FINAL

ENGINEERING DEVELOPMENT OF SLURRY BUBBLE COLUMN REACTOR (SBCR) TECHNOLOGY

Final Technical Report

Volume 1 of 2

Contractor
AIR PRODUCTS AND CHEMICALS, INC.
7201 Hamilton Blvd.
Allentown, PA 18195-1501

Bernard A. Toseland, Ph.D.
Program Manager and Principal Investigator

Robert M. Kornosky
Contracting Officer's Representative

Prepared for the United States Department of Energy
Under Cooperative Agreement No. DE-FC22-95PC95051
Project Period 3 April 1995 – 30 September 2002

ENGINEERING DEVELOPMENT OF SLURRY BUBBLE COLUMN REACTOR (SBCR) TECHNOLOGY

Final Technical Report

Project Objectives

The major technical objectives of this program are threefold: 1) to develop the design tools and a fundamental understanding of the fluid dynamics of a slurry bubble column reactor to maximize reactor productivity, 2) to develop the mathematical reactor design models and gain an understanding of the hydrodynamic fundamentals under industrially relevant process conditions, and 3) to develop an understanding of the hydrodynamics and their interaction with the chemistries occurring in the bubble column reactor. Successful completion of these objectives will permit more efficient usage of the reactor column and tighter design criteria, increase overall reactor efficiency, and ensure a design that leads to stable reactor behavior when scaling up to large diameter reactors.

COMPREHENSIVE TABLE OF CONTENTS

Abstract

This report summarizes the results of a Department of Energy-funded study on slurry bubble column reactors (SBCR). Alternate fuels projects need high reactor throughput for competitive economics so that reactors must operate in the churn-turbulent region of flow. Little data in this flow regime, especially at the conditions of high pressure and temperature for organic fluids found in an industrial reactor, existed at the inception of this project. This report summarizes the large body of fundamental data that was developed on these flows. It covers both the local liquid turbulence and large-scale liquid internal circulation aspects of flow in the SBCR. Where understood, the underlying mechanisms, which result in the macro-scale phenomena, are elucidated and modeled. Finally, new models for reactor design are also presented.

Executive Summary

The state of the art in design and modeling of bubble columns before the initiation of this project relied solely on the use of ideal flow patterns (e.g., perfectly mixed liquid and plug flow of gas) or on the use of the axial dispersion model (ADM). The use of ideal flow patterns can lead to serious over design, and the uncertainty in the values of the axial dispersion coefficients precludes a more accurate design based on the ADM. Since these models represent crude descriptions of the flow pattern in bubble columns and do not account for input from the fluid dynamics of the system, the scaleup of SCBR has been uncertain.

The need for rapid scaleup and optimal commercialization for gas conversion processes necessitated an improved understanding and quantification of fluid dynamics and transport in slurry bubble column reactors. This report presents the results of an extensive experimental and theoretical program on SBCR.

This program was conducted by a team comprising Air Products (APCI), Washington University in St. Louis (WU), The Ohio State University (OSU), Iowa State University (ISU) and Sandia National Laboratory (SNL). SNL participated as an active team member, but was supported by separate DOE funds; therefore, SNL's work will not be reported here.

Bubble columns are complex. The complexity can be simplified in breaking up the phenomena occurring in bubble columns according to scale. Molecular-scale investigations are needed to properly understand the catalysts and the chemistry of the gas conversion processes. These have been studied at APCI under additional grants. Bubble-scale phenomena are essential to understand the transport of gaseous reactant to the catalyst particle, where reaction with the liquid reactant takes place. Moreover, bubble-scale phenomena affect the global phase holdup and velocity distribution. These bubble-scale phenomena were studied extensively at OSU, and to a lesser extent at WU, SNL and APCI. Reactor-scale phenomena of gas holdup distribution, liquid recirculation, liquid and gas backmixing are critical in sizing the reactor properly for the

desired performance and in achieving optimal performance. These areas have been the focus of studies at WU, SNL, and APCI, and to a lesser extent at OSU. Reactor modeling is essential for development of scaleup rules. New phenomenological models have been developed at WU and tested at the DOE-owned, APCI-operated facility at LaPorte. More fundamental modeling efforts, based on solving the Navier-Stokes equations, were conducted at ISU and WU.

When we embarked on this endeavor, the understanding of bubble column reactor flow patterns at industrially relevant conditions was minimal, with no distinct features of the column behavior captured and scaleup rules extrapolated from ambient conditions using water as the model fluid. This program has elevated the understanding of bubble column hydrodynamics to the level at which the key physical features of the buoyancy-driven, two-phase flows are captured. The major areas of progress in the program are listed below:

- Reliable instrumentation and techniques for measurement of physical properties, velocities and holdups throughout the column have been developed. Methods for measurement of bubble characteristics, heat transfer and mass transfer have been modified and demonstrated in high-pressure, high-temperature columns. CARPT-CT, PIV and a variety of probes were tested, developed and used to compile an extensive database.

- A reliable database for flow in bubble columns under conditions of relatively high pressure and temperature has been developed. This database is useful in its own right for understanding flow behavior in large bubble column reactors. Furthermore, the database forms the basis for evaluation of parameters in both physically based engineering models and for computational fluid dynamic (CFD) models. This work presents data on the effects of gas velocity, solids concentration, pressure and temperature on the macroscopic and microscopic behavior of the column. Correlations for important engineering parameters such as gas holdup and holdup profiles are presented. The somewhat surprising lack of significance of sparger design on column flow, at industrially relevant conditions, is shown.

- Both macro- and micro-scale models of SBCR flow behavior have been developed. An engineering reactor model, firmly based on the observed phenomena for liquid recirculation and gas flow and backmixing, has been formulated and tested. Parameters of this model are tied to first principles as much as possible. These engineering models have been tested with tracer data taken at the AFDU in LaPorte, Texas. Furthermore, models for flow phenomena such as bubble size, circulation flows and mass and heat transfer have been developed.

- Identification of suitable CFD models for bubble columns has been initiated, and validation of these models has begun. 2D and 3D CFD computations are starting to yield results that are comparable to experimental observations. A search for reliable models and closures has been initiated.

Future Work

This program has been discontinued, but a considerable amount of work remains to be done before fully predictive models of slurry bubble column behavior are a reality. At the same time, it is clear that fully predictive models could become a reality, if a similar program would be executed successfully. The program would be difficult, but if a world-class team could be assembled as in this project, the goal is attainable. Furthermore, the models would be key in implementing the goal of finding the lowest cost method to convert synthesis gas (syngas) derived from advanced coal gasification processes to clean liquid chemicals and fuels.

This program would consist of developing improved methods for describing the SBCR using computational fluid dynamics and macroscopic models using the insights gained from the CFD program. This work scope includes both the computational work and the experimental program necessary to verify computations. Methods to measure the distribution of all three phases, including the bubble size distribution, at industrially relevant conditions are necessary for this verification. Verification under industrially relevant conditions would help in establishing the validity of the models. In addition, an experimental program to develop a better understanding of heat and mass transfer within the SBCR should be initiated both because of its intrinsic value and its value to model verification.

Detailed suggestions for future work are presented in each of the reports from the universities.

Introduction

This report summarizes the work done under cooperative agreement DE-FC 22 95 PC 95051 with the U.S. Department of Energy (DOE) to study the hydrodynamics of slurry bubble column reactors. Air Products and Chemicals, Inc. Washington University in St. Louis, The Ohio State University and Iowa State University performed the work under this agreement. Although Sandia National Laboratories was also part of the consortium, their work was performed under a separate agreement and will not be reported here.

The approach taken by the DOE to achieve energy independence and to improve the global competitiveness of U.S. energy conversion technology has been to promote the development of technologies that use clean synthesis gas produced from coal, natural gas, and other non-traditional feedstocks to produce a variety of alternative transportation fuels and chemicals.

At the time of the initiation of this program a major accomplishment of the DOE-supported program had been the development of high-capacity, slurry bubble column reactors -- the heart of liquid-phase technology. A slurry bubble column reactor (SBCR) is an attractive option for converting synthesis gas to selective products because it can process a hydrogen-lean synthesis gas produced by a typical modern gasifier. A slurry

bubble column reactor is essentially a hollow tube containing a heat transfer area (tubes) and a sparger system for introducing gas. The catalyst used in the reactor is a powdered solid that is suspended in a neutral liquid medium. The gas flow provides the mixing. While this type of reactor is a relatively simple device, it exhibits two characteristics that are very desirable for processing syngas:

- It provides for very efficient heat transfer.
- It provides a high degree of backmixing.

The combination of good heat transfer and improved mass transfer results in improvements in the performance of dispersed-phase catalysts. Furthermore, due to the simplicity of reactor design and vessel internals, the SBCR requires low initial capital and operating cost.

The development of bubble-column technology had been accomplished in conjunction with the development of liquid-phase processes for chemical reactions, which was the main thrust of the DOE-funded program. Nevertheless, this program pushed the rates of production of slurry bubble columns far above what had been practiced previously. In addition, the program verified that bubble columns exhibit the characteristics of stirred-tank reactors in series. It also used this phenomenon to demonstrate certain processing advantages for the conversion of synthesis gas to alternate fuels.

Despite the fact that slurry-bubble-column technology development became an important part of the liquid-phase program, studies of the fluid mechanics and modeling of this technology had not been pursued adequately. The models used for scaleup and economic calculations -- the dispersion model and the CSTR model -- are simple one-parameter models. Though these models are a useful starting point, major improvement is needed to develop a truly scaleable design model that can be used to sharpen economic estimates as well as to design more efficient columns. A good picture of the flow hydrodynamics at industrially relevant reaction conditions of high temperature and pressure was also lacking.

The major goal of the proposed project was to develop the design tools and the fundamental understanding of the fluid dynamics of a SCBR to maximize reactor productivity. If successful, completion of such a project will have the following technical benefits:
- More efficient usage of the column and tighter design
- Increased overall reactor efficiency by gaining insight into the interaction between the chemistry and the physics occurring in the reactor
- Stable reactor behavior when scaling up to large diameter columns

Another major goal of this research program was to develop the design models and to gain an understanding of the hydrodynamic fundamentals under industrially relevant conditions.

The tasks of this program are summarized below:

Task 1: Technical Assessment of the State-of-the-Art of SBCR Technology
This task included reviewing the literature with respect to the current SBCR state of the art, identifying the deficiencies, specifying the need for improvements regarding predictive equations, and identifying needs for additional data for design, operation, and technical risk reduction.

Task 2: Component Diagnostics Development
The objective of this task was to develop the required diagnostic components for characterizing the physical processes occurring inside an SBCR.

Task 3: Model Selection and Development
The objective of this task was to establish an engineering database for SBCR technology development that can be used for the design and operation of commercial reactors for producing alternative fuels and chemicals from synthesis gas.

Subtask 3.1: Experimental Design/Data Generation for Model Development
The goal of this task was to gather information that gives a physical picture of flow in a bubble column so that physically sound engineering models, which can be extrapolated to the larger scale, can be developed. This same information is also necessary for the validation of a computational fluid dynamic model.

Subtask 3.2: Model Development
The objective was to develop two different types of models: 1) a fundamental fluid-mechanic model based upon solutions of the time-averaged Navier-Stokes equations and 2) a phenomenological model based upon PFR (plug flow reactor) and CSTR (continuous stirred tanks in series) theory.

Subtask 3.3: Sparger/Entrance Region Modeling
This work encompassed an experimental study on the effect of sparger shape on bubble generation, development of a mathematical model of the generation of bubbles, and on sparger design.

Task 4: SBCR Experimental Program
This task involved characterizing the SBCR reaction system at the LaPorte AFDU facility. It was anticipated that radioactive tracer measurements, similar to those that were used in the past, would be utilized in this work.

Task 5: Slurry Behavior
The effect of slurry characteristics on the hydrodynamics of the SCBR has received little attention, despite the fact that it may be extremely important at the high concentration levels required for the commercial processing of synthesis gas. Thus, this task focused on developing a better understanding of slurry behavior.

Task 6: Data Processing

With the reactor model and parametric correlations selected in Tasks 1 to 3, computational strategies were determined and calculations performed to verify selected models and correlations derived in this program.

Task 7: Management and Reporting

7.1 Planning and Reports

Upon completion of the project, a final detailed project report was written covering all phases of the project.

This report structure is a summary of the accomplishments of the project under each task. Detailed reports from each of the universities are attached.

Results and Discussion

Task 1: State of the Art

The state of the art is discussed in each of the attached reports under the appropriate sections. This format allows the reader to understand the work in each section in context.

This work has been directed towards industrially relevant conditions. An extensive database of information had been gathered for air-water systems, at near atmospheric temperature and ambient temperature, operating at low superficial gas velocities such that the columns operate in bubbly flow. Indeed many papers at these conditions are still being written. SBCRs converting syngas for fuel production (methanol [MEOH], Fischer Tropsch [FT] or dimethyl ether [DME] synthesis) operate at high temperature (250°C), relatively high pressure (up to 80 atmospheres), with organic liquid at high enough gas flow rates (15-30 cm./sec.) to give churn turbulent flow. Little work is available for these industrially relevant conditions. Thus, this work concentrates on building a picture of the operation of SCBRs at these industrial relevant conditions.

This project has succeeded in moving the state of the art of SBCR forward significantly in many aspects:
- Development of a wealth of data on bubble columns at industrially relevant conditions
- Development of a model of flow in a reacting system that uses laboratory measurements at cold flow conditions to estimate parameters
- Demonstration of the use and pitfalls of computational fluid dynamic models for modeling bubble columns.

Task 2: Component Diagnostics Development

Since operation of an actual SBCR had outstripped data generation, a good part of this work was directed at understanding the behavior of the SBCR at industrially relevant conditions by making direct measurements. Since this work has stretched operating conditions, several existing techniques were modified, new techniques were devised, and

some techniques were shown to be inadequate. This section discusses these developments, organized by the property being measured to give the proper overview. The techniques are discussed individually in significantly more detail in the attached reports. (The major findings using these techniques are summarized in Task 3 and discussed in detail in the accompanying reports.)

Physical Property Measurement
The ability to measure physical parameters is vital to understanding the behavior of the SCBR. Physical properties of the gas and liquid greatly affect the hydrodynamic behavior of bubble/slurry bubble columns. The exact physical properties of the liquid phase at high pressure and temperature must be known in order to characterize the actual system. Moreover, the values of physical property parameters are generally found in dimensionless numbers used in generalized correlations, so that information can be transferred from one system to another.

During this project, the ability to measure density, viscosity and surface tension of liquids at elevated pressure and temperature was developed. Density, viscosity and surface tension of liquids at elevated pressure and temperature can be characterized by the hydrostatic weighing method, the dropping weight method, and the emerging bubble technique, respectively. Liquid properties can be characterized with maximum operating pressure and temperature of 21 MPa and 250ºC, respectively, in the high-pressure and high-temperature, multiphase visualization system developed at The Ohio State University. These limits are the limits of the apparatus, not the technique. In general, these techniques are useful for a wide range of pressures and temperatures. The use of this apparatus is discussed in the section entitled "Supplementary: Measurement of Liquid Physical Properties in Bubble/Slurry Bubble Column," which is contained in Ohio State's final report for the period January 2002 to June 2002. In this work, Paratherm is used as a test fluid. This apparatus has been employed to measure the properties of FT waxes for other projects. Thus, this contribution represents a flexible method to measure important physical properties of fluids at industrially relevant conditions.

Velocity Measurement

<u>CARPT</u>
At Washington University, the technique of Computer Aided Radioactive Particle Tracking (CARPT) was improved so that velocities everywhere in the column measurements could be measured reliably at industrially relevant conditions.

The basic principle of CARPT is simple. A single radioactive tracer particle, selected to be dynamically similar to the phase to be traced (e.g., solids or liquids), is released in the column surrounded by a set of scintillation detectors located at known positions. All the detectors sample the radioactive counts from the particle. The use of an appropriate reconstruction algorithm identifies the position of the particle. The reconstruction algorithm uses previously obtained calibration data to locate the particle. Lagrangian instantaneous velocities and eddy diffusivities are obtained directly from the trace of the

tracer particle. Mean velocities and turbulence intensities and stresses are calculated by invoking the ergodic hypothesis.

Although the principle is simple, the reduction of CARPT to practice is complex. This project has allowed the development of both a more precise technique and new applications of CARPT. Velocity measurements in Plexiglas columns had been demonstrated at Washington University. Improvements made during this contract extended these techniques to measurements of the velocity of solid particles and to measurements at high pressure by adapting the technique for use in a stainless steel column.

- Studies with slurry systems showed that the radioactive tracer particle had to resemble the solid phase particles in size and density. This required a reduction of size in the normally used Scandium particle, which is encased in polyethylene to make it neutrally buoyant. The new technique involves coating a Scandium particle of size 150 μm with Parylene for protecting the tracer particles from oxidation in CARPT experiments. Studies with these small tracers revealed that they could follow the solid motion reasonably well in slurry systems.

- The calibration step involves placing the tracer particle at numerous known locations in the column, operated under the actual experimental conditions. Extending CARPT to high-pressure measurements necessitated changes in calibration techniques. The original method of calibration, which relied on fishing lines and hooks to position the radioactive particle at desired locations, did not work when calibrating a stainless steel column. Hence, an automated calibration device was designed, constructed and successfully tested to accomplish the calibration in-situ at high pressure. The performance of this automated calibration device is excellent; it cuts calibration time to 25% of the original technique. When calibration experiments were performed in the stainless steel column, an unexpectedly large scatter was observed in the calibration curves. This scatter was attributed to radiation buildup at the column wall. It was found that buildup affects only the Compton scattering portion of the energy spectrum and not the photopeak fraction of the spectrum. Therefore, a new data acquisition strategy was developed to acquire only the photopeak fraction of the energy spectrum. Both of these improvements allow calibration in the stainless steel column so that high-pressure measurements can be made.

- Improvements in both location detection and noise filtering have been developed as a result of the work done under this contract. As the tracer particle moves through the reactor, the particle location needs to be reconstructed. In principle, a set of four distances should be sufficient to reconstruct the position of the particle. The real situation is more complex, however, as the photon emission from the source itself is a Poisson stochastic process. This leads to uncertainty in reconstructing the particle position based on counts obtained at any detector due to both the uncertainty associated with the source fluctuations and the detector anisotropy. The error associated with reconstructing the particle may be

minimized by different techniques. Improved tracer reconstruction strategies were developed during this contract and are currently employed.

- The reliability and accuracy of the CARPT measurement largely depends on several key factors that include the tracer particle, calibration and signal processing. The issue of removing noise from CARPT raw data is important in ensuring accurate reconstruction of particle positions and, therefore, subsequently the velocities and turbulence estimates. Therefore, a wavelet-based filtering approach was developed. Processing the CARPT data for a controlled motion experimentally validated the efficiency of the wavelet filtering and its ability to improve the accuracy of the measurement.

The newly developed particle reconstruction algorithms and the wavelet filtering reduce the error in particle location to less than ± 0.3 cm. This allows accurate measurement of turbulent quantities such as the Reynolds stresses, in addition to improved velocity measurement.

PIV (Particle Imaging Velocimetry)
PIV uses a laser sheet to illuminate a section of the flow that has been seeded with small particles and a camera in conjunction with data imaging software, to track and measure the velocity of the fluid, gas and solid. It has been used at Ohio State for over a decade to measure flow characteristics in bubble columns. The PIV system used in this study was enhanced and modified from the original system to measure instantaneous full-field flow characteristics for a given plane. The modified PIV technique has sufficient accuracy to determine time/volume-averaged flow information for each phase, including velocities and dispersed phase size distributions. Further, the PIV technique developed for multiphase systems has the ability to discriminate between the different phases, and provides the instantaneous, full-field flow properties of each phase. This same system was further modified for use in the high-pressure bubble columns at Ohio State. These significant enhancements, which are discussed in the Ohio State report, allow measurement of particle, bubble, and liquid velocities at industrially relevant conditions.

HPA
An HPA (Heat Pulse Anemometer) system, which uses pulses of heat, a hot-wire anemometer and a computer analysis to infer flow velocity in liquid, was tested at Washington University. The technique was found to be useful for bubbly flow, but not for churn-turbulent flow. HPA is prone to errors, especially in churn-turbulent flows, where the assumptions of the existence of dominant unidirectional velocity are clearly violated. Thus, this technique was judged to be not useful in velocity measurements for industrially relevant conditions that usually involve columns operating in churn-turbulent flow.

Holdup of Gas, Liquid and Solids
At Ohio State, the overall gas and solids holdup in the slurry bubble column was measured using the dynamic gas disengagement technique. This technique involves shutting off the gas inlet and outlet simultaneously to maintain constant system pressure

after the flow in the column reaches steady state. The bubbles disengage from the column, while the particles gradually settle. The pressure is followed as a function of time during the shutdown period. The inference of solids concentration is a novel use of this fairly standard technique. The solids concentration in the slurry bubble column can also be monitored with this method to ensure that all the particles are completely suspended at various gas velocities.

Washington University uses gamma ray Computed Tomography (CT) for measuring density (holdup) profiles in the column at operating conditions. A narrow beam of radiation traveling along a straight path through an object is attenuated primarily by absorption and to a lesser extent by scattering. The strength of the radiation reaching multiple detectors is used to infer the density of the object. In this case the object is the gas and liquid in a bubble column. The CT scanner at Washington University uses the third-generation fan-beam scanning configuration at various axial positions. This technique already existed and was adapted for use at high-pressure and -temperature operation. From CT scans, time-averaged cross-sectional gas holdup distributions are reconstructed at different axial locations. Thus, the radial gas holdup profiles can be calculated by azimuthal averaging.

Combination Measurements in the AFDU
A combination of the use of differential pressure and gamma densitometry (a simplified form of gamma ray CT) was implemented at the AFDU (Alternate Fuels Development Unit) to measure holdup at several axial positions and to infer the presence of the radial holdup distribution. While differential pressure has been used in slurry-free situations, this is the first use with slurries. The existence of the slurry particles makes this technique difficult to implement. The data from this technique was combined with data from the NDG (nuclear density gauge) previously installed at the LaPorte facility to estimate the holdup distribution in the column under reaction conditions. Attempts to do simple densitometry and CT at the AFDU were made; however, a lack of precise positioning thwarted these attempts. A suitable unit has been designed and awaits installation at a later date.

Bubble Size Distribution
Probes
Direct measurements of bubble sizes in the high-pressure slurry bubble column were attempted using fiber optic probes. The probe utilizes the difference in refractive index of gas and liquid to distinguish the gas phase from the liquid-solid suspension. Since the probes can distort the bubble interface, they must be calibrated using a camera, and the proper bubble surface must be used to note the time of passage. Given this development, the probe can be used to accurately determine the presence of a bubble and its time of passage.

At Ohio State, a dual-probe system was used. This system can only measure the bubble chord length, not the true bubble diameter. If a uniform bubble shape is assumed (either spherical or ellipsoidal), the bubble chord length distribution can be converted to the size

distribution. However, the bubbles in slurry bubble columns can have irregular shapes. The data from the probe can thus only represent the chord length distribution.

At Washington University, a four-point probe system is being developed. This work is an attempt to accurately measure bubble size directly and is continuing. The system itself has been demonstrated. The interpretation of the signals to infer bubble size directly is currently being analyzed.

DDG (Dynamic Gas Disengagement)
The DGD technique was first used in bubble columns at low gas velocities (Ug <2 cm/s) to quantify the bubble size and size distribution in the columns. Various models that relate gas disengagement phenomena to bubble size or size distribution have been proposed. However, the reliability of the DGD technique applied to the slurry bubble columns operated at high pressure and high gas velocity depends on whether the models account for the transient characteristics of bubble flow during the DGD process. Little has been reported on the evolutions of the instantaneous distributions of the bubble size and bubble rise velocity during the gas disengagement process.

Since observations based on the DGD technique have been used to propose a "two-bubble class" model, this technique was investigated by Ohio State in some detail. They found that in slurry bubble column reactors operated at high gas velocities, such as those in the methanol synthesis process, the bubble size distribution cannot be reasonably estimated by the DGD technique without the quantification of bubble-bubble interactions.

Heat Transfer
Ohio State used a heat transfer probe, which is specifically designed for high-pressure and high-temperature conditions, to determine the heat transfer coefficient. This probe uses a microfoil heat-flow sensor that can directly measure the local heat flux through the heating surface of the probe by detecting the temperature difference across a thermal barrier of known resistance. The temperature of the bulk fluid is measured with a T-type thermocouple. For each measurement, the heat flux and temperature difference between the probe surface and the bulk fluid are sampled simultaneously by using a computer data acquisition system at a rate of 100 Hz for 30 seconds. The time-averaged heat transfer coefficient can be calculated from the heat flux and temperature difference by integration.

Mass Transfer
The gas-liquid mass transfer coefficient was measured using an oxygen-stripping method with a discontinuous switch from air to nitrogen. A high-pressure optical fiber oxygen probe was developed to measure the oxygen concentration up to a pressure of 3000 psi. For this measurement, a 470 nm light source is sent to the probe. The tip of the oxygen optical fiber probe is coated with a fluorescence dye that is excited by the light source. When the fluorescence gel is excited, it gives out light of wavelength 590 nm. The dye fluoresces most brightly when no oxygen is present and decreases with increasing oxygen concentration. At the beginning of the experiment, the liquid is saturated with air. Then the airflow is shut down so that all bubbles escape from the liquid. Nitrogen is then fed into the column, and simultaneously, the oxygen concentration is monitored. To verify

the validity of the measuring technique, the mass transfer coefficient measurement was first conducted in the air-water system under ambient conditions and compared to known values.

Task 3: Model Selection and Development
The work summarized in this section has three main purposes:
- to provide qualitative answers regarding the effect of specific variables on observed flow patterns in the column,
- to allow estimation of engineering type models for flow and mixing in bubble columns, and
- to provide data for holdup and velocity profiles and turbulence intensities for validation of CFD codes.

The conclusions from this work are summarized in this section. The detailed data and interpretation are found in the individual final reports. This body of work forms a substantial contribution to the information about SBCRs operating at high pressures and temperatures. Work at ambient conditions is also presented so that general correlations that span the whole range of operating conditions can be developed.

Subtask 3.1: Experimental Design/Data Generation for Model Development
<u>Flow Phenomena</u>
- Perhaps the most striking feature of a SBCR is the high degree of mixing and heat transfer obtained in these reactors with little mechanical energy input. The familiar time-averaged "gulf stream" pattern of up-flow of liquid in the center of the column and down-flow at the sides coupled with the high degree of turbulence induced by the buoyancy of the individual bubbles induces the high degree of mixing. This flow pattern is found for all conditions of industrial interest studied.
  - Superficial gas velocity is the dominant variable that affects liquid recirculation, with recirculation increasing with increased velocity.
  - An increase in column diameter increases liquid recirculation.
  - The effects of liquid physical properties and solids concentration, while significant, are secondary in comparison to the effect of gas velocity and column diameter.
  - Correlations for axial liquid velocity and gas holdup radial profile have been developed. The main advantage of these correlations is their simplicity, as they require as input only the superficial gas velocity, physical properties and column dimensions. They can be readily used for prediction of the axial liquid velocity profiles for superficial gas velocities ranging from 2 to 60 cm/s and column diameters of 10 - 63 cm, as well as different liquid properties.
- Gas holdup is a key parameter that characterizes the transport phenomena of bubble column systems. The gas holdup generally increases with an increase in gas velocity. The rate of increase is larger in the dispersed-bubble regime than in the churn-turbulent regime.
  - Pressure has a significant effect on gas holdup in the column. The gas holdup increases with pressure, and the pressure effect is more pronounced in slurries of higher concentration. Particle concentration also

affects gas holdup, especially at ambient pressure. At elevated pressures, the effect of the solids concentration is relatively small at gas velocities above 25 cm/s. An empirical correlation, which takes into consideration the experimental data obtained from this study and in the literature, was developed to account for the overall gas holdup in both the high-pressure bubble columns and the slurry bubble columns in the work presented by Ohio State. The correlation covers a wide range of liquid and gas properties and flow conditions.

- o Correlations have been developed by Washington University for prediction of both gas holdup and liquid velocity profiles. These correlations are accurate for atmospheric pressure conditions and remain to be tested at high pressures.
- o Gas holdup and its radial profile are not affected much by pressure in bubbly flows. In fully churn-turbulent flow, gas holdup rises with pressure and becomes increasingly parabolic. Liquid recirculation is enhanced at high pressure.
- o When churn-turbulent flow is established at a given fixed superficial gas velocity, gas holdup profiles become slightly steeper with increased pressure. When the superficial gas velocity is sufficiently high so that at all pressures studied the flow is clearly churn-turbulent, the effect of increasing pressure at constant superficial gas velocity is equivalent to increasing the gas momentum, which leads to steeper holdup profiles.

- The effect of pressure on gas holdup in slurry bubble columns is related to the changes in bubble size distribution, which in turn affects bubble velocity in the column.
  - o Bubble size (as estimated from chordal measurements) at elevated pressures is significantly smaller than at ambient pressure, under all experimental conditions. Somewhat of a surprise is the finding at Ohio State that the largest size bubbles dominate the bubble rise velocity. The dominant effect of large bubbles on bubble rise velocity in slurry bubble columns is due to bubble wake attraction.
  - o The presence of particles in liquids leads to a larger bubble size, especially at ambient pressure. However, the solids concentration does not affect the maximum bubble size at gas velocities above 25 cm/s at 5.6 MPa.
  - o A model has been derived to quantify the observed pressure effect on maximum bubble size. This model includes the effect of internal circulation of gas in the bubble as a major driving force that determines bubble size. This effect has not been included in previous models used to explain the effect of pressure on bubble size in SBCRs. Centrifugal force induced by internal circulation of the gas inside a bubble can disintegrate the bubble at high pressures. As pressure increases, gas inertia increases and surface tension decreases, and therefore the maximum stable bubble size decreases. The model reveals that the gas inertia and gas-liquid surface tension dictate the maximum stable bubble size at high pressures, which explains the relatively small effects of solids concentration on the maximum bubble size and on the gas holdup as observed in this study. A

hydrodynamic similarity rule based on the similarity of three dimensionless groups is also proposed for high-pressure operations.

- Since flow in bubble columns is determined to a large extent by the bubbles themselves, understanding the factors that determine bubble size in a column will help to elucidate flow structure in the column. To fully understand bubble dynamics, it is necessary to quantify the initial bubble formation in both liquid and liquid-solid media. The work done in this program concentrates on high-pressure conditions, since this is a little explored region.
  - o Initial bubble size in the suspension, i.e., in the presence of solids, is generally larger than that in the liquid.
  - o The initial bubble size in the liquid is determined through the balance of various forces, including buoyancy, gas momentum, bubble inertial, surface tension, and liquid viscosity. Additional forces on the bubble in liquid-solid suspensions, induced by bubble-particle collision and liquid-solid suspension inertia, contribute to the larger initial bubble size in the suspension compared to that in the liquid. A model describing initial bubble size is formulated in this work.
  - o The effect of pressure on the initial bubble size is insignificant under constant flow conditions from the sparger. Through the analysis of forces used in developing the model, this effect is attributed to the balance of effects of pressure on the overall upward and overall downward forces.
- Observations and quantitative measurements allow both an understanding of the flow phenomena and an experimental basis for testing computational fluid dynamic simulations.
  - o The Reynolds normal stresses are an order of magnitude larger than the Reynolds shear stress. The Reynolds stresses decrease with increasing pressure.
  - o As the pressure increases, the magnitudes of the averaged velocity of the liquid phase at the center and in the wall region decrease.
  - o The fluctuation of the liquid phase caused by bubbles is damped out as the pressure increases because of a narrower bubble size distribution with a smaller mean bubble size at elevated pressures.
  - o The fluctuation of the liquid velocity is of the same order of magnitude as the averaged velocity. From the pdf's and the power spectral density functions, it was observed that the vortical structure dominates the low-frequency fluctuations in bubble column systems.

<u>Column Design Considerations</u>

- Gas distributor design does not significantly affect holdup and liquid velocity profiles in the fully developed flow region of the column, which occupies most of the column at high H/D ratios. It also does not tend to be an important factor anywhere in a column at the relatively high velocity and pressure of industrial reactors. Any effect of distributors is generally smaller at high-pressure and high-temperature conditions. This is attributed to the fact that bubble formation is dominated by the physical properties of the liquid phase instead of the distributor type. There is some sparger effect, especially at low gas velocities, e.g., in general, porous plate distributors give lower gas holdup than sparger and perforated plate gas distributors with larger holes.
- Liquid mixing in bubble columns is controlled by the combined mechanism of local liquid turbulence and large-scale liquid internal circulation. Thus, both large- and small-scale phenomena must be considered in column design.
- The axial liquid dispersion coefficient increases with increasing gas velocity and decreases with increasing pressure. Liquid properties, liquid-phase motion and column dimension have significant effects on liquid-phase mixing; however, distributor design does not have a significant effect.
- Axial eddy diffusivities exceed radial diffusivities by an order of magnitude. Both increase with increased superficial gas velocity. Correlations have been developed to estimate both axial and radial eddy diffusivities.
- Heat exchange tubes in vertical bundles occupying 5% of the cross-sectional area do not significantly affect the gas holdup or the liquid recirculation profiles, but do reduce the radial eddy diffusivities to some extent.

<u>Heat Transfer Coefficients</u>

- The heat transfer coefficient in gas-liquid or gas-liquid-solid systems is higher than that in single-phase systems. The high heat transfer rate in multiphase flows is attributed to turbulence induced by gas bubbles. The objective of this study was to investigate heat transfer behavior in a high-pressure slurry bubble column. The major conclusions are summarized below:
    - The heat transfer coefficient increases as the gas velocity increases and then levels off.
    - The heat transfer coefficient decreases significantly with increasing pressure. This behavior can be attributed to the variations in physical properties of the liquid phase, bubble size and gas holdup with pressure.
    - The heat transfer coefficient increases significantly with an increase in solids concentration, at least for the small particles studied here. The extent of the increase varies with pressure. Increasing solids concentration increases the heat transfer coefficient more at ambient pressure than at high pressure. The change in effect is attributed to the observation that the effect of solids concentration on bubble size is much greater at ambient pressure than at elevated pressures.
    - The heat transfer coefficient increases significantly with increasing temperature. This phenomenon can be explained by the significant decrease in liquid viscosity with increasing temperature.

- o The heat transfer behavior in a slurry bubble column under the pressure range is described using the consecutive film and surface renewal model. A correlation is contained in the Ohio State report.

Mass Transfer Coefficients

- The objective of this study was to develop a suitable measurement technique and to investigate the gas-liquid mass transfer coefficient in a hydrocarbon liquid at high pressures. The work was carried out in a small-diameter (50 mm) column. The Ohio State work shows that the gas-liquid mass transfer coefficient is higher in smaller diameter columns than in large-diameter columns, so that additional work is needed before the work can be of general design use.

- The general conclusion reached is that the mass transfer coefficient increases significantly with increasing gas velocity at high as well as ambient pressures. At high gas velocities, the gas-liquid mass transfer coefficient tends to level off.

- The effect of gas velocity change on mass transfer is complex. In general, the mass transfer coefficient, $k_l a$, is dominated by the variation of interfacial area, and decreasing the mean bubble diameter by increasing gas velocities provides a larger interfacial area. Simultaneously, as the gas velocity increases, the contact time between the liquid and bubbles is reduced, resulting in a lower mass transfer coefficient. Moreover, the turbulence generated by the gas bubbles, as well as the liquid internal circulation at higher gas velocities, contributes to the increase in the gas-liquid mass transfer. An example of this complexity is seen in the effect of column diameter mentioned above. In small columns, the column wall effect is significant, and the bubble size is limited by the column size. Bubble size is, of course, related to surface area and influences mass transfer. As column diameter increases, the bubble size is no longer limited by the column dimension, but by the gas and liquid properties. The rate of bubble coalescence and breakup will then dictate the bubble size.

Subtask 3.2: Model Development
Three types of chemical engineering reactor models to model flow in reactors are in general use: (1) idealized flow model, which uses abstract conceptions, e.g., the perfectly stirred tank or "plug" flow that models each molecule having the same residence time; (2) modifications of the idealized flow models, e.g., the axial dispersion model (ADM), which adds a diffusion-like term to account for residence time distribution, or combinations of idealized models; and (3) models based on the Navier Stokes equations. The state of the art in design and modeling of bubble columns before the initiation of this project relied solely on the use of ideal flow patterns (e.g., perfectly mixed liquid and plug flow of gas) or on the use of the axial dispersion model (ADM). The use of ideal flow patterns can lead to serious over design, while the uncertainty of the axial dispersion coefficients precludes a more accurate design based on ADM. All of these models represent the crude descriptions of the flow pattern in bubble columns, which do not take into account the fluid dynamics of the system. Two new kinds of models were developed during this project; each is discussed below.

Phenomenological Models
The extensive database for gas holdup and liquid velocity distribution provides the basis for engineering models for the description of flow and mixing in bubble column reactors. The models are based on observed physical phenomena, i.e., phenomenological models. All experimental results indicate that gas holdup (with rationally designed distributors) is almost axisymmetric and can be represented as a function of radial dependence. This holdup profile drives the buoyancy-driven liquid recirculation. Hence, the methodology was to quantify the liquid recirculation as a function of gas holdup profile, estimate the eddy diffusivities from the database, and superimpose these on the time-averaged liquid recirculation profile. The models were built up using each as the basis to go further:

- An extensive parametric study confirmed that the one-dimensional liquid recirculation model could predict some of the essential features of the bubble-driven turbulent flow in bubble columns. The axial liquid velocity profile calculated from this one-dimensional model compares well with the experimental data determined from CARPT. A correlation for the liquid recirculation has also been developed. This ability to predict the liquid recirculation pattern was used as a physical basis for the rest of the modeling effort.
- The first model, the one-dimensional Recycle with Cross Flow and Dispersion Model (RCFDM), was derived using a combination of the ideal flow patterns. The model breaks the reactor into four regions: an upflow region, a downflow region and two stirred-tank regions representing the sparger and disengagement zones. It uses seven input parameters to the model obtained from the experimental database to predict flow in the reactor. The model prediction of the tracer outlet response, based on CARPT/CT data for the fluid dynamic parameters, and without fitting parameters, matches the tracer impulse response in an air-water system remarkably well. Given its initial success, the idea of a compartmentalized model was used in the rest of the work.
  - Scaleup based on this model uses the experimental data in air-water systems to evaluate the mean liquid circulation velocity and turbulent eddy diffusivity in other systems and in larger columns. Thus, laboratory data

is used to set most of the parameters for the model and for the subsequent models. The only experimental information required by the model in the system of interest is the gas holdup and its radial distribution.

- The two-dimensional convection-diffusion model for liquid mixing in a bubble column followed a natural extension of the RCFDM. Since it is two-dimensional, this model accounts not only for the liquid recirculation and gas holdup (as done in the RCFDM), but also for their profiles as well as axial and radial eddy diffusivities. The improvement in this model is that it provides more information about the variance of the tracer concentration in the radial direction. It can capture, in a statistical sense, the large-scale transient flow patterns in the column. Thus, this model can represent meso- and macro-scale mixing in the column, which is of importance for modeling bubble column reactors.
  - For scaleup, model predictions for liquid mixing in bubble columns are truly "predictions," involving no fitting parameters. Thus, they represent first-of-their-kind capability. The two-dimensional convection-diffusion model, together with the scaleup strategy, results in fairly good predictions of the characteristic mixing times within the column as measured by the radiation detectors at various axial locations. This indirectly substantiates the proposed methodology of using the gas holdup profiles in churn-turbulent flows, at sufficiently high gas velocities, for characterizing the systems of interest.
- The final improvement in this series of models, the gas phase recirculation and dispersion, adds the ability to predict the gas mixing in bubble columns to the previous models. The only experimental information required by the model is the gas holdup and its radial distribution, which can be determined, with one floating parameter, by the same procedure used by the previous models. This model can be formulated for the popular "two-bubble class" hypothesis as well. Four-zone (SBCM) and five-zone (DBSM) mechanistic reactor models were used to describe the distribution, generation, and consumption of the reactant or tracer species that are transported in both phases to good effect.

This work represents a considerable step forward in the ability to model flow in a slurry bubble column. This new class of models is fundamentally based; additional testing is needed. Since these models have shown the ability to predict flow, some additional work is needed to make them more predictive by gaining a better understanding of the radial gas holdup profiles.

Computational Fluid Dynamic-based Models

The Holy Grail of reactor flow description is a predictive model for the calculation of the flow patterns in a reactor. Computational Fluid Dynamics (CFD) holds the promise of being able to calculate the flow for any given set of starting conditions. Indeed, for many single-phase flows, this promise has been fulfilled. However, a predictive model to calculate flow patterns in a reactor remains elusive.

Three major obstacles stand in the path of discovery:
- The size of the problem is much too large for present-day, state-of-the-computers.

- o The flow field of interest is composed of flow structures that may be as large as the diameter of the reactor, but that are only dissipated by viscosity at the molecular level. Thus, the size of the flow field ranges from meters to micrometers. One must have a huge computational grid with a very large number of computational cells in order to obtain the correct resolution of both the large and small structures. This is beyond the capabilities of even advance computers.
  - o Computation time becomes very long. The direct solution of the flow equations (Navier-Stokes equations) takes an extremely long time on even the fastest computers. Calculations for even a few milliseconds of actual flow are the longest that have been done. Even if one limits the problem by averaging and limiting the size of the computational grid, the computational time required for modern computers is very long for the three-dimensional problem. Computational times on the order of weeks are common. When multiple bubble sizes are added, the computational time becomes much longer. Thus, testing models and computational schemes becomes very long and difficult.
- The non-linear nature of the equations makes simplification difficult. The standard method of reducing the size of the problem is to use ensemble averaging. However, new terms are generated during the averaging procedure because of the nonlinearity of the equations. Models for these new terms, "Reynolds stress," which are generated by the averaging procedure, have been developed and tested for single-phase flow, but not for multiphase flow. Introduction of these models leads to further questions about small-scale fluctuations. Thus, a great deal of research is required to find the correct equations that will allow closure of the non-linear equation system.
- The state-of-the-art solution to the problem, the two-fluid approach, requires that the forces representing interphase momentum exchange, i.e., the forces between the gas and liquid phases, be described. The importance of the individual forces is currently the subject of a great deal of research. As yet, exactly what forces are necessary to give an accurate and predictive simulation is still the subject of much debate and active research. In addition, the physics needed for these descriptions is not yet clear.

Despite the difficulties in the CFD approach, the promise of a fully detailed description of multiphase flow and the importance of the prize are enough to warrant the initiation of CFD studies. Such studies have been carried out at various levels at each of the three universities. Reasonable progress has been made so that this work represents the state-of-the-art in CFD of bubble column flows. This work is covered in the individual summaries from each of the universities. The summary below will provide an overview so that each report can be seen in context.

Problem Size
Our studies have shown that long computation times are a fact of life when trying to simulate slurry bubble column reactors. The major issues are summarized below, while details are given in the reports from Iowa State University and Washington University.

22

- The basic conclusion reached in this study is that 3D simulations take much too long on a single processor or by auto-tasking multiprocessor computers. There is a continuing need for a parallel computing code, which will make excellent use of the distributed memory afforded by this system.
- The long computational time is intrinsic to the computation itself, so that one can try to find methods to deal with the issue, but cannot eliminate it. Techniques to reduce the computational time have been worked on extensively at Iowa State University. They have switched from the commercially available solution code from Fluent to the CFDLIB computation code from Los Alamos. The latter code allows parallel computation to speed up calculations. Parallel computation breaks the problem up so that several processors can work on the same problem. Results have been mixed in that a decrease in computational speed is, unfortunately, not directly proportional to the number of processors used. This behavior is typical in large simulations. Furthermore, the parallel computing scheme did not work in the cases used to try to understand the effect of the walls of the column on flow. An alternative solution method has been found, but calculations still take a long time.

  Both Iowa State University and Washington University have used two-dimensional simulations instead of three-dimensional simulations to reduce computation time. Although these 2D simulations may not be completely accurate, they have been used effectively to study issues and to make inferences that can be confirmed in more lengthy 3D computations.
- One consequence of the long computational time is that relatively small bubble columns have been simulated in all previous studies. This acts to reduce the size of the problem. The study at Iowa State University has shown that large turbulent structures are predicted by simulation of large-diameter columns when no turbulence model is used, i.e., when the turbulence is allowed to decay without using a turbulence model. Thus, simulations of small-diameter columns miss some essential features of large-diameter bubble column performance. The consequence of this finding is that simulation of large-diameter columns, although computationally intensive, may be necessary when scaling up columns to diameters of 4 to 5 meters for fuels applications.
- Since the computational time is so long, previous studies have used relatively coarse computational grids to reduce solution time. (As discussed below, the use of turbulence models allows fully resolved solutions to be obtained, despite the coarse grid size.) However, the dynamics of bubble column flows depend strongly on grid resolution. Iowa State studies show that coarse grids may not capture some essential features of bubble column dynamics. Unfortunately, the fine grid increases computation time. Thus, there is a tradeoff between details and time.

Closures needed for Non-Linear Equations
Solution of the Navier-Stokes equations presents two issues. The computation time is excessive, and the results of the computation, a rapidly fluctuating flow field, are difficult to interpret. Traditionally, ensemble averaging has been used to calculate the

average flow field. The ensemble-averaged flow field is more easily interpreted, and the use of averaging reduces computing time. Unfortunately, the averaging procedure introduces a further unknown, "the Reynolds Stresses," so that the averaged equation must also be solved by computer simulation.

Various ways have been proposed to deal with the Reynolds Stresses, i.e., various closures have been developed. The commonly used closure, the k-ε model has been developed for shear driven isotropic turbulence. It is not clear that this approach can be used to provide accurate simulations for bubble columns. Thus, a good deal of work concentrated on testing which closures are most appropriate.

- The Washington University approach is to test how well these closures simulate existing data. They have found that good agreement can be obtained between computed solutions and data, at least for low gas flow rates. The bubble-induced turbulence model, which they have used, looks promising. Their results are summarized in Chapter 6 of the attached final report.

  One disturbing factor they have uncovered is that either the flow or the holdup can be calculated accurately. However, flow and holdup are related. This implies that something is still missing from the physics included in the simulation. Thus, while Washington University has had good success in its computational program, it is also clear that further work is needed to develop a model that gives predictive simulations for the general case.

  Washington University has attempted to get more accurate solutions by explicitly calculating bubble sizes during the computation. Standard simulation methods implicitly use only one bubble size in their calculations. The only place that bubble size appears in the calculation is through the drag force term. The standard solution method is to use a single value for the drag force term, which is equivalent to picking a single bubble size. In their research program, Washington University has explicitly included bubble size by simultaneously solving the equations for a number of different drag force values. This implies the use a number of different bubble size classes. To do this in a predictive manner, Washington University has modeled coalescence and breakup of bubbles through yet another set of models. Several models of coalescence and breakup have been compared with each other. The model that gave the most accurate simulation has been determined, at least for 2D simulations. They have also determined that the minimum number of classes of bubble sizes to give accurate simulation is six, again for 2D simulations. The major issue with this approach is that using six bubble classes means that six solutions must be determined simultaneously. Thus, computational time and expense is increased dramatically. Work in this area continues.

- The approach at Iowa State University has been to try to understand what closure is needed by first solving the equations without using a closure assumption to see what the structure of the flow is. Once the structure of the flow is understood, the appropriate closure may be chosen or devised. The basis of the need for this work is the understanding that the currently available closures have been developed for

shear-driven turbulent flow, but that bubble columns have bubble-driven flow, and the existing closures may not accurately represent this class of flows.

Iowa State has found that relatively small grid sizes are needed to capture the structure of the eddies in bubble-driven turbulent flow. The implication of this work is that the turbulence closures generally used mask some of the detail of the flow structure. In essence, the turbulence closures normally used add too much turbulent viscosity and over-damp the solution. Recent work has implied that a turbulent closure is needed, or else the problem will be under-damped. The major reason for this is that the eddies persist at a small grid size so that a closure is needed or else the effect of turbulence is not modeled correctly. One of the major implications of this work is that all previous simulations using standard closure approximations should be reconsidered.

Interfacial Forces needed for Accurate Simulation
The Euler-Euler Two-Fluid approach, the commonly used model for two-phase flow, considers both phases as interpenetrating continua. This approach requires that the forces between the two phases, the liquid and the gases, must be modeled. Many forces are known. The basic questions are which are most important and what formulations are most effective in bubble column simulations. The present work at Washington University shows that at least three forces are important. The drag force is the predominant force while the virtual mass force and the lift force are needed to obtain accurate simulations. Iowa State has also studied the importance of the virtual mass force and lift, rotational forces. In recent work at Iowa State, a formulation just developed at Los Alamos using attraction and repulsion forces has been shown to give better agreement between simulated and measured results. This new formulation captures many of the features of the three forces used previously so that it may be a more generalized form of an interfacial force law. Additional work is needed in this area so that more accurate simulations may be obtained.

In summary, significant progress has been made in CFD modeling during this program. Formulations that allow reasonable simulations of bubble columns have been devised. However major issues still need to be resolved before a fully predictive model will be available. This work offers the best promise of understanding new situations so that CFD should be high on the list of ongoing projects.

Subtask 3.3: Sparger/Entrance Region Modeling
The experimental studies on the effect of the sparger have been covered in the discussions of Subtask 3.1. Spargers have some effect on this region, but not as large as initially thought. The downward flow reverses direction in this region, and turbulence is high so that the effect of the sparger is mitigated. This area of the SBCR represents a region of growing importance as the column diameter increases while the column height is limited by practical considerations of economics and shipping. While the sparger effect is minimal on the column as a whole for long columns currently in use, the sparger studies show that a region of developing flow exists. The volume of this region, and therefore the amount of reaction in this region, will take on more importance as the aspect

ratio of bubble columns changes. Of course, CFD studies will be the main tool for studying flow in this region. Until such time as CFD solutions are perfected, it may be premature to attempt detailed studies of this region. Thus, little work on this region has been done per se.

Task 4: SBCR Experimental Program
This task's purpose was to characterize the SBCR reaction system at the LaPorte AFDU facility. This work has two aspects: gathering experimental data and modeling. It forms a useful adjunct to Task 3, since it allows testing of the engineering models described in the previous section. The ability of a model to predict, without fitting parameters, the observed dynamics of the system in response to injection of an inert (or linearly decaying) liquid or gas tracer is a stringent test of the model. This ability to test models in conjunction with their development was one of the real strengths of this program.

Radioactive tracer testing was done during all AFFDU runs (except for runs that were stopped before the scheduled end of the run). For all the runs, both gas and "liquid" phases were measured. In the latter runs, catalyst particles were also used as tracers. The general physical results show that liquid mixing is rapid; complete mixing is obtained in less than 90 sec. The gas phase shows some degree of mixing as the pulse passes up the column. Peclet number is on the order of one. Tests on the alumina catalyst in the DME run indicated that this material is uniformly dispersed in the reactor. Similar good dispersion was found for the other catalyst particles in the reactor. The differences in the responses from the catalyst and fine powdered Mn_2O_3 tracer injections were minimal, indicating the validity of the pseudo-homogeneous assumption for the liquid (FT-wax) plus the solid (catalyst) phases.

Knowledge of the radial gas distribution profile is needed for the new models. A measurement of these profiles would be useful in verifying the model's utility. Gamma scans were performed during the demonstration runs of the slurry phase Fischer-Tropsch technology at the Alternate Fuels Development Unit (AFDU), LaPorte, Texas, to evaluate the technique as a future non-invasive diagnostic for measurement of cross-sectional gas holdup distribution. Uncertainties in the estimation of chordal averaged gas holdup from the gamma scans data are large and significant, making the estimates unsuitable for any quantitative use in reactor models. The sources of error include inaccuracies in source-detector positioning and repositioning, use of mockup fluids and calculated absorptivity corrections, and movement of internals. Therefore, incorporation of the holdup profile information from these scans in the liquid and gas phase mixing models for prediction of tracer responses cannot be reliably accomplished. A test protocol and procedure have been proposed to improve these measurements.

Task 5: Slurry Behavior
Notwithstanding the difficulty of understanding the fluid dynamics of a SBCR, slurry behavior, especially for slurries of high concentration, is the least understood part of this project. We undertook a preliminary study of the effect of slurry characteristics on the hydrodynamics of the SCBR. Considerably more work is needed.

Our preliminary study on the factors affecting the behavior of a catalyst particle in a slurry system was aimed at relating the physical properties of a powdered catalyst to its performance in a slurry phase bubble column. One goal was to be able to screen a commercial catalyst for its use in slurry solely based on its physical properties. Among the properties that have been shown relevant are viscosity, void volume, surface property, and particle size distribution. The methods for characterizing these properties have been established and used for assessing commercial methanol catalysts. Although these methodologies and results are preliminary and incomplete, they form a framework for future studies.

The causes of adhesion of catalyst powders to reactor internals were also studied. This work has importance since adhesion is the cause for greater catalyst aging rates in lab reactors, compared to plant reactors, and could potentially lead to fouling inside plant reactors. The preliminary results showed that the static charge on the surface of catalyst powders might be responsible for the adhesion.

Task 6: Data Processing
One of the major results of this program is the new reactor models that have arisen from the studies. Development of these models involved the understanding of bubble column flow as well as testing by using the tracer data from the AFDU. All of the knowledge is combined to test reactor models. The results of this testing are summarized below:

- The standard model, the ADM axial dispersion model, can be fitted to the tracer responses observed by the detectors positioned at various levels for the methanol run. However, the model still seems inadequate in properly describing liquid mixing in bubble columns. A consistent value of an axial dispersion coefficient that fits all the data cannot be found for liquid mixing. Fitting the data for various detectors produces a large scatter in liquid axial dispersion coefficients, and the range of values dramatically increases when responses at the lower level of the column are included.
- The two-dimensional convection-diffusion model, together with the scaleup strategy for evaluating the model parameters in the AFDU slurry bubble column reactor during methanol synthesis, results in good predictions of the characteristic mixing times as measured by the radiation detectors at various axial locations. This indirectly substantiates the proposed methodology of using the gas holdup in churn-turbulent flows, at sufficiently high gas velocities, for characterizing the systems of interest.
- The single bubble-class gas-liquid recirculation model was used to simulate the gas tracer responses acquired during the FT-IV and DME runs in the AFDU. The model is able to predict the characteristic features of the observed experimental responses without any fitting parameters. This is a strong indication of the accuracy of these models.

Thus, this project has resulted in the development of a new set of models that significantly add to understanding of the behavior of bubble columns.

Task 7: Management and Reporting

This report constitutes the required final project report. Detailed reports from each of the universities summarize their accomplishments.

FINAL

ENGINEERING DEVELOPMENT OF SLURRY BUBBLE COLUMN REACTOR (SBCR) TECHNOLOGY

Final Technical Report

Volume 2 of 2

Contractor
AIR PRODUCTS AND CHEMICALS, INC.
7201 Hamilton Blvd.
Allentown, PA 18195-1501

Bernard A. Toseland, Ph.D.
Program Manager and Principal Investigator

Robert M. Kornosky
Contracting Officer's Representative

Prepared for the United States Department of Energy
Under Cooperative Agreement No. DE-FC22-95PC95051
Project Period 3 April 1995 – 30 September 2002

FLUID AND BUBBLE DYNAMICS OF SLURRY BUBBLE COLUMNS AT HIGH PRESSURES AND HIGH TEMPERATURES

Contract No. DE-FC-22-95 PC 95051

Final Report (Reporting Period: 1996 – 2001)

From

Dr. Liang-Shih Fan
Distinguished University Professor and Chair
Department of Chemical Engineering
The Ohio State University
140 West 19th Ave.
Columbus, OH 43210

Submitted to

Table of Contents

Executive Summary

Gas-liquid bubble columns and three-phase fluidization systems are widely used in industry, particularly chemical and petrochemical industries. Three-phase fluidization describes a gas-liquid-solid flow system in which particles are in motion induced by gas and/or liquid phases. High pressure operations are common in industrial applications of slurry bubble columns for reactions, such as resid hydrotreating, Fischer-Tropsch synthesis and methanol synthesis. The design and scale-up of slurry bubble column reactors require knowledge of the hydrodynamics and heat transfer characteristics. Studies reported in the literature for such characteristics have been limited to ambient conditions. Little has been reported for high-pressure conditions.

The studies conducted under this program examine the effects of pressures and temperatures on some areas pertaining to fundamental hydrodynamics in slurry bubble columns. These area include single bubble formation in liquid-solid suspensions, gas holdup and maximum bubble size, pressure effect on the flow fields and Reynolds stresses, axial liquid mixing, and heat transfer behavior.

The specific findings in this study for each of these areas are summarized below:

Bubble formation from a single nozzle is investigated analytically and experimentally in non-aqueous liquid and liquid-solid suspensions at pressures up to 17.3 MPa. A mechanistic model is proposed to predict the initial bubble size in liquid-solid suspensions, by taking into account the various forces affecting the bubble growth including those induced by the presence of the particles, such as the suspension inertial force and the particle–bubble collision force. It is found that the initial bubble size in the suspensions is generally larger than that in the liquid mainly due to the inertia effect of the suspension. The initial bubble size increases with the solids holdup. The pressure has an insignificant effect on the initial bubble size in both the liquid and liquid-solid suspensions under the conditions of this study. The model can reasonably predict the initial bubble sizes obtained in this study and those reported in the literature.

Experiments are conducted to investigate the effects of pressure on gas holdup and bubble size in slurry bubble columns at pressures up to 5.6 MPa and at gas velocities up to 45 cm/s. The results indicate that the gas holdup increases with an increase in pressure, especially at high slurry concentration. At ambient pressure, a higher solids concentration leads to a significantly lower gas holdup over the entire gas velocity range, while at a pressure of 5.6 MPa, the effect of solids concentration on gas holdup is relatively small at gas velocities above 25 cm/s. An empirical correlation is developed based on the present data and those in the literature to predict gas holdup in bubble columns and slurry bubble columns over a wide range of operating conditions. An analysis of the flow characteristics of the bubbles during dynamic gas disengagement indicates that large bubbles play a key role in determining gas holdup due to the large bubble volume and large wake volume, which induce the acceleration of small bubbles. Direct measurement of bubble size reveals that elevated pressures lead to smaller bubble size and narrower bubble size distributions. It is also shown that bubble size increases significantly with increasing solids concentration at ambient pressure, while at high pressures this effect is less pronounced. A theoretical analysis of circulation of gas inside the bubble yields an analytical expression for maximum stable bubble size in high pressure slurry bubble columns. Based on this internal circulation model, the maximum stable bubble size at high pressures is significantly smaller due to the high gas inertia and low gas-liquid surface tension. The smaller bubble size as well as its reduced bubble rise velocity account for the observed effect of pressure on gas holdup.

The hydrodynamics of bubble columns operated at pressures up to 7.0 MPa are investigated using a laser Doppler velocimetry system. Laser Doppler velocimetry is a non-invasive optical technique, which is used to conduct *in situ* measurements of velocity, with high spatial resolution, fast dynamic response and the ability to detect flow. The axial and radial velocities and the Reynolds shear and normal stresses are analyzed and discussed in relation to large-scale structures present in the flow. This study demonstrates the significance of the pressure effect on the flow field in bubble column systems.

Axial dispersion coefficients of the liquid phase in bubble columns at high pressure are investigated using the thermal dispersion technique. Water and hydrocarbon liquids are used as the liquid phase. The system pressure varies up to 10.3 MPa and the superficial gas velocity varies up to 0.4 cm/s, which covers both the homogeneous bubbling and churn-turbulent flow regimes. Experimental results show that flow regime, system pressure, liquid properties, liquid-phase motion and column size are the main factors affecting liquid mixing. The axial dispersion coefficient of the liquid phase increases with an increase in gas velocity, and decreases with increasing pressure. The effects of gas velocity and pressure on liquid mixing can be explained based on the combined mechanism of global liquid internal circulation and local turbulent fluctuations. The axial liquid dispersion coefficient also increases with increasing liquid velocity due to enhanced liquid-phase turbulence. The scale-up effect on liquid mixing reduces as the pressure increases.

The heat transfer behavior between an immersed heating surface and the surrounding gas-liquid-solid medium in a slurry bubble column is studied experimentally and analytically. The operating pressures and temperatures vary up to 4.2 MPa and 81°C, respectively. Nitrogen, Paratherm NF heat transfer fluid and 53 μm glass beads are used as the gas, liquid and solid phases, respectively. The solids concentrations are varied up to 35 vol.%, while the superficial gas velocities are varied up to 20 cm/s. The effects of gas velocity, solids concentration, pressure and temperature on the heat transfer coefficient are examined. It is found that pressure has a significant effect on heat transfer characteristics. The heat transfer coefficient in a slurry bubble column decreases appreciably with an increase in pressure. It is noted that the variation in heat transfer coefficient with pressure is attributed to the counteracting effects of the increased liquid viscosity, decreased bubble size, and increased gas holdup or frequency of bubble passage over the heating surface as the pressure increases. The addition of particles to the liquid phase enhances heat transfer substantially. The effect of temperature on the heat transfer behavior is mainly determined by the change in liquid viscosity. An empirical correlation is proposed to predict the heat transfer coefficient in a slurry bubble column under high-pressure conditions. A consecutive film and surface renewal model is used to analyze the heat transfer results. Based on the model analysis, it is found that the major heat transfer resistance in high-pressure slurry bubble columns is within a fluid film surrounding the heating surface.

The future research needs in the areas of the heat transfer involving internals and gas-liquid mass transfer at high pressure and high temperature conditions in slurry bubble columns are notably indicated.

Chapter 1: Single Bubble Formation in Liquid-Solid Suspensions

Introduction

Studies in the literature have indicated significant effects of pressure on the hydrodynamics and transport phenomena in bubble columns (Idogowa et al., 1986; Wilkinson, 1991), slurry bubble columns (Tarmy et al., 1984), and three-phase fluidized beds (Jiang et al., 1992; Luo et al., 1997a). Elevated pressures lead to an increased gas holdup in these systems, and this phenomenon has been mainly attributed to the small bubble size at high pressures (Luo et al., 1997b). The bubble size in multiphase fluidization systems is dictated by three processes: initial bubble formation, bubble coalescence, and bubble breakup. The increased gas momentum in the bubble-formation process has been suggested as one factor behind the bubble size reduction at high pressures, especially at low gas velocities. To fully understand the high pressure fluidization phenomena, it is necessary to quantify the initial bubble formation in both liquid and liquid-solid media under high pressure conditions.

Numerous experimental and modeling studies have been conducted over the past decades on the bubble formation from a single orifice or nozzle submerged in liquids, mostly under ambient conditions (e.g., Kumar and Kuloor, 1970; Azbel, 1981). Various models were established to predict the initial bubble size from a single nozzle in liquids, as summarized by Azbel (1981). Only a few studies were conducted at elevated pressures (LaNauze and Harris, 1974; Idogawa et al., 1987; Tsuge et al., 1992; Wilkinson and Van Dierendonck, 1994). The high pressure studies indicate that an increase in gas density reduces the size of bubbles formed from single orifices. However, these results were limited to water systems only. The pressure effect on the initial bubble size in hydrocarbon liquids systems are not understood. Furthermore, it is known that the volume of the gas chamber connected to the nozzle is an important factor in determining the initial bubble size (Tadaki and Maeda, 1963). When the volume of the gas chamber is large, the bubble formation process is considered to be under constant pressure conditions. Conversely, when the volume of the gas chamber is very small, the bubble formation can be considered to be under constant flow conditions. When the gas chamber volume is between these two extremes, the bubble formation is considered to be under an intermediate condition. Most of the results at the elevated pressures mentioned above were obtained in systems with finite gas chamber volumes (constant pressure or intermediate conditions). Clearly, the effect of pressure on initial bubble size may vary significantly with the bubble formation process dictated by the three conditions (Wilkinson and Van Dierendonck, 1994).

Although the initial bubble formation in liquids has been studied extensively, studies of the initial bubble formation in liquids with the presence of solid particles, as in slurry bubble column and three-phase fluidized bed systems, are very limited. The experimental data of Massimilla et al. (1961) in an air-water-glass bead three-phase fluidized bed revealed that the bubbles from a single nozzle in the fluidized bed are larger in size than those in water and the initial bubble size increases with the solids concentration. Yoo et al. (1997) recently investigated the initial bubble formation in pressurized liquid-solid suspensions. They used 18.6% (wt.) glycerol aqueous solution and 0.1 mm polystyrene beads as the liquid and solid phases, respectively. The densities of the liquid and the particles are identical and thus the particles are neutrally buoyant in the liquid. The results of this study indicated that the initial bubble size decreases inversely with pressure under otherwise constant conditions, i.e., gas flow rate, temperature, solids concentration, orifice diameter, and gas chamber volume. Their results also

indicated that the particle effect on initial bubble size is insignificant. The difference in the finding regarding the particle effects on initial bubble size between Massimilla et al. (1961) and Yoo et al. (1997) may possibly be due to the difference in particle density. To clarify the particle effect on initial bubble size, further work is clearly needed.

The objective of this study is to investigate the particle effect and the effect of pressure on initial bubble size from a single nozzle in non-aqueous liquid and liquid-solid suspensions under constant flow conditions. The liquid used in this study is a hydrocarbon-based heat transfer fluid and the particles used are glass beads. A mathematical model is developed to predict initial bubble size in the liquid-solid suspension. The mechanisms underlining the particle and pressure effects are discussed in light of the model.

Mathematical Model

Two types of models have been developed for bubble formation, namely, the spherical bubble formation model, including the one-stage model (Davidson and Schuler, 1961) and the two-stage model (Ramakrishnan et al., 1969), and the non-spherical bubble formation model (Pinczewski, 1981; Tan and Harris, 1986; Tsuge et al., 1992). The two-stage spherical bubble formation model assumes that the bubbles are spherical in shape and the bubble detaches from the orifice when the distance between the bubble and the nozzle reaches a certain value. The non-spherical bubble formation model calculates the shape of the bubble based on the local force balance. For simplicity, in this work the two-stage spherical bubble formation model is adopted to quantify the initial bubble size in high pressure liquid-solid suspensions.

In the two-stage spherical bubble formation model, bubbles are assumed to be formed in two stages, namely, the expansion stage and the detachment stage, as shown in Fig. 1-1 (Ramakrishnan et al., 1969). The bubble expands with its base attached to the nozzle during the first stage. In the detachment stage, the bubble base moves away from the nozzle, although the bubble remains connected with the nozzle through a neck. The shape of the bubble is assumed to remain spherical in the entire bubble formation process. It is also assumed in this model that a liquid film always exists around the bubble. During the expansion and detachment stages, particles collide with the bubble and stay on the liquid film. The particles and the liquid surrounding the bubble are set in motion as the bubble grows and rises.

The volume of the bubble at the end of the first stage and during the second stage can be described by considering a balance of all the forces acting on the bubble being formed (Fig. 1-2). The forces induced by the liquid include the upward forces [effective buoyancy (F_B) and gas momentum (F_M) forces], and the downward resistance [liquid drag (F_D), surface tension force (F_σ), bubble inertial force ($F_{I,g}$), and Basset force (F_{Basset})]. It is assumed that the particles affect the bubble formation process only through two additional downward forces on the bubble, i.e., the particle-bubble collision force (F_C) and the suspension inertial force ($F_{I,m}$) due to the acceleration of the liquid and particles surrounding the bubble. Therefore, the overall force balance on the bubble can be written as

$$F_B + F_M = F_D + F_\sigma + F_{Basset} + F_{I,g} + F_C + F_{I,m}. \qquad (1-1)$$

The expansion stage and the detachment stage follow the same force balance equation, Eq. (1-1), although the expression for the same force in the two stages may be different.

Expansion Stage

The effective buoyancy force (F_B) on the bubble can be expressed as

$$F_B = V_B(\rho_l - \rho_g)g = \frac{\pi}{6}d_b^3(\rho_l - \rho_g)g \,. \tag{1-2}$$

The gas momentum force is

$$F_M = \frac{\pi}{4}D_0^2\rho_g u_0^2 \,. \tag{1-3}$$

The surface tension force (F_σ) can be written as

$$F_\sigma = \pi D_0 \sigma \cos\gamma \tag{1-4}$$

where the measured contact angle, γ, is 52° for the present system. The liquid drag force (F_D) can be expressed in terms of drag coefficient:

$$F_D = \frac{1}{2}C_D\rho_l\frac{\pi}{4}d_b^2 u_b^2 \qquad (C_D = 24/\text{Re}) \tag{1-5}$$

where the Reynolds number, Re, is based on bubble size and the viscosity and density of the liquid. In the expansion stage, the rise velocity of the bubble center, u_b, is equal to the bubble expansion velocity, u_e, while the bubble base is attached to the nozzle:

$$u_e = \frac{dr_b}{dt} = \frac{d}{dt}\left(\frac{3V_b}{4\pi}\right)^{1/3} = \frac{1}{3}\left(\frac{3}{4\pi}\right)^{1/3}V_b^{-2/3}\frac{dV_b}{dt} = \frac{u_0}{4}\left(\frac{D_0}{d_b}\right)^2 \tag{1-6}$$

where the bubble volume, V_b, is simply the product of the volumetric gas flow rate, Q, and the time, t:

$$V_b = Qt = \frac{\pi}{4}D_0^2 u_0 t \,. \tag{1-7}$$

The bubble inertial force ($F_{I,g}$) is due to the acceleration of the bubble and can be related to the mass and the acceleration of the bubble by

$$F_{I,g} = \frac{d(u_b V_b \rho_g)}{dt} = \rho_g V_b\frac{du_b}{dt} + \rho_g u_b\frac{dV_b}{dt} \,. \tag{1-8}$$

Thus, the bubble inertial force can be related to Q and V_b by substituting Eqs. (1-6) and (1-7) into Eq. (1-8) as

$$F_{I,g} = \frac{\rho_g Q^2 V_b^{-2/3}}{12\pi(3/4\pi)^{2/3}} \,. \tag{1-9}$$

The history of the bubble acceleration gives rise to a further resistance to the bubble motion (Fan and Zhu, 1998), that is, the Basset force (F_{Basset}). However, the bubble acceleration is negligible in the expansion stage and thus the Basset force in this stage can be neglected.

The particle-bubble collision force can be accounted for by considering the rate of particle momentum change before and after the collision. The expression of the collision force for the expansion stage is different from that for the detachment stage because of the different characteristics of the bubble motion in these two stages. In the expansion stage, the vertical velocity of the bubble is negligible compared to the radial expansion velocity of the bubble surface; while in the detachment stage, the bubble vertical velocity is dominant. From Fig. 1-3, the particle-bubble collision force in the vertical direction can be derived as

$$F_C = \int_0^{r_0} dr \int_0^{2\pi}\rho_p(1+e)\varepsilon_s u_e^2 r\,d\phi = \frac{\pi}{4}D_0^2\rho_p(1+e)\varepsilon_s u_e^2 \,. \tag{1-10}$$

In deriving Eq. (1-10), note that only the collision on the bubble surface directly above the nozzle opening appears in the integral since the collision force on the rest of the bubble surface cancels out.

The resistance that remains to be accounted for is the inertial force induced by the acceleration of the surrounding particles and liquid. Assume that the slip velocity between the liquid and the solid particles is small and that the liquid and solid inertial force can be approximated by the suspension inertial force, $F_{I,m}$, which is essentially the rate of momentum change of the liquid and particles with respect to time, based on Newton's second law:

$$F_{I,m} = \frac{d[\iiint(\varepsilon_s\rho_s u_s + \varepsilon_l\rho_l u_l)\delta V]}{dt} \approx \frac{d(\iiint\rho_m u_m \delta V)}{dt} \tag{1-11}$$

where the apparent density of the suspension is defined as

$$\rho_m = \varepsilon_s\rho_s + \varepsilon_l\rho_l. \tag{1-12a}$$

and the suspension velocity is

$$u_m \approx u_l \approx u_s \tag{1-12b}$$

The evaluation of the suspension inertial force requires knowledge of the flow field around the bubble. A simplified form for the suspension inertial force used for the model calculation is given in the Results and Discussion section.

Substituting Eqs. (1-2), (1-3), (1-4), (1-5), (1-9), (1-10), and (1-11) into Eq. (1-1) results in the force balance equation. The resulting algebraic equation can be expressed explicitly in terms of bubble volume and can be solved to obtain the bubble volume at the end of the expansion stage, V_E, or the radius of the bubble at the end of the expansion stage, r_E.

Detachment Stage

In the detachment stage, the rise velocity of the bubble center is the sum of the expansion velocity, u_e, and the bubble base rise velocity, u,

$$u_b = u_e + u. \tag{1-13}$$

As a result of the additional motion of the bubble base, the bubble inertial force and particle-bubble collision force in the detachment stage are more complicated than those in the expansion stage. The bubble volume is also different from that in the expansion stage:

$$V_b = V_E + Qt_2 \tag{1-14}$$

where t_2 is the time elapsed in the second stage.

The bubble inertial force can be expressed in terms of the bubble volume and the volumetric gas flow-rate, by substituting Eqs. (1-6) and (1-14) into Eq. (1-8):

$$F_{I,g} = \rho_g V_b \frac{du}{dt} + \rho_g Qu + \frac{\rho_g Q^2 V_b^{-2/3}}{12\pi(3/4\pi)^{2/3}}. \tag{1-15}$$

Figure 1-4 shows the collision between the bubble and the particle in the detachment stage. Since the bubble motion is dominated by its vertical movement in the detachment stage, the expression derived by Jean and Fan (1990) for evaluating the particle-bubble collision force during the bubble rise can be used to account for that during the detachment stage in the bubble formation process:

$$F_C = \frac{\pi}{2}r_b^2\varepsilon_s\rho_s u^2\eta\frac{H}{\sin^2\beta}, \tag{1-16}$$

where

7

$$H = \frac{1+\sin\beta}{\pi/2\beta+1} + \frac{\sin 3\beta-1}{\pi/2\beta-3} + e\left(\frac{1+\sin 3\beta}{\pi/2\beta+3} + \frac{\sin\beta-1}{\pi/2\beta-1}\right), \tag{1-17}$$

and β is the maximum collision angle, defined as

$$\beta = \frac{1}{2}\left(\frac{\pi}{2} + \sin^{-1}\sqrt{\eta}\right). \tag{1-18}$$

Consider the restitution coefficient, e, to be zero, i.e., the particles stay on the bubble surface after the collision. Also, the collection coefficient, η, is assumed to be unity. Equation (1-16) can then be simplified to

$$F_C = \pi r_b^2 \varepsilon_s \rho_s u^2. \tag{1-19}$$

As the bubble acceleration becomes significant, the Basset force needs to be taken into account:

$$F_{Basset} = \frac{3}{2}d_b^2\sqrt{\pi\rho_l\mu_l}\int_0^t \frac{du/dt}{\sqrt{t-\tau}}d\tau. \tag{1-20}$$

Equation (1-20) can be simplified by assuming a constant acceleration:

$$F_{Basset} = 3d_b^2\sqrt{\pi\rho_l\mu_l}\,\frac{du}{dt}\sqrt{t} \approx 3d_b^2\sqrt{\pi\rho_l\mu_l}\,\frac{du}{dt}\sqrt{t}. \tag{1-21}$$

This assumption is justified by the results of the calculation of bubble acceleration based on the model.

The governing equation for the detachment stage can be obtained by substituting Eqs. (1-2), (1-3), (1-4), (1-5), (1-11) (more specifically (1-26)), (1-15), (1-19), and (1-21) into Eq. (1-1). The resulting equation is a second-order ordinary differential equation. The initial condition of this differential equation is $u = 0$ at $t = 0$. In solving the governing equation, a criterion for the bubble detachment is used, i.e., the bubble detaches from the nozzle when the distance between the bubble base and the nozzle tip is equal to r_E.

The governing equation can be solved to obtain the relationship between u and t. The distance between the bubble base and the nozzle tip, i.e., the neck length, can be obtained by

$$x = \int_{t_2=0}^{t_2} u dt_2. \tag{1-22}$$

When the neck length reaches r_E, the calculation is terminated. The bubble volume at this instant represents the final volume of the bubble.

Experimental
Initial Bubble Formation

The high pressure three-phase fluidized bed used in this work for measuring the initial bubble size in high pressure liquid-solid suspensions is shown in Fig. 1-5. The fluidized bed is a stainless steel column (1,372 mm in height and 101.6 mm I.D.) and can be operated at pressures up to 21 MPa and temperatures up to 180ºC. Three pairs of quartz windows are installed on the front and rear sides of the column. Each window is 12.7 mm wide and 93 mm long. A liquid-solid suspension is generated by fluidizing a fixed amount of particles with a uniform liquid flow. The liquid enters the column through a perforated plate distributor with 120 square-pitched holes of 1.0 mm diameter. The height of the suspension is maintained at 150 mm from the distributor and the solids concentration is determined from the particle weight. A high-speed

video camera (240 frames/s) is used to capture the images of bubbles emerging from the bed surface. The bubble size and frequency are obtained via the image analysis. Nitrogen is injected into the liquid-solid medium through a stainless steel tubing of 3.175 mm O.D. and 1.585 mm I.D. The distance between the orifice and the distributor is 70 mm. The flow rate of nitrogen is controlled by adjusting a metering valve, across which the pressure drop is kept at 3.44 MPa to maintain a constant flow during the bubble formation process. In this study, the liquid phase is Paratherm NF heat transfer fluid (viscosity = 0.028 Pa·s, surface tension = 0.029 N/m, and density = 869 kg/m^3 at 26.5^{o}C and 0.1 MPa). The particles used in this study are glass beads of 210 μm in diameter and 2450 kg/m^3 in density. The physical properties of the gas and liquid phases vary with pressure. To fully understand the pressure effect on the initial bubble size, the variations of these properties should be taken into account. Table 1-1 shows the physical properties of the gas and liquid at various pressures.

PIV Experimental Setup

To evaluate the inertial force of the liquid-solid suspension based on Eq. (1-11), the flow field of the liquid-solid suspension around a growing bubble from an injector must be known. The flow field is measured in a 2-dimensional (2-D) liquid-solid suspension with a high-speed particle image velocimetry (PIV) technique. Figure 1-6 shows the experimental apparatus. The 2-D fluidized bed is made of Plexiglas, and the viewing section of the column is 30 cm in width, 130 cm in height and 0.6 cm in depth. Below the viewing section is the liquid distributor, which consists of a packed particle section and a liquid calming section. Compressed air and glycerin solution are used as the gas and liquid phases. The gas is injected by a tube flush mounted on the column wall. The gas injector opening is 1.6 mm ID. A manual solenoid valve, creating single bubbles of various sizes, regulates the gas flow through the injector.

Activated carbon particles with a size range from 500 to 800 μm are used as the solid phase. Approximately 2% of the particles are colored white, which are utilized as the tracers. The CCD image recorded by the high-speed camera features 765 pixels across by 246 lines. The framing rate of the camera can be selected up to 480 fields/sec. A frame grabber, which is equipped with 40 MHz max pixel clock to support the high-framing rate, simultaneously digitizes the CCD image from the camera. Further, the high-speed camera is connected to the high-speed video recorder to store the images for further studies. The PIV technique used here utilizes a particle-tracking algorithm developed by Chen and Fan (1992) to determine the velocity fields of the particles. The particle-tracking algorithm involves with matching of the particles in three or more consecutive fields. The PIV system provides data on the full-field velocities of the tracer particles.

Results and Discussion
Suspension Inertial Force

Acceleration of the liquid-solid mixture associated with the bubble induces significant resistance to the motion of the bubble. The suspension inertial force can be evaluated by considering the flow field of the mixture around the bubble as described by Eq. (1-11). Figure 1-7 shows the particle velocity field obtained from the PIV analysis. Since the particle terminal velocity in the liquid is small, the particle velocity can be used to approximate the flow field of the liquid-solid suspension. It can be seen from Fig. 1-7 that the particles on the bubble surface

9

have the same velocity as the bubble. As the distance of the particle from the bubble surface increases, the particle velocity decreases. The particle velocity field shown in the figure can be approximated by

$$u_m = u_b \, \exp\left[k\left(\frac{r}{r_b} - 1 \right) \right]$$

(1-23)

where $k = -0.64$. For a 2-dimensional flow field, the suspension inertial force is evaluated by

$$F_{I,m} = \frac{\mathrm{d} \iint \rho_m u_m \delta A}{\mathrm{d}t}.$$

(1-24)

Integration of Eq. (1-24) from r_0 to R where $u_m = 0.01 u_b$ gives

$$F_{I,m} = \frac{\mathrm{d}\left(\iint \rho_m u_m \delta A \right)}{\mathrm{d}t} = \frac{\mathrm{d}}{\mathrm{d}t} \int_0^\pi \mathrm{d}\theta \int_{r_b}^R \rho_m u_b \, \exp\left[k\left(\frac{r}{r_b} - 1 \right) \right] r \, \mathrm{d}r$$

$$= \left\{ \frac{\left(\frac{kr}{r_b} - 1 \right) \exp\left[k\left(\frac{r}{r_b} - 1 \right) \right]}{k^2} \frac{\mathrm{d}}{\mathrm{d}t} \left[\rho_m \left(\pi r_b^2 \right) u_b \right] \right\} \Bigg|_{r_b}^R$$

(1-25)

$$= 3.86 \frac{\mathrm{d}}{\mathrm{d}t} \left[\rho_m \left(\pi r_b^2 \right) u_b \right].$$

Equation (1-25) indicates that the suspension inertial force is equivalent to 3.86 times the change rate of the momentum of the suspension that is displaced by the bubble. Assume that the suspension inertial force from the 2-dimensional measurement can be extended to describe the suspension inertial force under 3-dimensional conditions, i.e.,

$$F_{I,m} = \iiint \rho_m u_m \delta V = 3.86 \frac{\mathrm{d}}{\mathrm{d}t} \left[\rho_m \left(\frac{1}{6} \pi d_b^3 \right) u_b \right].$$

(1-26)

In principle, the coefficient (3.86) in Eq. (1-26) is a function of solids holdup, particle properties, and liquid properties. In this study, the value of 3.86 is used for the coefficient as an approximation in the prediction of the initial bubble size in liquid-solid suspensions. When the solids holdup is zero or the particle density is equal to the liquid density, the coefficient would assume a value of 11/16, the value that characterizes the added mass effects for liquid (Davidson and Shuler, 1961; Ramakrishnan et al., 1969).

Initial Bubble Size and Simulation Results
 Particle Effects. Figure 1-8 shows the particle effect on initial bubble size. Various solids holdups in the suspension are obtained by varying the fluidizing liquid velocity. The fluidizing liquid velocity is so small that it does not affect the bubble formation behavior. At both the ambient and 4.2 MPa pressures, the bubbles formed in the liquid-solid suspension are larger in size than those formed in the liquid for a given u_0. The bubble size increases with an increase in solids holdup. It can be seen from Fig. 1-8 that the model developed in this work can reasonably predict the initial bubble size in the liquid-solid suspensions under various pressure conditions.

The experimental data of Massimilla et al. (1961) showed a similar trend. The above results apparently contradict the conclusions drawn by Yoo et al. (1997) who indicated that particles do not have a significant effect on the initial bubble size in their experimental system. The experimental data under constant flow conditions reported by Yoo et al. (1997) can also be reasonably predicted by the model proposed in this study, as shown in Fig. 1-9. Thus, the effect of particles on the initial bubble size depends on the physical properties of the liquid and solids phases employed.

The initial bubble size is determined based on the balance of various forces acting on the bubble formed at the nozzle, given in Eq. (1-1). In liquids, the upward forces (driving forces) include buoyancy and gas momentum forces, and the downward forces (resistances) include liquid drag, surface tension, gas bubble inertial force, and Basset force. The presence of particles induces two additional downward forces on the bubble: particle-bubble collision force [Eqs. (1-10) or (1-16)] and liquid-solid suspension inertial force [Eq. (1-26)]. Based on these equations, both the collision and suspension inertial forces increase linearly with the solids holdup. Figure 1-10 compares the magnitude of all the forces involved in the bubble formation process. Among the resistances, the suspension inertial force is the dominant force, while the buoyancy force is dominant as a driving force compared to the gas momentum force. With a much smaller inertial force for the liquid compared to the liquid-solid suspension, the bubble center accelerates and moves faster in liquid than in the liquid-solid suspension under the same pressure, temperature, and gas flow-rate conditions; hence, the bubble detaches from the nozzle at an earlier time in the liquid. Therefore, the initial bubble size in the liquid is much smaller than that in the liquid-solid suspension. When the solids holdup increases, the suspension inertial force increases, leading to an increased initial bubble size.

Pressure Effect. The experimental data shown in Fig. 1-11 indicate that the effect of pressure on the initial bubble size is insignificant in the liquid-solid suspension as well as in the liquid under the conditions of this study. Increasing pressure does not significantly change the bubble sizes for a given solids holdup, orifice gas velocity, and temperature. The model's prediction is consistent with the experimental results obtained in this study, as shown in Fig. 1-11. As discussed in the preceding section, the initial bubble size is determined based on the balance among various forces acting on the bubbles. The magnitudes of all the forces are pressure dependent (Fig. 1-12). When the pressure increases, the gas momentum increases significantly. However, the effect of the increase in gas momentum force is counterbalanced by the decrease in the buoyancy force and the increases in the Basset and liquid drag forces. Under the constant flow conditions, the effect of pressure on the overall upward forces and overall downward forces is comparable, leading to an insignificant net effect of pressure on the initial bubble size in liquid-solid suspensions. This mechanism can also explain the negligible pressure effect on bubble formation under constant flow conditions as indicated by the results of Wilkinson and Van Dierendonck (1994) and Yoo et al. (1997).

Concluding Remarks

The bubble formation behavior from a single nozzle is studied analytically and experimentally in the liquid and the liquid-solid suspension. The initial bubble size in the suspension is generally larger than that in the liquid. The initial bubble size in the liquid is determined through the balance of various forces including the buoyancy, gas momentum,

11

bubble inertial, surface tension, liquid viscous, and Basset forces. Additional forces on the bubble in liquid-solid suspensions, induced by bubble-particle collision and liquid-solid suspension inertia, contribute to the larger initial bubble size in the suspension compared to that in the liquid. The effect of pressure on the initial bubble size is found to be under the constant flow conditions, due to the comparable effects of pressure on the overall upward forces and overall downward forces.

Notations

C_D Drag coefficient
D_0 Orifice diameter
d_b Bubble diameter
e Restitution coefficient
F_B Buoyancy force
F_{Basset} Basset force
F_C Particle-bubble collision force
F_D Liquid drag force
$F_{I,g}$ Bubble inertial force
$F_{I,m}$ Suspension inertial force
F_M Gas momentum force
F_σ Surface tension force
Q Volumetric gas flow-rate
Re   Reynolds number, $\rho_l u_b d_b / \mu_l$
r_E Bubble radius at the end of expansion stage
r_b Bubble radius
r_0 Orifice radius
t Time
t_2 Time elapsed in the second stage
u Rise velocity of bubble base
u_b Rise velocity of bubble center
u_e Bubble expansion velocity
u_l Liquid velocity
u_s Particle velocity
u_m Velocity of suspension
u_0 Orifice gas velocity
V_B Bubble volume
V_E Bubble volume at the end of the expansion stage
β Maximum angle of collision between a particle and a bubble in the detachment stage
ε_s Solids holdup
ε_l Liquid holdup
ϕ Azimuthal angle
η Collection coefficient
γ Contact angle
μ_l Liquid viscosity

ρ   Density
ρ_m Density of liquid-solid suspension
σ   Surface tension

Subscript
g   Gas phase
l   Liquid phase
s   Solids phase

References

Azbel, D., *Two-Phase Flows in Chemical Engineering*, Cambridge Univ. Press, Cambridge, UK (1981).

Chen, R. C. and L.-S. Fan, "Particle image velocimetry for characterizing the flow structure in three-dimensional gas-liquid-solid fluidized beds," *Chem. Eng. Sci*., 47, 3615 (1992).

Davidson, J. F. and B. O. G. Schuler, "Bubble formation at an orifice in an inviscid liquid," *Trans. Instn. Chem. Engrs*., 38, 335 (1961).

Fan, L.-S., *Gas-Liquid-Solid Fluidization Engineering*, Butterworths, Stoneham, MA (1989).

Fan, L.-S. and C. Zhu, *Principles of Gas-Solid Flows*, Cambridge University Press, Cambridge, UK (1998).

Idogowa, K., K. Ikeda, T. Fukuda and S. Morooka, "Behavior of bubbles of air-water system in a column under high pressure," *Int. Chem. Eng*., 26, 468 (1986).

Idogawa, K., K. Ikeda, T. Fukuda and S. Morooka, "Formation and flow of gas bubbles in a single orifice or nozzle gas distributor," *Chem. Eng. Comm*., 59, 201 (1987).

Jean, R.-H. and L.-S. Fan, "Rise velocity and gas-liquid mass transfer of a single large bubble in liquids and liquid-solid fluidized beds," *Chem. Eng. Sci.*, 45, 1057 (1990).

Jiang, P., D. Arters and L.-S. Fan, "Pressure effects on the hydrodynamic behavior of gas-liquid-solid fluidized beds," *Ind. Eng. Chem. Res.*, 31, 2322 (1992).

Kumar, R. and N. R. Kuloor, "The formation of bubbles and drops," *Advances in Chemical Engineering*, 8, 255 (1970).

LaNauze, R. D. and I. J. Harris, "Gas bubble formation at elevated system pressures," *Trans. Instn Chem. Engrs.*, 52, 337 (1974).

Luo, X., P. Jiang and L.-S. Fan, "High-pressure three-phase fluidization: hydrodynamics and heat transfer," *AIChE J.*, 43, 2432 (1997a).

Luo, X., J. Zhang, K. Tsuchiya and L.-S. Fan, "On the rise velocity of bubbles in liquid-solid suspensions at elevated pressure and temperature," *Chem. Eng. Sci.*, 52, 3693 (1997b).

Massimilla, L., A. Solimando and E. Squillace, "Gas dispersion in solid-liquid fluidized beds," *Brit. Chem. Eng.*, 6, 232 (1961).

Pinczewski, W. V., "The formation and growth of bubbles at a submerged orifice," *Chem. Eng. Sci.*, 36, 405 (1981).

Ramakrishnan, S., R. Kumar and N. R. Kuloor, "Studies in bubble formation – I: bubble formation under constant flow conditions," *Chem. Eng. Sci.*, 24, 731 (1969).

Tadaki, T. and S. Maeda, "The size of bubbles from a single orifice," *Kagaku Kogaku*, 27, 147 (1963).

Tan, R. B. H. and I. J. Harris, "A model for non-spherical bubble growth at a single orifice," *Chem. Eng. Sci.*, 41, 3175 (1986).

Tarmy, B., M. Chang, C. Coulaloglou and P. Ponzi, "Hydrodynamic characteristics of three phase reactors," *The Chemical Engineer*, October, 18-23 (1984).

Tsuge, H., Y. Nakajima and K. Terasaka, "Behavior of bubbles formed from a submerged orifice under high system pressure," *Chem. Eng. Sci.*, 47, 3273 (1992).

Wilkinson, P. M., "Physical aspects and scale-up of high pressure bubble columns," Ph.D. dissertation, University of Groningen, The Netherlands (1991).

Wilkinson, P. M. and L. Van Dierendonck, "A theoretical model for the influence of gas properties and pressure on single-bubble formation at an orifice," *Chem. Eng. Sci.*, 49, 1429 (1994).

Yoo, D.-H., H. Tsuge, K. Terasaka and K. Mizutani, "Behavior of bubble formation in suspended solution for an elevated pressure system," *Chem. Eng. Sci.*, 52, 3701 (1997).

Table 1-1. Physical Properties of the Gas and Liquid Phases at Various Pressures (T = 30ºC)

	P = 0.1 MPa	P = 2.0 MPa	P = 4.2 MPa	P = 17.3 MPa
Gas Density (kg/m^3)	1.1	22.6	44.7	192.5
Liquid Density (kg/m^3)	868	871	873	892
Liquid Viscosity (Pa•s)	0.023	0.026	0.029	0.039
Surface Tension (N/m)	0.0292	0.0274	0.0262	0.0237
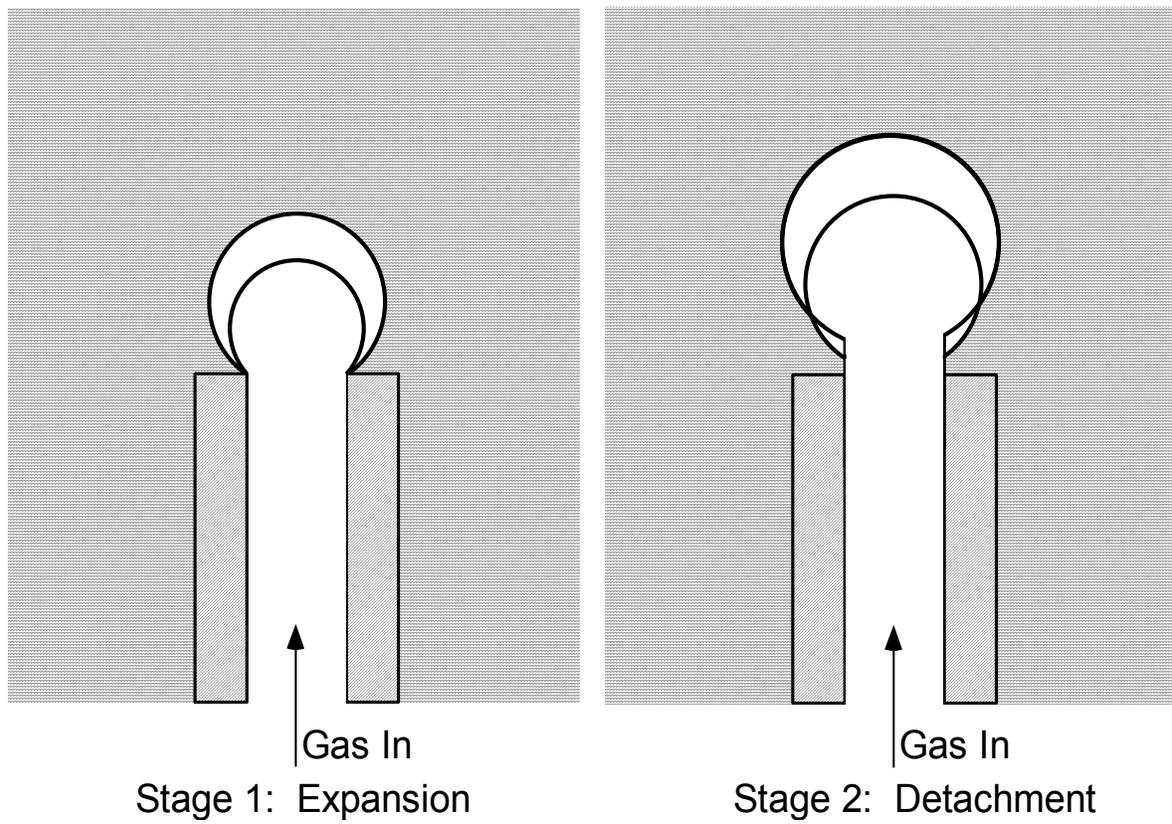
Figure 1-1. The schematic representation of the 2-stage model employed in this study to account for the bubble formation from a single nozzle in a liquid-solid suspension (Ramakrishnan et al., 1969).
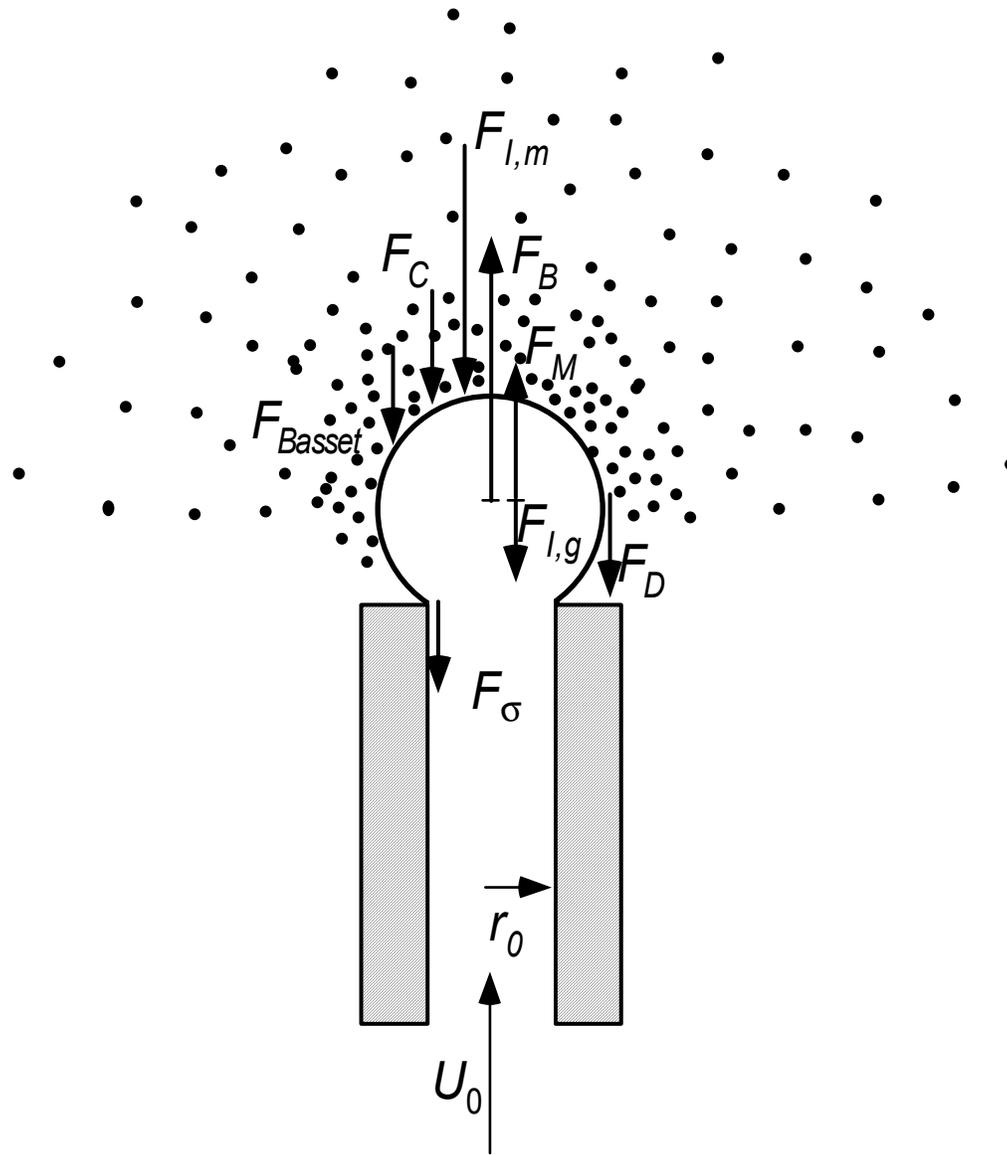
Figure 1-2. The balance of all the forces acting on a growing bubble.
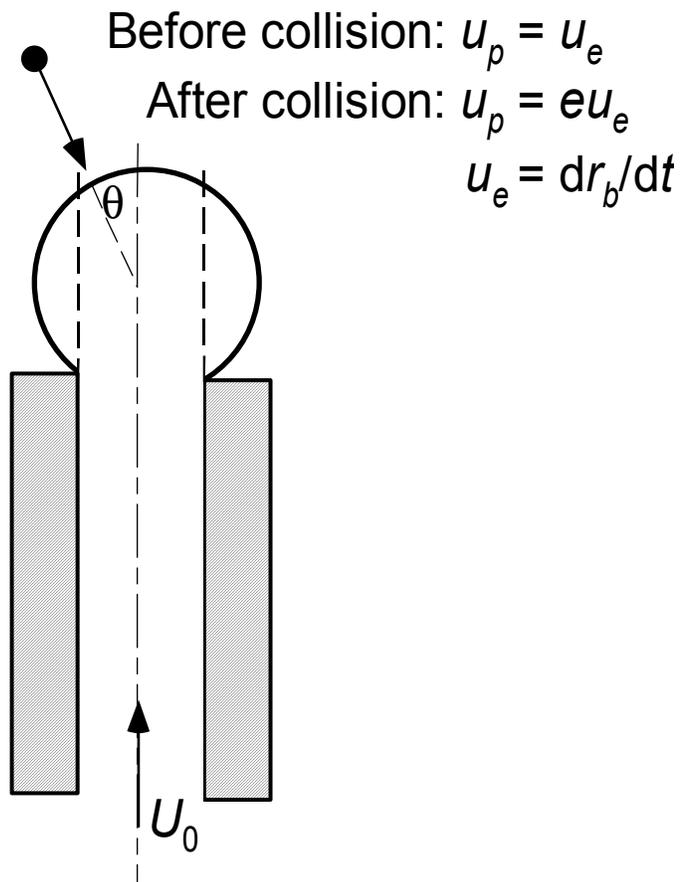
Figure 1-3. Particle-bubble collision force in the expansion stage.
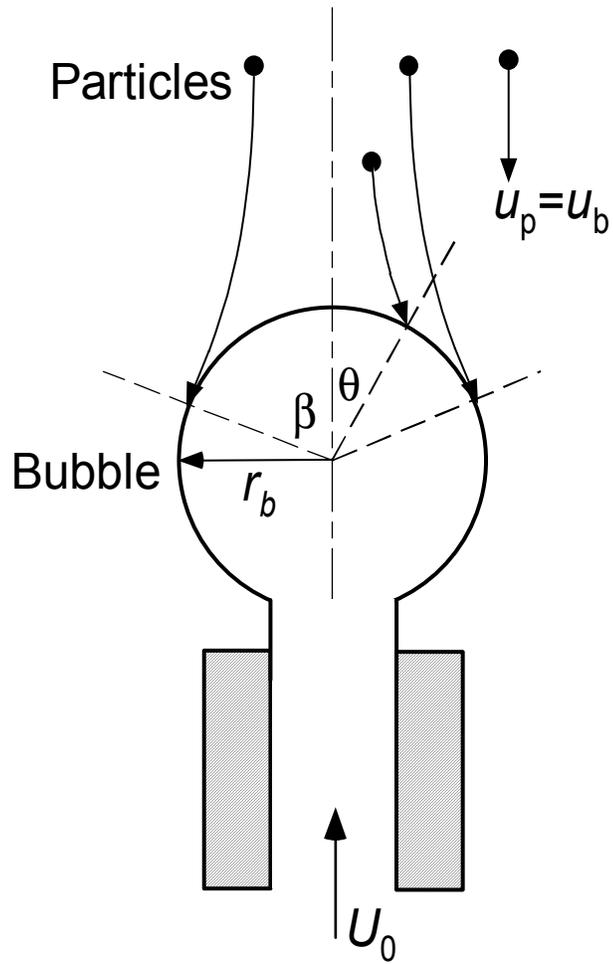
Figure 1-4. Particle-bubble collision force in the detachment stage.
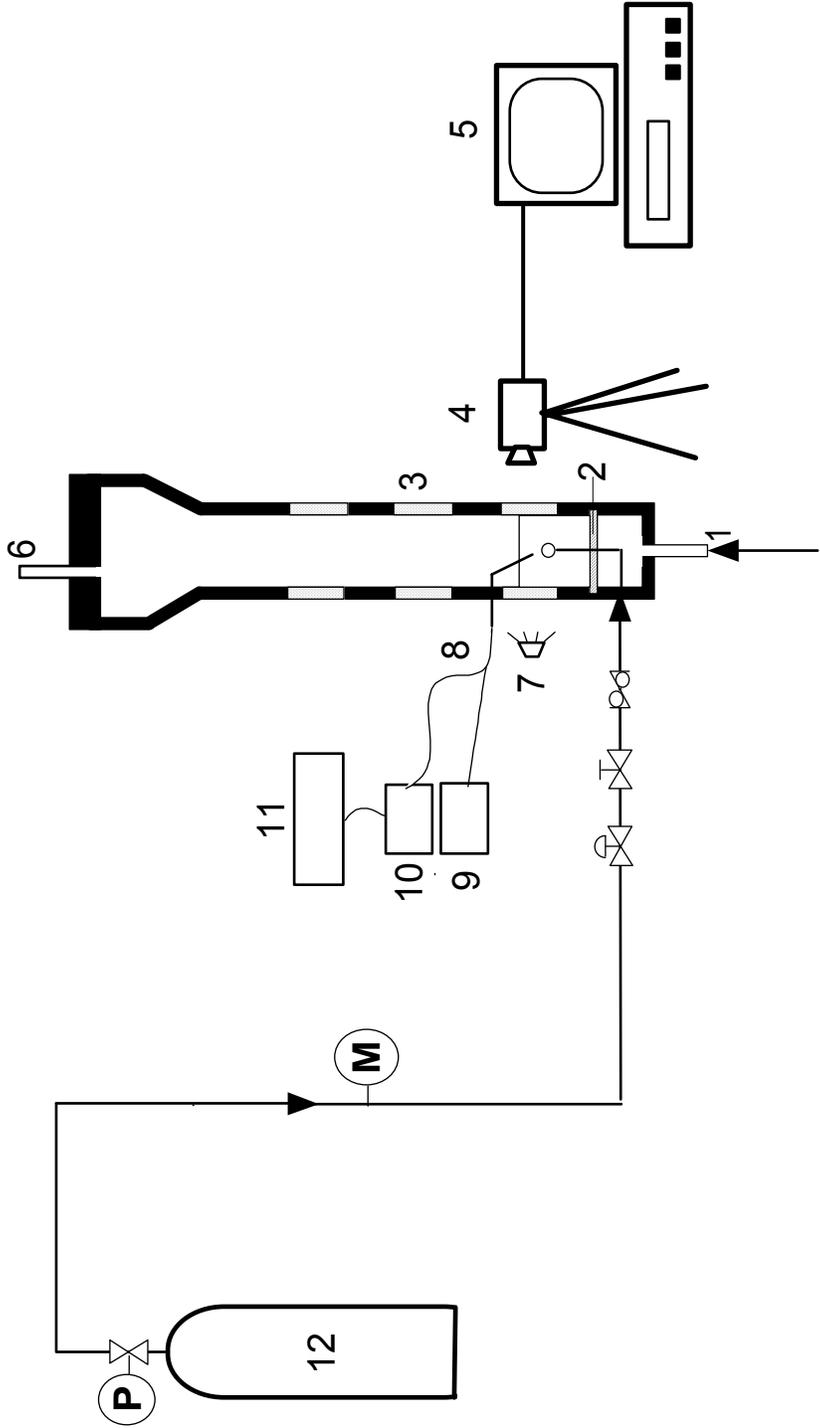
Figure 1-5. Experimental setup for the measurement of initial bubble size in high pressure liquid-solid suspensions (1. Liquid inlet; 2. Perforated plate distributor; 3. Quartz windows; 4. High-speed video camera; 5. Monitor and high-speed VCR; 6. Gas and liquid outlet; 7. Lighting; 8. Optical fiber probe; 9. Light source; 10. Photomultiplier; 11. Data acquisition system; 12. Nitrogen cylinder).
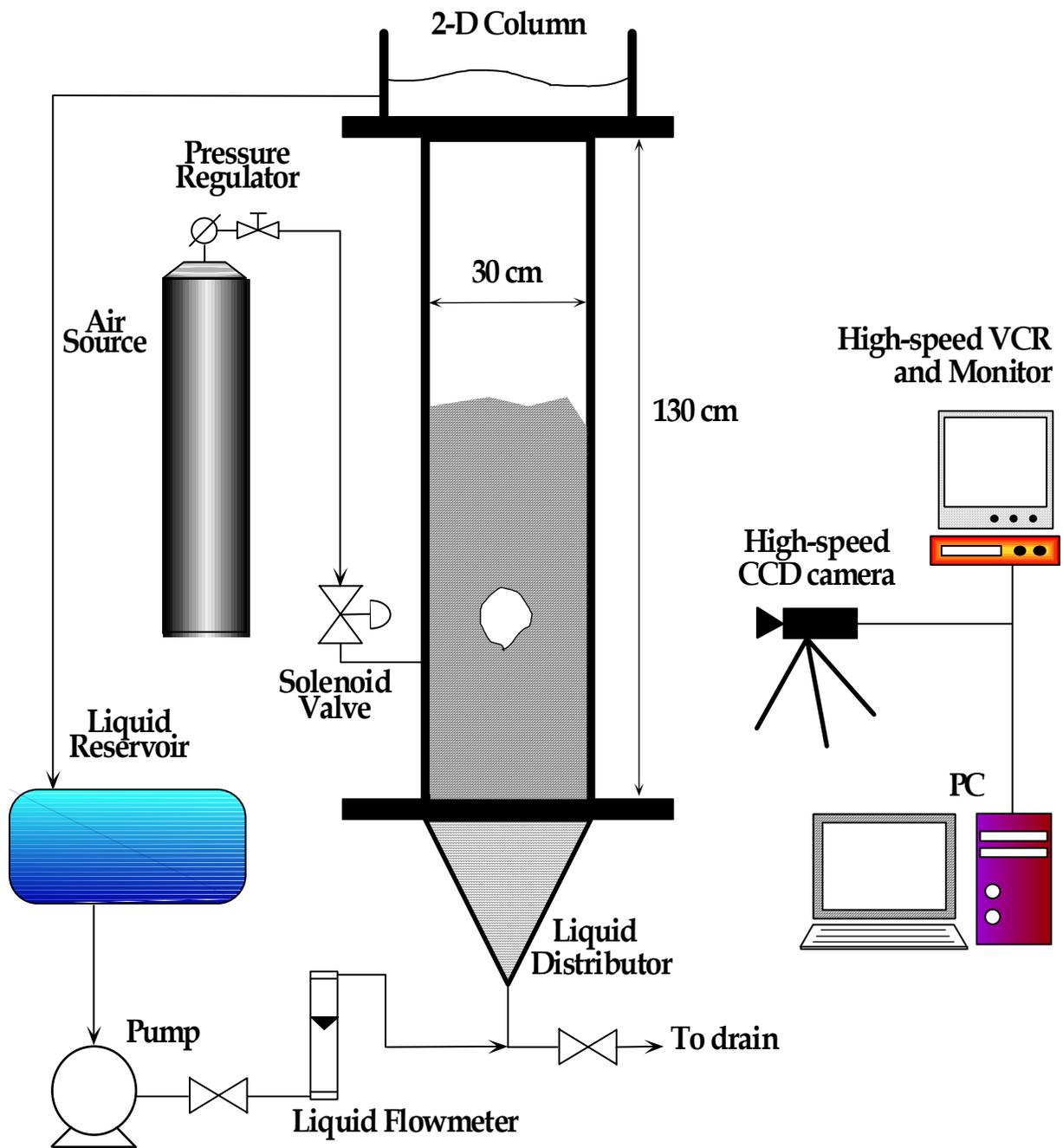
Figure 1-6. Experimental setup for the measurement of the flow field around a growing bubble in liquid-solid suspensions.
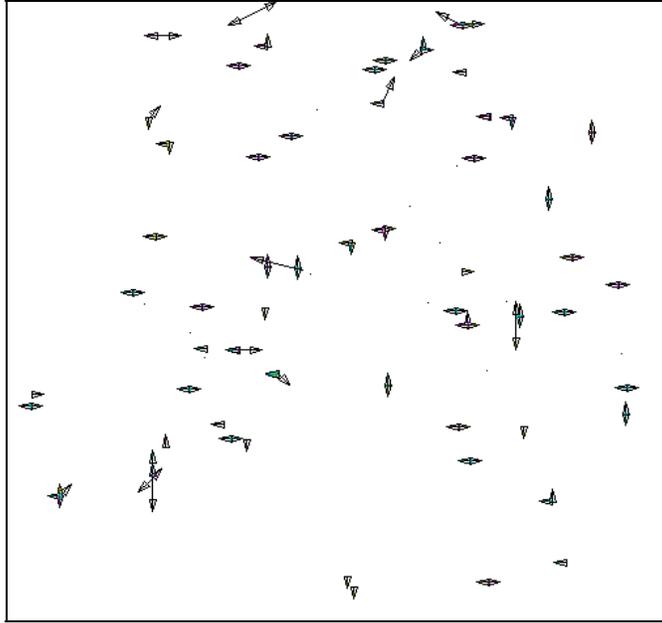
(a)
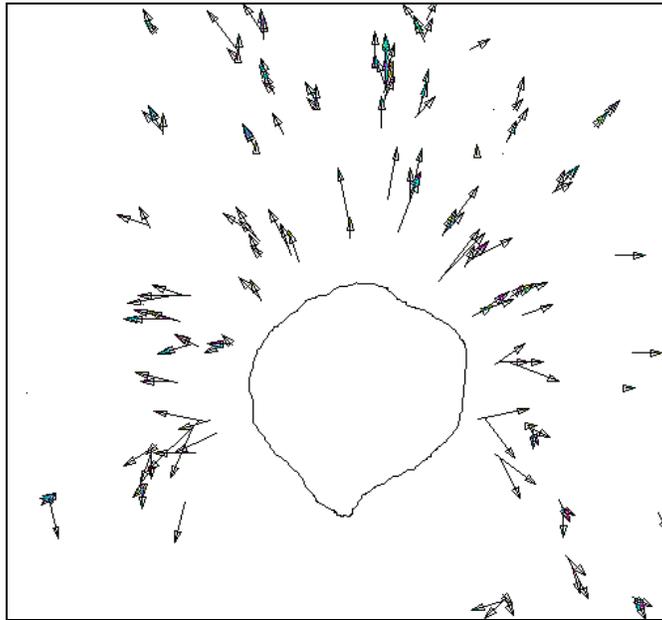
(b)

Figure 1-7. (a) Particle velocities before bubble injection; (b) Particle velocities around a growing bubble.
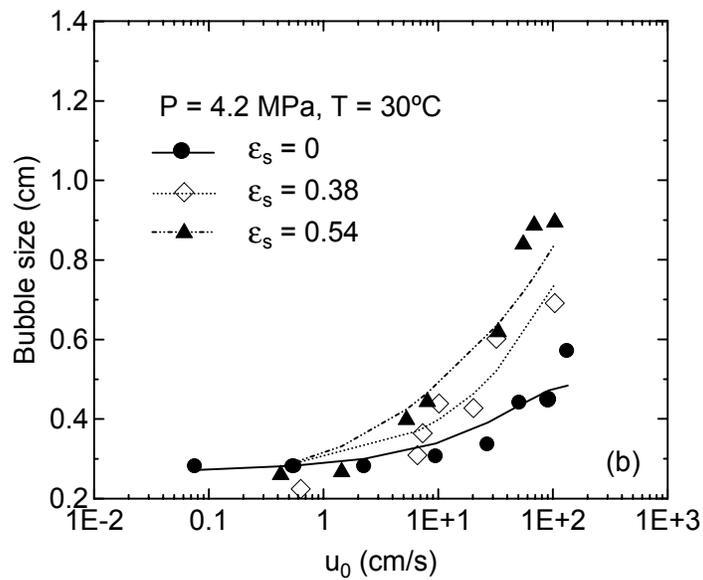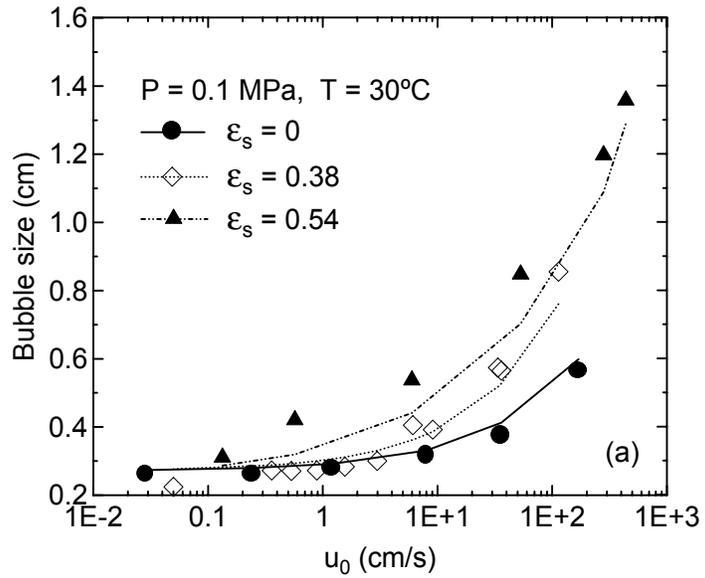
Figure 1-8. Effect of solids holdup on initial bubble size (a) Pressure = 0.1 MPa; (b) Pressure = 4.2 MPa (symbols: experimental data; lines: model predictions).
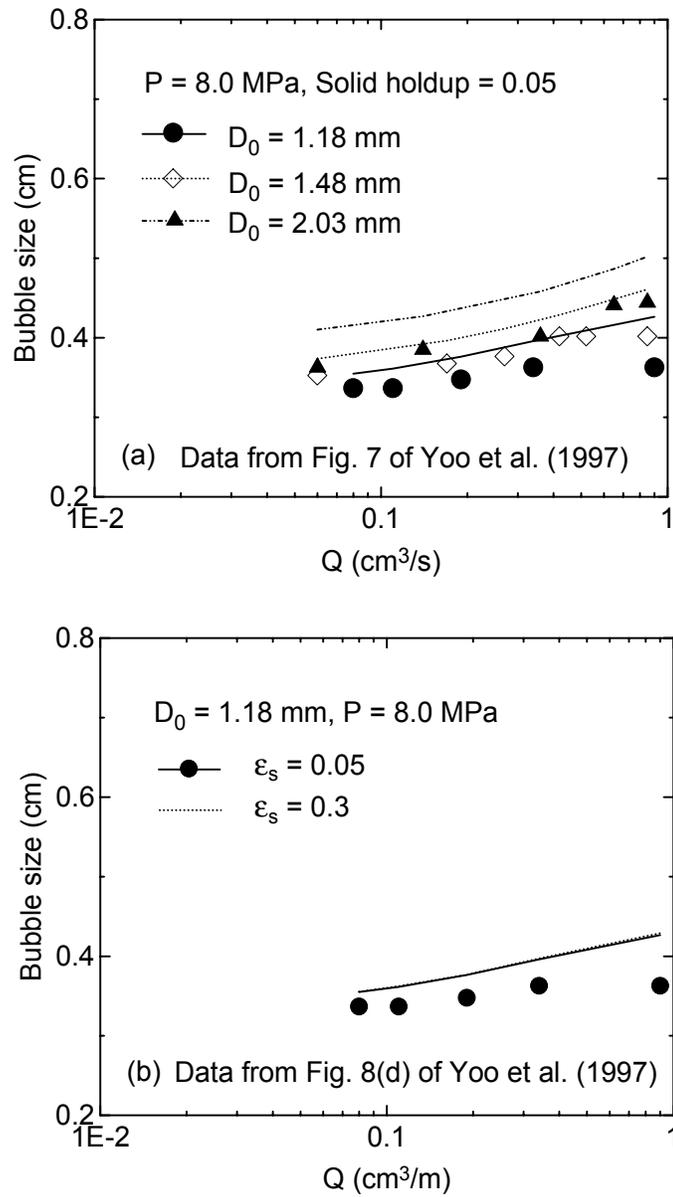
Figure 1-9. Comparison between the experimental data of Yoo et al. (1997) and the predictions by the present model (symbols: experimental data; lines: model predictions).
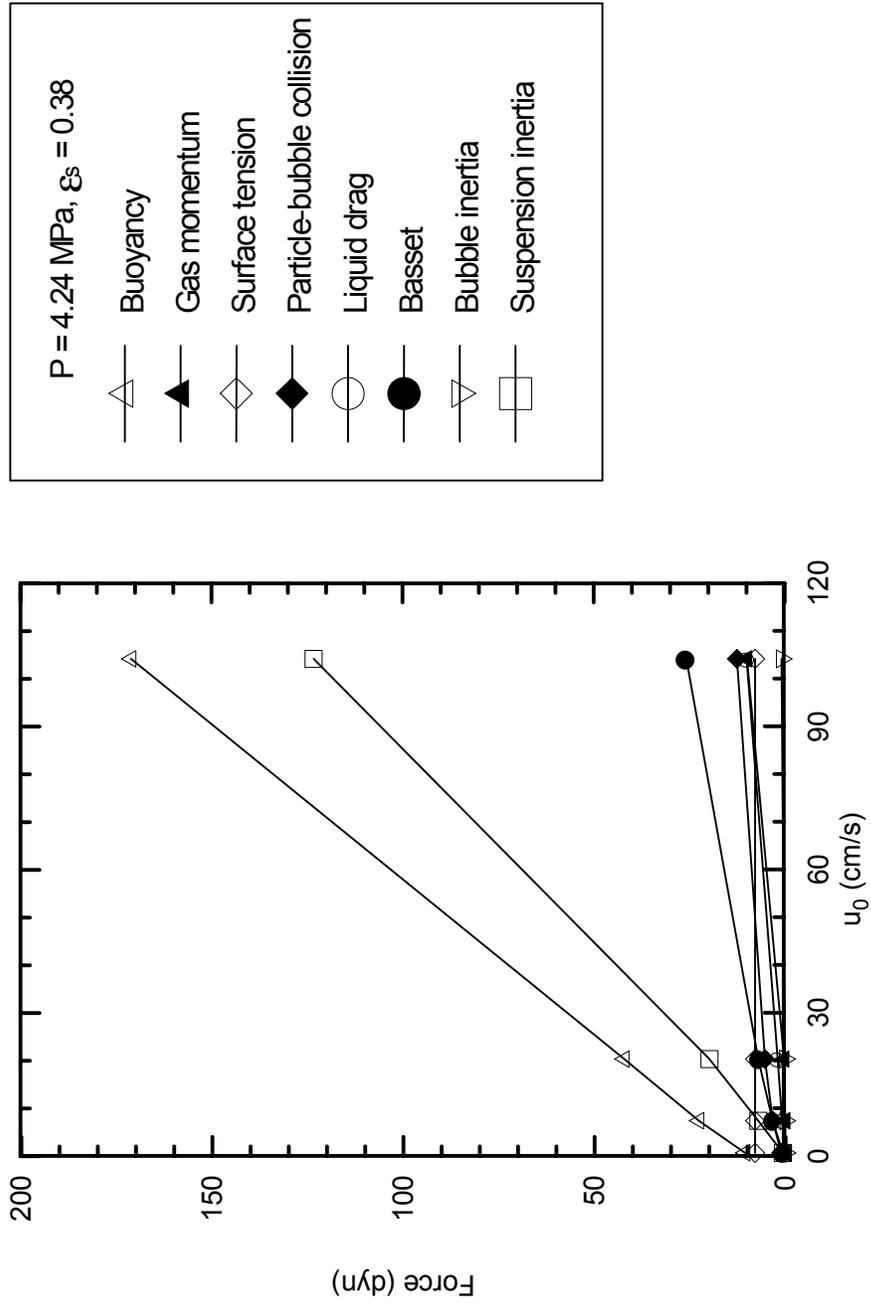
Figure 1-10. Comparison of various forces acting on the growing bubble in the bubble formation process.

25
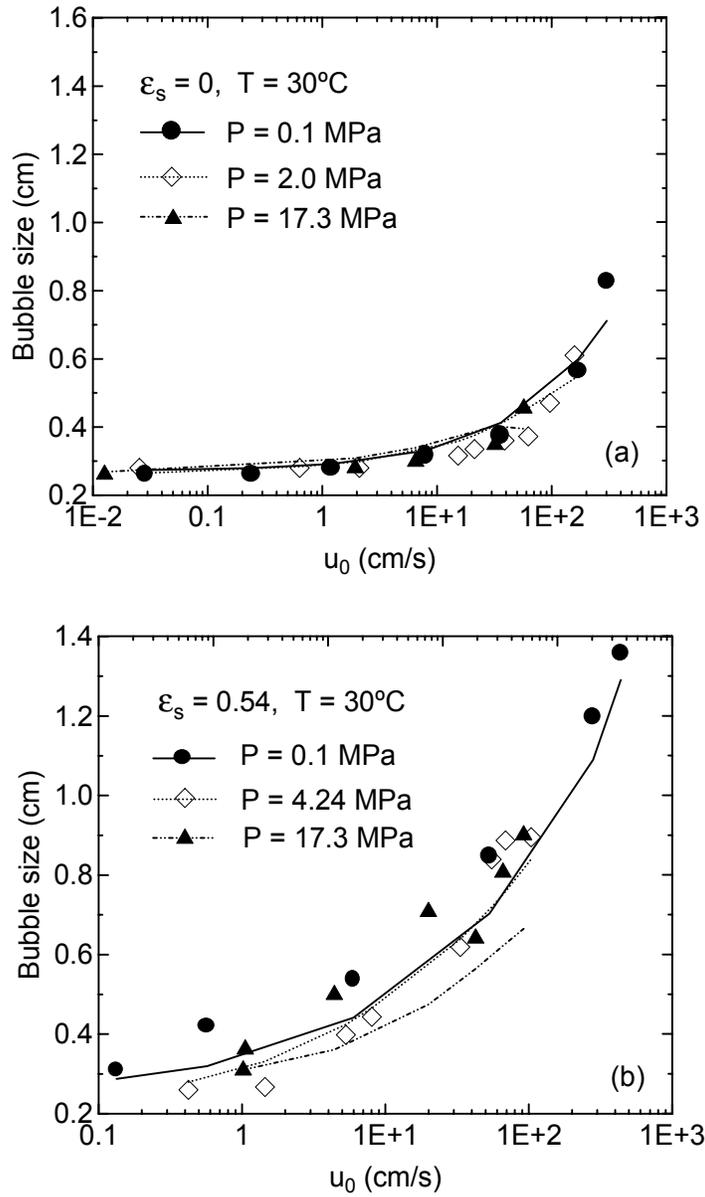
Figure 1-11.   Effect of pressure on initial bubble size in liquid and in liquid-solid suspensions (symbols: experimental data; lines: model predictions).

26
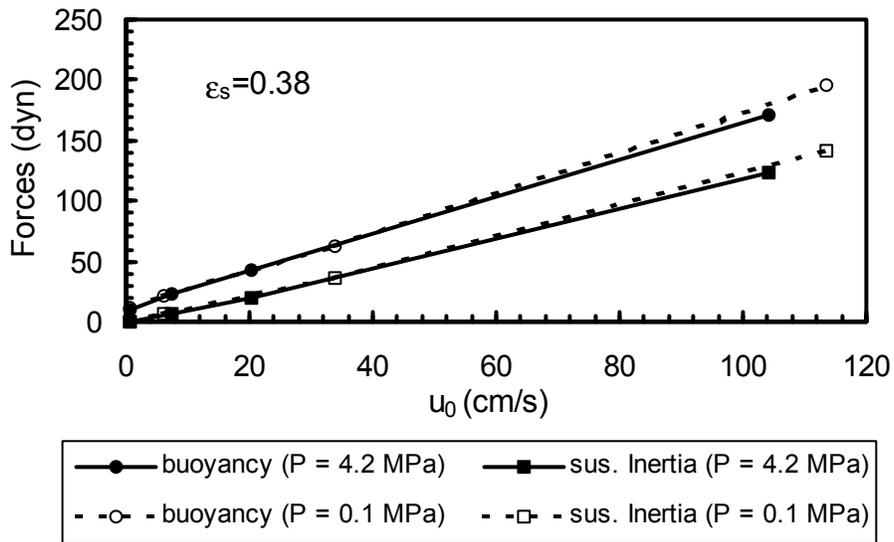
(a)
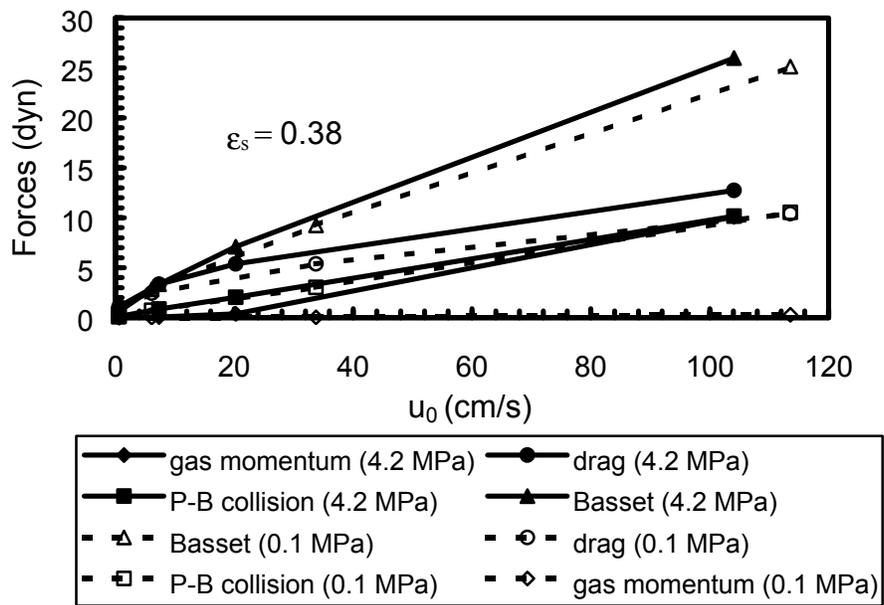
(b)

Figure 1-12. Effect of pressure on the various forces acting on a growing bubble.

Chapter 2: Gas Holdup and Maximum Stable Bubble Size in Slurry Bubble Columns

Introduction

Gas holdup is a key parameter that characterizes the transport phenomena of bubble column systems. The gas holdup generally increases with an increase in gas velocity, with a larger increasing rate in the dispersed bubble regime than in the churn-turbulent regime. The distributor design affects the gas holdup significantly only at low gas velocities. In bubble columns, the effect of column size on gas holdup is negligible when the column diameter is larger than 0.1–0.15 m (Shah et al., 1982). The influence of the column height is insignificant if the height is above 1-3 meters and the ratio of the column height to the diameter is larger than 5 (Kastaneck et al., 1984). The gas holdup decreases as liquid viscosity and/or gas-liquid surface tension increase. The addition of particles into a bubble column leads to a larger bubble size and thus a decreased gas holdup, especially when the particle concentration is low. The particle size effect on the gas holdup can be neglected in the particle size range of 44–254 μm.

Some studies have been conducted to investigate the effect of pressure on the gas holdup of bubble columns (Tarmy et al., 1984; Idogawa, 1986; Wilkinson et al., 1992; Deckwer et al., 1993; Reilly et al., 1994; Jiang et al., 1995; Lin et al., 1998) and three-phase fluidized beds (Luo et al., 1997a). It is commonly accepted that elevated pressures lead to higher gas holdups in both bubble columns and three-phase fluidized beds except in those systems which are operated with porous plate distributors and at low gas velocities. The increased gas holdup is directly related to the smaller bubble size and, to a lesser extent, the slower bubble rise velocity at higher pressures (Luo et al., 1997b). The most fundamental reason for the bubble size reduction can be attributed to the variation in physical properties of the gas and liquid with pressure. Three mechanisms are involved: smaller initial bubble size from the gas distributor (larger gas density), reduced bubble coalescence rate (lower surface tension and larger liquid viscosity), and increased bubble breakup rate (larger gas density and smaller surface tension). Empirical correlations have been proposed for the gas holdup in bubble columns operated at elevated pressure and temperature (Wilkinson et al., 1992; Reilly et al., 1994).

Significant pressure effects on the gas holdup should exist in slurry bubble columns; however, little is reported concerning such effects. Deckwer et al. (1980) found little effect of pressure on the gas holdup in a Fisher-Tropsch slurry bubble column with a porous plate distributor (P = 0.4–1.1 MPa; T = 143–260ºC; U_g = 0–3.5 cm/s). The experimental data of Kojima et al. (1991) indicated that the gas holdup increases with the pressure; but no pressure effect was observed at the 30 wt.% solids concentration (P = 0.1–1.1 MPa, U_g = 1.7–9 cm/s, single orifice distributor). Inga (1997) measured the gas holdup in slurry bubble columns for Fischer-Tropsch synthesis at pressures up to 0.72 MPa and a significant pressure effect was observed. No viable model or correlation is presently available to predict the gas holdup in high pressure slurry bubble columns.

The knowledge of bubble flow characteristics and bubble size is essential to a fundamental understanding of gas holdup behavior in slurry bubble columns. Lee et al. (1998) studied the flow structure and the bubble characteristics in bubble columns utilizing the particle image velocimetry (PIV) and dynamic gas disengagement (DGD) techniques. The DGD technique was first used in bubble columns at low gas velocities (U_g < 2 cm/s)

by Sriram and Mann (1977) to quantify the bubble size and size distribution in the columns. Various models that relate gas disengagement phenomena to bubble size or size distribution have been proposed in the literature (Vermeer and Krishna, 1981; Schumpe and Grund, 1986; Patel et al., 1989; Daly et al., 1992). However, the reliability of the DGD technique applied to the slurry bubble columns operated at high pressure and high gas velocity depends on whether the models account for the transient characteristics of bubble flow during the DGD process.   Little has been reported on the evolutions of the instantaneous distributions of the bubble size and bubble rise velocity during the gas disengagement process.

The objective of this work is to investigate the effects of pressure on the hydrodynamics of slurry bubble columns under conditions of industrial relevance. In this study, experiments are conducted to measure gas holdup at pressures up to 5.6 MPa and at gas velocities up to 45 cm/s. An empirical correlation is developed to account for the gas holdup behavior in high pressure slurry bubble columns. The PIV system is applied to examine the flow characteristics and to substantiate the applicability of the DGD technique for the measurement of the bubble size distribution in the slurry bubble column operated under the present conditions. The bubble size and its distribution are directly measured using a fiber optic probe in the high pressure slurry bubble column. A mechanistic model is proposed to illustrate the bubble breakup mechanism at high pressures. The mechanism is verified by comparing the model predictions of maximum stable bubble size with the experimental data.

Experimental
High Pressure Slurry Bubble Column and Gas Holdup Measurement
The experiments are conducted in a high pressure multiphase flow and visualization system, as shown in Figure 2-1. The maximum operating pressure and temperature of this system are 21 MPa and 180ºC, respectively. The high pressure slurry bubble column is 0.102 m in diameter and 1.37 m in height. The column is divided into three sections: plenum region, test section, and disengagement section. Three pairs of quartz windows are installed on the front and rear sides of the column. Each window is of 12.7 mm in width and of 93 mm in height. The windows cover the entire test section. A perforated plate is used as the gas distributor, with 120 square-pitched holes of 1.5 mm diameter. The volume of the plenum region beneath the distributor is 1.18 liter.

In this study, the liquid is in batch mode. Nitrogen from the high pressure cylinders is introduced into the slurry bubble column after the pressure and temperature are adjusted to desired values.   The gas exiting from the column flows through a back pressure regulator and is vented into an exhaustion system. The back pressure regulator controls the system pressure. The gas flow rate is measured using a high pressure turbine flowmeter. In this study, Paratherm NF heat transfer fluid is used as the liquid phase. The physical properties of this liquid are shown in Table 2-1. The solids phase is alumina particles with a wet density of 2440 kg/m^3. The particle sizes are uniformly distributed between 90 μm and 110 μm with an averaged diameter of 100 μm. The clear liquid level is maintained at 0.5 m above the distributor. Experiments are performed in two slurries of different solids volume fractions (ϕ_s) of 0.081 and 0.191.

The gas holdup in the slurry bubble column is measured using the dynamic gas disengagement technique. After the flow in the column reaches steady state, the gas inlet

29

and outlet are simultaneously shut off to maintain constant system pressure. The bubbles disengage from the column and the particles gradually settle down. A differential pressure transducer is used to monitor the variation of the dynamic pressure drop during the process. The positive port of the transducer is located at 0.18 m above the distributor while the negative port is located at 0.36 m above the distributor.

Figure 2-2 shows an example of the differential pressure signal during the disengagement process. The column is at steady state before the gas flow is shut off at $t =$ 9.0 s. It can be seen from the figure that the entire process can be divided into 6: (1) Immediately following gas shutoff, a sudden jump of the differential pressure signal corresponds to the simultaneous disengagement of bubbles of all sizes; (2) The increase of the signal value is much more gradual, since only relatively small bubbles escape from the column; (3) The differential pressure remains at a relatively constant value for a period of about 150 seconds because the particles are still fully suspended by the liquid motion induced by bubbles; (4) Starting from $t = 150$ s, the pressure drop increases gradually. During this time period, the liquid motion dies down and particles start settling down, which leads to an increased solids concentration in the region between the two pressure ports. A solids surface can be seen to move downward at this stage; (5) The solids surface continues to move down and drops into the region between the two pressure ports, which causes a steep drop in the differential pressure value ($550 < t < 800$ s); (6) The particle surface is below the lower pressure port ($t > 800$ s) and the pressure drop approaches zero.

The gas holdup can then be calculated from the dynamic pressure drops at the steady state together with that at stage (3). The ratio of the solids holdup to the liquid holdup, K, remains constant in the region between the two pressure ports from the initial stage to stage (3). The dynamic pressure drop in stage (3) can be approximated as

$$\left(\frac{\Delta P}{\Delta z}\right)_d^0 = \left(\rho_l \varepsilon_l^0 + \rho_s \varepsilon_s^0 - \rho_l\right)g = \varepsilon_s^0(\rho_s - \rho_l)g .$$ (2-1)

Fu et al. (1995) used a similar equation to measure the solids holdup in slurry bubble columns. Based on Eq. (2-1), K can be written as

$$K = \frac{\varepsilon_s}{\varepsilon_l} = \frac{(\Delta P/\Delta z)_d^0}{(\rho_s - \rho_l)g - (\Delta P/\Delta z)_d^0} .$$ (2-2)

With K known, the differential pressure signals at steady state and at bubble escape can be related to the phase holdups and densities of the three phases by

$$\left(\frac{\Delta P}{\Delta z}\right)_d = \left(\rho_g \varepsilon_g + \rho_l \varepsilon_l + \rho_s \varepsilon_s - \rho_l\right)g$$

$$= \left\{\frac{K(\rho_s - \rho_l)}{1+K} + \left[\frac{(1+K)\rho_g - (\rho_l + K\rho_s)}{1+K}\right]\varepsilon_g\right\}g .$$ (2-3)

Solving Eq. (2-3) for ε_g and replacing K with Eq. (2-2) yields

$$\varepsilon_g = \frac{\left[(\Delta P/\Delta z)_d^0 - (\Delta P/\Delta z)_d\right]/g}{(\Delta P/\Delta z)_d^0/g + (\rho_l - \rho_g)} .$$ (2-4)

The particle density is not present in Eq. (2-4); hence, the gas holdup can be calculated without knowledge of the particle density. The advantage of this technique is that the gas holdup and solids holdup can be evaluated simultaneously when the particle density is known. The solids concentration in the slurry bubble column can also be monitored with

this method to ensure that all the particles are completely suspended at various gas velocities.

Bubble Flow Characteristics and Bubble Size Measurement

PIV Measurements in DGD Process. Dynamic gas disengagement experiments are conducted in a two-dimensional (2-D) Plexiglas column under ambient conditions as well as in a 3-D column under high pressures. The instantaneous flow fields during the DGD process are analyzed using a PIV system to study the characteristics of bubble flow and to examine the assumptions used in the existing DGD models. The detailed experimental setup for the 2-D column is given in Lee et al. (1998). In the 2-D column, the liquid phase used is tap water, and is operated under batch conditions with the static liquid height maintained near 120 cm. Compressed air and alumina particles of 100 μm mean diameter are used as the gas and solid phases, respectively. After steady state operation is reached, the gas supply is shut off with a three-way valve, with one outlet being connected to the atmosphere, to prevent trickling bubbles from leaking into the column after shutoff.

The image of the flow field during the DGD process is recorded with a high framing-rate and high resolution CCD camera equipped with a variable electronic shutter ranging from 1/60 to 1/10,000 s. A framing rate of 240 fields/sec is used in this study. The images are analyzed using the PIV system. The PIV system used here was originally developed by Chen and Fan (1992) and was enhanced and modified to measure instantaneous full-field flow characteristics for a given plane. The modified PIV technique has sufficient accuracy to determine time/volume averaged flow information for each phase including velocities and dispersed phase size distributions. Further, the PIV technique developed for multiphase systems has the ability to discriminate between the different phases, and provides the instantaneous, full-field flow properties of each phase. With the PIV system, the transient flow behavior during the DGD process can be analyzed and compared to the assumptions made in various models.

Fiber Optic Probe Measurement. Direct measurements of bubble sizes in the high pressure slurry bubble column are conducted using a fiber optic probe. The probe utilizes the difference in refractive index of gas and liquid to distinguish the gas phase from the liquid-solid suspension. The probe is of U-shape, similar to that of de Lasa et al. (1982). There are variations in the tip designs for U-shaped probes used by various researchers to obtain maximum internal light reflection intensity for multiphase flow measurements. In the present probe, the fiber cladding in the tip portion is partially removed in such a manner that it yields the most distinctive signals for gas void detection. The cross section of the tip perpendicular to the flow direction in this probe has a dimension of 1.2×4 mm. The output of the photomultiplier is interfaced with a computer data acquisition system, which samples the signal for four seconds at a frequency of 2,000 Hz. The tip of the probe is located at the center of the column and 0.35 m above the distributor.

The probe is calibrated in a chain of bubbles; bubbles passing through the tip periodically. The bubble rise velocity, u_b, can be calculated by

$$u_b = \frac{\Delta h}{\Delta \tau_2},$$
(2-5)

where Δh is the vertical distance between the two tips and $\Delta \tau_2$ is the time lag between the rear surface of the bubbles intercepting the upper and lower tips. The result is calibrated

against the bubble rise velocity measured with a video camera. It is noted that $\Delta\tau_2$ is consistently less than the other time lag, $\Delta\tau_1$, corresponding to the frontal surface, due to the deformation of the frontal surface upon the interception. The comparison between the two bubble velocities reveals that $\Delta\tau_2$ should be used instead of $\Delta\tau_1$. The average error for the bubble rise velocity by the probe is less than 5%. The bubble chord length, l, is evaluated as

$$l = u_b\tau, \tag{2-6}$$

where τ is the time period when the bubble is in contact with the lower tip of the probe. The probe actually measures the vertical chord length of the bubble rather than the bubble diameter.

Results and Discussion
Overall Gas Holdup

Figures 2-3 through 2-6 show the gas holdup in the slurry bubble columns under various temperature, solids concentration, and pressure conditions. Two temperatures of 28ºC and 78ºC are considered in the experiments. Specifically, the effect of the solids concentration on the gas holdup is shown in Figure 2-3. The presence of particles reduces the gas holdup at both the ambient and 5.6 MPa pressures, especially when the solids fraction is increased from 0 to 0.081. At ambient pressure, the gas holdup in the bubble column ($\phi_s = 0$) is almost 100% higher than in the slurry of 0.191 solids volume fraction over the entire gas velocity range. In contrast, at the pressure of 5.6 MPa, the effect of the solids concentration on the gas holdup is relatively small at gas velocities above 25 cm/s. For example, at 5.6 MPa, the gas holdup decreases from 0.55 to 0.48 (12%) as the solids fraction increases from 0 to 0.191 at a constant gas velocity of 30 cm/s; while at ambient pressure the gas holdup decreases from 0.35 to 0.18 (49%) for the same solids concentration increase and at the same gas velocity.

The pressure effect on the gas holdup can be seen in Figures 2-4 through 2-6. In general, elevated pressures lead to higher gas holdups under all the experimental conditions in the present study. The pressure effect is more significant at low pressures. Examination of the pressure effect on gas holdup at different solids concentrations indicates that the pressure effect is more pronounced at higher solids concentrations. For example, at a gas velocity of 30 cm/s and a temperature of 78ºC, the gas holdup increases from 0.34 to 0.55 (62% increase) in the bubble column ($\phi_s = 0$) when the pressure is elevated from 0.1 MPa to 5.6 MPa. At the same gas velocity and temperature, and for the same pressure change, the gas holdup changes from 0.25 to 0.49 (96%) in the slurry system with the solids fraction of 0.081, and from 0.2 to 0.45 (125%) in the slurry system with a solids concentration of 0.191.

For design purposes, an empirical correlation is developed to account for the gas holdup in high pressure slurry bubble columns operated in the coalesced bubble regime, as given below:

$$\frac{\varepsilon_g}{1-\varepsilon_g} = \frac{2.9\left(\dfrac{U_g^4\rho_g}{\sigma g}\right)^{\alpha}\left(\dfrac{\rho_g}{\rho_{sl}}\right)^{\beta}}{\left[\cosh\left(Mo_{sl}^{0.054}\right)\right]^{4.1}}, \tag{2-7}$$

where Mo_{sl} is the modified Morton number for the slurry phase, $(\xi\mu_l)^4 g/\rho_{sl}\sigma^3$, and

$$\alpha = 0.21 \text{Mo}_{sl}^{0.0079} \quad \text{and} \quad \beta = 0.096 \text{Mo}_{sl}^{-0.011}. \tag{2-7a}$$

ρ_g, ρ_l, μ_l, and σ are respectively the gas density, liquid density, liquid viscosity, and gas-liquid surface tension at operating pressure and temperature. The effective slurry density, ρ_{sl}, is given by

$$\rho_{sl} = \phi_s \rho_s + \phi_l \rho_l, \tag{2-8}$$

where ϕ_s and ϕ_l are the volume fractions of the solids and the liquid in the gas-free slurry. In Eq. (2-7), ξ is a correction factor which accounts for the effect of particles on slurry viscosity:

$$\ln \xi = 4.6 \phi_s \left\{ 5.7 \phi_s^{0.58} \sinh \left[-0.71 \exp(-5.8 \phi_s) \ln \text{Mo}^{0.22} \right] + 1 \right\} \tag{2-9}$$

where Mo is the Morton number of the liquid, $g\mu_l^4 / \rho_l \sigma^3$. When the solids volume fraction approaches zero, this correlation reduces to the form for bubble columns. The correlation takes into account not only the experimental data obtained in this work, but also the data obtained in systems of various gas, liquid, and solids and by different authors. Table 2-2 lists the various experimental systems and their corresponding references. The column diameter in the selected systems is larger than 0.1 m and the ratio of column height to diameter is larger than 5. The gas distributors are perforated plate, sparger, or bubble cap distributor. The average error of the predictions is 13% for both the slurry and gas-liquid systems and the maximum error is 53%. Figure 2-7 shows the comparison between the predictions by the correlation and the experimental data. Oyevaar (1989) measured the gas holdup of an air/water system at pressures up to 7.8 MPa in a column of 0.08 m diameter. Although the error of the predictions by the correlation is 40% at ambient pressure, the error at the high pressure is only 10%, which implies that the scale effect on the gas holdup is relatively small at high pressures due to the smaller bubble sizes. The applicable ranges of the correlation are summarized in Table 2-3.

Flow Characteristics and Bubble Size Distribution

Flow Characteristics from DGD Experiments. To fundamentally explain the effect of pressure on the gas holdup in the slurry bubble column, it is essential to understand the flow characteristics and the bubble size variation with the pressure in the system. The frame by frame analysis of the instantaneous flow fields of the bubble phase reveals the importance of the interaction between the small and large bubbles. A wake is formed when the bubble Reynolds number is above 20 for a single bubble (Fan and Tsuchiya, 1990). The wake behind the bubble generates a low pressure region. Smaller bubbles are frequently attracted into the region and are accelerated to almost the same rise velocity as the leading bubble. This attraction phenomenon is evident in the results obtained from the DGD experiments. Figures 2-8(a) and 2-8(b) show the variations of the number of the largest bubbles and the number of bubbles with the largest rise velocity during a DGD process. As the number of the large bubbles gradually decreases during the DGD process, so does the rise velocity of the small bubbles. It is noted that the bubbles larger than 2.0 cm rise at velocities of approximately 50 cm/s. The initial number of bubbles with rise velocity larger than 50 cm/s is around 12 while the initial number of bubbles larger than 2.0 cm is only 2. Further, the number of fast rising bubbles becomes zero only after the largest bubbles completely disengage at 1.5 s. The above observations clearly show the bubble wake attraction effect. Without such attraction only the largest bubbles can reach this high velocity. Note that the superficial gas velocity in Figure 2-8 is 3.0 cm/s; as the

superficial gas velocity increases, the effect of the large bubbles on the rise velocity of the smaller bubbles becomes more dominant. Lee et al. (1998) studied the amount of the small bubbles attracted by the large bubbles with the PIV system in a 2-D bubble column at various superficial gas velocities. They concluded that at gas velocities above 11 cm/s, over 70% of the initial small bubbles disengage from the column with the large bubbles; at gas velocities below 4 cm/s, the number is around 20%. The above observations undoubtedly indicate the dominant effect of the large bubbles on the rise velocity of the bubbles in bubble columns and slurry bubble columns. Moreover, the volume of a bubble is proportional to the cube of the bubble size. Since the gas holdup is basically dictated by the size and rise velocity of bubbles, the large bubbles play a key role in determining the gas holdup in these systems.

The significance of the bubble wake attraction calls for examination of the existing models that describe the DGD profiles, i.e., the gas holdup or liquid height variation with time during the DGD process. The various existing DGD models are summarized in Figure 2-9, in which the gas is shut off at t_0. If a bimodal bubble size distribution is assumed, the DGD profile can be approximated by two straight lines. The line with a steeper slope corresponds to the escape of both large and small bubbles in stage one; the other line corresponds to the escape of the small bubbles in stage two. If the rise velocity of the small bubbles is assumed to be constant throughout the entire disengagement process, the line for stage two can be extrapolated to t_0 to obtain the initial holdup of the small bubbles (Sriram and Mann, 1977), marked as Model 1 in Figure 2-9. If it is assumed that the small bubbles do not disengage in stage one due to the liquid backflow (Model 2), the initial small bubble holdup is simply the gas holdup at t_1, i.e., at the end of stage one (Vermeer and Krishna, 1981). The other assumption made regarding the disengagement rate of bubbles is that the slip velocity between the gas and the liquid is constant (Patel et al., 1989). In this case, the calculated small-bubble holdup falls in between the values of Model 1 and Model 2. However, since all the three assumptions regarding the small bubble rise velocity do not recognize the bubble acceleration due to the large bubbles at the first stage, the models may lead to errors in estimating holdups for both small and large bubbles especially at high superficial gas velocities, as shown in Figure 2-9. The above analysis is based on a bimodal bubble size assumption; the true bubble disengagement behavior is even more complex as the bubble size distribution is known to be continuous. The liquid circulation in the column further complicates the analysis of the DGD processes (Desphande et al., 1995).

In addition to the bubble wake attraction, strong bubble coalescence and breakup are also observed during the DGD process, which invalidates the first assumption made in the existing DGD models, i.e., no bubble coalescence and breakup. However, the error due to this assumption is minimal if a dynamic equilibrium between the bubble coalescence and the bubble breakup can be assumed.

In summary, the intrinsic bubble flow behavior in the dynamic gas disengagement process is complex in nature. Through the bubble wake attraction, the gas holdups in bubble columns or slurry bubble columns are closely associated with the size and number of the large bubbles. A fundamental explanation of the pressure effect on gas holdup should be based on a full understanding of the variation of bubble size, especially of the large bubble size, with the pressure. The existing DGD models can only provide preliminary estimations about the holdup structure and bubble size distribution in slurry

bubble columns at low gas velocities. In slurry bubble column reactors operated at high gas velocities, such as those in the methanol synthesis process, the bubble size distribution cannot be reasonably estimated by the DGD technique without the quantification of bubble-bubble interactions. Therefore, direct measurement is the only accurate means to quantify bubble size distribution.

Pressure Effect on Bubble Size. A fiber optic probe can give a reliable measurement of the bubble size distribution in the high pressure slurry bubble column. It is noted that the probe can only measure the bubble chord length instead of the true bubble diameter. If a uniform bubble shape is assumed (either spherical or ellipsoidal), the bubble chord length distribution can be converted to the size distribution (Liu et al., 1996). However, the bubbles in slurry bubble columns have irregular shapes. The data from the probe can thus only represent the chord length distribution.

Special attention should be placed on the maximum chord length for the dominant effect of large bubbles on the gas holdup. In addition, the measured maximum chord length can be interpreted as the height of the largest bubble (h_{max}) in the system if the number of bubbles detected by the probe is large enough. In general, the maximum bubble height differs from the maximum bubble size. Nevertheless, the large bubbles in 2-D slurry bubble columns of different solids concentrations have approximately the same maximum dimensions in the horizontal and vertical directions, based on the photos shown by de Swart et al. (1996) and observations from the 2-D experiments. The maximum bubble size can thus be approximated by the maximum bubble height in 2-D slurry bubble columns. It is further assumed here that this approximation holds also for 3-D columns; thus, the maximum bubble chord length is approximated as the maximum bubble diameter in the following analysis.

Figure 2-10 shows the bubble chord length distributions of slurry at ambient pressure. The *y*-axis and the *x*-axis represent the probability density distribution function and the bubble chord length in the vertical direction, respectively. It can be seen that the bubbles at ambient pressure have a wide size distribution. The maximum bubble size increases with an increase in gas velocity. The maximum bubble size is about 7.2 cm at a gas velocity of 38.5 cm/s. The slurry bubble column is apparently operated in the slugging regime. The slugging regime is also confirmed by a visual observation of the flow through the quartz windows. The periodical penetration of light is evident from the opposite side lighting in the experiments. At high gas holdup, for the ambient pressure case, the column is opaque except for a flash of light as the large bubble rises past the window. In contrast, for the 5.6 MPa case, the column is opaque over the entire gas velocity range. This indicates a much smaller bubble size in the high pressure case. A comparison of the data shown in Figures 2-10 and 2-11 indicates that pressure has a significant effect on the breakage of the large bubbles. At a pressure of 5.6 MPa, the bubble size is much smaller and the bubble size distribution is narrower, similar to the results obtained in high pressure bubble columns and three-phase fluidized beds. The maximum bubble size is around 2.4 cm at a gas velocity of 30 cm/s. In addition to the bubble size reduction, bubbles rise at slower velocities at high pressures. The increase in gas holdup with pressure is a consequence of the decreases both in the bubble size and in the bubble rise velocity, i.e. larger bubbles broken into smaller ones and their rise velocities further reduced by pressure.

The maximum bubble size under different conditions can be seen from Figure 2-12. Under otherwise constant conditions, the maximum bubble size decreases with an increase in pressure, especially at pressures lower than 1.5 MPa. Increasing particle concentration leads to significantly larger bubble sizes at ambient pressure over the entire gas velocity range. On the other hand, the particle concentration has a significant effect on the maximum bubble size only in the gas velocity range of 8–23 cm/s at the pressure of 5.6 MPa. At gas velocities above that range, the maximum bubble size is virtually independent of solids concentration. Due to the dominant role of the large bubbles in determining the gas holdup, the above observation can explain the similar solids concentration effect on gas holdup shown in Figure 2-3. The effect of solids concentration on gas holdup is significant over the entire gas velocity range at ambient pressure; the solids concentration effect on gas holdup is relatively small at gas velocities above 25 cm/s at the pressure of 5.6 MPa.

Maximum Stable Bubble Size - Background. The upper limit of the bubble size is set by the maximum stable bubble size, D_{max}, above which the bubble is subjected to breakup and is hence unstable. Several mechanisms have been proposed to predict the maximum stable bubble size in gas-liquid systems. Hinze et al. (1955) proposed that the bubble breakup is caused by the dynamic pressure and the shear stresses on the bubble surface induced by different liquid flow patterns, e.g., shear flow and turbulence. When the maximum hydrodynamic force in the liquid is larger than the surface tension force, the bubble disintegrates into smaller bubbles. This mechanism can be quantified by the liquid Weber number; when the Weber number $= \rho_l \overline{u^2} D_{max} / \sigma$ is larger than a critical value, the bubble is not stable and disintegrates. This theory was adopted to predict the breakup of bubbles in gas-liquid systems (Walter and Blanch, 1986). Calculations by Lin et al. (1998) showed that the theory under-predicts the maximum bubble size and cannot predict the observed effect of pressure on bubble size.

A maximum stable bubble size exists for bubbles rising freely in a stagnant liquid without the external stresses (Grace et al., 1978). The Rayleigh-Taylor instability has been regarded as the mechanism for the bubble breakup under such conditions. A horizontal interface between two stationary fluids is unstable with respect to disturbances having wavelengths exceeding a critical value if the upper fluid has a higher density than the lower one (Bellman and Pennington, 1954). Chen and Fan (1988) obtained an expression for the critical wavelength for a curved surface as in the case of bubble. Grace et al. (1978) applied the Rayleigh-Taylor instability theory by considering the time available for the disturbance to grow and the time required for the disturbance to grow to an adequate amplitude. Batchelor (1987) pointed out that the observed maximum air bubbles in water were considerably larger than that predicted by the model of Grace et al. (1978). Batchelor (1987) further took into account the stabilizing effects of the liquid acceleration along the bubble surface and the non-constant growth rate of the disturbance. In his model, the information of disturbances is required for the prediction of the maximum bubble size. The models based on the Rayleigh-Taylor instability predict an almost negligible pressure effect on the maximum bubble size; in fact, the Rayleigh-Taylor instability implies that the bubble is slightly more stable when the gas density is higher.

Kitscha and Kocamustafaogullari (1989) applied the Kelvin-Helmhotz instability theory to model the breakup of large bubbles in liquids, using the same concept of Grace et

al. (1978). Wilkinson and Van Dierendonck (1990) applied the critical wavelength to explain the maximum stable bubble size in high pressure bubble columns. Their results showed that the critical wavelength decreases with an increase in pressure and therefore bubbles are easier to disintegrate by the disturbances. However, the critical wavelength is not necessarily equivalent to the maximum stable bubble size and their approach alone cannot quantify the pressure effect on bubble size.

All the models mentioned above neglected the effect of the internal circulation of the gas. For the continuity of the tangential velocity in the gas and liquid phases, the internal circulation velocity is of the same order of magnitude as the bubble rise velocity. A centrifugal force is induced by this circulation, pointing outwards to the bubble surface, which can suppress the disturbances at the gas-liquid interface and act as a stabilizing force. This force may be another reason to explain the underestimation of D_{max} by the model of Grace et al. (1978), besides that discussed by Batchelor (1987). On the other hand, centrifugal force can also disintegrate the bubble as it increases with an increase in bubble size. The bubble breaks up when the centrifugal force exceeds the surface tension force, especially at high pressures when gas density is high.

Levich (1962) recognized the fact of internal gas circulation and assumed the centrifugal force to be equal to the dynamic pressure induced by the gas moving at the bubble rise velocity, and proposed a simple equation to calculate the maximum stable bubble size:

$$D_{max} \approx \frac{3.63\sigma}{u_b^2 \sqrt[3]{\rho_l^2 \rho_g}} \quad . \tag{2-10}$$

Equation (2-10) shows a significant effect of pressure on the maximum bubble size; however, it severely under-predicts the maximum bubble size.

Maximum Stable Bubble Size - Proposed Mechanistic Model. An analytical criterion for the bubble breakup can be derived by considering a single large bubble rising in a stagnant liquid at a velocity of u_b, without any disturbances on the gas-liquid interface. The bubble is subjected to breakup when its size exceeds the maximum stable bubble size due to the circulation and centrifugal force. Large bubbles normally assume a spherical cap shape; in this work, the spherical-cap bubble is approximated by an ellipsoidal bubble with the same volume and the same aspect ratio (height to width). The bubble is described in a cylindrical coordinate system which moves with the bubble and has the center of the ellipsoidal bubble as its origin, as shown in Figure 2-13(a). The bubble surface is formed by rotating an ellipse around the vertical axis, z:

$$\frac{r_c^2}{a^2} + \frac{z^2}{c^2} = 1, \tag{2-11}$$

where r_c is the distance from the z axis. The aspect ratio of the ellipse ($\alpha = c/a$) is the same as that of the real spherical cap bubble. The internal circulation can be described by Hill's vortex (Hill, 1894) because of the high Reynolds number of the gas in the bubble. The flow field is symmetrical about the z axis and has no azimuthal component. The circulation velocity in the r_c and z directions are, respectively,

$$u = \frac{3u_b}{2c^2}zr_c = \frac{3u_b}{2\alpha^2 a^2}zr_c \tag{2-12a}$$

and

$$w = \frac{3u_b}{2a^2}\left[\left(a^2 - 2r_c^2\right) - \frac{z^2}{\alpha^2}\right]. \tag{2-12b}$$

In the presence of contaminants, a small bubble would behave like a rigid particle and thus, the circulation of the gas inside the bubble could be suppressed. For large bubbles, as encountered in the model, the high shear force generated by the high relative velocity between the bubble and the liquid or slurry could readily sweep away the contaminants on the surface and thus, the contaminants induce negligible effects on the internal circulation of the gas (Levich, 1962).

To model the bubble breakup, it is necessary to evaluate the x-component of the centrifugal force, F_x, on the entire bubble surface as shown in Figure 2-13(c). Based on Eqs. (2-12a) and (2-12b), there is a surface within the bubble, S, on which the z component of the circulation velocity, w, is zero and the circulation velocity has only the component in the r_c direction, u, as shown in Figures 2-13(a) and 2-13(b). This surface can be described as

$$\frac{2r_c^2}{a^2} + \frac{z^2}{\alpha^2 a^2} = 1. \tag{2-13}$$

Surface S passes through the vortex center and intercepts all the vortex streamlines, as shown in Figure 2-13(a). Because the pressure field inside the bubble is symmetrical about the x-y plane, F_x is simply the rate of change of momentum across the surface S in the x direction, based on a momentum balance for the gas phase. In addition, the streamlines inside the bubble are symmetrical about the x-y plane and x-z plane, and thus, F_x is 4 times the rate of the x-component of the gas momentum flowing across an octant of surface S shown in Figure 2-13(c),

$$F_x = 4\iint_S \left(\rho_g \vec{u} \cdot \overrightarrow{\delta S}\right) u_x = 4\rho_g \iint_S u^2 \cos\phi \, r_c d\phi dz. \tag{2-14}$$

where $\left(\rho_g \vec{u} \cdot \overrightarrow{\delta S}\right)$ is the mass flow rate across a surface element of S. Substituting Eq. (2-12a) into Eq. (2-14) and integrating the resulted equation yields F_x:

$$F_x = 4\rho_g \int_0^{\pi/2} \cos\phi \, d\phi \int_0^c \left(\frac{3u_b z r_c}{2\alpha^2 a^2}\right)^2 r_c dz$$

$$= 4\rho_g \int_0^c \left(\frac{3u_b z r_c}{2c^2}\right)^2 r_c dz = \frac{9\rho_g u_b^2}{\alpha^4 a^4} \int_0^c r_c^3 z^2 dz. \tag{2-14a}$$

From Eq. (2-13), r_c can be expressed as

$$r_c = \sqrt{\frac{1}{2}\left[a^2 - \left(\frac{z}{\alpha}\right)^2\right]}. \tag{2-15}$$

Substituting Eq.(2-15) into Eq. (2-14a) and integrating the resulting equation yields F_x:

$$F_x = \frac{9\rho_g u_b^2}{2\sqrt{2}\alpha^4 a^4} \int_0^c z^2 \left[a^2 - \left(\frac{z}{\alpha}\right)^2\right]^{3/2} dz$$

$$= \frac{9\pi}{64\sqrt{2}\alpha}\rho_g u_b^2 a^2 = \frac{0.312}{\alpha}\rho_g u_b^2 a^2. \tag{2-16}$$

The surface tension force is the product of the surface tension and the circumference of the ellipse described by Eq. (2-11),

$$F_\sigma = \sigma L = \sigma \int_{ellipse} \sqrt{(\delta r_c)^2 + (\delta z)^2} = 4\sigma a\, E(\sqrt{1-\alpha^2})$$

(2-17)

where $E(\sqrt{1-\alpha^2})$ is the complete second kind elliptic integral which decreases with a decrease in α. Also, the volume equivalent bubble diameter, d_e, is related to a and α by

$$\frac{\pi}{6}d_e^3 = \frac{4\pi}{3}\alpha a^3$$

(2-18)

or

$$a = \frac{d_e}{\sqrt[3]{8\alpha}}.$$

(2-18a)

Note that the centrifugal force is affected significantly by the aspect ratio of the bubble as well as by the bubble size and the bubble rise velocity. The bubble is not stable if F_x is larger than the surface tension force, F_σ, i.e.,

$$\frac{0.312}{\alpha}\rho_g u_b^2 \left(\frac{d_e}{\sqrt[3]{8\alpha}}\right)^2 \geq 4\sigma\left(\frac{d_e}{\sqrt[3]{8\alpha}}\right)E(\sqrt{1-\alpha^2})$$

(2-19)

or

$$u_b^2 d_e \geq \frac{8\alpha^{4/3}\,E(\sqrt{1-\alpha^2})}{0.312}\frac{\sigma}{\rho_g}.$$

(2-19a)

When the centrifugal force is larger than the surface tension force, the bubble should be stretched in the x direction. During the stretching, the aspect ratio, α, becomes smaller while d_e and u_b can be assumed to remain constant. As a result, the centrifugal force increases, the surface tension force decreases, and the bubble stretching becomes an irreversible process. When the bubble is stretched to an extent where the necking phenomenon occurs, the bubble would split into two smaller bubbles. A sequence of events in the photographs shown in Figure 2-14 confirm the proposed mechanism of bubble breakup. The bubble images in the figure are obtained at a pressure of 3.5 MPa. It can be seen from the figure that bubble stretching during rising takes place from $t = 0$ to 68 ms and the necking starts at $t = 68$ ms. At $t = 85$ ms, the bubble splits into two smaller bubbles.

Equation (2-19a) indicates that the breakup of bubbles is dictated by various factors, including bubble size, bubble rise velocity, aspect ratio of the bubble, gas density, and gas-liquid surface tension. In addition to the direct contribution to the centrifugal force as illustrated by Eqs. (2-17) and (2-19), increasing the bubble size also leads to a larger bubble rise velocity and a smaller aspect ratio of the bubble which both favor bubble breakup. As the pressure increases, the gas density increases and the surface tension decreases; thus, bubbles are less stable.

The bubble rise velocity in high pressure slurries can be calculated by a correlation developed by Luo et al. (1997b). The simplified form of that correlation for a large bubble is

$$u_b = \sqrt{\frac{2.8\sigma}{\rho_{sl}d_e} + \frac{gd_e}{2}\frac{\rho_{sl}-\rho_g}{\rho_{sl}}}$$

(2-20)

Equation (2-20) has the similar form as the modified Mendelson equation (Mendelson, 1967) of Maneri (1995), except that the slurry density here is replaced with the liquid

density in Maneri's equation. By substituting Eq. (2-20) into Eq. (2-19a), d_e can be solved from the resulting equation:

$$d_e \geq \sqrt{\frac{2\sigma}{g}\left[\frac{8\alpha^{4/3}\,\mathrm{E}\left(\sqrt{1-\alpha^2}\right)}{0.312\rho_g}\frac{\rho_{ls}}{\rho_{sl}-\rho_g} - \frac{2.8}{\rho_{sl}-\rho_g}\right]} \cong \sqrt{\frac{16\alpha^{4/3}\sigma\,\mathrm{E}\left(\sqrt{1-\alpha^2}\right)}{0.312 g\rho_g}} \qquad (2\text{-}21)$$

Therefore, the maximum stable bubble size is

$$D_{max} \approx 7.16\alpha^{2/3}\,\mathrm{E}(\sqrt{1-\alpha^2})^{1/2}\sqrt{\frac{\sigma}{g\rho_g}} \qquad (2\text{-}22)$$

The aspect ratio of bubble, α, is related to the wake angle, θ_w, by

$$\alpha = \frac{1-\cos\theta_w}{2\sin\theta_w} \qquad (2\text{-}23)$$

and the wake angle for bubbles in liquids depends on the bubble Reynolds number (Clift et al., 1978),

$$\theta_w = 50 + 190\exp\left(-0.62\,\mathrm{Re}^{0.4}\right). \qquad (2\text{-}24)$$

The wake angle of large bubbles in the liquids can be approximated as 50º since the Reynolds number is normally high. The aspect ratio is hence about 0.21 for the large bubbles in liquids and $\mathrm{E}(\sqrt{1-\alpha^2})^{1/2}$ is close to unity. For large bubbles rising in liquid-solids suspensions, the aspect ratio is approximated as 0.3 (Fan and Tsuchiya, 1990) and $\mathrm{E}(\sqrt{1-\alpha^2})^{1/2}$ is 1.018. The simplified forms of Eq. (2-22) are

$$D_{max} \approx 2.53\sqrt{\frac{\sigma}{g\rho_g}} \qquad \text{(for } \alpha = 0.21) \quad (2\text{-}25a)$$

or

$$D_{max} \approx 3.27\sqrt{\frac{\sigma}{g\rho_g}} \qquad \text{(for } \alpha = 0.3) \quad (2\text{-}25b)$$

The internal circulation model provides an estimation of the upper limit of the maximum stable bubble size, since the external stresses in the liquid phase are neglected. In actual bubble columns or slurry bubble columns, the observed maximum bubble size should be smaller than the predictions by Eqs. (2-25a) and (2-25b). Figure 2-15 shows the comparison between the experimental maximum stable bubble size obtained in the present experimental system and the predictions by different models. The experimental data of maximum stable sizes in Figure 2-15 are approximated by the maximum bubble sizes measured over the entire gas velocity range under the specified pressure, temperature, and solids concentration conditions. The comparison between the predictions and the experimental data indicates that the internal circulation model can reasonably predict the maximum stable bubble size at high pressures in the present experimental system while the observed effect of pressure on bubble size can not be explained by the Rayleigh-Taylor instability or the Kelvin-Helmhotz instability. For an air/water system, the prediction by Eq. (2-25a) for the maximum stable bubble size is 5.7 cm at 1.5 MPa, while Wilkinson (1991) observed a maximum bubble size of about 3 cm. However, Eqs. (2-25a) and (2-25b) over-predict the maximum stable size at ambient pressure, as shown in Figure 2-15. For an air/water system, the predicted maximum stable bubble size is 22 cm and the reported value is 13.2 cm, as discussed above. The over-prediction by the internal

circulation model of this work at ambient pressure suggests that the bubbles are disintegrated by disturbances in the liquid or slurry through other types of mechanisms, e.g., Rayleigh-Taylor instability (Grace et al., 1978) and Kelvin-Holmhotz instability (Kischa and Kocamustafaogullari, 1989), before the bubble size reaches the value predicted by the internal circulation model. It can be seen from Figure 2-15 that the maximum stable bubble size can be estimated by the internal circulation model at pressures higher than 5 atm; at lower pressures, models based on Rayleigh-Taylor instability (Grace et al., 1978) or Kelvin-Helmhotz instability (Kitscha and Kocamustafaogullari, 1989) should be used. To improve the prediction of the internal circulation model at low pressures, the physical properties of the liquid or the slurry and the external stresses would need to be taken into account.

Based on the internal circulation model, the inertia of the gas and gas-liquid surface tension are the dominant factors dictating the maximum stable bubble size at elevated pressures. The model illustrates an insignificant effect of solids concentration on the maximum bubble size at high pressures since the stresses in the slurry are neglected. However, at ambient pressure, the solids concentration has an indirect effect on the maximum bubble size through the variations of the shape or the aspect ratio. The maximum stable bubble size would be larger in the slurry than that in the liquid, as exhibited by Eqs. (2-25a) and (2-25b). Note that the aspect ratio in the slurry (0.3) is larger than that in the liquid (0.21) for a given pressure at high bubble Reynolds numbers.

The importance of the large bubbles to the hydrodynamics in slurry bubble columns can further be manifested through the relationship between the gas holdup correlation, given by Eq. (2-7), and the rise velocity of the maximum stable bubble, V_{max}, by

$$V_{max} = \sqrt{\frac{2.8\sigma}{\rho_{sl}D_{max}} + \frac{gD_{max}}{2}} \approx 0.71\sqrt{gD_{max}} \ . \tag{2-26}$$

Substituting Eq. (2-25a) into Eq. (2-26) yields

$$V_{max} = 1.1g^{1/2}\left(\frac{\sigma}{g\rho_g}\right)^{1/4} \tag{2-27a}$$

or

$$V_{max}^4 = 1.6g^2\frac{\sigma}{g\rho_g} = \frac{1.6g\sigma}{\rho_g} \ . \tag{2-27b}$$

Thus, the dimensionless group of $U_g^4\rho_g / \sigma g$ in Eq. (2-7) can be rearranged to

$$\frac{U_g^4\rho_g}{\sigma g} \propto \left(\frac{U_g}{V_{max}}\right)^4 \ . \tag{2-28}$$

Therefore, Eq. (2-7) can be rearranged to

$$\frac{\varepsilon_g}{1-\varepsilon_g} \propto \frac{\left(U_g/V_{max}\right)^{4\alpha}\left(\rho_g/\rho_{sl}\right)^\beta}{\cosh\left(Mo_{sl}^{0.054}\right)^{4.1}} \ . \tag{2-29}$$

The gas holdup is thus a function of a set of dimensionless groups, including U_g/V_{max}, Mo_{sl}, and ρ_g/ρ_{sl}. Thus, it is clear that the gas holdup behavior in high pressure and high temperature systems can be mimicked using low pressure and low temperature systems based on the matching of these dimensionless groups. As the gas holdup is the principal

variable that characterizes the hydrodynamic properties of bubble columns or slurry bubble columns, for high pressure bubble columns and slurry bubble columns operated under a wide range of conditions outlined in Table 2-3, the hydrodynamic similarity requires these three dimensionless groups to be similar. It is noted that this similarity rule is applicable for columns of diameters greater than 0.1 m and with the column height to diameter ratio larger than 5, under high pressure batch-liquid operating conditions.

Concluding Remarks

Experiments are conducted to investigate the effect of pressure on the hydrodynamics of a slurry bubble column. The pressure has a significant effect on the gas holdup in the column. The gas holdup increases with pressure and the pressure effect is more pronounced in slurries of higher concentration. The particle concentration also affects the gas holdup, especially at ambient pressure. At elevated pressures, the effect of the solids concentration is relatively small at gas velocities above 25 cm/s. An empirical correlation, which takes into consideration the experimental data obtained from this study and in the literature, is developed to account for the gas holdup in both the high pressure bubble columns and the slurry bubble columns. The correlation covers a wide range of liquid and gas properties, and flow conditions.

To fully understand the effect of pressure on the gas holdup in slurry bubble columns, the bubble flow characteristics during dynamic gas disengagement is analyzed using particle image velocimetry (PIV). The results indicate a dominant effect of large bubbles on bubble rise velocity in slurry bubble columns due to bubble wake attraction. Without considering bubble wake attraction, the existing DGD models may severely underestimate the holdup of small bubbles and overestimate the large bubble holdup, and thus lead to errors in estimating the gas holdup structure and the bubble size distribution, especially at high gas velocities. The PIV results also indicate that strong bubble-bubble interactions, i.e., bubble coalescence and breakup and bubble wake attraction, exist during the DGD process at ambient and high pressures.

The bubble size distribution is measured using a fiber optic probe in the high pressure slurry bubble column. It is found that bubble size at elevated pressures is significantly smaller than at ambient pressure, under all experimental conditions. The presence of particles in liquids leads to a larger bubble size, especially at ambient pressure. However, the solids concentration does not affect the maximum bubble size at gas velocities above 25 cm/s at 5.6 MPa. An internal circulation model is derived to quantify the observed pressure effect on maximum bubble size. Centrifugal force induced by internal circulation of the gas inside a bubble can disintegrate the bubble at high pressures. As pressure increases, gas inertia increases and surface tension decreases; and therefore the maximum stable bubble size decreases. The model reveals that the gas inertia and gas-liquid surface tension dictate the maximum stable bubble size at high pressures, which explains the relatively small effects of solids concentration on the maximum bubble size and on the gas holdup as observed in this study. A hydrodynamic similarity rule based on the similarity of three dimensionless groups is also proposed for high pressure operations.

Notations

a	Width of ellipse
c	Height of ellipse
D_c	Column diameter
D_{max}	Maximum stable bubble size
$d_{b,max}$	Maximum bubble size at a given gas velocity
d_e	Volume equivalent bubble diameter
d_p	Particle diameter
E	Complete second kind elliptic integral
F_x	x-component of the centrifugal force generated by gas circulation
F_σ	Surface tension force
g	Gravitational acceleration
H	Column height
h_{max}	Height of the largest bubble
K	Ratio of solids holdup to liquid holdup
l	Bubble chord length measured by probe
Mo	Morton number of the liquid
P	Pressure
Re	Bubble Reynolds number, $\rho_l d_e u_b / \mu_l$
r_c	Radius in a cylindrical coordinate system
S	Surface within bubble on which the z-component of the circulation velocity is zero
T	Temperature
t	Time
U_g	Superficial gas velocity
U_l	Superficial liquid velocity
$\overline{u^2}$	Average value of the squares of velocity differences over a distance of D_{max} across the whole flow field
u_b	Bubble rise velocity
u	r_c-component of the circulation velocity of gas inside a bubble
u_x	x-component of the circulation velocity of gas inside a bubble
V_{max}	Rise velocity of maximum stable bubble
w	z-component of the circulation velocity of gas inside a bubble
z	z-coordinate in a cylindrical coordinate system

Greeks

α	Aspect ratio of bubbles defined in Eq. (18)
Δh	Vertical distance between the two tips of the probe
τ	Time period when the bubbles is in contact with the lower tips
$\Delta\tau_1$	Time lag between the frontal surface of the bubbles intercepting the upper and lower tips
$\Delta\tau_2$	Time lag between the rear surface of the bubbles intercepting the upper and lower tips
ε	Phase holdup, or the energy input per unit mass per unit time
ϕ	Azimuthal angle in spherical coordinates or cylindrical coordinates, or volume fractions of liquid or solids in a slurry

μ	Liquid viscosity
θ	Polar angle in a spherical coordinate system
θ_w	Wake angle
ρ	Density
σ	Gas-liquid surface tension
τ	Time period during bubble contact with the probe
ξ	Parameter accounting for the effect of particles on the viscosity

Superscript
0	Gas-free liquid-solids suspension stage in a dynamic gas disengagement process

Subscripts
d	Dynamic pressure
e	Volume equivalent
g	Gas phase
l	Liquid phase
s	Solids phase
sl	Slurry

References

Akita, K., and F. Yoshida, "Gas Holdup and Volumetric Mass Transfer Coefficient in Bubble Columns," *Ind. Eng. Chem. Process Des. Develop.*, 12, 76 (1973).

Bach, H.F., and T. Pilhofer, "Variation of Gas Hold-Up in Bubble Columns with Physical Properties of Liquids and Operating Parameters of Columns," *Ger. Chem. Eng.*, 1, 270 (1978).

Batchelor, G.K., "The Stability of a Large Gas Bubble Rising through Liquid," *J. Fluid Mech.*, 184, 399 (1987).

Bellman, R. and R.H. Pennington, "Effect of Surface Tension and Viscosity on Taylor Instability," *Q. Appl. Math.*, 51, 151 (1954).

Chen, R.-C. and L.-S. Fan, "Particle Image Velocimetry for Characterizing the Flow Structure in Three-Dimensional Gas-Liquid-Solid Fluidized Beds," *Chem. Eng. Sci.*, 47, 3615 (1992).

Chen, Y.-M. and L.-S. Fan, "On the Criteria of Rayleigh-Taylor Instability at a Curved Interface by a Local Force Balance," unpublished results (1988).

Clift, R., J.R. Grace, and M.E. Weber, *Bubbles, Drops, and Particles*, Academic Press, New York (1978).

Daly, J.G., S.A. Patel, and D.B. Bukur, "Measurement of Gas Holdups and Sauter Mean Bubble Diameters in Bubble Column Reactors by Dynamic Gas Disengagement Method," *Chem. Eng. Sci.*, 47, 3647 (1992).

de Lasa, H., S.L.P. Lee, and M.A. Bergougnou, "Bubble Measurement in Three-Phase Fluidized Beds Using a U-Shaped Optical Fiber," *Can. J. Chem. Engng.*, 62, 1029 (1982).

de Swart, J.W.A., R.F. van Vliet, and R. Krishna, "Size, Structure and Dynamics of "Large" Bubbles in a Two-Dimensional Slurry Bubble Column," *Chem. Eng. Sci.*, 51, 4619 (1996).

Deckwer, W.-D., Y. Louisi, A. Zaidi, and M. Ralek, "Hydrodynamic Properties of the Fisher-Tropsch Slurry Process," *Ind. Eng. Chem. Process Des. Dev.*, 19, 699 (1980).

Deckwer, W.-D., *Bubble Column Reactors*, John Wiley and Sons, Chichester, England (1992).

Deckwer, W.-D., and A. Schumpe, "Improved Tools for Bubble Column Reactor Design and Scale-up, " *Chem. Eng. Sci.*, 48, 889 (1993)

Desphande, N.S., M. Dinkar, and J.B. Joshi, "Disengagement of the Gas Phase in Bubble Columns," *Int. J. Multiphase Flow*, 21, 1191 (1995).

Fan, L.-S., *Gas-Liquid-Solid Fluidization Engineering*, Butterworths, Stoneham, MA (1989).

Fan, L.-S. and K. Tsuchiya, *Bubble Wake Dynamics in Liquids and Liquid-Solid Suspensions*, Butterworth-Heinemann, Stoneham, MA (1990).

Fox, J. M., "Fisher-Tropsch Reactor Selection," *Catal. Lett.*, 7, 281 (1990).

Fu, W., Y. Chisti, and M. Moo-Young, "A New Method for the Measurement of Solids Holdup in Gas-Liquid-Solid Three Phase Systems," *Ind. Eng. Chem. Res.*, 34, 928 (1995).

Grace, J.R., T. Wairegi, and J. Brophy, "Break-Up of Drops and Bubbles in Stagnant Media," *Can. J. Chem. Eng.*, 56, 3 (1978).

Hill, M.J.M., "On a Spherical Vortex, " *Phil. Trans. Roy. Soc. London*, 185, 213 (1894).

Hinze, J.O., "Fumdamentals of the Hydrodynamic Mechanism of Splitting in Dispersion Processes," *AIChE J.*, 1, 289 (1955).

Idogawa, K., K. Ikeda, T. Fukuda, and S. Morooka, "Behavior of Bubbles of the Air-Water System in a Column under High Pressure," *Int. Chem. Eng.*, 26, 468 (1986).

Inga, J.R., "Scaleup and Scaledown of Slurry Reactors: A New Methodology," Ph.D. thesis, University of Pittsburgh, PA (1997).

Jiang P., T.-J. Lin, X. Luo, and L.-S. Fan, "Visualization of High Pressure (21MPa) Bubble Column," *TranIChemE*, 73, Part A, 269 (1995).

Kastaneck, F., J. Zahradnik, J. Kratochvil, and J. Cermak, "Modelling of Large-Scale Bubble Column Reactors for Non-Ideal Gas-Liquid Systems," in *Frontiers in Chemical Reaction Engineering*, ed. by Doraiswamy, L.K. and Mashelkar, R.A., 1, 330, Whiley, Bombay, India (1984).

Kitscha, J. and G. Kocamustafaogullari, "Breakup Criteria for Fluid Particles," *Int. J. Multiphase Flow*, 15, 573 (1989).

Koide, K., A. Takazawa, and M. Komura, "Gas Holdup and Volumetric Liquid-Phase Mass Transfer Coefficient in Solid-Suspended Bubble Columns, " *J. Chem. Engng. Japan*, 17, 459 (1984).

Kojima, H., B. Okumura, and A. Nakamura, "Effect of Pressure on Gas Holdup in a Bubble Column and a Slurry Bubble Column," *J. Chem. Engng. Japan*, 24, 115 (1991).

Krishna, R., P.M. Wilkinson, and L.L. VAN Dierendonck, "A Model for Gas Holdup in Bubble Columns Incorporating the Influence of Gas Density on Flow Regime Transitions," *Chem. Eng. Sci.,* 46, 2491 (1991).

Krishna, R., J.W.A. de Swart, J. Ellenberger, G. B. Martina, and C. Maretto, "Gas Holdup in Slurry Bubble Columns: Effect of Column Diameter and Slurry Concentrations," AIChE J., 43, 311 (1997).

Lee, D.J., X. Luo, and L.-S. Fan, "Gas Disengagement Technique in a Slurry Bubble Column Operated in the Coalesced Bubble Regime," paper P-14 presented at the 15th International Symposium of Chemical Reaction Engineering, Newport Beach, California, September 13-16 (1998).

Levich, V.G., *Physiochemical Hydrodynamics*, Prentice Hall, Englewood Cliffs, NJ (1962).

Li, H., and A. Prakash, "Heat Transfer and Hydrodynamics in a Three-Phase Slurry Bubble Column, " *Ind. Eng. Chem. Res*., 36, 4688 (1987).

Lin, T.-J., K. Tsuchiya, and L.-S. Fan, "Bubble Flow Characteristics in Bubble Columns at Elevated Pressure and Temperature, " *AIChE J*., 44, 545 (1998).

Liu W., N.N. Clark, and A.I. Karamavruc, "General Method for the Transformation of Chord-Length Data to a Local Bubble-Size Distribution," *AIChE J*., 42, 2713 (1996).

Luo, X., P. Jiang, and L.-S. Fan, "High Pressure Three-Phase Fluidization: Hydrodynamics and Heat Transfer," *AIChE J.*, 43, 2432 (1997a).

Luo, X., J. Zhang, K. Tsuchiya, and L.-S. Fan, "On the Rise Velocity of Bubbles in Liquid-Solid Suspensions at Elevated Pressure and Temperature," *Chem. Eng. Sci.*, 52, 3693 (1997b).

Maneri, C. C., "New Look at Wave Analogy for Prediction of Bubble Terminal Velocities," *AIChE J.*, 41, 481 (1995).

Mendelson, H. D., "The Prediction of Bubble Terminal Velocities from Wave Theory," *AIChE J.*, 13, 250 (1967).

O'Dowd, W., D.N. Smith, J.A. Ruether, and Saxena, S.C., "Gas and Solids Behavior in a Baffled and Unbaffled Slurry Bubble Column," *AIChE Journal*, 33, 1959 (1987).

Oyevaar, M., *Gas-Liquid Contacting at Elevated Pressures*, Ph.D. thesis, Twente University, The Netherlands (1989).

Petukhov, V.I. and V.A. Kolokol'tsev, "Effect of liquid viscosity on droplet entrainment and volumetric air content," *Therm. Eng.*, 12, 41-44 (1965).

Patel, S.A., J. Daly, and D. Bukur, "Holdup and Interfacial Area Measurements using Dynamic Gas Disengagement," *AIChE J.*, 35, 931 (1989).

Reilly, I.G., D.S. Scott, T.J.W. de Bruijn, and D. MacIntyre, "The Role of Gas Phase Momentum in Determining Gas Holdup and Hydrodynamic Flow Regimes in Bubble Column Operations," *Can. J. Chem. Eng.*, 72, 3 (1994).

Saxena, S.C., R. Vadivel, and A.C. Saxena, "Gas Holdup and Heat Transfer from Immersed Surfaces in Two- and Three-Phase Systems in Bubble Columns," *Chem. Eng. Comm.*, 85, 63 (1989).

Saxena, S.C. and Z.D. Chen, "Hydrodynanics and Heat Transfer of Baffled and Unbaffled Slurry Bubble Columns," *Reviews in Chemical Engineering*, 10, 193 (1994).

Saxena, S.C., "Bubble Column Reactors and Fischer-Tropach Synthesis," *Catal. Rev.-Sci. Eng.*, 37, 227 (1995).

Schumpe, A., and G. Grund, "The Gas Disengagement Technique for Studying Gas Holdup Structure in Bubble Columns," *Can. J. Chem. Eng.*, 64, 891 (1986).

Shah, Y.T., B.G. Kelkar, S.P. Godbole, and W.-D. Deckwer, "Design Parameters Estimations for Bubble Column Reactors," *AIChE J.*, 28, 353 (1982).

Shollenberger, K.A. and T.J. O'Hern, "Characterization of Slurry-Phase Flow in the LaPorte Alternative Fuels Development Unit (AFDU) Using Differential Pressure Measurements," U.S. DOE Report, under contract number DE-FC22-95 PC 95051 (1997).

Sriram, K., and R. Mann, "Dynamic Gas Disengagement: A New Technique For Assessing the Behaviour of Bubble Columns," *Chem. Eng. Sci*., 32, 571 (1977).

Tarmy, B., M. Chang, C. Coulaloglou, and P. Ponzi, "Hydrodynamic Characteristics of Three Phase Reactors," *The Chemical Engineer*, October, 18-23 (1984).

Vermeer, D.J. and R. Krishna, "Hydrodynamics and Mass Transfer in Bubble Columns Operating in the Churn-Turbulent Regime," *Ind. Eng. Chem. Process Des. Dev*., 20, 475 (1981).

Walter, J.F., and H.W. Blanch, "Bubble Break-Up in Gas-Liquid Bioreactors: Break-Up in Turbulent Flows," *Chem. Eng. J*., 32, B7 (1986).

Wilkinson, P. and L.L. van Dierendonck, "Pressure and Gas Density Effects on Bubble Break-Up and Gas Holdup in Bubble Columns," *Chem. Eng. Sci*., 8, 2309 (1990).

Wilkinson, P.M., *Physical Aspects and Scale-Up of High Pressure Bubble Columns*, Ph.D. thesis, University of Groningen, The Netherlands (1991).

Wilkinson, P., A.P. Spek, and L.L. van Dierendonck, "Design Parameters Estimation for Scale-Up of High Pressure Bubble Columns," *AIChE J.*, 38, 544 (1992).

Table 2-1. Physical properties of the Paratherm NF heat transfer fluid

(a) $T = 28°C$

P (MPa)	ρ_g (kg/m^3)	ρ_l (kg/m^3)	μ_l (Pa s)	σ_l (N/m)
0.1	1.13	870	0.026	0.029
1.48	16.5	872	0.028	0.028
2.86	32.0	874	0.031	0.027
5.62	62.8	878	0.034	0.026

(b) $T = 78°C$

P (MPa)	ρ_g (kg/m^3)	ρ_l (kg/m^3)	μ_l (Pa s)	σ_l (N/m)
0.1	0.97	846	0.0051	0.026
1.48	14.2	850	0.0054	0.024
2.86	27.4	852	0.0056	0.023
5.62	53.9	857	0.0059	0.021

Table 2-2. List of the various experimental systems and references selected

GAS/LIQUID/SOLIDS SYSTEMS	REFERENCES	SYMBOLS IN FIG. 7
Air/methanol, air/water, air/glycol, He/water, CO_2/water	Akita and Yoshida (1973)	▬
Air/tetrabromoethane, air/n-octanol, air/ethylene glycol, air/butan-diol(1,3)	Bach and Pilhofer (1978)	-
CH_4/C6/FeOx, CO/C6/FeOx, N_2/C6/FeOx, H_2/C6/FeOx	Inga (1997)	□
Air/water, air/water/glass beads	Koide et al. (1984)	+
Ar/water, N_2/water, N_2/turpentine, N_2/butanol, N_2/MEG	Krishna et al. (1991)	▲
Air/water/glass beads	Li and Prakash (1997)	◇
N_2/water/glass beads	O'Dowd et al. (1987) Saxena et al. (1989)	□
Nitrogen/water	Oyevaar (1989)	■
N_2/water	Petukhov and Kollo'tsev (1965)	△
Air/Isopar G, He/water, air/water, air/trichloroethylene	Reilly et al. (1994)	×
N_2/Drakeol-10/ZnO_x, N_2/Drakeol-10/CuO_x, N2/Drakeol-10/Alumina	Schollenberger et al. (1997)	△
N_2/n-heptane	Tarmy et al. (1984)	◆
N_2/n-heptane, N_2/MEG, N_2/water	Wilkinson et al. (1992)	○

Table 2-3. Applicable range of the gas holdup correlation

PARAMETER (UNITS)	RANGE
ρ_l (kg/m^3)	668 - 2965
μ_l (mPa-s)	0.29 - 30
σ_l (N/m)	0.019 - 0.073
ρ_g (kg/m^3)	0.2 - 90
ϕ_s (-)	0 - 0.4
d_p (μm)	20 - 143
ρ_s (kg/m^3)	2200 - 5730
U_g (m/s)	0.05 - 0.69
U_l (m/s)	0 (batch liquid)
D_c (m)	0.1 - 0.61
H/D_c (-)	> 5
Distributor types	Perforated plate, sparger, and bubble cap
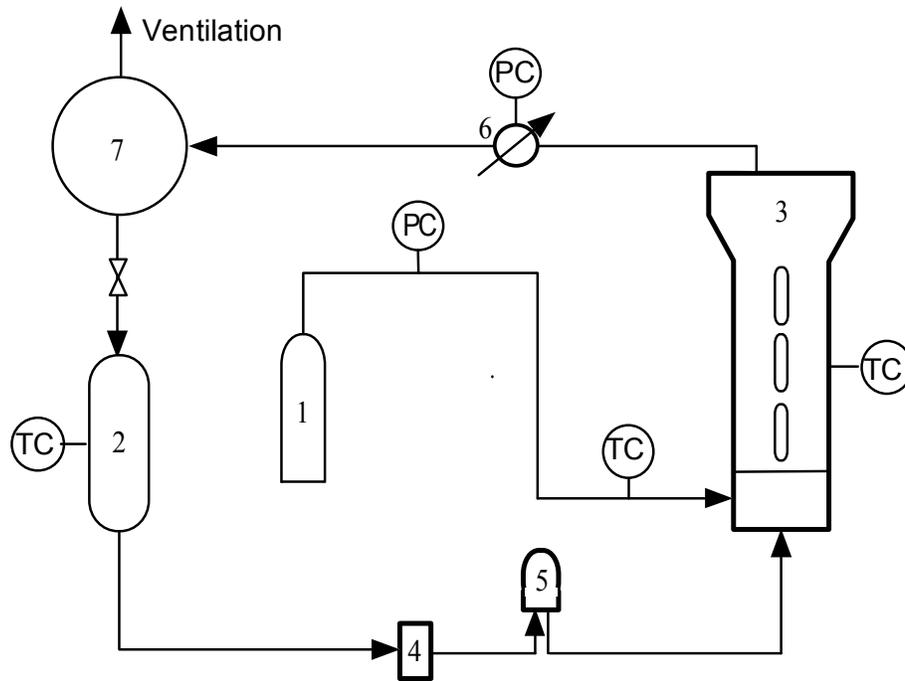
1. Nitrogen cylinders (17 MPa)
2. Liquid storage tank
3. High pressure three-phase fluidized bed
4. Liquid piston pump
5. Liquid pulsation damper

6. Back pressure regulator
7. Gas-liquid separation tank

(PC: pressure control;
TC: temperature control)

(a)
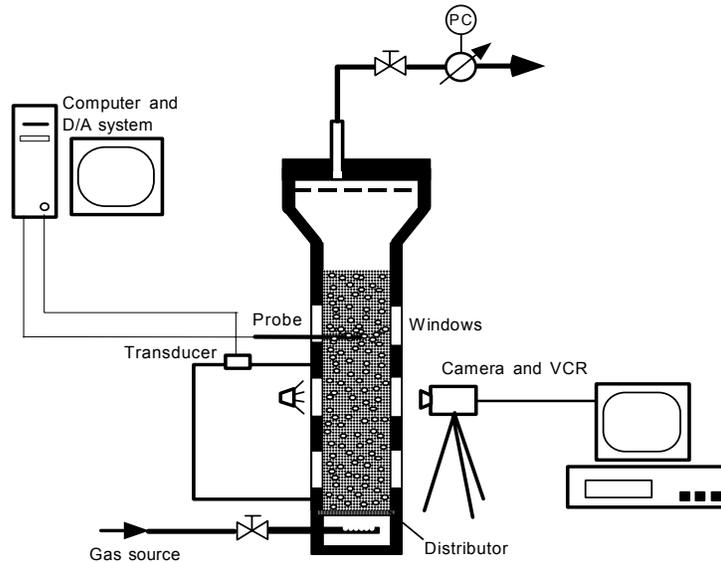
(b)

Figure 2-1.(a) Schematic of the high pressure multiphase flow and visualization system;
(b) High pressure slurry bubble column and instrumentation setup.
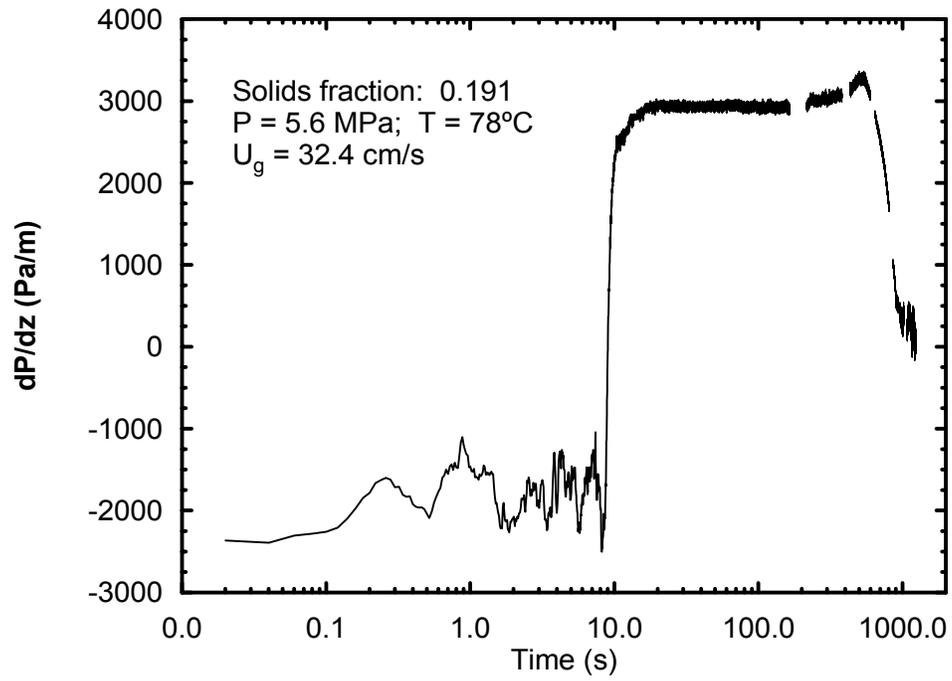
Figure 2-2. Variation of dynamic pressure drop with time in a bed collapse process.
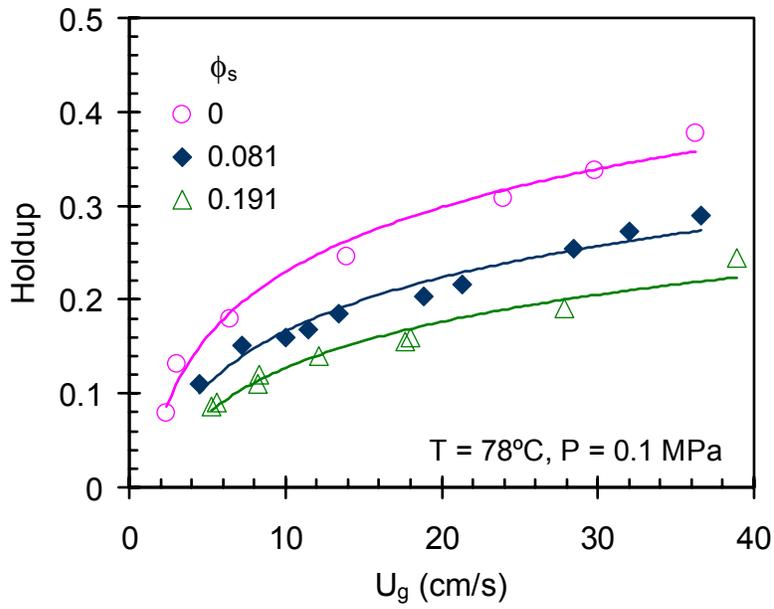
(a)
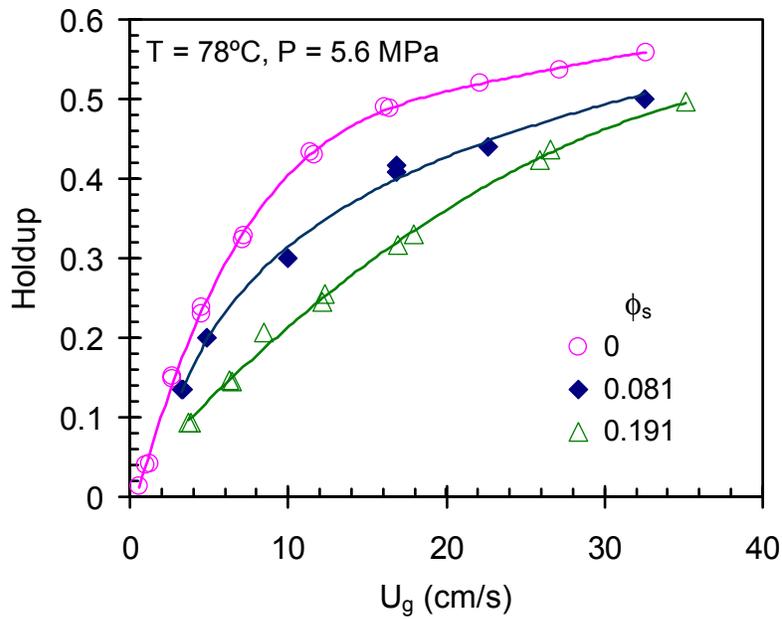
(b)

Figure 2-3. Effect of solids concentration on the gas holdup at two pressures: (a) $P = 0.1$ MPa; (b) $P = 5.6$ MPa.
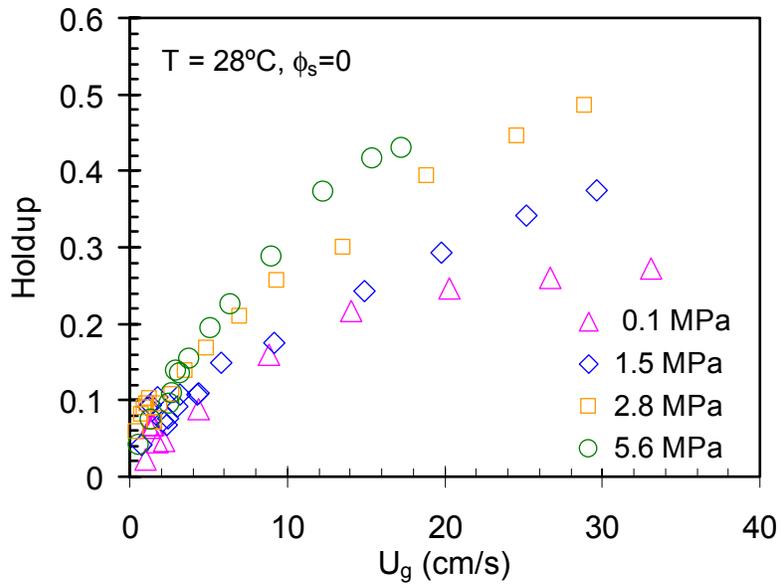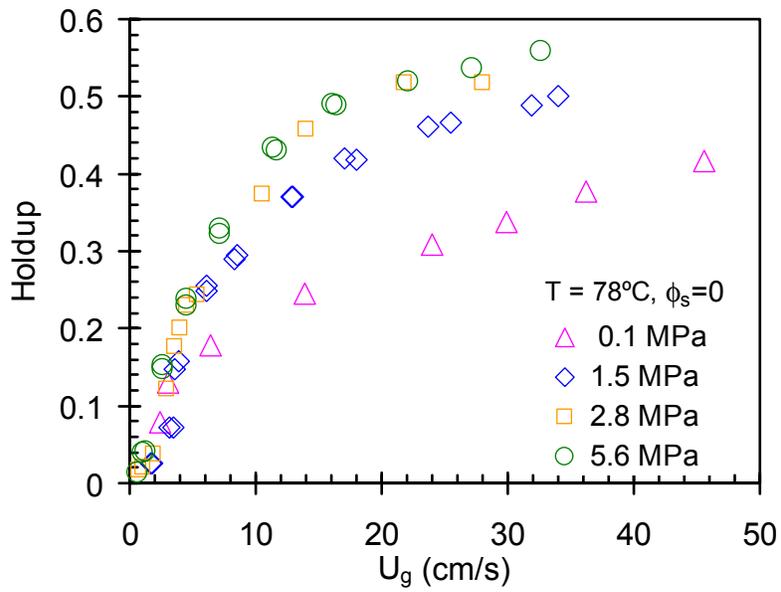
Figure 2-4. Gas holdup as a function of gas velocity at various pressures and temperatures in a bubble column (ϕ_s=0): (a) T = 28°C; (b) T = 78°C.
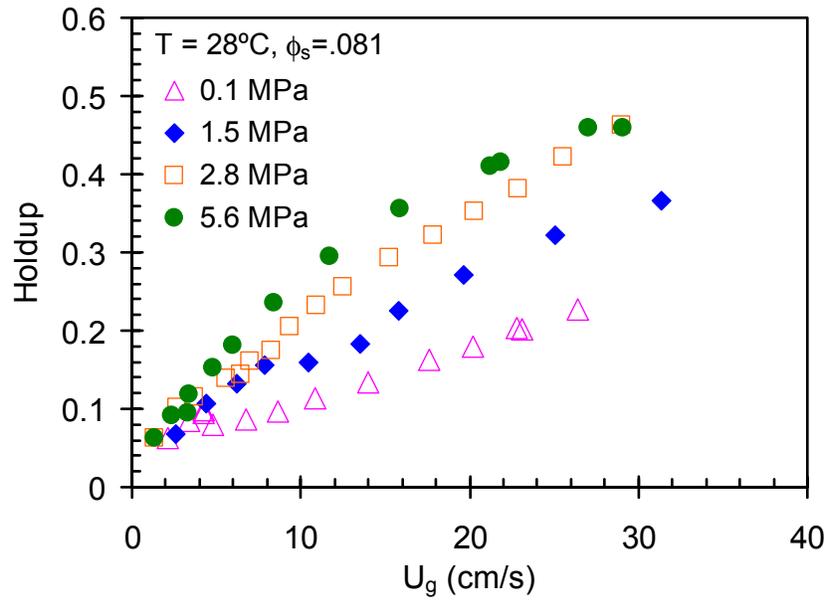
(a)
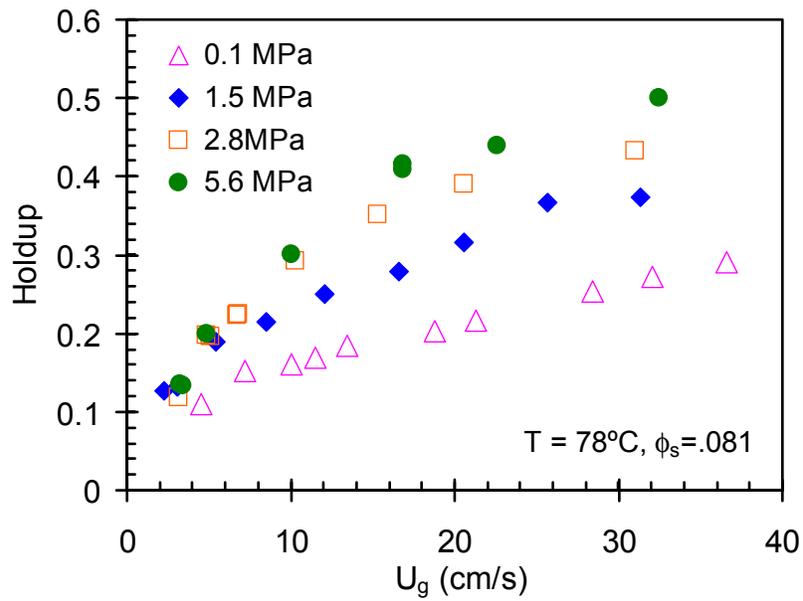
(b)

Figure 2-5. Gas holdup as a function of gas velocity at various pressures and temperatures in a slurry bubble column (ϕ_s=0.081): (a) T = 28°C; (b) T = 78°C.
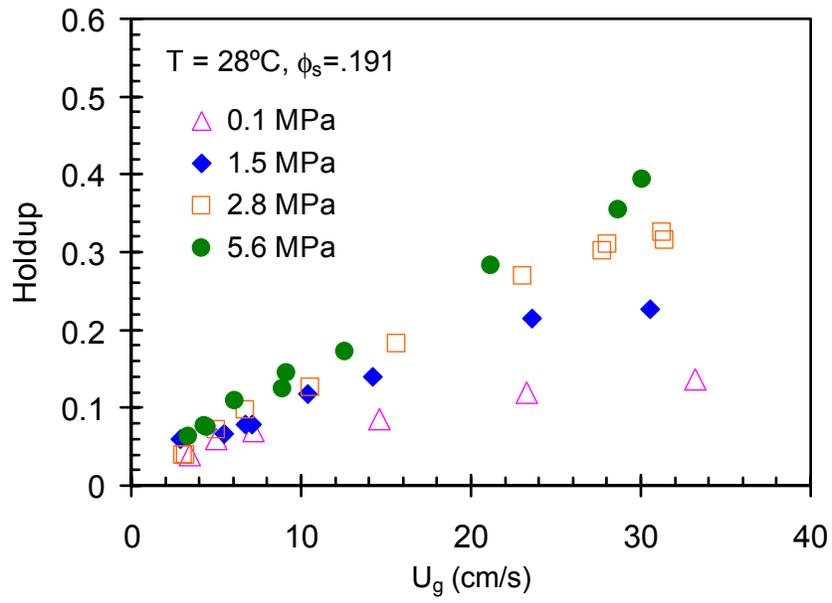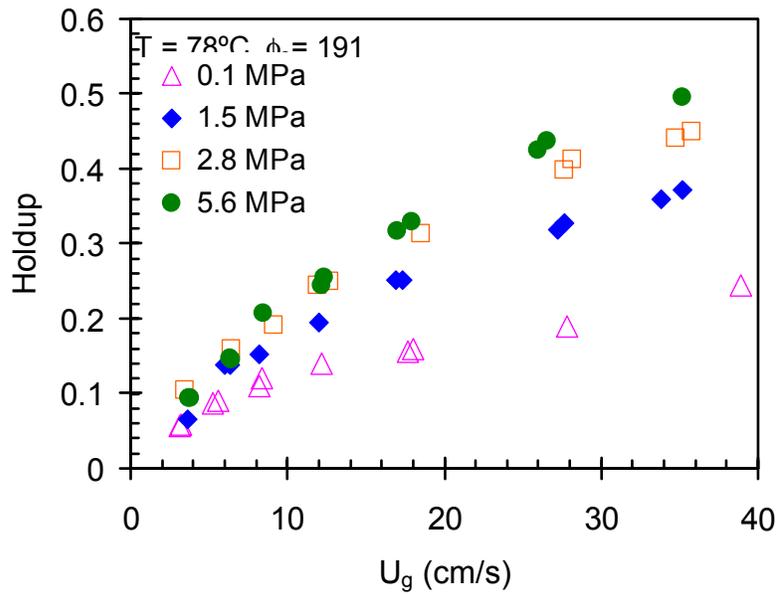
Figure 2-6. Gas holdup as a function of gas velocity at various pressures and temperatures in a bubble column (ϕ_s = 0.191): (a) T = 28°C; (b) T = 78°C.
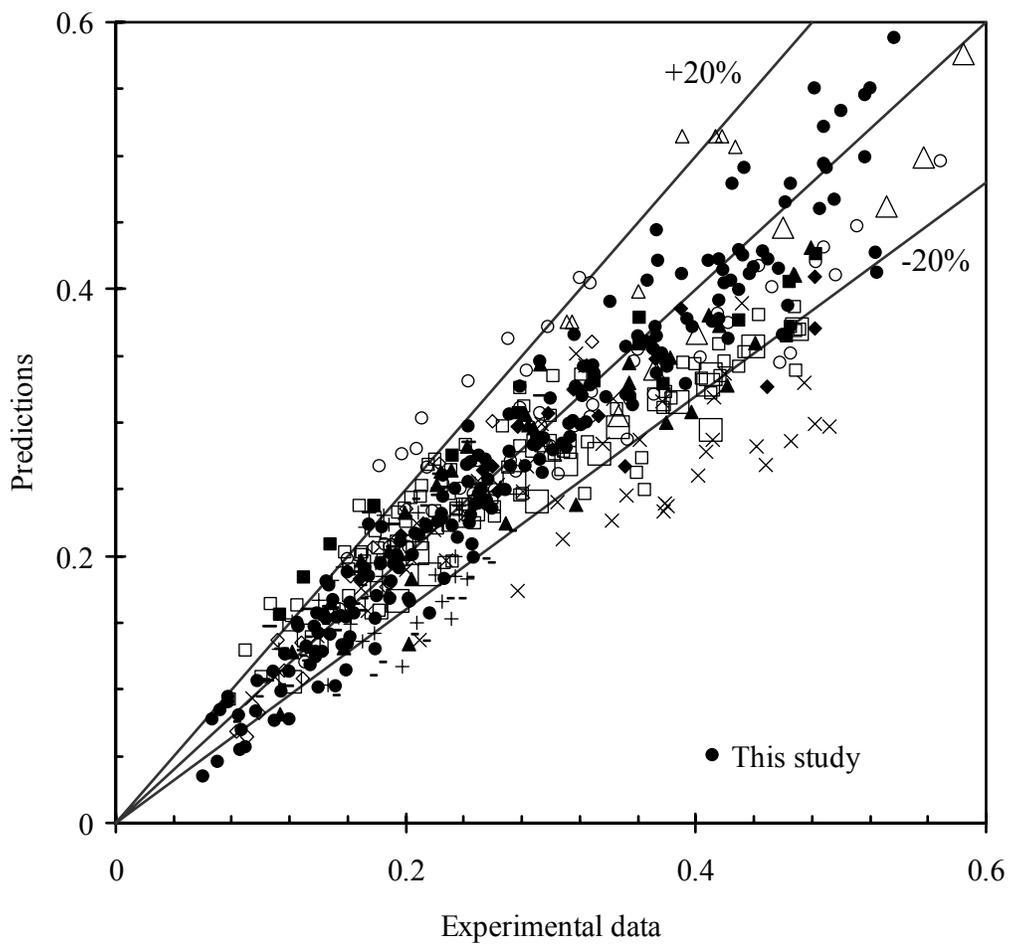
Figure 2-7. Comparison between the predicted gas holdup and the experimental data. (For literature data, see Table 2)
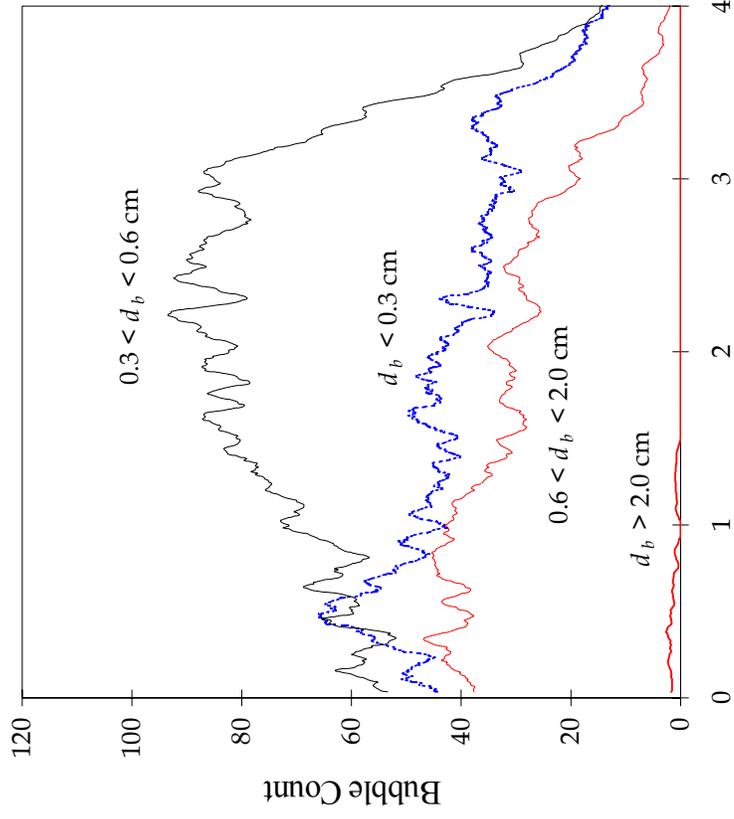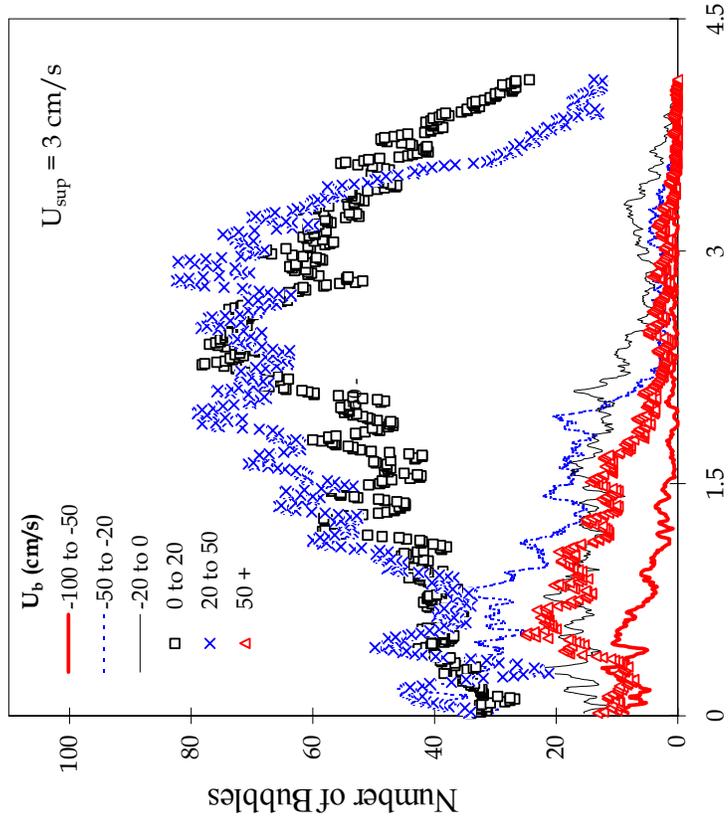
Figure 2-8. Bubble flow characteristics during a DGD process: (a) bubble size variation (U_g = 3.0 cm/s, from Lee et al., 1998); (b) bubble rise velocity variation.
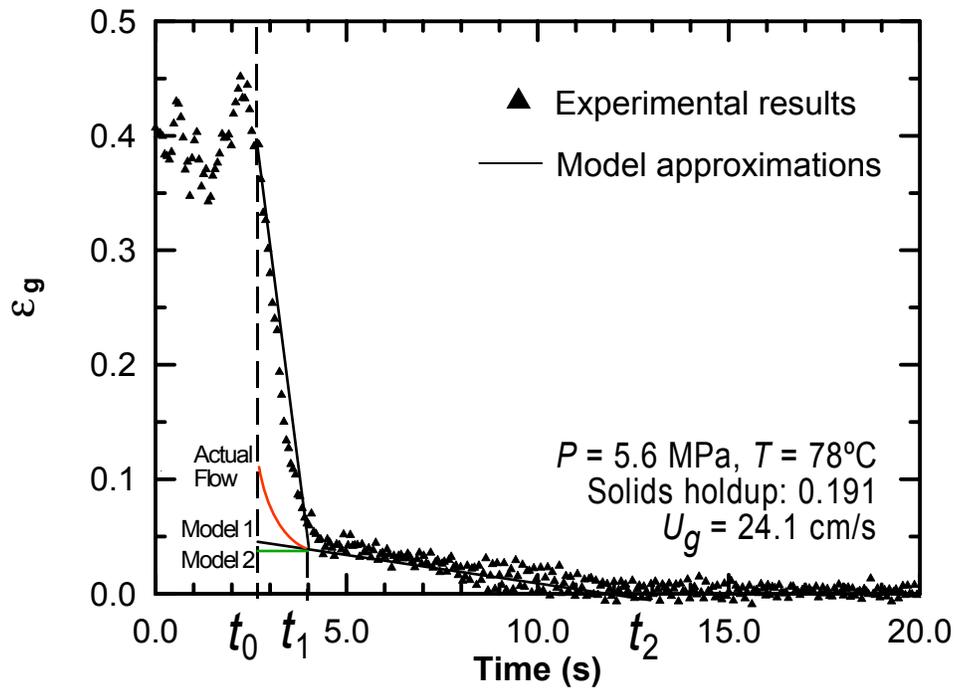
Figure 2-9. Characteristics of models 1, 2 in accounting for the experimental gas holdup variation during the gas disengagement process.
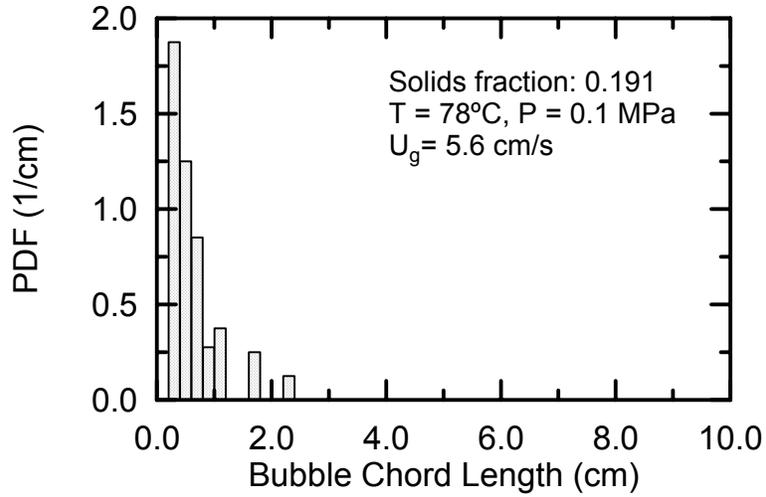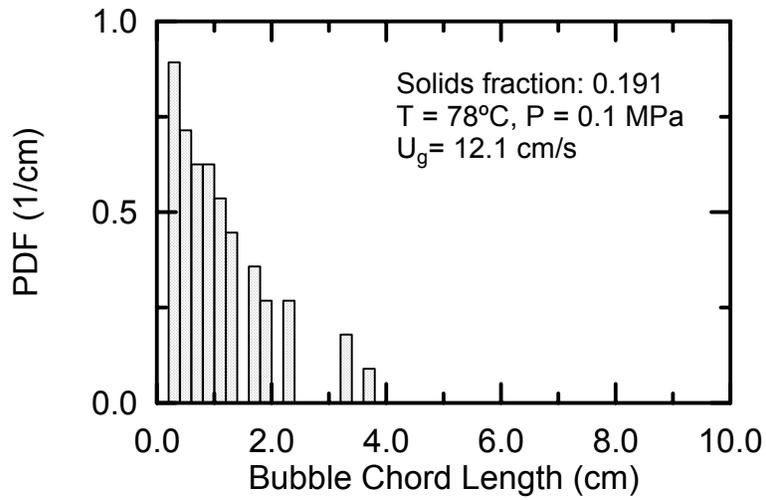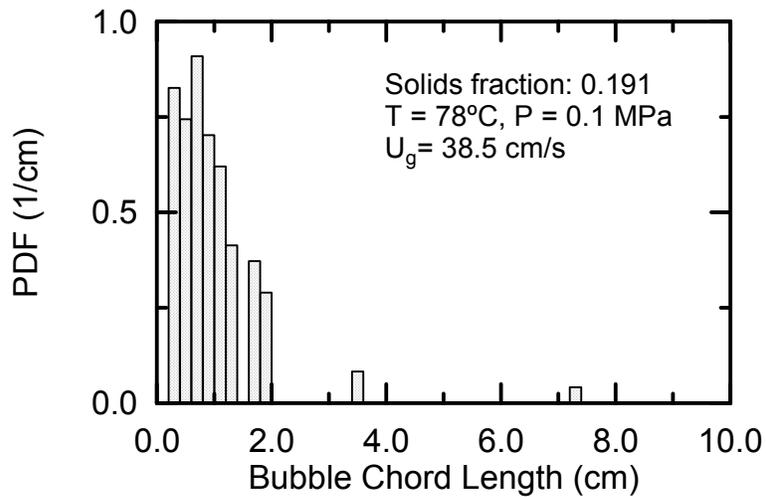
Figure 2-10.   Bubble size distribution in the slurry bubble column at ambient pressure.
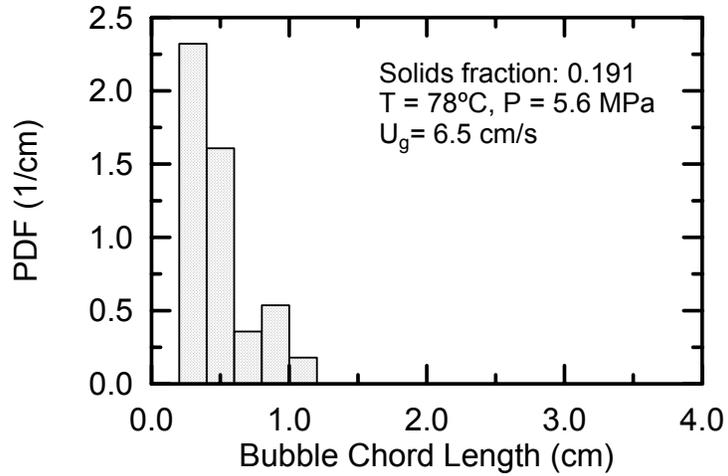
(a)
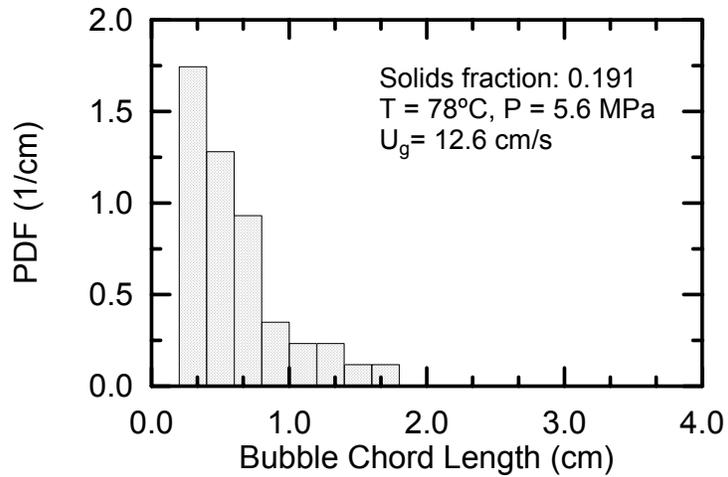
(b)
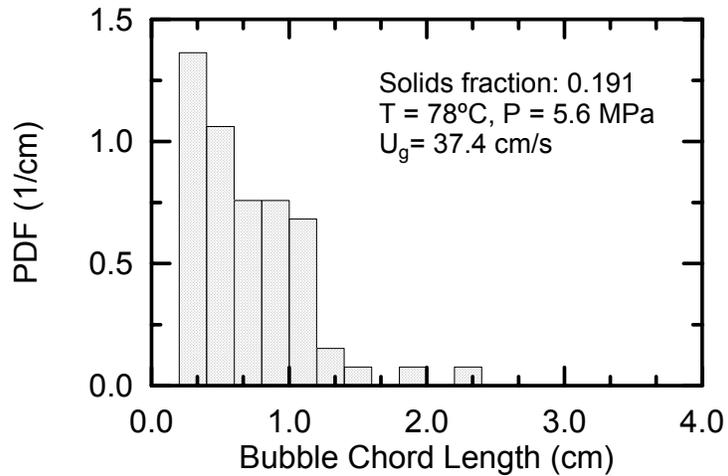
c)

Figure 2-11.   Bubble size distribution in the slurry bubble column at a pressure of 5.6 MPa.
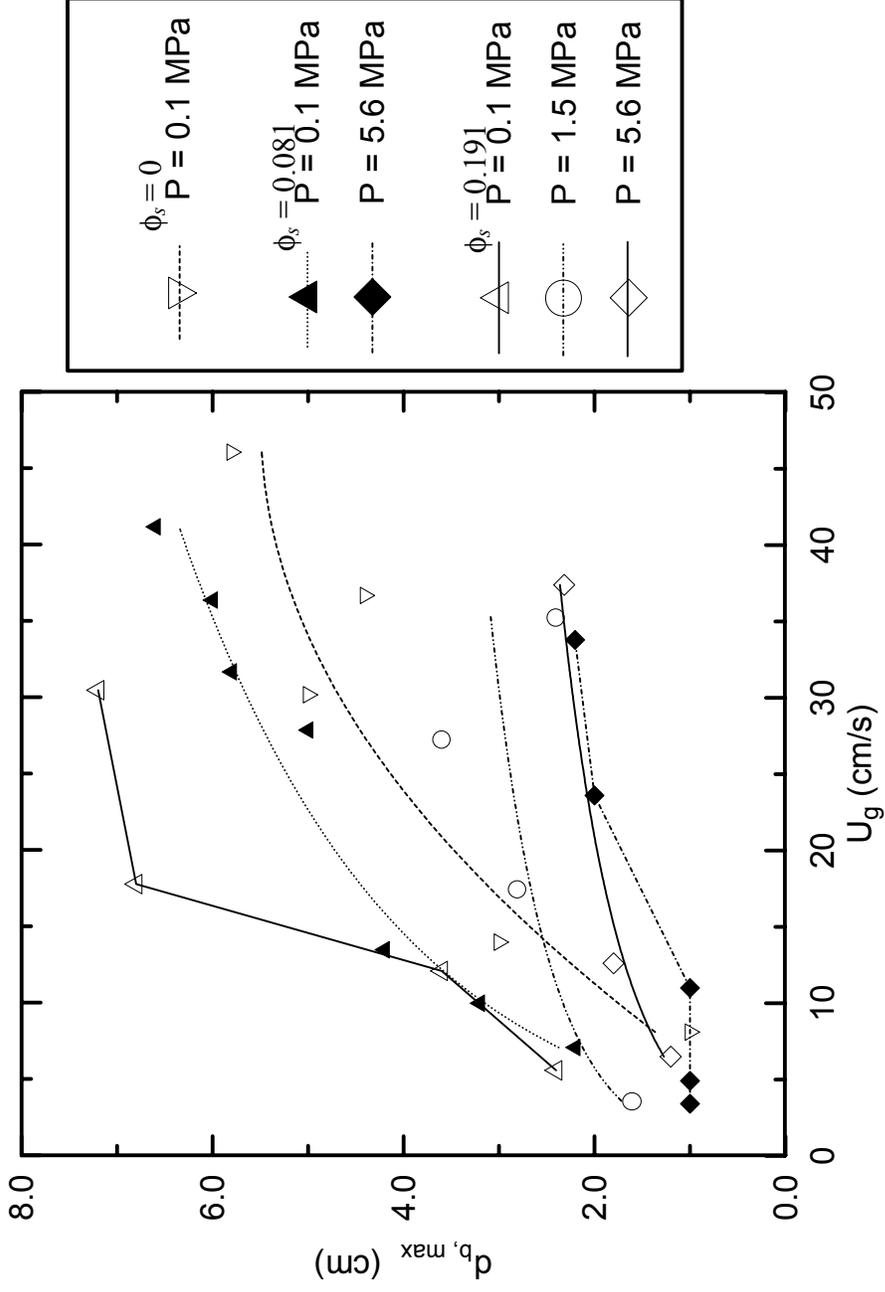
Figure 2-12. Effect of pressure on maximum bubble size in a slurry bubble column ($T = 78°C$).

63
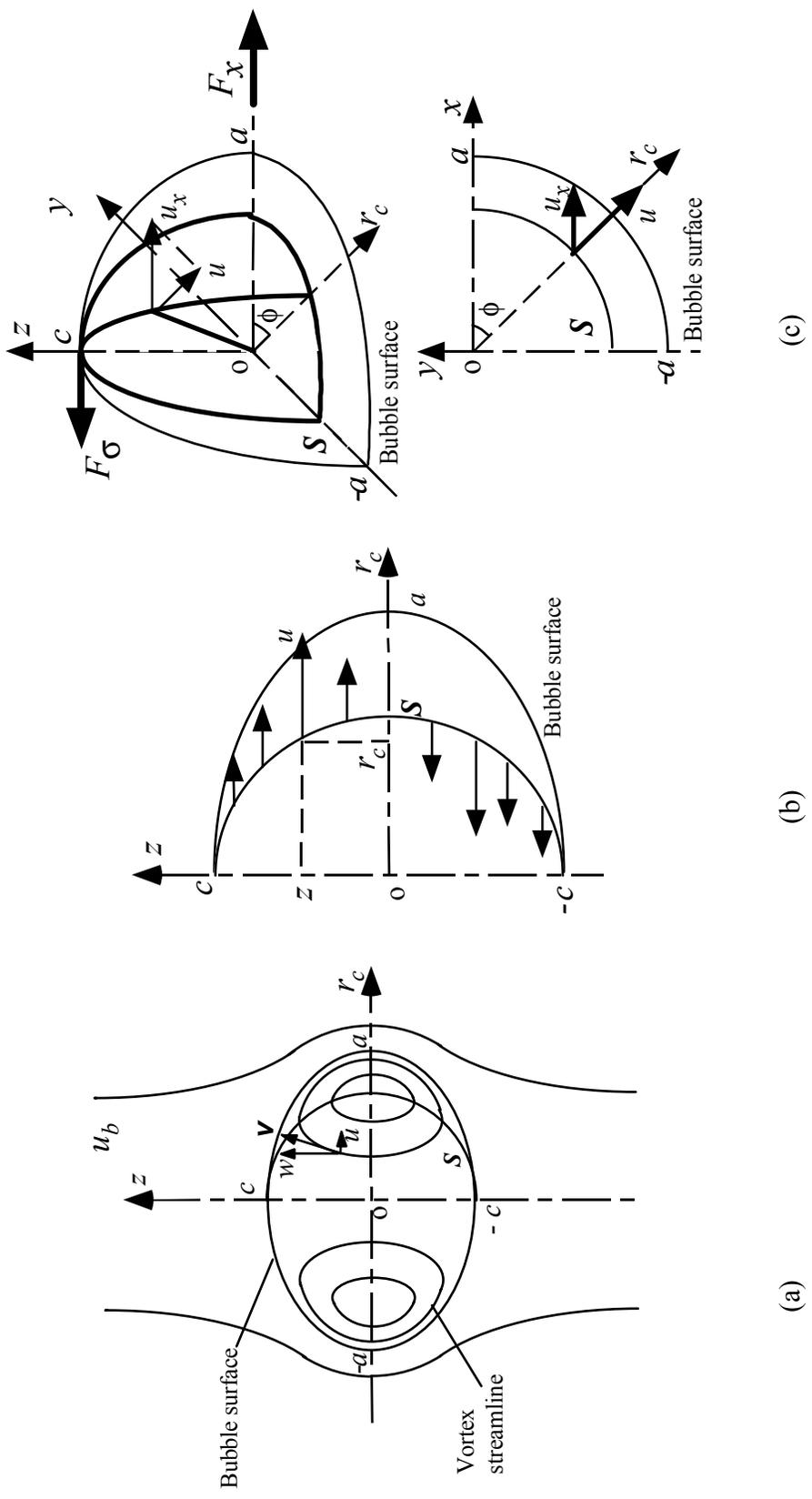
Figure 2-13. Schematic of the internal circulation model for bubble breakup: (a) internal and external flow fields; (b) circulation velocity on surface **S**; (c) force balance and 3-D view of surface **S** and the flow pattern on **S**.

64

(a) t = 0 ms (b) t = 17 ms (c) t = 34 ms

(d) t = 51 ms (e) t = 68 ms (f) t = 85 ms
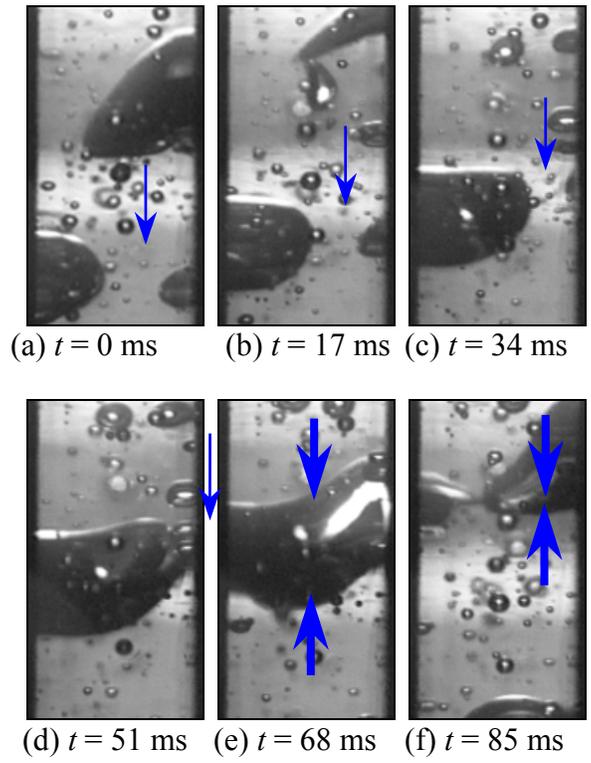
Figure 2-14. A sequence of bubble images showing the process of bubble breakup (P = 3.5 MPa).
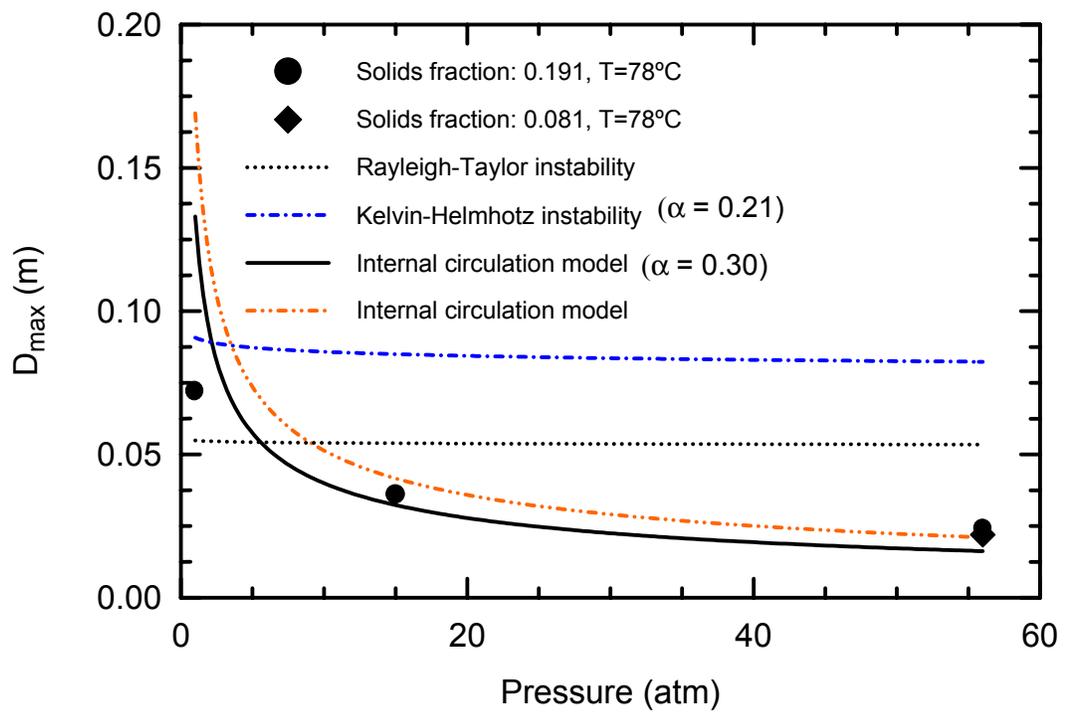
Figure 2-15. Comparison of the maximum stable bubble size between the experimental data and the predictions by the internal circulation model.

Chapter 3: Flow Fields and the Reynolds Stresses in a Bubble Column

Introduction

The use of computational fluid dynamics (CFD) has contributed to the understanding of such complicated hydrodynamic behaviors in a bubble column; however, to establish closure relationships for CFD formulations, fundamental understanding of hydrodynamic flow phenomena and gas-liquid interactions is necessary. Franz *et al.* (1984) and Menzel *et al.* (1990) used an intrusive hot-film anemometer technique to measure the liquid velocities and turbulent intensities at ambient conditions. They revealed the dynamic nature of the flow behavior in a bubble column system. They noted that the largest turbulent intensity exists in the vortical structure region between the center and the downward region close to the wall. Non-intrusive measurement techniques, *e.g.*, computer-automated radioactive particle tracking (CARPT), particle image velocimetry (PIV), and laser Doppler velocimetry (LDV) techniques, have been utilized to investigate the flow behavior in bubble column systems. Devanathan *et al.* (1990) and Yang *et al.* (1993), using the CARPT technique, measured the Reynolds stresses in a bubble column system. By tracking a neutrally buoyant single radioactive particle over a long period of time, they determined the radial profiles of the Reynolds shear and normal stresses. Chen and Fan (1992) used a PIV system to quantify the instantaneous flow field of bubble columns. The PIV system allows for the measurement of the full-field flow information; thus, the PIV system has the capability of assessing the coupling effects of the flow field that may be lost when using point measurement techniques. Chen *et al.* (1994) studied the instantaneous flow phenomena of a bubble column using flow visualization and the PIV system. The instantaneous macroscopic flow phenomena were delineated. Furthermore, through the use of the PIV system, Mudde *et al.* (1997) demonstrated that the instantaneous macroscopic phenomena were lost when the flow information was averaged. They provide further insight into the instantaneous behavior of bubble columns by refining the significance of the contribution of the vortical structures to the Reynolds stresses, thus separating out the contribution of smaller-scale or higher-frequency fluctuations. These microscopic phenomena can be associated with the gas phase in forms such as bubble coalescence and breakup, bubble wake, and bubble motion, and with the liquid phase in the form of fluctuating velocities.

Another non-intrusive fluid flow measurement technique is LDV. Numerous applications have been reported in single-phase flows as well as in dilute bubbly flows. However, its application to a bubble column system with higher gas holdup is more challenging. Mudde *et al.* (1997) used the LDV technique to investigate the dynamic flow behavior in bubble columns. They showed the fluctuating nature of the velocity field and the profiles of the Reynolds stresses. They also showed that by the frequency analysis the vortical structures are present at low frequencies of 0.1 – 0.2 Hz; furthermore, a –5/3 power law is satisfied at the high frequencies.

In this study, an LDV system is utilized to measure the flow structure in high-pressure bubble column systems. The axial and radial velocities and the Reynolds shear and normal stresses are analyzed. This study examines the effect of pressure on the flow field in bubble column systems at pressures up to 7 MPa and superficial gas velocities up to 11 cm/s.

Experimental

High-pressure multiphase flow visualization system

The experiments are conducted in a high-pressure multiphase flow visualization system, as shown in Figure 3-1. The maximum operating pressure and temperature of this system are 21 MPa and 180ºC, respectively. Two high-pressure bubble columns of 5.1 and 10.2 cm in inner diameter are used. The heights of 5.1 and 10.2-cm columns are 95.9 and 137 cm, respectively. The column is divided into three sections: plenum region, test section, and disengagement section. Three pairs of flat quartz windows are installed on the front and rear sides of the column. Each window is of 1.27 cm in width and of 9.3 cm in height. A perforated plate is used as the gas distributor, with 120 square-pitched holes of 1.5 mm diameter.

Water and Paratherm NF heat transfer fluid are used as the liquid phase and are operated in batch mode. The physical properties of Paratherm NF heat transfer can be found in Lin *et al.* (1999). The static liquid level is maintained at 70 cm above the distributor. Nitrogen from the high-pressure cylinders is introduced into the bubble column after the pressure is adjusted to desired values. The gas exiting from the column flows through a backpressure regulator and is vented into an exhaust system. The backpressure regulator controls the system pressure. The gas flow rate is measured using a high-pressure turbine flow meter.

Laser Doppler velocimetry system

A two-dimensional laser Doppler velocimetry system is used in the backscatter mode. A 300-mW air-cooled argon-ion laser and a beam separator are used to generate two pairs of beams of known wavelengths of 514.5 and 480 nm. The light is transmitted through a fiber optic cable and a probe with 25-cm focal-length lens. This configuration yields 48 fringes with fringe spaces of 3.40 and 3.22 μm and measurement volumes of $0.164 \times 0.164 \times 2.162$ mm and $0.156 \times 0.156 \times 2.05$ mm for the 514.5 and 480-nm wavelengths, respectively. The scattered light is collected through the same probe (backscatter) and a detector and processed with a signal processor.

The application of the LDV technique in bubbly flows is not as trivial as in single-phase flows because of the existence of a dispersed phase. One of the most challenging issues in the application of the LDV technique in bubbly flows is proper discrimination between the different phases. Mudde *et al.* (1997) showed that threshold technique does not contribute to the discrimination of the signals from the two phases in a bubble column system and the signals obtained in the backscatter mode predominantly represent the liquid phase.

All LDV measurements were taken at 40 and 63 cm above the distributor (in the top window) for 5.1 and 10.2-cm ID columns, respectively. Neutrally buoyant Pliolite particles of 1.02 g/cm^3 in density with a size range of $20 - 50$ μm are used as the liquid seeding particles. The distortion of the laser beams does not occur through the cylindrical column because of the flat quartz window on the cylindrical column. All measurements in this study are sampled between 600 and 1200 seconds. Only the coincident signals of axial and radial components are validated. The data rate ranges from 10 to 100 Hz. The sampling rate is relatively low because of the system limitation, *e.g.*, low power source of the laser system, thick visualization window of the high-pressure column, and, as a consequence, relatively large liquid tracers. For the cases where Paratherm NF heat

transfer fluid is used as the liquid phase, no seeding particles are used. Paratherm NF heat transfer fluid creates very tiny bubbles (< 5 μm) that make the laser beams very difficult to penetrate into the column. Measurements at the wall region are obtained for these cases and the tiny bubbles are used as liquid tracers.

The sampling rate is a strong function of the distance between the measurement point and the wall due to the light scattering caused by bubbles. Ohba *et al.* (1976) showed that the exponential relationship of the intensity of the scattered light, I, in bubbly flows with the penetration depth of the laser beams, l, and the gas holdup, ε_g, is

$$\frac{I}{I_o} = \exp\left(-\frac{3}{2}\frac{l}{d_b}\varepsilon_g\right) \tag{3-1}$$

where I_o is the light intensity without bubbles and d_b is the distance occupied by a bubble in the direction parallel to the laser beam.

Results and Discussion
Averaged velocity

The averaged radial and axial liquid velocities are obtained directly from the LDV measurements by ensemble averaging,

$$\langle u \rangle = \frac{1}{N}\sum_{i=1}^{N} u(i) \text{ and} \tag{3-2}$$

$$\langle v \rangle = \frac{1}{N}\sum_{i=1}^{N} v(i) \tag{3-3}$$

where u and v represent the radial and axial velocities, respectively, and N is the total number of samples. The ensemble-averaged properties are denoted by < >. Table 3-1 shows the averaged vertical velocity at the wall region ($r/R = 0.9$) in a 10.2-cm ID nitrogen-Paratherm NF heat transfer fluid bubble column at different U_g and P. Table 3-1 reveals the pressure effect on the axial velocity. The magnitude of downward flow at the wall region increases as the superficial gas velocity increases and as the pressure decreases. An example of the pressure effect on the profile of the averaged velocity in a 5.1-cm ID nitrogen-water bubble column at a superficial gas velocity of 5.0 cm/s is shown in Figure 3-2. The familiar gross-scale circulation is evident from the figure. At the center, the upward velocity is decreased by 25% from 0.1 MPa to 7.0 MPa. Also, a lower magnitude of downward velocity at the wall is observed at higher pressures.

Figure 3-3 shows a radial profile of the averaged axial and radial liquid velocities. The profile of the axial velocity shows that the flow is symmetrical and the net upward flow of the liquid phase agrees with the net downward flow. The radial velocity is close to zero. Note that the complete profile of the radial velocity is not obtained because only one-dimensional LDV measurement in the axial direction is performed due to the width of the visualization window on the high-pressure column, *i.e.*, the window is 1.27 cm in width and the separation of blue beams (480 nm), which measure the radial component, at the transmitter is 1.8 cm. It should be noted that the profiles are the result of averaging the swirling or spiraling motion of the large bubbles in the central bubble stream and the related structures present in the flow.

The flow behavior in a bubble column is directly related to the bubble behavior. Pressure has a significant effect on bubble dynamics, *e.g.*, bubble size, bubble rise velocity, and gas holdup, in a bubble column system (1999). As the pressure increases, gas inertial

force increases and surface tension force decreases, and thus, the stable bubble size decreases[13]. In general, the bubble size and bubble rise velocity decrease with increasing pressure. The effect of pressure on the mean bubble size in a bubble column is due to the change of bubble size distribution with pressure. At atmospheric pressure, the bubble size distribution is broader; while under high pressure, the bubble size distribution becomes narrower and is in smaller size ranges. The bubble size is affected by bubble formation at the gas distributor, bubble coalescence and bubble breakup. When the pressure is increased, the bubble size at the distributor is reduced, bubble coalescence is suppressed, and large bubbles tend to break up due to a bubble instability (1999). The combination of these factors causes the decrease of mean bubble size with increasing pressure in bubble columns, and thus, a smaller magnitude of velocities.

Probability density function of the velocity

The flow is characterized by the appearance of vortical structures that move downward adjacent to the wall regions. The alternating vortices dominate the form of the probability density functions (pdf) of the vertical component of the liquid velocity. For instance, in Figure 3-4, at the wall region the contribution of the vortices to the pdf causes a high negative peak [Figure 3-4(a)], whereas the vortex that flows downward at the opposite side gives a smaller local maximum at positive velocity in the pdf. Moving toward the center of the column, the significance of the positive peak increases and the negative peak decreases so that a 'shoulder' is formed in the pdf [Figure 3-4(b)]. In the center the negative peak is hidden in the bell-shaped curve; however, negative velocities are still observed showing the dynamic nature of the flow [Figure 3-4(c)]. As seen in the figures, the high fluctuations are present in all locations in the column. The velocity fluctuations are of the same order as the averaged velocity.

As the pressure increases, the velocity distribution narrows as shown in Figure 3-5. As mentioned earlier, the bubble size distribution is broader at ambient pressure; while under high pressures, the bubble size distribution becomes narrower and is in smaller size ranges. The bubble size distribution plays a direct role in the liquid velocity.

Reynolds stresses

The Reynolds radial and axial normal stresses and shear stresses are obtained by Equations (3-4), (3-5), and (3-6), respectively,

$$\langle u'u' \rangle = \frac{1}{N} \sum_{i=1}^{N} \{u(i) - \langle u \rangle\}^2 , \qquad (3\text{-}4)$$

$$\langle v'v' \rangle = \frac{1}{N} \sum_{i=1}^{N} \{v(i) - \langle v \rangle\}^2 , \text{ and} \qquad (3\text{-}5)$$

$$\langle u'v' \rangle = \frac{1}{N} \sum_{i=1}^{N} \{u(i) - \langle u \rangle\}\{v(i) - \langle v \rangle\} . \qquad (3\text{-}6)$$

The fluctuating velocity components in the radial, *u'*, and axial, *v'*, directions are defined by *u* - *<u>* and *v* - *<v>*, respectively. As shown in Figure 3-6, the Reynolds normal stresses are an order of magnitude higher than the shear stress; moreover, the axial normal stress is higher than the tangential normal stress.

Figure 3-7 shows the significant effect of pressure on the axial normal stress. The stress decreases as the pressure increases. Again the bubble size plays an important role.

The mean bubble size becomes smaller and the bubble size distribution as well as the velocity distribution become narrower at higher pressures, and thus, the fluctuations of the liquid phase induced by the gas phase, *e.g.*, bubble wake, bubble motion, *etc.*, become smaller.

The nature of the normal stresses is evident by considering the swirling motion of the central bubble stream. In the center of the column, the flow is more frequently upward, whereas in the vortical region, the flow dynamically changes from upward to downward depending on the location of the central bubble stream. The flow in this region, therefore, experiences large fluctuations in the axial component of the liquid velocity, leading $\langle v'v' \rangle$ to peak closer to the center of vortical structures rather than in the center where the motion is primarily directed upward. The swirling motion of the central bubble stream leads to the peaking in $\langle u'u' \rangle$ at the central portion of the column, since the horizontal velocity attains its highest magnitude in the center while the rather uniform downflow or upflow closer to the wall regions does not contribute as significantly to the radial fluctuations. Alternatively, the nature of the normal stresses can be explained by the dominance of the flow by the vortical structures.

Table 3-2 shows the Reynolds stresses for various U_g and P at the wall region (r/R = 0.9) in a 10.2-cm ID bubble column using nitrogen-Paratherm NF heat transfer fluid. The Reynolds normal stresses increase with U_g, but it decreases with P as shown in the table. The table also shows that a significant increase in the Reynolds stress is observed in the heterogeneous flow regime from the homogeneous flow regime (U_g = 0.5 cm/s). It should be noted that the liquid-phase turbulence plays a critical role during the regime transition. A higher gas density has a stabilizing effect on the flow, and the gas fraction at the instability point increases with gas density, while the gas velocity at the instability point only slightly increases with gas density. Increasing pressure delays the regime transition.

Time series

Analyzing a time series of the instantaneous velocity yields more detailed information in the flow of the liquid phase. Figure 3-8(a) shows a series for the axial velocity obtained in the 5.1-cm ID nitrogen-water bubble column at U_g = 5.0 cm/s and P = 3.5 MPa. The velocity is taken at r/R = 0.8. From the figure, the low-frequency vortical structure is evident. The time series for other radial positions have a similar trend, except at the wall region where the downward flow dominates and the fluctuation of the radial velocity is damped by the wall, and at the center where the presence of the vortical structure is less dominant in the vertical velocity. Also, Figure 3-8(b) shows the bubble interfering with the signal, which causes the sampling interval to be random.

Due to the nature of the LDV burst, the LDV velocity data are obtained at irregular time intervals as shown in Figure 3-8(b). To obtain a power spectral density of the time series from the LDV velocity data, linear interpolation is applied to the data. Figure 3-9 shows the power spectral density of the axial velocity shown in Figure 3-8. Again, the low-frequency vortical structure dominates the flow, *i.e.*, the power spectral density shows a distinct peak at frequencies of 0.1 – 0.2 Hz. The time series shows that the velocity field can be decomposed into a low-frequency contribution due to the vortical structure and high-frequency contributions[8]. The contribution from the vortical structure is very similar for all cases. The pressure effect on the power spectral density is not clearly shown in this

study. Due to the relatively low sampling frequency, as mentioned earlier, the high-frequency analysis is limited in this study.

Concluding Remarks

The investigation of the flow behavior in bubble columns using the LDV measurement technique reveals that the pressure has a significant effect on the flow. The ensemble-averaged velocity shows the gross-circulation pattern in a bubble column, and, as the pressure increases, the magnitudes of the averaged velocity of the liquid phase at the center and in the wall region decrease. The Reynolds normal stresses are an order of magnitude larger than the Reynolds shear stress. The Reynolds stresses decrease with increasing pressure. The fluctuation of the liquid phase caused by bubbles is damped out as the pressure increases because of a narrower bubble size distribution with a smaller mean bubble size at elevated pressures. The fluctuation of the liquid velocity is of the same order of magnitude as the averaged velocity. From the pdf's and the power spectral density functions, it is observed that the vortical structure dominates the low-frequency fluctuations in bubble column systems.

Notations

d_b	bubble diameter
I	scattered light intensity in bubbly flows
I_o	scattered light intensity without bubbles
l	penetration length of laser beam
f	frequency
N	total number of sampled data
P	pressure
r	radial coordinate in the column
R	column radius
t	time
u	radial velocity of the liquid phase
u'	fluctuating component of the radial velocity of the liquid phase
u''	high-frequency fluctuating component of the radial velocity of the liquid phase after removing the average and the contribution of the vortical structures
v	axial velocity of the liquid phase
v'	fluctuating component of the axial velocity of the liquid phase
u''	high-frequency fluctuating component of the axial velocity of the liquid phase after removing the average and the contribution of the vortical structures
U_g	superficial gas velocity

Greek letter
ε_g	gas holdup

Symbol
$<>$	averaging operator

References

Fan, L.-S. *Gas-Liquid-Solid Fluidization Engineering*, Butterworths; Stoneham: MA, 1989.

Franz, K.; Börner, T.; Kantorek, H. J.; Buchholz, R. Flow structures in bubble columns. *Ger. Chem. Eng.* 1984, *7*, 365.

Menzel, T.; In Der Weide, T.; Staudacher, O.; Wein, O.; Onken, U. Reynolds shear stress for modeling of bubble column reactors. *Ind. Eng. Chem. Res.* 1990, *29*, 988.

Devanathan, N.; Moslemian, D.; Dudukovic, M.P. Flow mapping in bubble columns using CARPT. *Chem. Eng. Sci.* 1990, *45*, 2285.

Yang, Y. B.; Devanathan, N.; Dudukovic, M. P. Liquid backmixing in bubble columns via computer-automated radioactive particle tracking (CARPT). *Exp. Fluids.* 1993, *16*, 1.

Chen, R.C.; Fan, L.-S. Particle image velocimetry for characterizing the flow structure in three-dimensional gas-liquid-solid fluidized beds. *Chem. Eng. Sci*. 1992, *47*, 3615.

Chen, R.C.; Reese, J.; Fan, L.-S. Flow structure in a three-dimensional bubble column and three-phase fluidized bed. *AIChE J.* 1994, *40*, 1093.

Mudde, R. F.; Lee, D. J.; Reese, J.; Fan, L.-S. Role of coherent structures on Reynolds stresses in a 2-D bubble column. *AIChE J.* 1997, *43*, 913.

Mudde, R. F.; Groen, J. S.; Van Den Akker, H. E. A. Liquid velocity field in a bubble column: LDA experiments. *Chem. Eng. Sci.* 1997, *52*, 4217.

Lin, T.-J.; Tsuchiya, K.; Fan, L.-S. Bubble flow characteristics in bubble columns at elevated pressure and temperature. *AIChE J.* 1999, *44*, 545.

Ohba, K.; Kishimoto, I.; Ogasawara, M. Simultaneous measurement of local liquid velocity and void fraction in bubbly flows using a gas laser – Part I: Principle and measuring procedure. *Tech. Rep. Osaka Univ.* 1976, *26*, 547.

Fan, L.-S.; Yang, G. Q.; Lee, D. J.; Tsuchiya, K.; Luo, X. Some aspects of high-pressure phenomena of bubbles in liquids and liquid-solid suspensions. *Chem. Eng. Sci.* 1999, *54*, 4681.

Luo, X.; Lee, D. J.; Lau, R.; Yang, G. Q.; Fan, L.-S. Maximum stable bubble size and gas holdup in high pressure slurry bubble columns. *AIChE J.* 1999, *45*, 665.

Table 3-1. Averaged downward velocity (cm/s) in a 10.2-cm ID nitrogen-Paratherm NF
heat transfer fluid bubble column at $r/R = 0.9$ and various U_g and P

P (MPa) U_g (cm/s)	0.1	1.48	4.24
0.5	-7.76	-5.20	-4.20
5.5	-11.3	-10.9	-9.95
11.0	-14.5	-13.0	-12.9

Table 3-2. The Reynolds normal stresses in a 10.2-cm ID nitrogen-Paratherm NF heat
transfer fluid bubble column at $r/R = 0.9$ and various U_g and P

P (MPa) U_g (cm/s)		0.1	1.48	4.24
0.5	$<u'u'>$	144.6	49.72	38.35
	$<v'v'>$	452.9	94.31	109.3
5.5	$<u'u'>$	409.9	280.8	193.8
	$<v'v'>$	1052.0	566.4	445.0
11.0	$<u'u'>$	588.75	321.8	228.3
	$<v'v'>$	1501	657.0	502.2

Figure 3-1. Schematic diagram of a high-pressure multiphase visualization system.
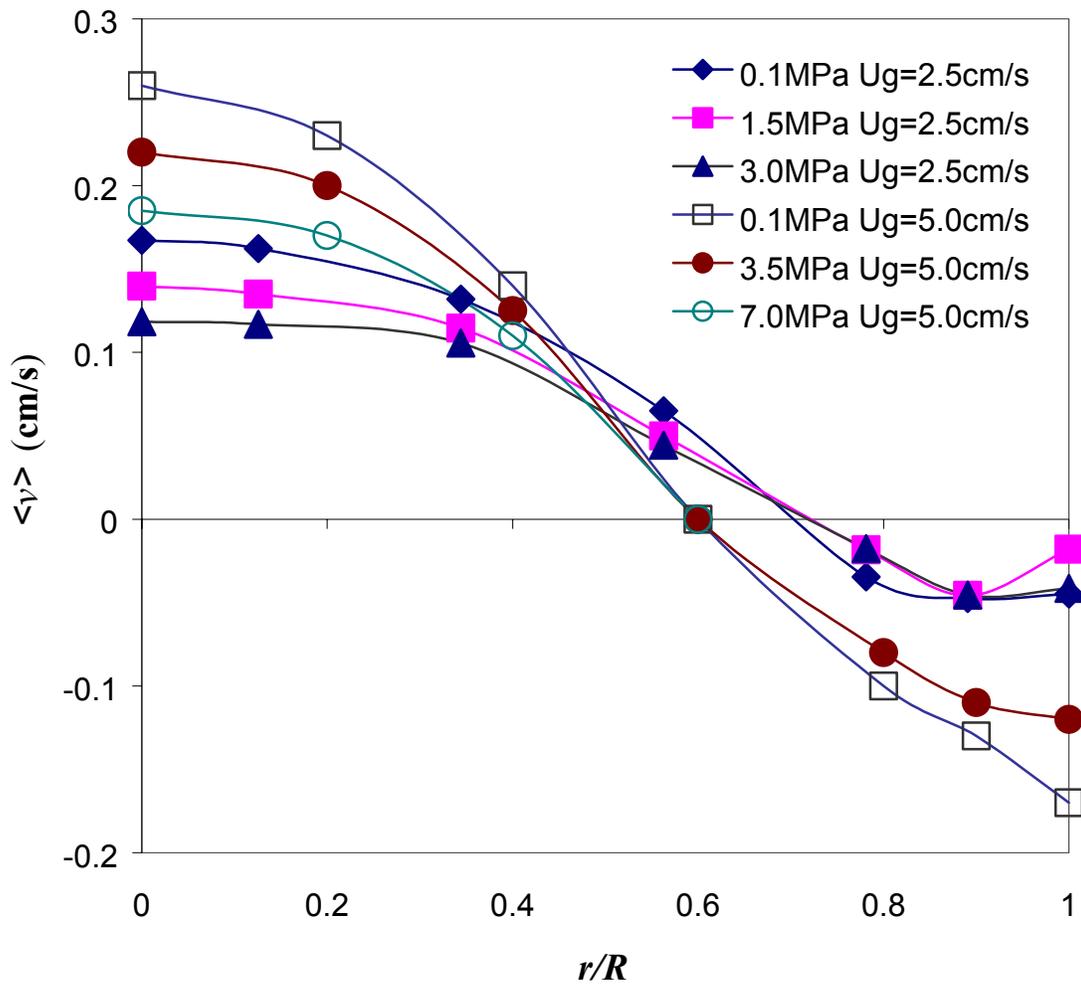
Figure 3-2. Pressure effect on the averaged liquid velocity in a 5.1 cm i.d. nitrogen-water bubble column at Ug = 2.5 and 5.0 cm/s and + = 0.1, 1.5, 3.5 and 7.0 MPa.
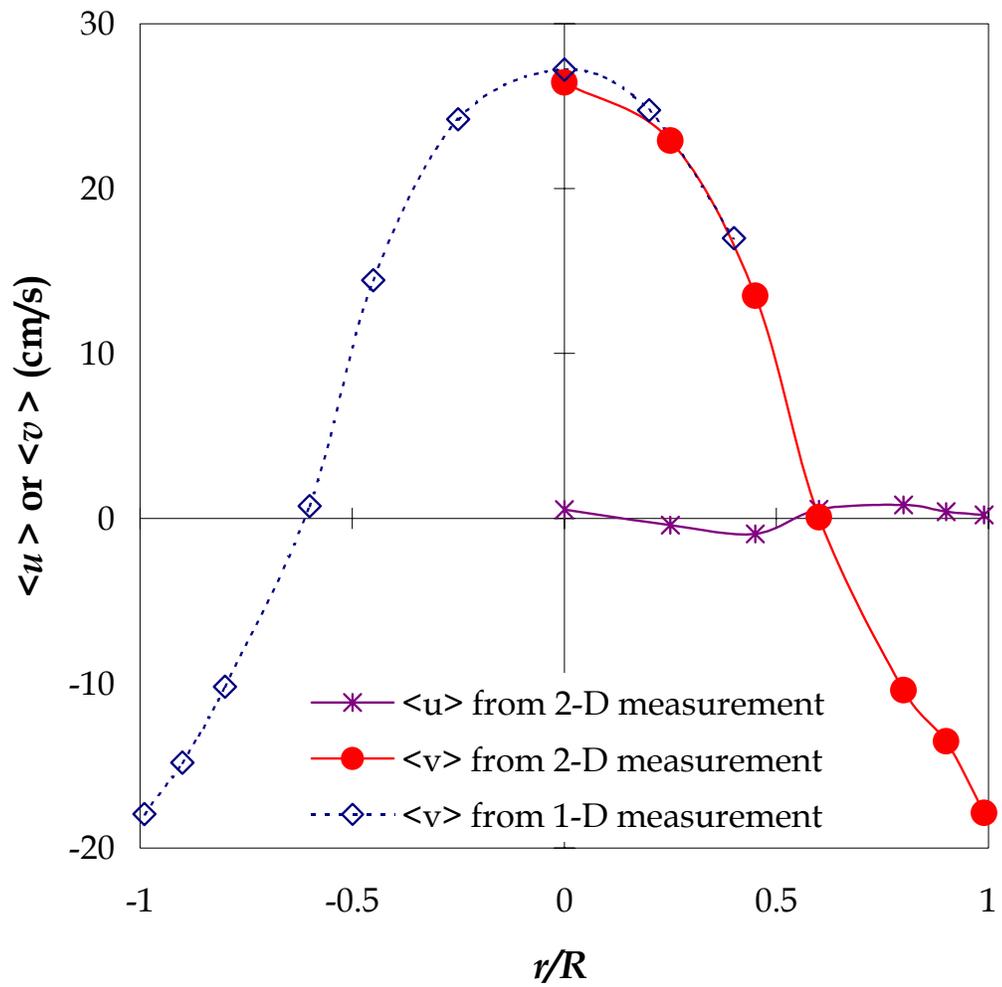
Figure 3-3. Complete profile of the averaged liquid velocity in a 5.1 cm i.d. nitrogen-water bubble column at $U_g = 5.0$ cm/s and ambient conditions.
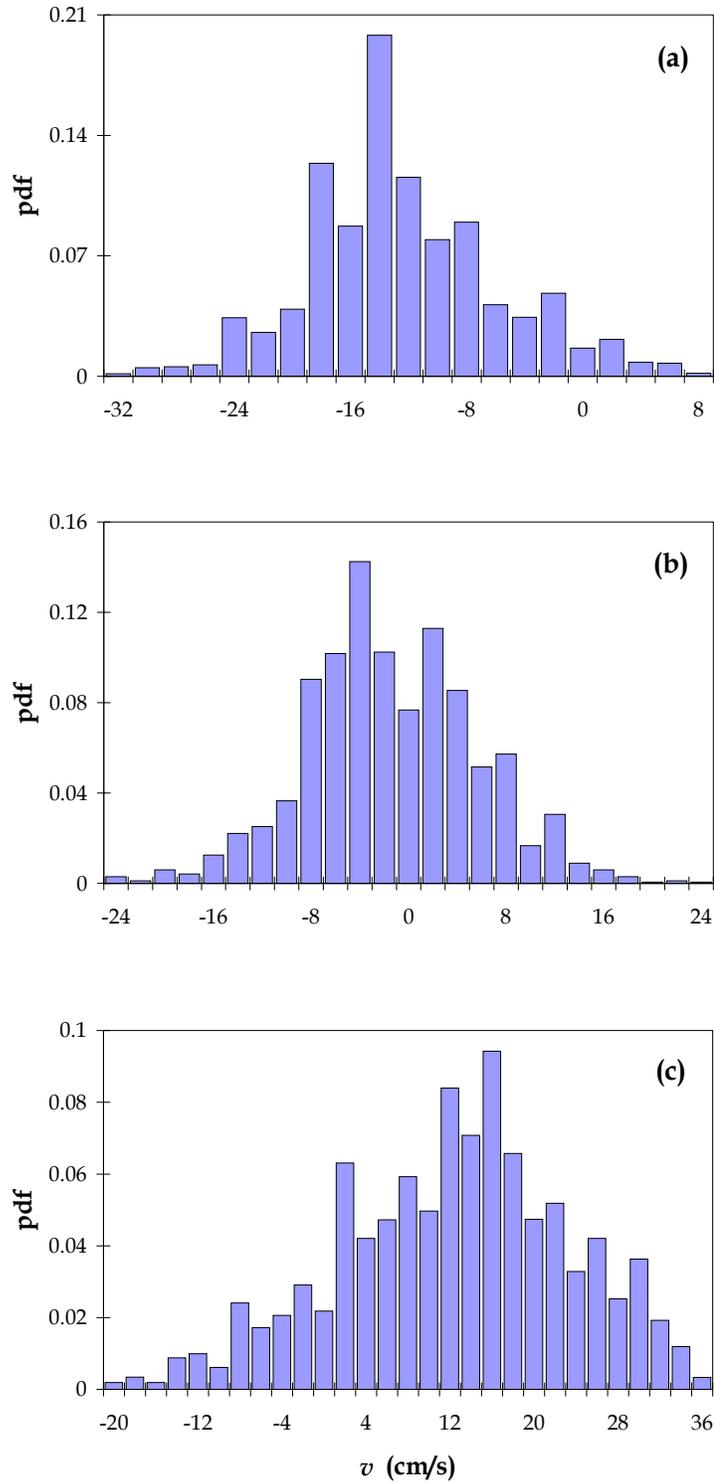
Fgure 3-4. pdf's of the axial liquid velocity component for the 5.1 cm i.d. nitrogen-water bubble column at Ug = 5.0 cm/s, P = 7.0 MPa, and r/R = (a) 0.99, (b) 0.5, and (c) 0.
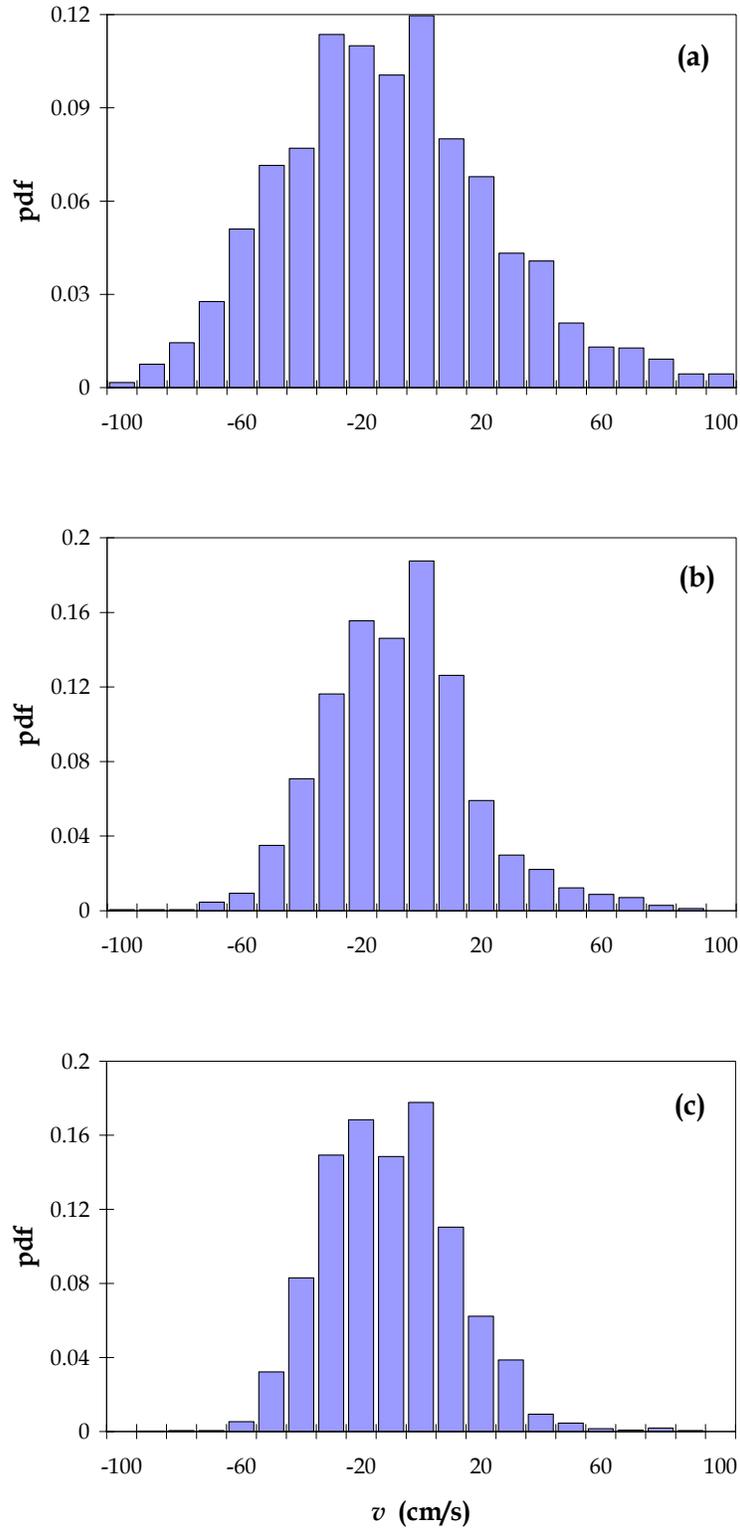
Figure 3-5. Pressure effect on pdf's of the axial liquid velocity component for the 10.2 cm
i.d. nitrogen-Paratherm NF heattransfer fluid bubble column at $U_g = 11$ cm/s, r/R = 0.9,
and P = (a) 0.1, (b) 1.48, and (c) 4.24 MPa.
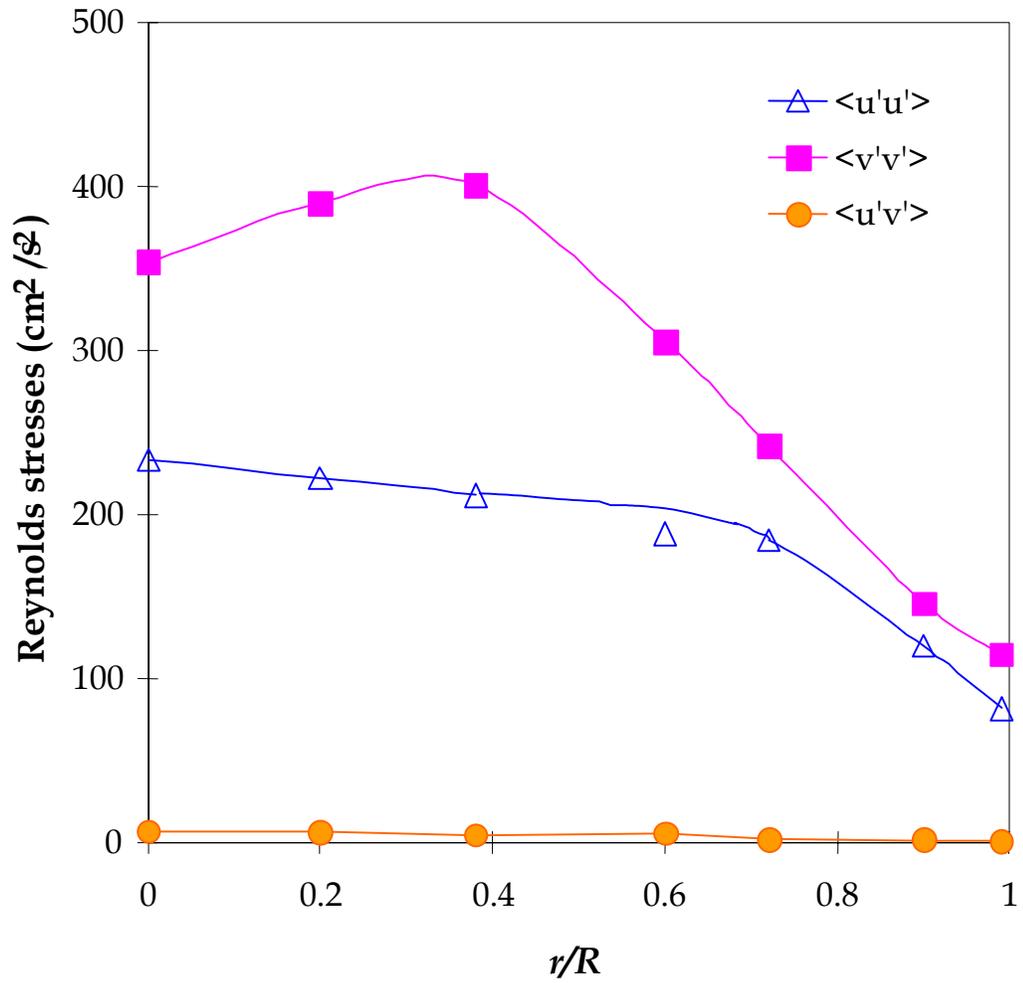
Figure 3-6. Profiles of the Reynolds stresses component for the 5.1 cm i.d. nitrogen-water bubble column at U_g = 5.0 cm/s and P = 7.0 MPa.
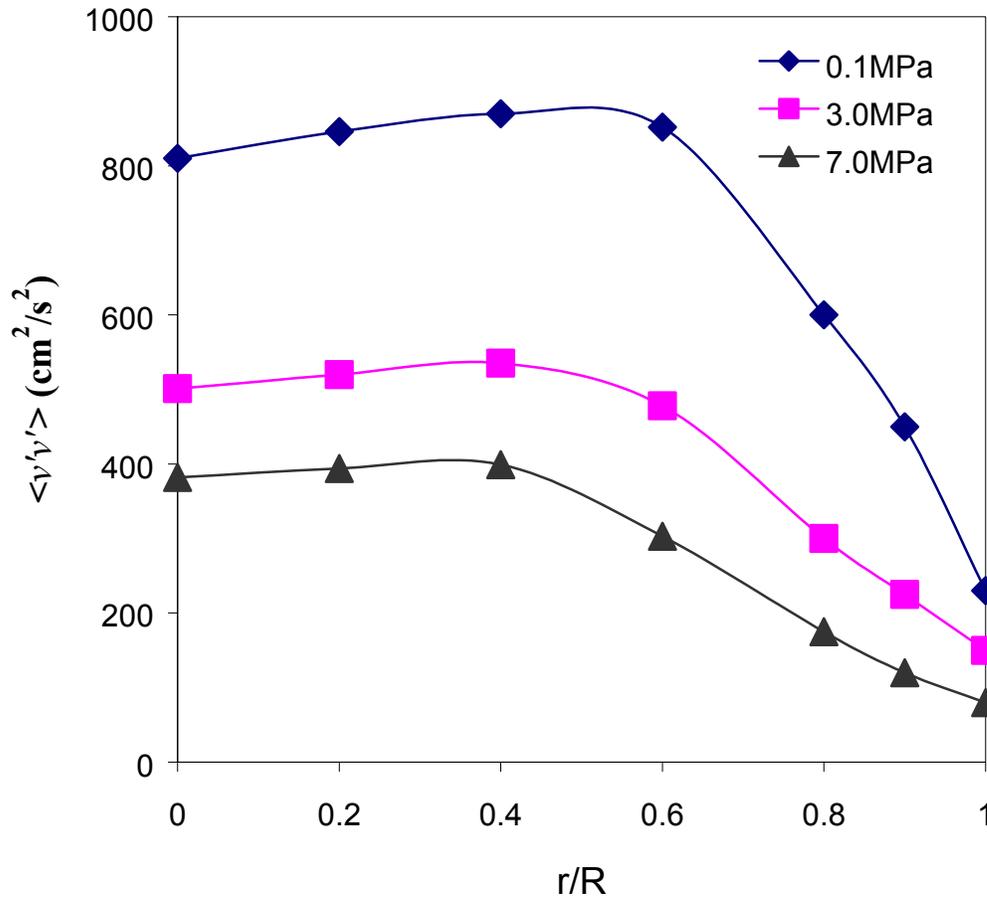
Figure 3-7. Pressure effect on the Reynolds stresses for the 5.1 cm i.d. nitrogen-water bubble column at $U_g = 5.0$ cm/s and $P = 0.1$, 3.0 and 7.0 MPa.
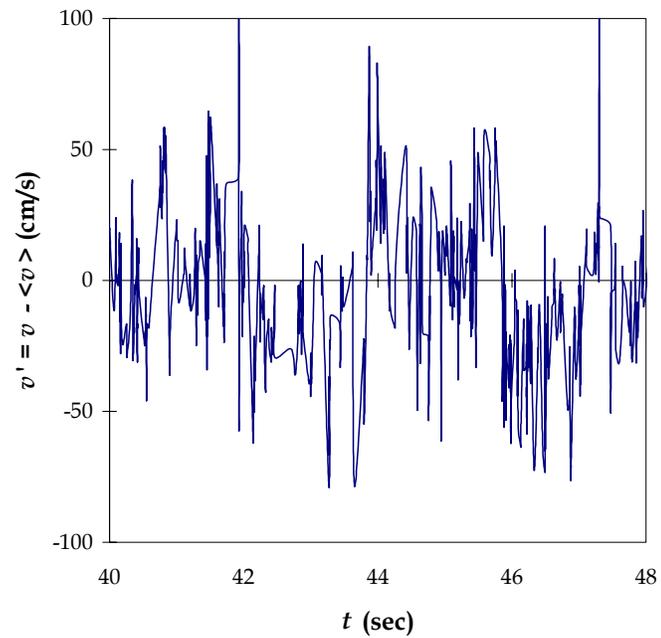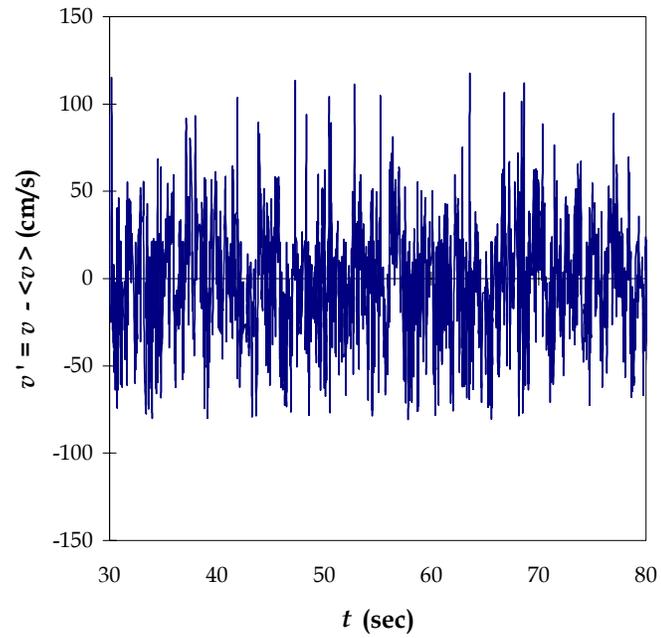
Figure 3-8. Time series of the axial liquid velocity for the 5.1 cm i.d. nitrogen-water bubble column at U_g = 5.0 cm/s and P = 3.5 MPa at r/R = 0.8 over (a) 30<t<80 and (b) 40<t<80.
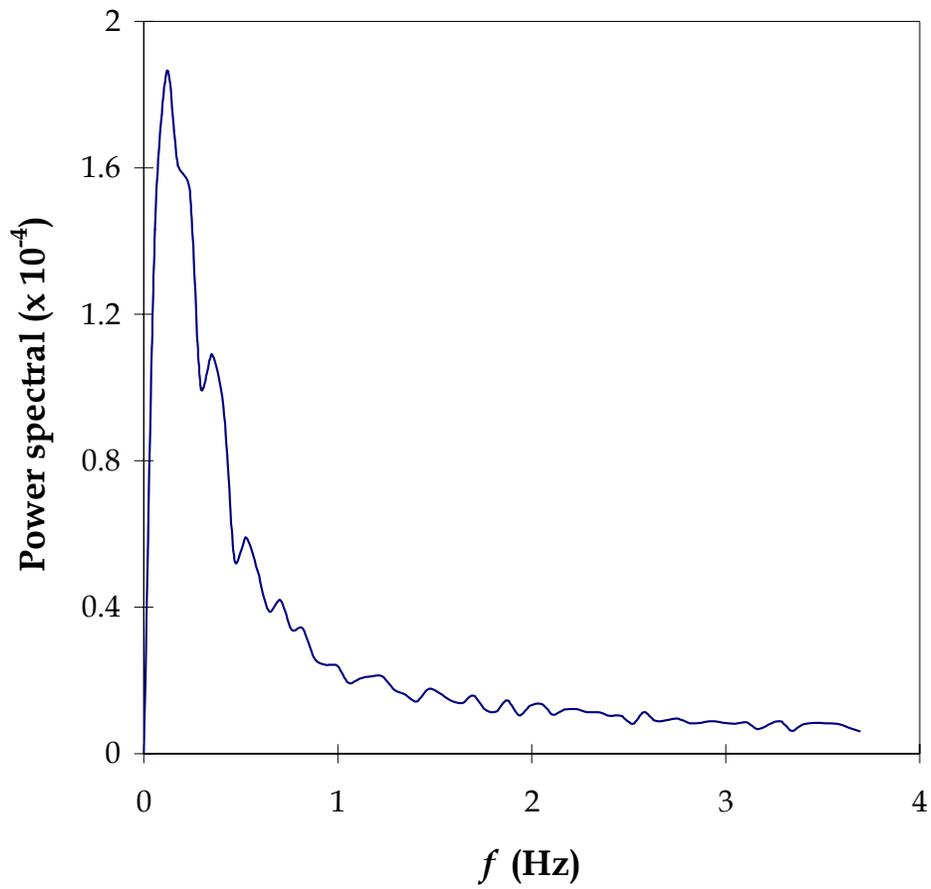
Figure 3-9. Power spectrum of the time series of the axial liquid velocity for the 5.1 cm i.d. nitrogen-water bubble column at $U_g = 5.0$ cm/s and $P = 3.5$ MPa at r/R = 0.8 for sampling period of 300s.

Chapter 4: Axial Liquid Mixing in a Bubble Column

Introduction

One feature of bubble column reactors is the nonideal flow pattern of each individual phase, which significantly influences reactant conversion and selectivity. In bubble columns, the dispersed gas phase moves in a continuous liquid medium, and thus the mixing behavior of the liquid phase is mainly affected by the agitating action of rising bubbles. Many studies have shown that pressure has a significant effect on bubble characteristics. Therefore, study of the effect of pressure on liquid mixing behavior is necessary for the design of industrial reactors.

Studies regarding the axial liquid-phase mixing in bubble columns at atmospheric conditions are extensive, especially for the air-water system; however, studies under high-pressure conditions are very scarce. Houzelot et al. (1985) investigated the axial dispersion behavior of the liquid phase in a 5-cm bubble column. An insignificant effect of pressure on the axial dispersion was observed, which was limited by the narrow experimental conditions in their study, that is, very low superficial gas velocity (< 6 mm/s) and pressure (< 3 atm). Under such conditions, the flow is always in the homogeneous bubbling regime and a significant change in liquid-phase mixing within such narrow operating conditions is not expected. Sancnimnuan et al. (1984) experimentally investigated the extent of liquid-phase backmixing under industrial coal hydroliquefaction conditions (temperature between 164 and 384°C and pressure between 4.5 and 15 MPa) in a small bubble column reactor (1.9 cm in diameter). They did not describe the effect of pressure on axial mixing and their study was limited by the small scale of the reactor.

Holcombe et al. (1983) determined the axial liquid dispersion coefficient in a 7.8-cm bubble column under pressures in the range of $3.0 - 7.1$ atm. The superficial gas velocity varied up to 0.6 m/s. They used heat as a tracer to measure the thermal dispersion coefficient, which is comparable to the mass dispersion coefficient. They found that the effect of pressure on thermal dispersion coefficients was negligible in the pressure range of their study. Wilkinson et al. (1993) measured the liquid axial dispersion coefficient in a batch-type bubble column 15.8 cm in diameter for the water-nitrogen system at pressures between 0.1 and 1.5 MPa using the electrical conductivity method. It was found that the axial liquid dispersion coefficient actually increases with increasing pressure, especially under high gas velocity conditions ($U_g > 0.10$ m/s). They noted that the available theories in the literature to describe liquid mixing under the atmospheric pressure cannot explain the pressure effect observed in their study. Their study was also limited by the narrow experimental conditions (low pressure range and batch operation) and limited system (air-water), and the observed pressure effect needs to be further verified under a wide range of operating pressures and in different gas-liquid systems.

The most common approach to account for the nonideality of liquid flow pattern in bubble columns is based on a one-dimensional axial dispersion model (ADM). Because of its simplicity and ease of use, the ADM remains popular in reactor design, and numerous correlations for the axial liquid dispersion coefficient in bubble columns have been developed over the years. Most of the existing correlations were developed for air-water systems at atmospheric conditions. As a result, these correlations severely underpredict the axial dispersion coefficient in industrial reactors operating under high pressure conditions, and cannot be applied directly to the reactor design. Tarmy et al. (1984) investigated liquid

backmixing in industrial coal liquefaction reactors using radioactive tracers. The operating pressure in their study varied up to 17 MPa and they found that the measured dispersion coefficients at high pressures were up to 2.5 times smaller than the values predicted by literature correlations, which were developed based on experimental data under ambient conditions. Recently, Onozaki et al. (2000a, 2000b) studied gas-liquid dispersion behavior in coal liquefaction reactors using a neutron absorption tracer technique. They also found that the axial dispersion coefficients of the liquid phase under coal liquefaction conditions ($P = 16.8 - 18.8$ MPa) were much smaller than those estimated from literature correlations obtained at ambient conditions. Those observations imply a decreasing trend for the pressure effect on liquid mixing.

In summary, although some research work has been done to study the pressure effect on liquid mixing in bubble columns, most of those studies were confined to low gas velocities or low pressures (normally less than 1.5 MPa), small column sizes and limited systems (air-water). To date, no systematic study is available to provide comprehensive data for axial liquid dispersion coefficients at high pressures. In this study, a thermal dispersion technique is developed to measure axial liquid dispersion coefficients in bubble columns. The study is conducted in systems close to industrial applications and covers a wide range of operating conditions. The inherent mechanisms underlying the pressure effect on liquid-phase mixing are also discussed.

Experimental Studies
Measurement technique

The mixing properties of bubble columns are usually described by a one-dimensional dispersion model, and the dispersion coefficient can be determined by steady and unsteady tracer injection methods. It has been verified that both methods lead to the same results (Deckwer et al., 1974). For the steady injection method, a tracer is injected at the exit or at another convenient point, and the axial concentration profile is measured upward of the liquid bulk flow. The dispersion coefficient is then calculated from the axial concentration profile. With the unsteady injection method, a variable flow of tracer is injected, usually at the contactor inlet, and samples are taken at the exit. Analysis of the response curve of the tracer input yields the dispersion coefficient. Electrolyte, dye and heat are normally applied as tracer for both methods and each of them yields identical dispersion coefficients.

In this study, the axial dispersion coefficients of the liquid phase are measured by the steady-state thermal dispersion method, that is, introducing heat close to the outlet of the liquid phase and measuring the upstream temperature profile in the liquid. The dispersion coefficient is determined from the axial temperature profile based on the one-dimensional dispersion model. Since the heat capacity of gas is much smaller than that of liquid, the temperature change in the column is mainly due to the backmixing of liquid. Taking the heat losses through the column wall and the gas-liquid interface to be negligible, the following differential energy balance equation applies (Aoyama et al., 1968; Wendt et al., 1984):

$$\frac{k_l}{\rho_l C_{pl}} \frac{d^2 T}{dz^2} + \frac{U_l}{1-\varepsilon_g} \frac{dT}{dz} = 0 \quad \text{with } E_l \equiv \frac{k_l}{\rho_l C_{pl}} \tag{4-1}$$

where E_l is the effective thermal dispersion coefficient and comparable to the mass dispersion coefficient. z is the axial distance from the liquid outlet, and $z = 0$ represents the

liquid outlet. This differential equation can be solved analytically after introducing the boundary conditions for a semi-infinite reactor, i.e.,

$$T = T_m \quad \text{at} \ z = 0$$
$$T = T_0 \quad \text{at} \ z = \infty$$

(4-2)

where T_0 and T_m are the inlet and outlet liquid temperatures, respectively. T is the liquid temperature at a distance z from the liquid outlet. The analytical solution of the differential equation with the above boundary conditions is:

$$\ln\left(\frac{T - T_0}{T_m - T_0}\right) = -\frac{U_l}{E_l(1 - \varepsilon_g)} z$$

(4-3)

Equation (4-3) indicates that the relationship between $\ln[(T-T_0)/(T_m-T_0)]$ and z is linear, and the dispersion coefficient, E_l, can be calculated from the slope of the temperature distribution profile, provided that the dispersion coefficient is constant and the gas holdup and superficial liquid velocity are known. The validity of the thermal dispersion technique has been verified by many studies (Aoyama et al., 1968; Holcombe et al., 1983; Wendt et al., 1984). Furthermore, the thermal dispersion technique is more easily applied to high-pressure systems with hydrocarbon liquids as the medium.

Experimental setup

 Liquid mixing experiments are conducted in two stainless steel high-pressure columns with an inner diameter of 5.08 cm and 10.16 cm, respectively. The aspect ratio for the 5.08-cm and 10.16-cm columns is 11 and 9, respectively. Three pairs of quartz windows are installed on the front and rear sides of the column, through which the bubble characteristics and flow phenomena under high-pressure conditions can be directly observed. The windows have a viewing area of 12.7 mm × 92 mm. The system pressure is controlled by a back-pressure regulator installed at the outlet of the column. Both columns can be operated up to 22 MPa. The details of the high-pressure columns were given in Luo et al. (1997). The schematic of the experimental setup is shown in Fig. 4-1.

 A heater with adjustable heating power is installed in the center of the column right below the liquid outlet. The maximum heating power is 750W. The axial temperature profile within the column is measured by several T-type copper-constantan thermocouples placed in the column center at different longitudinal positions after a steady temperature distribution is attained. The inlet temperatures of liquid and gas are kept constant during each run. Since the current high-pressure system has no cooling components, in order to maintain constant liquid inlet temperature, the liquid level in the liquid supply tank is kept relatively high, and in the meantime the maximum temperature difference across the column is controlled to within several degrees centigrade by adjusting the heater power. Therefore, such a small amount of heat does not increase the temperature in the liquid supply tank significantly. Typically, for each run the variation of the liquid inlet temperature is less than 1°C. The compressed gas is heated to the same temperature as the inlet liquid by a gas heater. In order to prevent heat loss through the column wall, insulation materials are installed to cover the entire vessel.

 The axial temperature distribution is measured by a 16-channel, high-accuracy thermocouple input board. The resolution of the board is 0.04°C for T-type thermocouples. For each gas velocity condition, 100 data points are sampled within 100 seconds and the average temperature is calculated. A differential pressure transducer is also installed to

measure the overall gas holdup in the column simultaneously with the temperature measurement, which is required for calculating the axial dispersion coefficient. For most experiments, a perforated plate with a number of square-pitched holes of 1.6 mm in diameter and 8 mm in pitch is used as the distributor for both the gas and liquid phases. The number of holes on the plate is 45 and 120 for the 5.08-cm and 10.16-cm columns, respectively. In order to investigate the effect of distributor design on liquid mixing, two other types of distributors, porous plate and sparger, are also employed for the measurements in the 5.08-cm column. The pore size of the porous plate is 200 μm and the sparger is a 1.27-cm diameter pipe with 13 holes on the side of the pipe. The hole diameter of the sparger is 0.32 cm.

Nitrogen is used as the gas phase, and water and Paratherm NF heat transfer fluid are used as the liquid phase. The physical properties of Paratherm NF heat transfer fluid (ρ_l = 870 kg/m^3, μ_l = 0.028 Pa·s, σ = 0.029 N/m at 27°C and 0.1 MPa) at different pressures and temperatures were given in Lin et al. (1998). The liquid is in continuous operation and the superficial liquid velocity varies up to 1.0 cm/s. The superficial gas velocity varies up to 40 cm/s, which covers both the homogenous bubbling and churn-turbulent flow regimes.

Results and Discussion
Temperature distribution

The measured axial temperature profiles in both water and Paratherm NF heat transfer fluid at different operating conditions are shown in Fig. 4-2. It can be seen that the relations between $\ln[(T\text{-}T_0)/(T_m\text{-}T_0)]$ and z are almost linear for various operating conditions and liquid systems, which indicates that the one-dimensional dispersion model is capable of describing the liquid mixing behavior in bubble columns. As the gas velocity increases, the axial temperature profile becomes flat, indicating an increased degree of liquid backmixing at higher gas velocities. The axial dispersion coefficient can be calculated based on the slope of the temperature distribution profile and the gas holdup.

Comparison with literature data

To verify the validity of the measurement technique, liquid mixing experiments are first conducted in the air-water system under ambient conditions, and the measured axial dispersion coefficients are compared with the literature data. The effects of gas and liquid velocities on the gas holdup and the axial dispersion coefficient in the air-water system under ambient conditions are shown in Fig. 4-3. It can be seen that the liquid velocity has an insignificant effect on the gas holdup, and the measured gas holdup values agree well with the reported literature data. The axial dispersion coefficient of the liquid phase increases significantly with increasing gas velocity. Generally, the axial liquid mixing in the nearly uniform dispersed bubbling regime is limited and the axial dispersion coefficient is small. When the gas velocity is increased, the flow is in the coalesced bubbling or slugging regime, and the non-uniform flow behavior creates significant backmixing. It is also found that the effect of liquid velocity on axial liquid mixing is small compared to the gas velocity effect. The axial dispersion coefficient in the air-water system slightly increases with an increase in the liquid velocity, especially at low gas velocities. The comparison of the measured axial dispersion coefficients with the available literature data obtained by various measurement techniques is also shown in Fig. 4-3(b). Since liquid mixing strongly depends on column size, for the purpose of comparison, the literature data

obtained in different sizes of columns are converted into the column size in this work (5.08 cm for Fig. 4-3), using the relationship between the axial dispersion coefficient and the column diameter reported in literature studies. If such a relation is not available in corresponding studies, the following general relation is used to convert the data between different columns:

$$E_l \propto D^{1.5} \qquad (4-4)$$

This relation can reasonably predict the scale-up effect on liquid mixing (Deckwer et al., 1974; Wendt et al., 1984). The comparison shows that the experimental data obtained in this study using the thermal dispersion technique agree well with most literature data. It is also found that the data converted from large columns (e.g., $D > 10$ cm) (Deckwer et al., 1974; Hikita and Kikukawa, 1974; Wilkinson et al., 1993) are lower than the experimental data actually obtained in small columns (Aoyama et al., 1968; Kato and Nishiwaki, 1972; Holcombe et al., 1983; Wendt et al., 1984). This may indicate different mixing behavior in small columns due to wall effects, and the scale-up effect on liquid mixing needs to be further investigated. Detailed information of various literature studies used in the comparison is shown in Table 4-1.

Effect of flow regime

In bubble columns, the dispersed gas phase moves in a continuous liquid medium, and therefore, the behavior of the gas phase is of importance for understanding the flow characteristics. Depending on the nature of gas dispersion, two main flow regimes are normally identified in the literature: homogeneous (or dispersed) bubbling flow and churn-turbulent (or coalesced bubbling) flow. The churn-turbulent flow can be further subdivided into the vortical-spiral flow condition and the turbulent flow condition (Chen and Fan, 1992; Chen et al., 1994). In the homogeneous bubbling flow regime predominating at low and intermediate gas velocities, no bubble coalescence occurs and the bubbles are of uniform, small size. In the churn-turbulent flow regime occurring at high gas velocities, bubbles coalesce intensively, and both the bubble size and rising velocity are large and exhibit wide distributions. Distinct bubble characteristics in these two flow regimes may result in different liquid mixing behaviors. Figure 4-4 shows the effect of flow regime on liquid mixing at different pressures. It can be seen that the axial dispersion coefficient of the liquid phase increases with increasing gas velocity, particularly in the homogeneous bubbling regime under ambient pressure. At high gas velocities, the axial dispersion coefficient tends to level off. The transition velocities from the homogeneous bubbling flow to the churn-turbulent flow indicated in Fig. 4-4 are identified based on the drift-flux model (Luo et al., 1997). For gas-liquid flows, the drift flux of gas is defined as the volumetric flux of the gas phase relative to a surface moving at the average velocity of gas-liquid systems. This flux can be expressed using the relative velocity between the gas and liquid phases as

$$j_{gl} = \varepsilon_g \left(1 - \varepsilon_g\right) \left(\frac{U_g}{\varepsilon_g} - \frac{U_l}{\varepsilon_l} \right) \qquad (4-5)$$

Figure 4-5 shows the overall gas holdup and the relationship between the drift flux and the gas holdup at different pressures in the 10.16-cm column. As can be seen from Fig. 4-5(a), at low gas holdups, the drift flux increases linearly with the gas holdup, indicating the prevalence of small dispersed bubbles. When the gas holdup or gas velocity exceeds a

certain value, the increase rate of drift flux with the gas holdup become larger, which indicates the existence of large coalesced bubbles. The point at which the increased rate of drift flux suddenly changes can be defined as the onset of the churn-turbulent flow. At both ambient and elevated pressures, the increased rates of drift flux with gas holdup are almost identical in the homogeneous bubbling regime. In contrast, in the churn-turbulent flow regime, the increased rate of drift flux at ambient pressure is higher than that at elevated pressure, because the bubbles become smaller and more uniform at elevated pressure. From Fig. 4-5(b), it is found that there is no significant difference in the gas holdup when the flow under both pressures is in the homogeneous bubbling regime; however, in the churn-turbulent flow regime, the gas holdup at the elevated pressure is much higher than that at the ambient pressure due to the smaller bubble size. The transition velocities identified based on the drift-flux method for the N_2-Paratherm liquid system at ambient pressure and the pressure of 0.8 MPa are about 6.0 cm/s and 11.0 cm/s, respectively. Increasing the system pressure markedly delays the transition from the homogeneous bubbling to the churn-turbulent flow regime. In other words, the existence of small bubbles in the system tends to delay the regime transition. In order to further verify the validity of the drift-flux method, the transition point in the air-water system under ambient pressure is also identified using the same approach. It is found that the transition velocity for the air-water system under ambient conditions is about 5.0 cm/s, and agrees with most literature data which are in the range of $4.0 - 5.2$ cm/s as shown in Table 4-2. Since the bubble size in the Paratherm liquid is normally smaller than that in water due to lower surface tension, the transition velocity in the Paratherm liquid (about 6.0 cm/s) is expected to be higher than that in the water (about 5.0 cm/s).

It is generally accepted that liquid-phase turbulence induced mainly by the movement of bubbles and the existence of large-scale liquid internal circulation are the main causes of liquid mixing in bubble columns. Many studies have indicated the presence of a large-scale liquid circulation cell in bubble columns, with liquid ascending in the central region and descending in the wall region (Joshi, 1980; Degaleesan et al., 1997). Liquid internal circulation is mainly driven by non-uniform radial gas distribution in the column. In the homogeneous bubbling flow regime, there is no pronounced large-scale liquid circulation in the column and the liquid-phase turbulence induced by rising bubbles is the main reason for liquid mixing. The scale of turbulence in the homogeneous bubbling flow regime depends on the bubble size. As the gas velocity increases, the bubble size increases and thus the bubble-induced turbulence increases, resulting in a rapid increase in the axial dispersion coefficient as shown in Fig. 4-4. In the churn-turbulent flow regime, both the convective liquid circulation and the liquid turbulent fluctuations play important roles in determining the mixing behavior of the liquid phase. The scale of turbulence in this flow regime is proportional to the column diameter and the intensity of the turbulence is not enhanced significantly by increasing gas velocity. Instead, increasing gas velocity induces an enhanced liquid internal circulation, which does not improve the mixing as efficiently as the local turbulent fluctuation does. Therefore, the axial dispersion coefficient levels off at high gas velocities. Similar observations were also found for heat transfer coefficients in bubble columns (Deckwer, 1980; Yang et al., 2000).

The effect of distributor design on the hydrodynamics and liquid-phase mixing in bubble columns is also investigated in this study. Three types of distributor plates are employed, that is, perforated plate, porous plate, and sparger. Detailed information about

the configuration of these distributors can be found in the experimental section. Figure 4-6 shows the experimental results of gas holdup and axial dispersion coefficients using different types of distributors in the 5.08-cm column at an elevated pressure. It can be seen that the effects of distributor design on both the gas holdup and axial dispersion coefficients are insignificant. It is commonly accepted that the distributor only affects a certain flow region above it, that is, in the area of height to diameter ratio less than 3.0 or even lower. Reese and Fan (1994) studied the transient flow structure in the entrance region of a bubble column using the particle image velocimetry technique. They found that the length of the entrance region affected by the distributor depends on the gas velocity. When the superficial gas velocity is higher than 3.0 cm/s, which is the typical experimental condition in this work, the entrance effects become insignificant and only a short height immediately above the distributor is required for the coherent flow structure to be developed. Figure 4-7 shows the gas holdups measured at different axial positions in a 15.24-cm bubble column at ambient conditions. It can be seen that the variation of gas holdup with the axial position becomes insignificant when the dimensionless axial height (L/D) is higher than 2.0 − 3.0. Since the measurements of gas holdup and axial dispersion coefficients in this study are conducted in the well-developed flow region ($L/D > 3.0$), no significant distributor effect is expected.

Effect of system pressure
The effect of pressure on the axial dispersion coefficient in the 5.08-cm and 10.16-cm columns for the nitrogen-Paratherm liquid system is shown in Figs. 4-8 and 4-9, respectively. It is found that the axial dispersion coefficient decreases significantly when the pressure is changed from the ambient to elevated pressures in both columns, indicating distinct flow behavior under ambient and elevated pressures. When the pressure is further increased, the decrease rate of the axial dispersion coefficient becomes smaller. The pressure effect is more pronounced at high gas velocities and in large columns. For example, as shown in Fig. 4-8(a), at a gas velocity of 20 cm/s and a liquid velocity of 0.18 cm/s, when the pressure increases from 0.1 MPa to 10.3 MPa (a factor of 103 increase), the axial dispersion coefficient in the 5.08-cm column decreases from 40 cm^2/s to 18 cm^2/s, i.e., a 55% decrease. In contrast, under similar gas and liquid velocities, the axial dispersion coefficient in the 10.16-cm column decreases from 104 cm^2/s to 40 cm^2/s (a 62% decrease) as the pressure varies only from 0.1 MPa to 4.2 MPa (a factor of 42 increase), as shown in Fig. 4-9(a). Reduced liquid backmixing at high pressures was also observed by other researchers (Tarmy et al., 1984; Onozaki et al., 2000a, 2000b). The insignificant pressure effect on liquid mixing in small columns (diameter normally less than 10.0 cm) observed by some researchers (Holcombe et al., 1983; Houzelot et al., 1985) is possibly due to the narrow operating conditions in their studies, that is, either low gas velocities or a narrow pressure range. As shown in Fig. 4-8, in small columns, the variation of axial dispersion coefficients with pressure is not pronounced at low gas velocities (i.e., in the homogeneous bubbling flow regime).

The gas holdup in both the 5.08-cm and 10.16-cm columns for the nitrogen-Paratherm liquid system at different pressures are shown in Fig. 10. As shown in the figure, the gas holdup increases significantly with increasing pressure, particularly in the low pressure range ($P < 4.2$ MPa). When the pressure is further increased, the gas holdup

90

slightly increases with pressure. A higher gas holdup at elevated pressures indicates the existence of small bubbles in the system.

The available theories in the literature describing liquid mixing under atmospheric pressure are based on either liquid turbulence induced by rising bubbles (Baird and Rice, 1975), large-scale liquid internal circulation (Joshi, 1980), or a combination of these two mechanisms (Degaleesan et al., 1997). Based on the internal circulation model, Joshi (1980) proposed the following equation to predict the average liquid circulation velocity in bubble columns:

$$V_c = 1.31 \left[gD \left(U_g - \frac{\varepsilon_g}{1-\varepsilon_g} U_l - \varepsilon_g U_{b\infty} \right) \right]^{1/3} \tag{4-6}$$

where $U_{b\infty}$ is the terminal bubble rise velocity. The second term on the right-hand side of Eq. (4-6) is normally negligible compared to the other two terms at low liquid velocities. It can be seen that both the gas holdup and bubble rise velocity affect the liquid circulation velocity, which can be treated as a measure of the extent of liquid circulation effect on liquid mixing. It is known that the gas holdup increases and the bubble size and rise velocity decrease with increasing pressure. Based on Eq. (4-6), the combined effects of gas holdup and bubble rise velocity on the liquid circulation velocity may result in unchanged or slightly changed liquid circulation pattern at elevated pressures. On the other hand, when the system pressure increases, bubbles become smaller, and liquid entrainment by bubble wakes and turbulence induced by the motion of bubbles are reduced. Therefore, the extent of liquid mixing is reduced at elevated pressures. Our recent study of flow fields and Reynolds stresses in high-pressure bubble columns using the laser Doppler velocimetry technique (Lee et al., 2001) also confirmed that the bubble-induced turbulence of the liquid phase is depressed as the pressure increases. The combined variations of liquid-phase turbulent fluctuations and internal liquid circulation give rise to the overall effect of pressure on liquid mixing.

Effect of liquid velocity

The effects of liquid velocity on liquid mixing and gas holdup in both columns are shown in Figs. 4-11 and 4-12, respectively. It is found that the effect of liquid velocity on the gas holdup is insignificant, indicating that the liquid-phase motion has little effect on bubble characteristics under low liquid velocity conditions (superficial liquid velocity less than 1.0 cm/s in this study). On the other hand, liquid-phase mixing is enhanced significantly with increasing liquid velocity in the range of this study. Comparing Fig. 4-11 to Fig. 4-3, it is also noted that the effect of liquid velocity on liquid mixing in the nitrogen-Paratherm liquid system is more pronounced than that in the air-water system. A similar trend of the liquid velocity effect was also observed by Zahardnik et al. (1997). They studied axial liquid mixing in a bubble column using a saturated solution of sodium benzoate as the tracer, and found that the axial dispersion coefficient increases with increasing liquid flow rate within the entire liquid velocity range in their study (superficial liquid velocity from 0.4 cm/s to 1.1 cm/s).

The enhancement of liquid-phase mixing with increasing liquid velocity is due to the enhanced liquid-phase turbulence at high liquid velocity conditions. Turbulent fluctuations in the liquid phase are important in determining the mixing behavior, and are mainly caused by two factors: the movement of bubbles and turbulent liquid eddies. Under

low liquid velocity conditions, liquid-phase motion does not change bubble characteristics significantly and hence does not affect bubble-induced turbulence; however, liquid-phase motion does enhance the energy exchange between micro-scale liquid eddies. Therefore, it enhances the overall turbulent fluctuations in the liquid phase yielding higher dispersion coefficients observed at high liquid velocities.

In this study, the axial dispersion coefficients in the air-water system are also measured at the ambient pressure. Figure 4-13 shows the comparison of liquid mixing and gas holdup between water and Paratherm NF heat transfer fluid at ambient pressure. As shown in Fig. 13, the gas holdup in Paratherm liquid is higher than that in water, indicating a smaller bubble size in the Paratherm liquid. The measured gas holdup data in the air-water system also agree with the literature data obtained in the column of similar size (Kato and Nishiwaki, 1972). Paratherm liquid has higher viscosity and lower surface tension compared to water. Higher liquid viscosity results in larger bubble size and thus lower gas holdup (Zahradnik et al., 1997); while lower surface tension favors the formation of small bubbles and thus increases gas holdup. The combination of these two effects gives rise to the overall gas holdup in the Paratherm liquid. According to the comparison of gas holdup between the water and Paratherm liquid as shown in Fig. 4-13, the effect of surface tension on bubble size and gas holdup is more pronounced compared to the viscosity effect, resulting in smaller bubble size and higher gas holdup in the Paratherm liquid.

A comparison of liquid mixing between these two liquids shows higher axial dispersion coefficients in the Paratherm liquid at the same gas and liquid velocities. The difference becomes more pronounced with increasing gas velocity. Bubbles in water are generally larger than those in Paratherm liquid, resulting in enhanced bubble-induced turbulence. Therefore, the axial dispersion coefficients are higher for water than those for Paratherm liquid. Based on this comparison, it is clear that axial dispersion coefficients obtained in water cannot be used directly to design bubble column reactors when a non-aqueous liquid medium is used.

Effect of column size

Mixing behavior strongly depends on column size and it is necessary to study the scale-up effect of liquid-phase mixing. In this study, the mixing experiments are carried out in both the 5.08-cm and 10.16-cm columns. The effects of column size on the gas holdup and axial dispersion coefficient can be seen clearly from Fig. 4-14. The gas holdup in the 5.08-cm column is much higher than that in the 10.16-cm column at both ambient and elevated pressures. This difference is more pronounced in the churn-turbulent flow regime. For example, at ambient pressure and a gas velocity of 20 cm/s, the gas holdup in the 5.08-cm and 10.16-cm columns is 0.21 and 0.30, respectively (about a 43% difference). When the pressure increases, the difference in the gas holdup between these two columns tends to be reduced. In order to further confirm the effect of column size, the gas holdup at ambient conditions is also measured in a larger column (15.24 cm in diameter) at the same dimensionless axial position (*L/D*=3.9) using the same liquid and the same type of distributor plate. The gas holdup data in the 15.24-cm column are also shown in Fig. 4-14(b). It can be seen that the difference between gas holdups in the 10.16-cm and 15.24-cm columns is small, which indicates that the effect of column size on the gas holdup is practically negligible when the column is larger than a certain size (about 10 cm observed in this study). Figure 4-15 further shows the effect of column size on the gas holdup at

ambient conditions in the air-water system obtained in this study and those reported in the literature. In the figure, the column diameter is up to 5.5 m. The solid line in the figure represents the predictions by the gas holdup correlation developed by Luo et al. (1999), which was mainly based on experimental data in columns of diameter larger than 10 cm. As shown in the figure, when the column diameter is larger than 10 cm, the difference in gas holdup among different sizes of columns is not significant. Shah et al. (1982) and Reilly et al. (1986) also found that the effect of column size on gas holdup is negligible when the column diameter is larger than 0.1 to 0.15 m.

The effect of column size on gas holdup occurs mainly through the variation in bubble characteristics. In small columns, the column wall effect is significant and the bubble size is confined by the column size, particularly in the slugging and churn-turbulent flow regimes. Therefore, the gas holdup in small columns is higher. When the column is larger than a certain size, the wall effect is negligible and thus the bubble size no longer depends on the column dimension. In this situation, the bubble size is mainly determined by the rates of bubble coalescence and breakup, and therefore, the gas holdup is no longer affected by the column size.

The effect of column size on the axial liquid dispersion coefficient is shown in Fig. 4-14(a). It is found that the axial dispersion coefficient strongly depends on the column size and liquid backmixing in the larger column is more apparent. As mentioned earlier, liquid-phase mixing is mainly determined by liquid-phase turbulence and large-scale liquid internal circulation. Both the scale of turbulence and the extent of liquid circulation strongly depend on the column size. Liquid turbulence and internal circulation are stronger in larger columns. Therefore, liquid mixing is enhanced significantly with increasing column size. The relationship between the axial dispersion coefficient and the column diameter is commonly expressed by

$$E_l \propto D^n \tag{4-7}$$

Many studies have shown that the scale-up index "n" is in the range of $1.4 - 1.5$ at ambient conditions (Deckwer et al., 1974; Wendt et al., 1984). As shown in Fig. 4-14(a), the effect of column size on liquid mixing is reduced with increasing pressure. Based on the experimental data in this study, the values of the scale-up index at different pressures are shown in Fig. 4-16. As can be seen, at ambient pressure, the index is about 1.5, which agrees with most literature studies. When the pressure increases, the index decreases significantly. At high pressures, the values of the index are in the range of $0.9 - 1.0$. The variation of scale-up index with gas density can be expressed by the following relation:

$$1 - \frac{n}{n_0} = 0.11 \ln\left(\frac{\rho_g}{\rho_{g0}}\right) \tag{4-8}$$

Here, n_0 (=1.5) is the value of the scale-up index at ambient pressure, and ρ_{g0} is the density of gas at ambient pressure.

The reduced effect of column size on the liquid mixing behavior at high pressures is mainly due to the variation of bubble characteristics. At ambient pressure, bubbles are large and unstable, and the behavior of large bubbles is easily affected by the column wall; while at elevated pressures, the bubble size is reduced significantly and small bubbles tend to be more stable. The effect of column size on the behavior of small bubbles is not as significant as that on the behavior of large bubbles. Therefore, the effect of column size on liquid mixing is reduced at elevated pressures.

Based on the scale-up relation (Eq. 4-7), the axial dispersion coefficient in industrial reactors can be estimated from the data in smaller laboratory-scale columns. Table 4-3 shows an example of a comparison between the axial dispersion coefficient actually measured in an industrial reactor and that calculated from the data in a laboratory-scale column based on the scale-up relation. The measured and simulated axial dispersion coefficients in the industrial reactor (1 m in diameter) are 1,100 and 670 cm^2/s, respectively, under the conditions listed in Table 4-3 (Onozaki et al., 2000a). The axial dispersion coefficient measured in the 10.16-cm column of this study under a condition of matched gas density and superficial gas and liquid velocities is 67 cm^2/s. Considering the scale-up index (n) of 1.02 for the gas density of 20 kg/m^3, the axial dispersion coefficient for the 1-m column can be estimated to be 688 cm^2/s based on the present result for the 10.16-cm column, which is comparable to the reported measured (1,100 cm^2/s) or simulated (670 cm^2/s) value. If, however, the scale-up index value of 1.5 for the ambient pressure is used, the estimated axial dispersion coefficient for the 1-m column becomes 2,057 cm^2/s, which would be much higher than the reported measured or simulated value. This example illustrates the importance of considering the variation of liquid mixing characteristics with pressure in the scale-up process.

Concluding Remarks

The thermal dispersion technique is developed to determine axial dispersion coefficients of the liquid phase at high pressure in the system close to industrial applications. The validity of the measuring technique is verified by the comparison of the measured results with the literature data. The study covers a wide range of operating gas velocity and pressure conditions. The axial liquid dispersion coefficient is found to increase with increasing gas velocity and decrease with increasing pressure. Liquid properties, liquid-phase motion and column dimension have significant effects on liquid-phase mixing; however, distributor design does not have a significant effect. Liquid mixing in bubble columns is controlled by the combined mechanism of local liquid turbulence and large-scale liquid internal circulation. Local turbulent fluctuation of the liquid phase is caused by the movement of both bubbles and turbulent liquid eddies.

Notations

C_{pl}	heat capacity of liquid, J/(kg·°C)
D	column diameter, m
E_l	axial dispersion coefficient of liquid phase, m^2/s
g	gravitational acceleration, m/s^2
j_{gl}	drift flux of gas, m/s
k_l	thermal conductivity of liquid, W/(m·°C)
L	axial height above distributor, m
n	scale-up index for liquid mixing, dimensionless
n_0	scale-up index for liquid mixing at ambient pressure, dimensionless
P	system pressure, Pa
T	temperature at axial position z, °C
T_0	liquid inlet temperature, °C

T_m liquid outlet temperature, °C
$U_{b\infty}$ terminal bubble rising velocity, m/s
U_g superficial gas velocity, m/s
$U_{g,tr}$ regime transition velocity, m/s
U_l superficial liquid velocity, m/s
V_c average liquid circulation velocity, m/s
z axial distance from the liquid outlet, m

Greek letters

ε_g gas holdup, dimensionless
$\varepsilon_{g,tr}$ gas holdup at the regime transition point, dimensionless
ε_l liquid holdup, dimensionless
μ_l liquid viscosity, Pa·s
ρ_g gas density, kg/m^3
ρ_{g0} gas density at ambient pressure, kg/m^3
ρ_l liquid density, kg/m^3
σ surface tension, N/m

References

Aoyama, Y., K. Ogushi, K. Koide, and H. Kubota, "Liquid Mixing in Concurrent Bubble Columns," *J. Chem. Eng. Japan*, **1**, 158 (1968).

Baird, M., and R. Rice, "Axial Dispersion in Large Scale Unbaffled Columns," *Chem. Eng. J.*, **9**, 171 (1975).

Bakshi, B. R., H. Zhong, P. Jiang, and L. S. Fan, "Analysis of Flow in Gas-Liquid Bubble Columns Using Multi-Resolution Methods," *Chem. Eng. Res. Des.*, **73**, 608 (1995).

Chen, R. C., and L. S. Fan, "Particle Image Velocimetry for Characterizing the Flow Structure in Three-Dimensional Gas-Liquid-Solid Fluidized Beds," *Chem. Eng. Sci.*, **47**, 3615 (1992).

Chen, R. C., J. Reese, and L. S. Fan, "Flow Structure in a Three-Dimensional Bubble Column and Three-Phase Fluidized Bed," *AIChE J.*, **40**, 1093 (1994).

Deckwer, W. D., "On the Mechanism of Heat Transfer in Bubble Column Reactors," *Chem. Eng. Sci.*, **35**, 1341 (1980).

Deckwer, W. D., R. Burckhart, and G. Zoll, "Mixing and Mass Transfer in Tall Bubble Columns," *Chem. Eng. Sci.*, **29**, 2177 (1974).

Degaleesan, S., M. P. Dudukovic, B. A. Toseland, and B. L. Bhatt, "A Two-Compartment Convective-Diffusion Model for Slurry Bubble Column Reactors," *Ind. Eng. Chem. Res.*, **36**, 4670 (1997).

Drahos, J., J. Zahradnik, M. Fialova, and F. Bradka, "Identification and Modelling of Liquid Flow Structures in Bubble Column Reactors," *Chem. Eng. Sci.*, **47**, 3313 (1992).

Gopal, J. S., and M. M. Sharma, "Mass Transfer Characteristics of Low H/D Bubble Columns," *Can. J. Chem. Eng.*, **61**, 517 (1983).

Hikita, H., and H. Kikukawa, "Liquid-Phase Mixing in Bubble Columns: Effect of Liquid Properties," *Chem. Eng. J.*, **8**, 191 (1974).

Holcombe, N. T., D. S. Smith, H. N. Knickle, and W. O'Dowd, "Thermal Dispersion and Heat Transfer in Nonisothermal Bubble Columns," *Chem. Eng. Commun.*, **21**, 135 (1983).

Houzelot, J. L., M. F. Thiebaut, J. C. Charpentier, and J. Schiber, "Contribution to the Hydrodynamic Study of Bubble Columns," *Int. Chem. Eng.*, **25**, 645 (1985).

Hyndman, C. L., and C. Guy, "Gas Phase Hydrodynamics in Bubble Columns," *Chem. Eng. Res. Des.*, **73**, 302 (1995).

Joshi, J. B., "Axial Mixing in Multiphase Contactors − a Unified Correlation," *Trans. Instn. Chem. Engrs.*, **58**, 155 (1980).

Kato, Y., and A. Nishiwaki, "Longitudinal Dispersion Coefficient of a Liquid in a Bubble Column," *Int. Chem. Eng.*, **12**, 182 (1972).

Koide, K., S. Morooka, K. Ueyama, A. Matsuura, F. Yamashita, S. Iwamoto, Y. Kato, H. Inoue, M. Shigeta, S. Suzuki, and T. Akehata, "Behavior of Bubbles in Large Scale Bubble Column," *J. Chem. Eng. Japan*, **12**, 98 (1979).

Koide, K., A. Takazawa, M. Komura, and H. Matsunaga, "Gas Holdup and Volumetric Liquid-Phase Mass Transfer Coefficient in Solid-Suspended Bubble Columns," *J. Chem. Eng. Japan*, **17**, 459 (1984).

Lee, D. J., B. K. McLain, Z. Cui, and L. S. Fan, "Pressure Effect on the Flow Fields and the Reynolds Stresses in a Bubble Column," *Ind. Eng. Chem. Res.*, **40**, 1442 (2001).

Lin, T. J., K. Tsuchiya, and L. S. Fan, "Bubble Flow Characteristics in Bubble Columns at Elevated Pressure and Temperature," *AIChE J.,* **44**, 545 (1998).

Luo, X., P. Jiang, and L. S. Fan, "High-Pressure Three-Phase Fluidization: Hydrodynamics and Heat Transfer," *AIChE J.*, **43**, 2432 (1997).

Luo, X., D. J. Lee, R. Lau, G. Q. Yang, and L. S. Fan, "Maximum Stable Bubble Size and Gas Holdup in High-Pressure Slurry Bubble Columns," *AIChE J.,* **45**, 665 (1999).

Mangartz, K. H., and T. H. Pilhofer, "Interpretation of Mass Transfer Measurements in Bubble Columns Considering Dispersion of Both Phases," *Chem. Eng. Sci.*, **36**, 1069 (1981).

Myers, K. J., M. P. Dudukovic, and P. A. Ramachandran, "Modelling Churn-Turbulent Bubble Columns − I. Liquid-Phase Mixing," *Chem. Eng. Sci.*, **42**, 2301 (1987).

Ohki, Y., and H. Inoue, "Longitudinal Mixing of the Liquid Phase in Bubble Columns," *Chem. Eng. Sci.*, **25**, 1 (1970).

Onozaki, M., Y. Namiki, N. Sakai, M. Kobayashi, Y. Nakayama, T. Yamada, and S. Morooka, "Dynamic Simulation of Gas-Liquid Dispersion Behavior in Coal Liquefaction Reactors," *Chem. Eng. Sci.*, **55**, 5099 (2000a).

Onozaki, M., Y. Namiki, H. Ishibashi, T. Takagi, M. Kobayashi, and S. Morooka, "Steady-State Thermal Behavior of Coal Liquefaction Reactors Based on NEDOL Process," *Energy & Fuels*, **14**, 355 (2000b).

Reese J., and L. S. Fan, "Transient Flow Structure in the Entrance Region of a Bubble Column Using Particle Image Velocimetry," *Chem. Eng. Sci.*, **49**, 5623 (1994).

Reilly, I. G., D. S. Scott, T. De Bruijn, A. Jain, and J. Piskorz, "A Correlation for Gas Holdup in Turbulent Coalescing Bubble Columns," *Can. J. Chem. Eng.*, **64**, 705 (1986).

Rice, R. G., and M. N. Littlefield, "Dispersion Coefficients for Ideal Bubbly Flow in Truly Vertical Columns", *Chem. Eng. Sci.*, **42**, 2043 (1987).

Sangnimnuan, A., G. N. Prasad, and J. B. Agnew, "Gas Hold-Up and Backmixing in a Bubble-Column Reactor Under Coal-Hydroliquefaction Conditions," *Chem. Eng. Commun.*, **25**, 193 (1984).

Shah, Y. T., B. G. Kelkar, S. P. Godbole, and W. D. Deckwer, "Design Parameters Estimations for Bubble Column Reactors," *AIChE J.*, **28**, 353 (1982).

Shnip, A. I., R. V. Kolhatkar, D. Swamy, and J. B. Joshi, "Criteria for the Transition from the Homogeneous to the Heterogeneous Regime in Two-Dimensional Bubble Column Reactors," *Int. J. Multiphase Flow*, **18**, 705 (1992).

Tarmy, B. L., M. Chang, C. A. Coulaloglou, and P. R. Ponzi, "Hydrodynamic Characteristics of Three-Phase Reactors," *The Chemical Engineer*, **407**, 18 (1984).

Wendt, R., A. Steiff, and P. M. Weinspach, "Liquid Phase Dispersion in Bubble Columns," *Ger. Chem. Eng.*, **7**, 267 (1984).

Wilkinson, P. M., H. Haringa, and F. P. A. Stokman, "Liquid Mixing in a Bubble Column Under Pressure," *Chem. Eng. Sci.*, **48**, 1785 (1993).

Yang, G. Q., X. Luo, R. Lau, and L. S. Fan, " Heat-Transfer Characteristics in Slurry Bubble Columns at Elevated Pressures and Temperatures," *Ind. Eng. Chem. Res.*, **39**, 2568 (2000).

Zahradnik, J., M. Fialova, M. Ruzicka, J. Drahos, F. Kastanek, and N. H. Thomas, "Duality of the Gas-Liquid Flow Regimes in Bubble Column Reactors," *Chem. Eng. Sci.,* **52**, 3811 (1997).

Table 4-1. Relevant information of various references used in Fig. 3 regarding liquid mixing in the air-water system under ambient conditions.

Reference	Measurement Technique	U_g (cm/s)	U_l (cm/s)	D (cm)	U_l effect	Relation between E_l and D
Aoyama et al. (1968)	steady injection; heat and KCl solution as tracer	0.3 – 8	0.18 – 0.62	5.0	insignificant	$E_l \propto D^{1.5}$
Kato and Nishiwaki (1972)	impulse injection; KCl solution as tracer	1 – 25	0.7 – 1.3	6.6	insignificant	*N/A*
Deckwer et al. (1974)	steady and impulse injection; NaCl solution as tracer	1 – 15	0.71	20	N/A	$E_l \propto D^{1.4}$
Hikita and Kikukawa (1974)	impulse injection; KCl solution as tracer	4.3 – 33.8	0	10	N/A	$E_l \propto D^{1.25}$
Mangartz and Pilhofer (1981)	steady injection; heat as tracer	0.5 – 18	0 – 6	10	insignificant	$E_l \propto D^{1.5}$
Holcombe et al. (1983)	steady injection; heat as tracer	0 – 60	0 – 2	7.8	N/A	$E_l \propto D^{1.33}$
Wendt et al. (1984)	steady injection; heat and NaCl solution as tracer	1.5 – 30	0.2 – 4.5	6.3	insignificant	$E_l \propto D^{1.4}$
Wilkinson et al. (1993)	unsteady injection; NaCl solution as tracer	2 – 20	0	15.8	N/A	N/A
This work	steady injection; heat as tracer	2 – 20	0.34 – 1.0	5.08	small	N/A

Table 4-2. Literature data regarding regime transition velocity for the air-water system under ambient conditions.

Reference	Transition Velocity (cm/s)	Identification Method
Rice and Littlefield (1987)	4.0	Based on experimental gas holdup and liquid mixing data
Shnip et al. (1992)	4.4 – 5.2	Based on linear stability theory
Drahos et al. (1992) Zahradnik et al. (1997)	4.0	Based on experimental gas holdup and gas mixing data
Reese and Fan (1994)	4.2	Based on experimental gas holdup data measured by PIV technique
Bakshi et al. (1995)	4.8	Based on wavelet-based multi-resolution analysis of local gas holdup signals
Hyndman and Guy (1995)	4.5	Based on experimental gas holdup data

Table 4-3. Comparison of axial dispersion coefficients measured in an industrial reactor and calculated based on the scale-up relation.

Parameters	Onozaki et al. (2000a)	This work
Column diameter (m)	1.0	0.102
Gas source	Mainly H_2	N_2
Operating pressure (MPa)	16.6 – 16.8	1.8
Operating temperature (°C)	40	27
Gas density inside reactor (kg/m³)	**20**	**20**
Liquid density (kg/m³)	964	872
Liquid viscosity (mPa·s)	7.0	28
Superficial gas velocity (cm/s)	**6.3**	**6.2**
Superficial liquid velocity (cm/s)	**0.31**	**0.32**
Axial dispersion coefficient (cm²/s)	1,100 (measured) 670 (simulated)	67
Axial dispersion coefficient (cm²/s) [converting the condition of this work to that of Onozaki et al. (2000a) using the scale-up index (*n*) of 1.02 (Fig. 16) for ρ_g of 20 kg/m³]	**1,100** (measured) **670** (simulated)	**688**
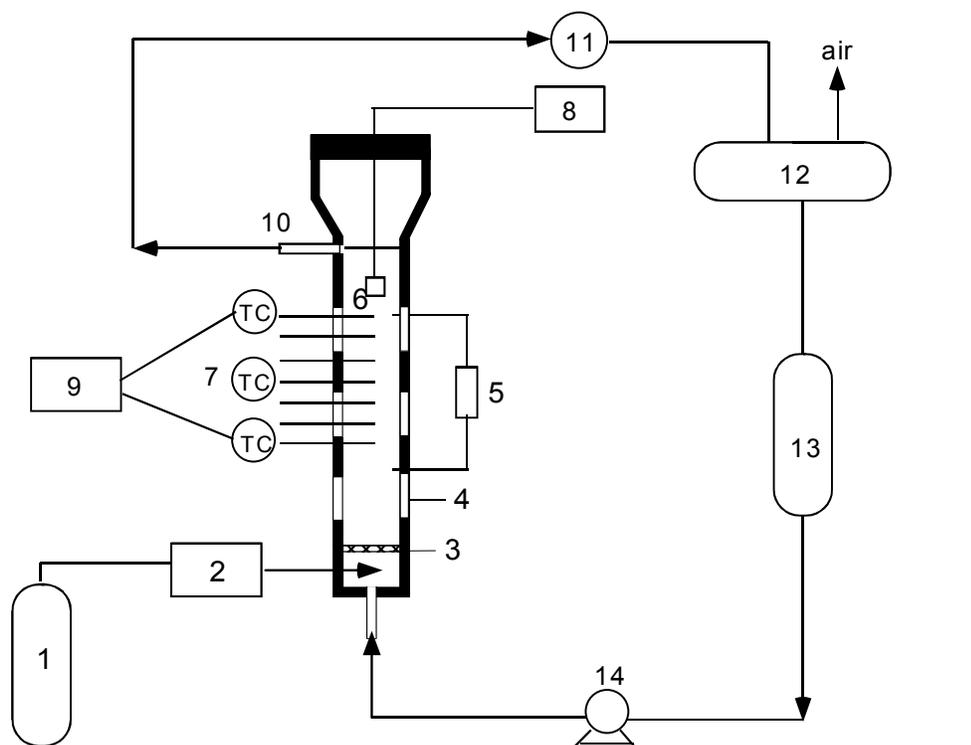
1. Gas supply
2. Gas heater
3. Perforated plate distributor
4. Quartz window
5. Pressure transducer
6. Heater
7. Thermocouples
8. DC power
9. Thermocouple input board (0.04°C)
10. Gas and liquid outlet
11. Back pressure regulator
12. Gas/liquid separation tank
13. Liquid supply tank
14. Liquid pump

Figure 4-1. Schematic of experimental setup for the measurement of liquid-phase mixing.
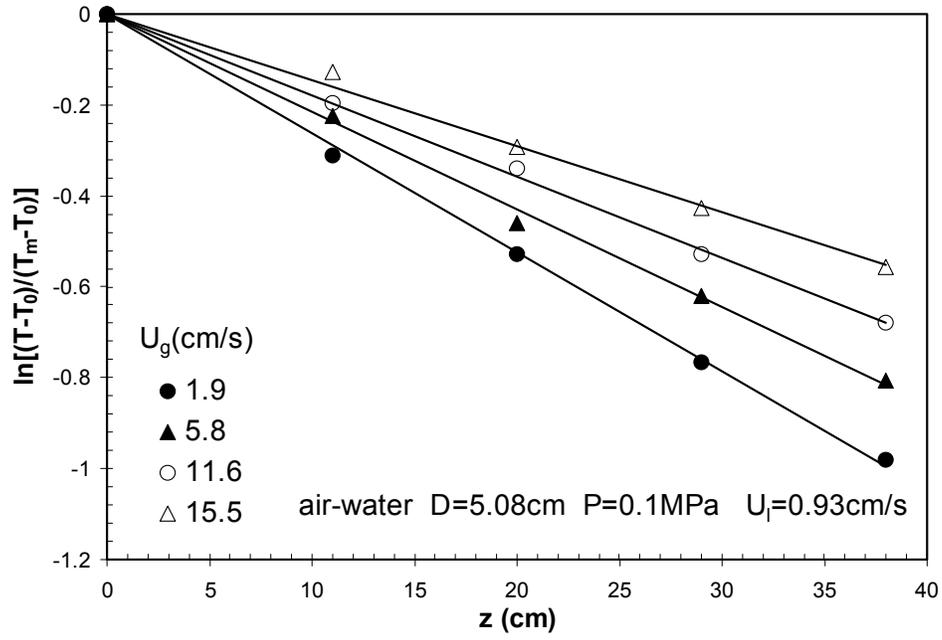
(a) water, ambient pressure
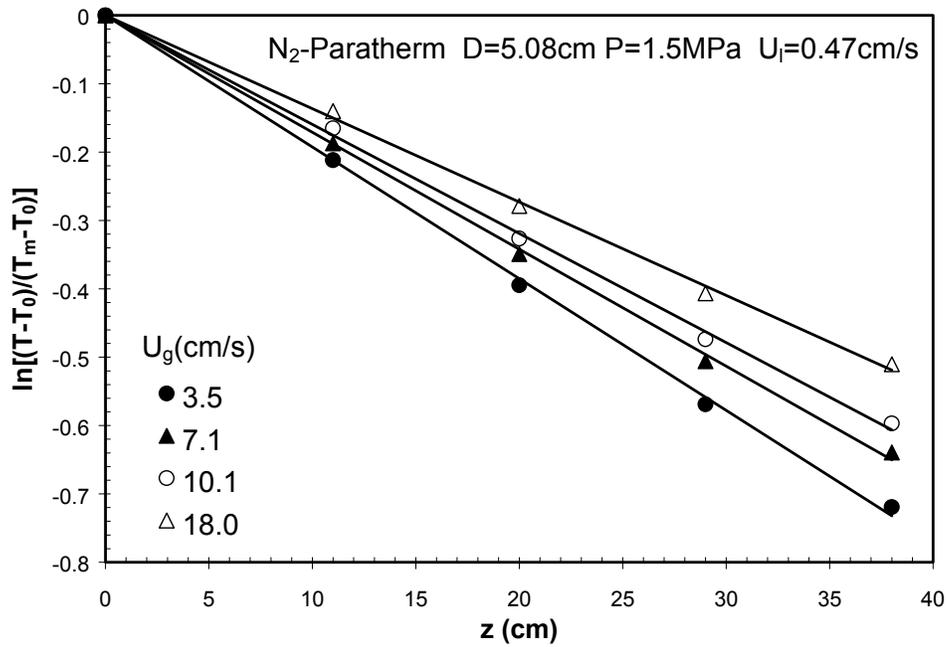
(b) Paratherm NF heat transfer fluid, elevated pressure

Figure 4-2. Typical temperature distribution profiles for both water and Paratherm NF heat transfer fluid at different operating conditions.

103
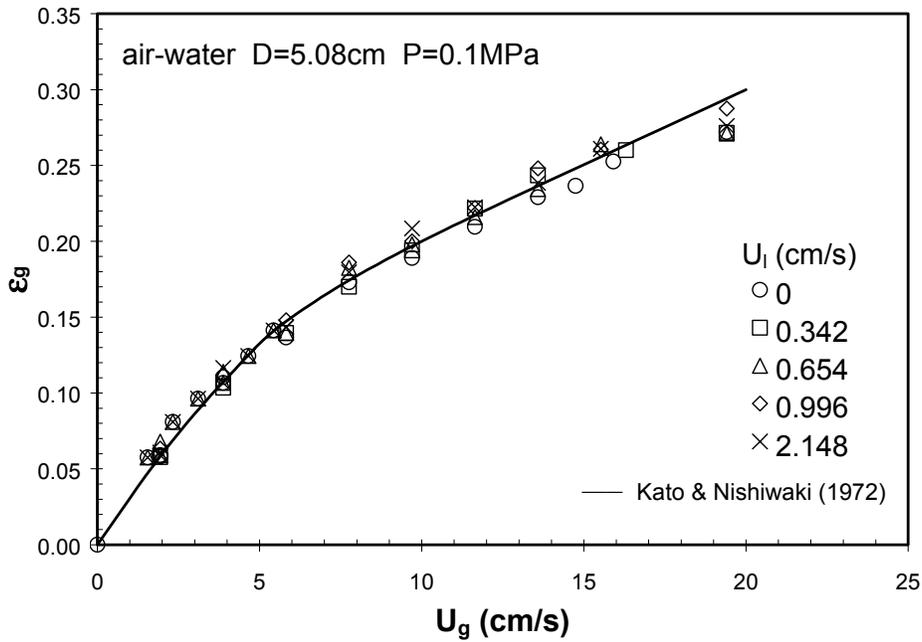
(a) gas holdup
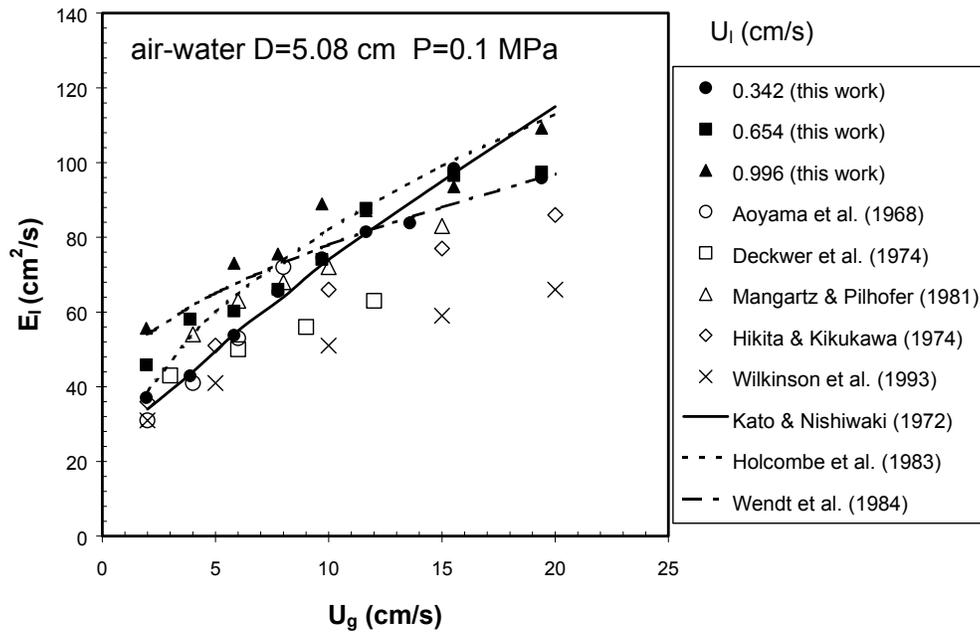
(b) dispersion coefficient

Figure 4-3. Comparison of experimental results with available literature data for the air-water system under ambient conditions.
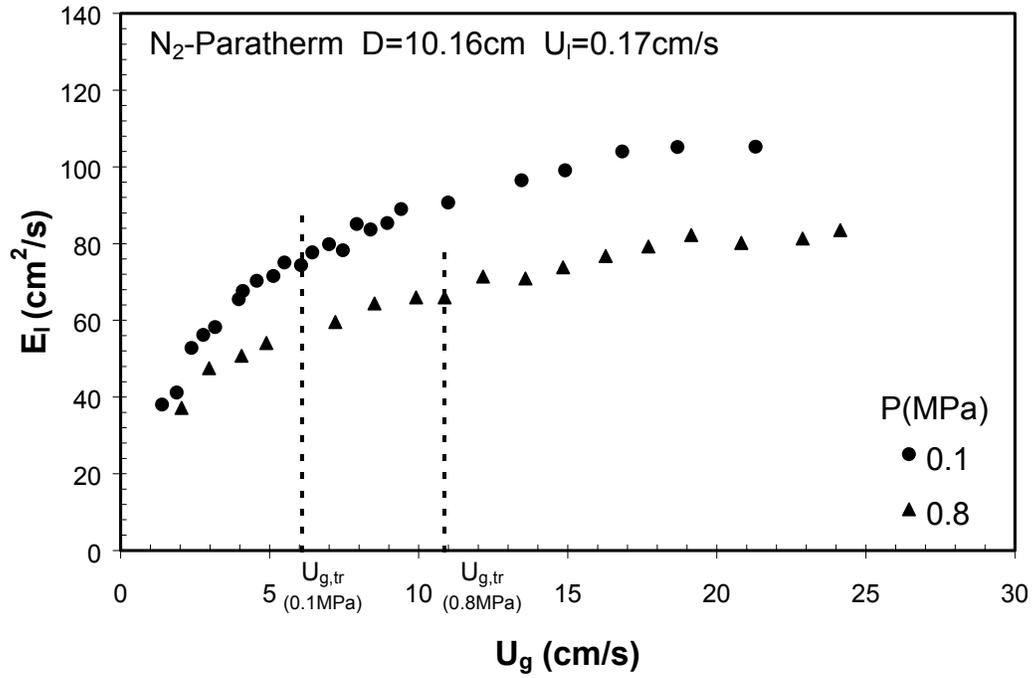
Figure 4-4. Effect of gas velocity on the axial liquid dispersion coefficient at different pressures in the 10.16-cm column.
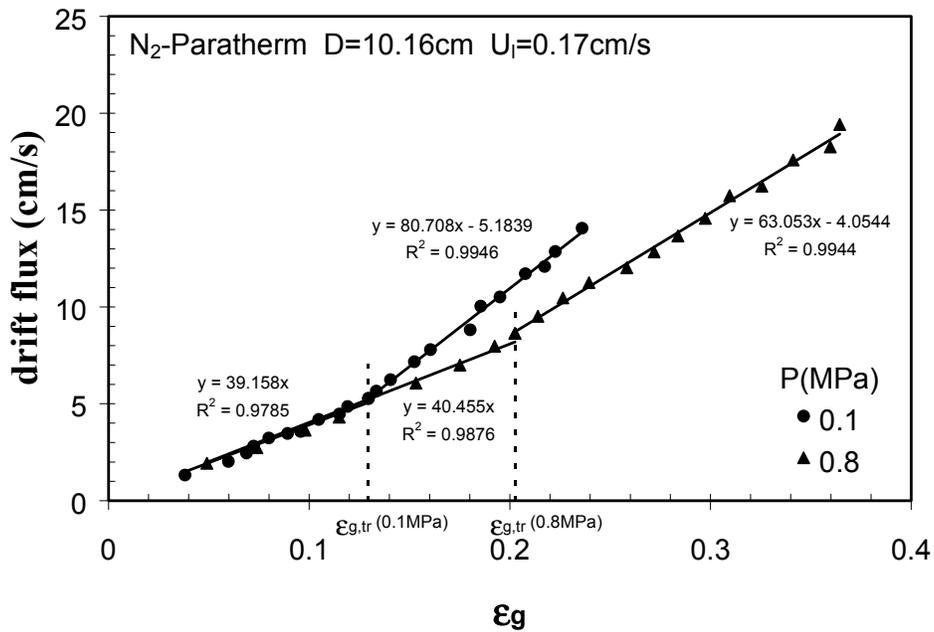
(a) drift flux vs. gas holdup
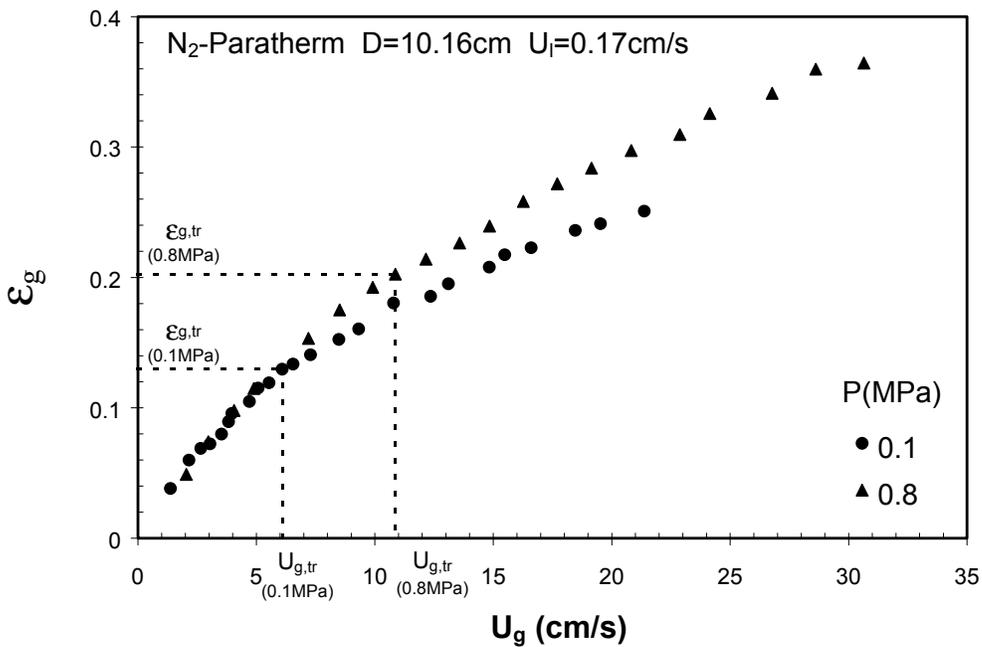
(b) gas holdup vs. gas velocity

Figure 4-5. Determination of transition velocity from homogeneous bubbling to churn-turbulent flow regimes at different pressures.
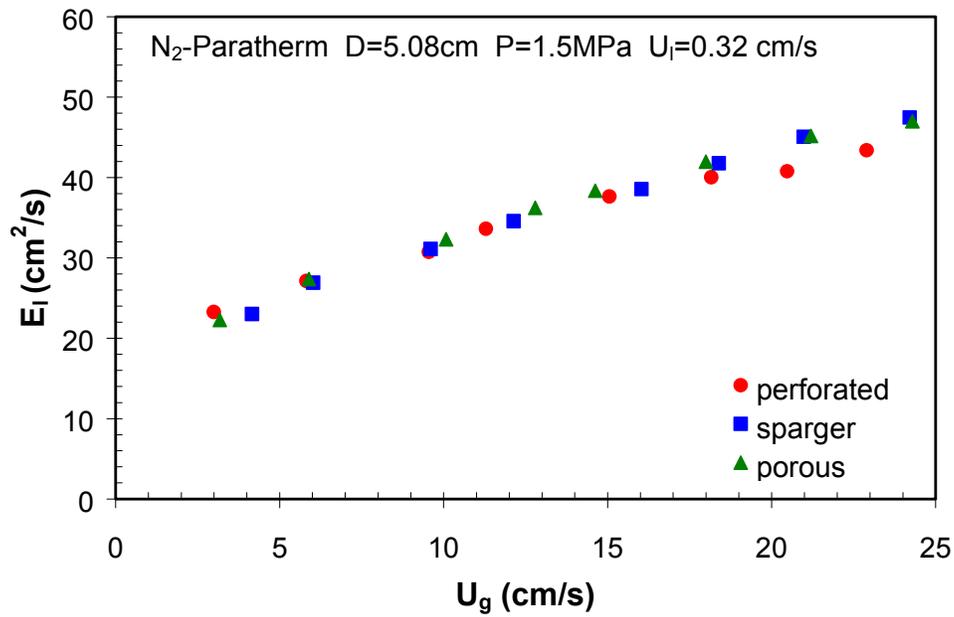
(a) dispersion coefficient
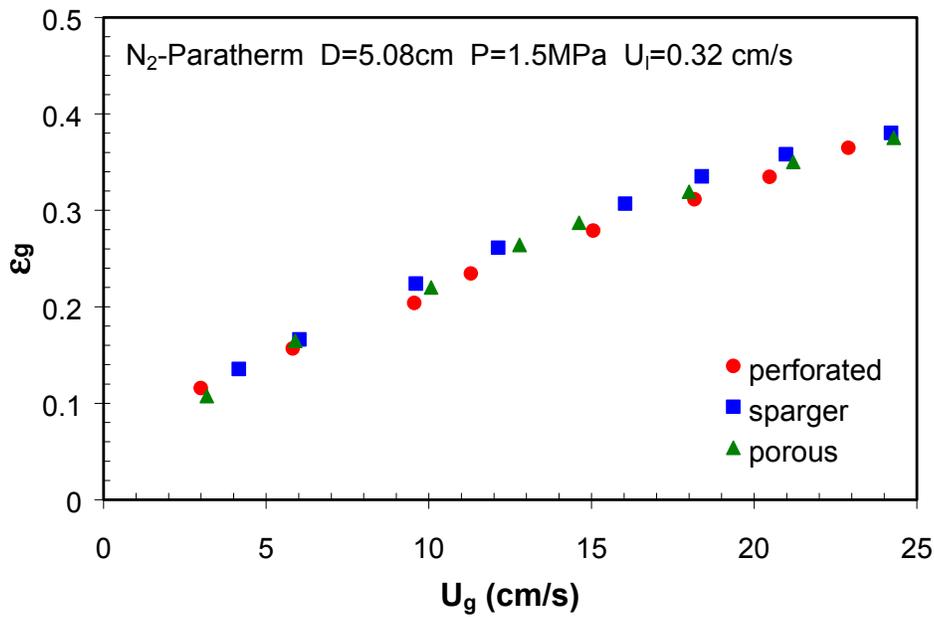
(b) gas holdup

Figure 4-6. Effects of distributor design on liquid mixing and gas holdup in the 5.08-cm column at elevated pressure.
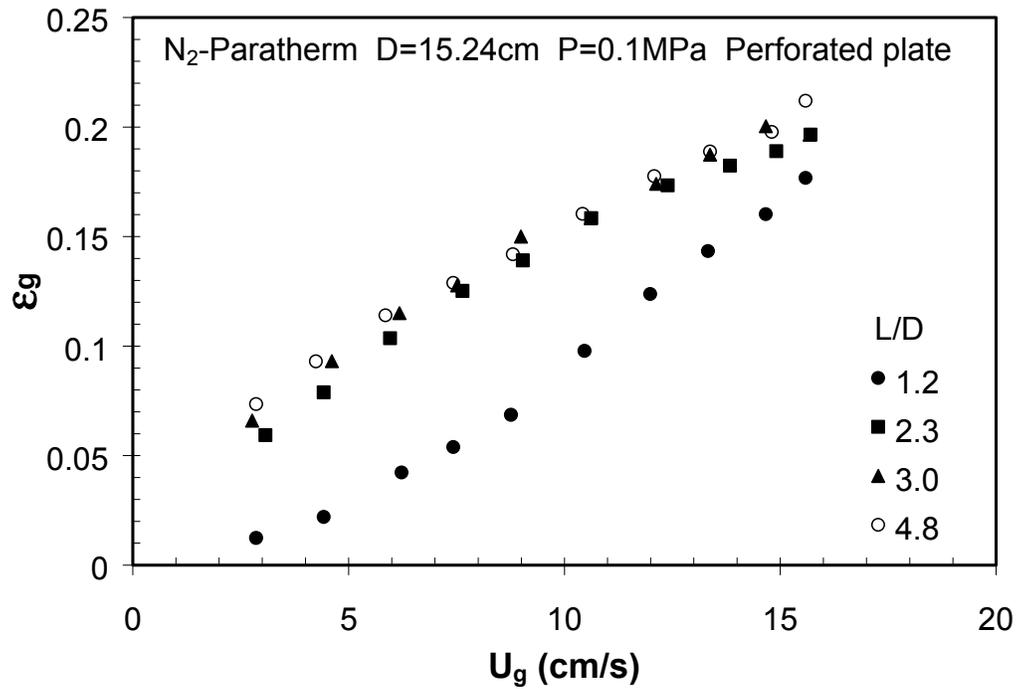
Figure 4-7. Gas holdups measured at different axial positions in a 15.24-cm bubble column at ambient conditions.
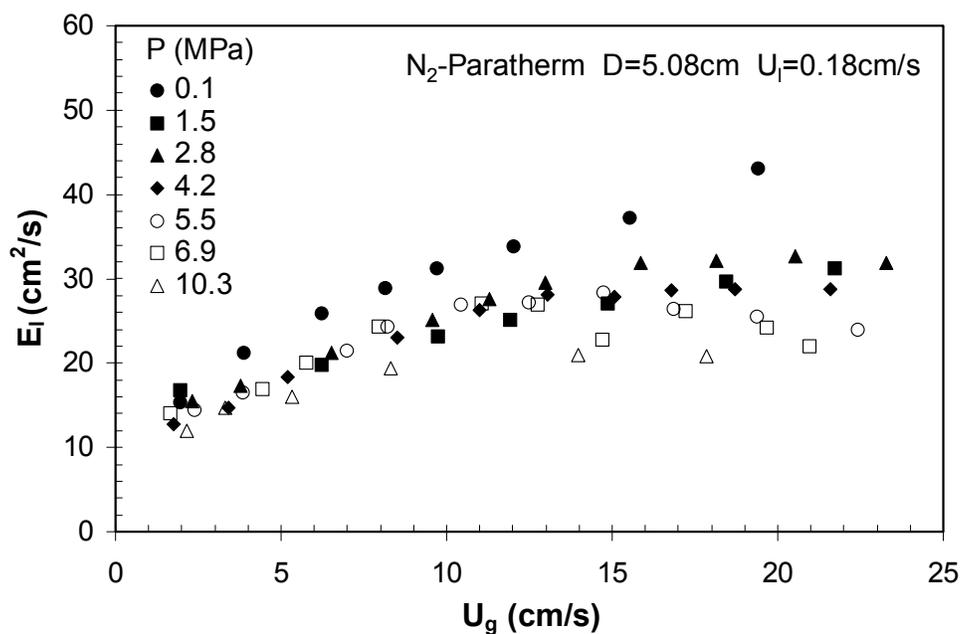
(a) U_l=0.18cm/s
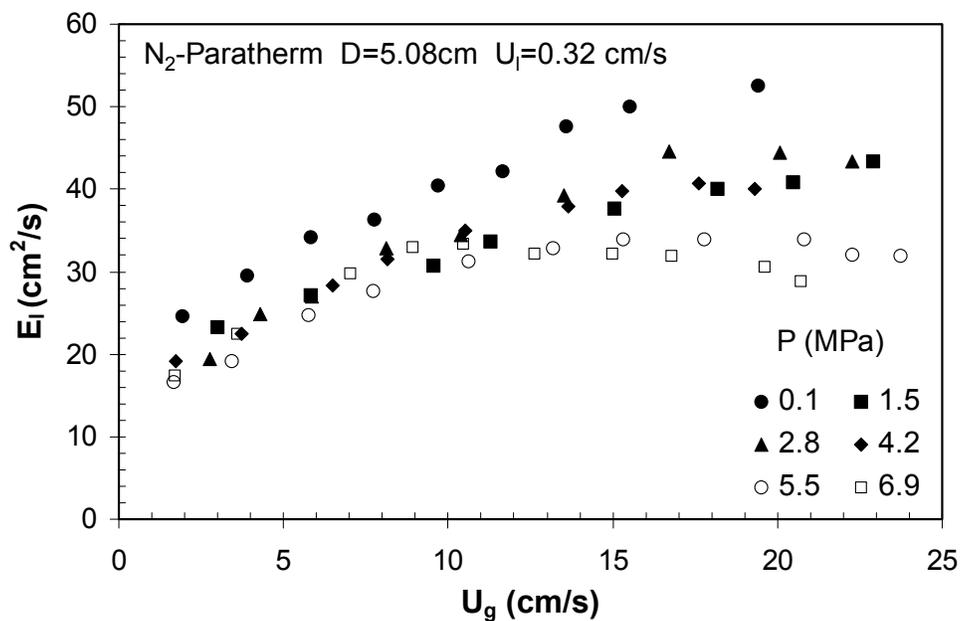
(b) U_l=0.32cm/s

Figure 4-8. Pressure effect on liquid-phase mixing in the 5.08-cm column at different liquid velocities.

(a) U_l=0.17cm/s
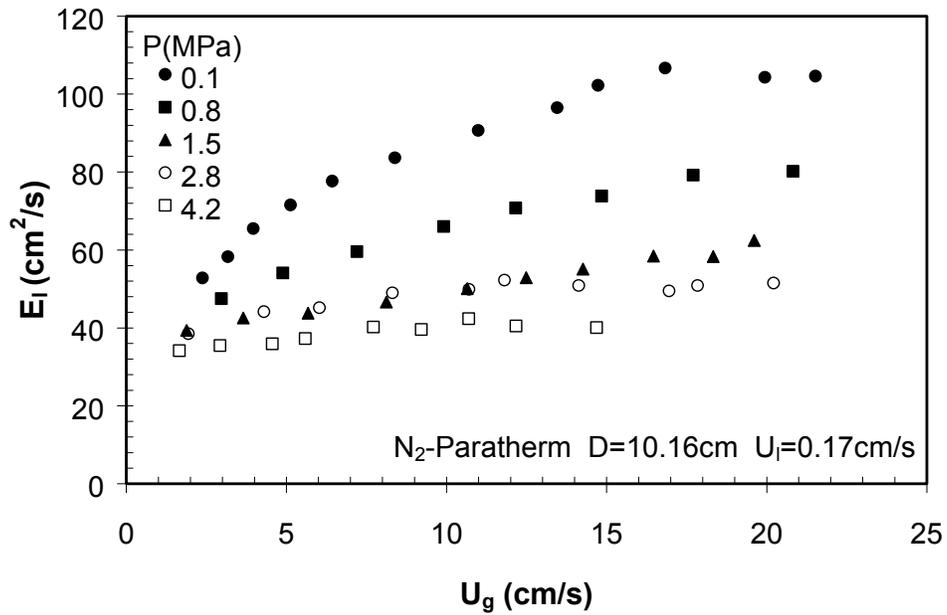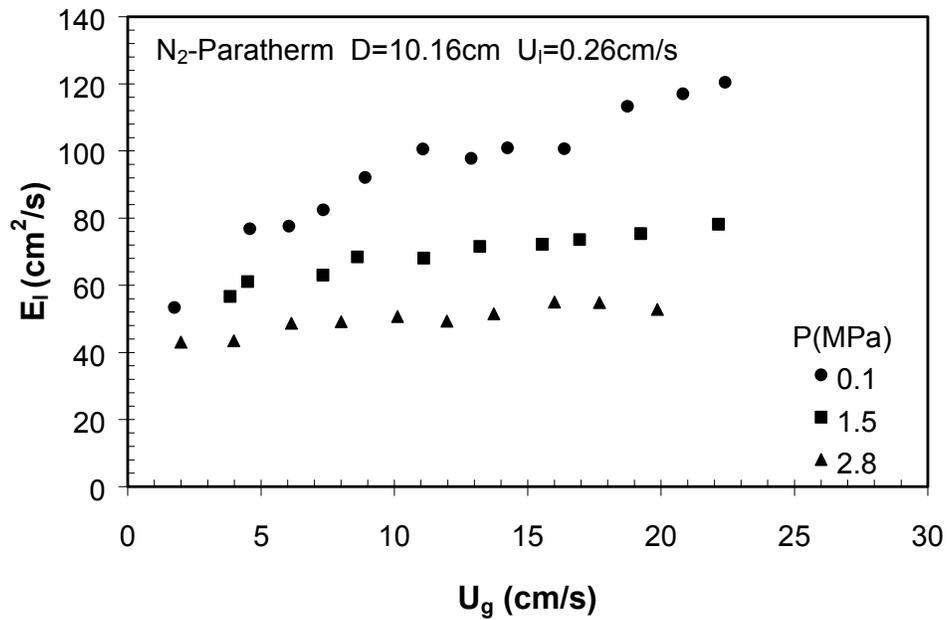
(b) U_l=0.26cm/s

Figure 4-9. Pressure effect on liquid-phase mixing in the 10.16-cm column at different liquid velocities.
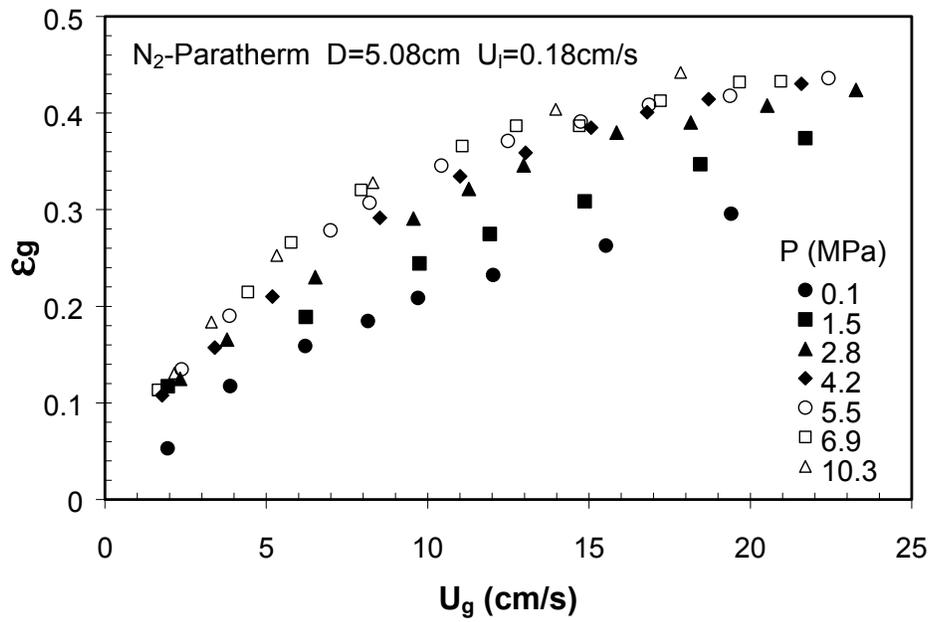
(a) 5.08-cm column
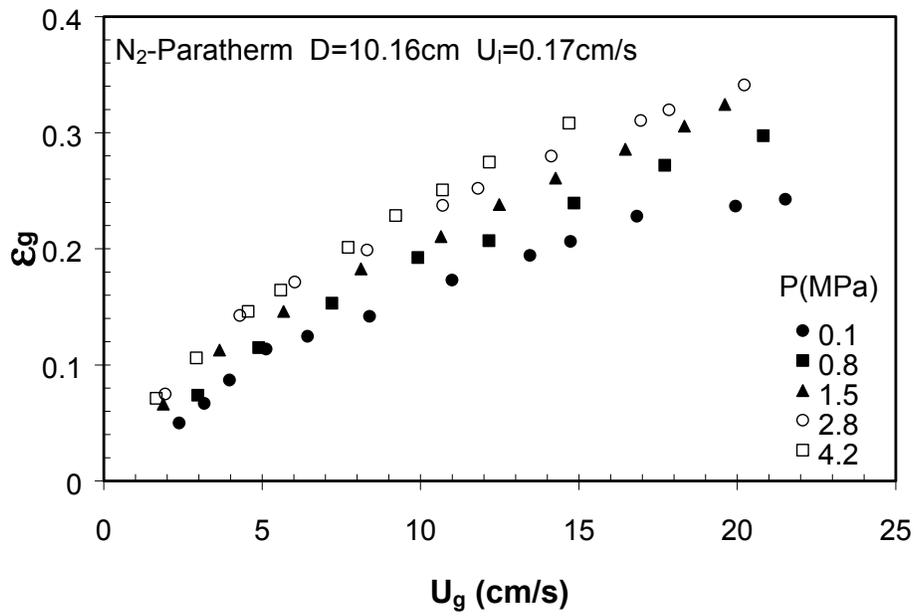
(b) 10.16-cm column

Figure 4-10. Pressure effect on the gas holdup in both the 5.08-cm and 10.16-cm columns.

111
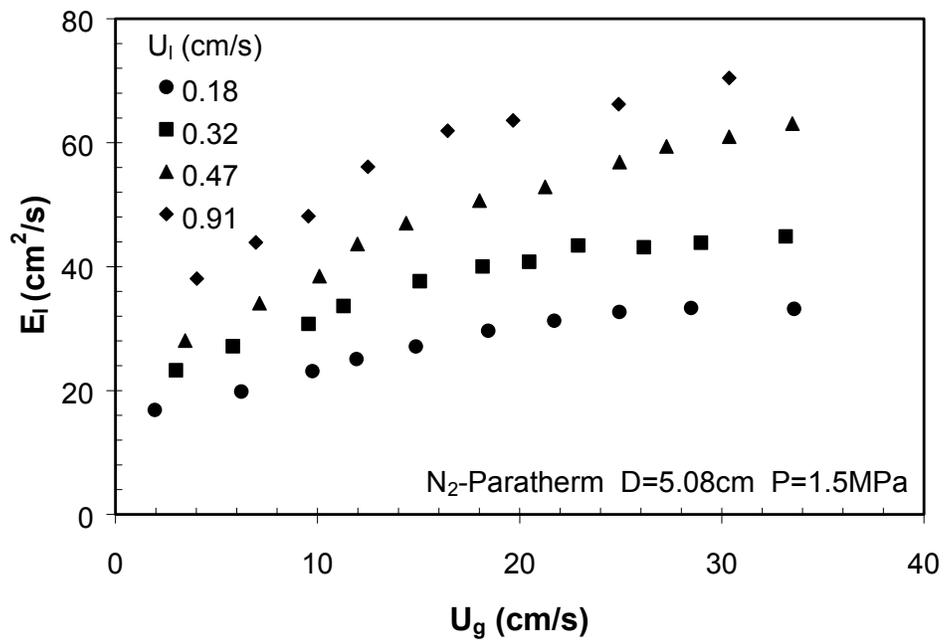
(a) 5.08-cm column

(b) 10.16-cm column

Figure 4-11. Effect of liquid velocity on liquid mixing in both the 5.08-cm and 10.16-cm columns.
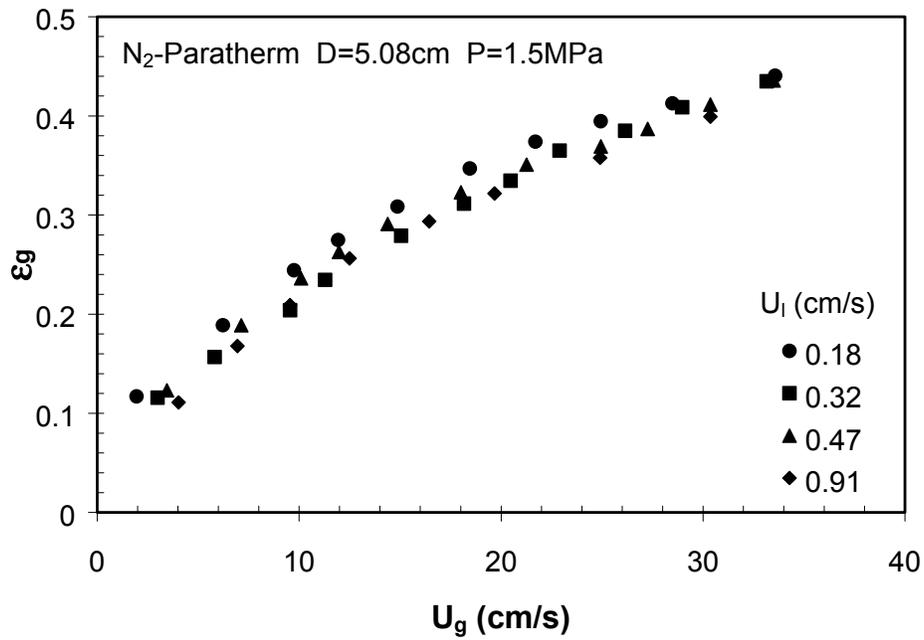
(a) 5.08-cm column
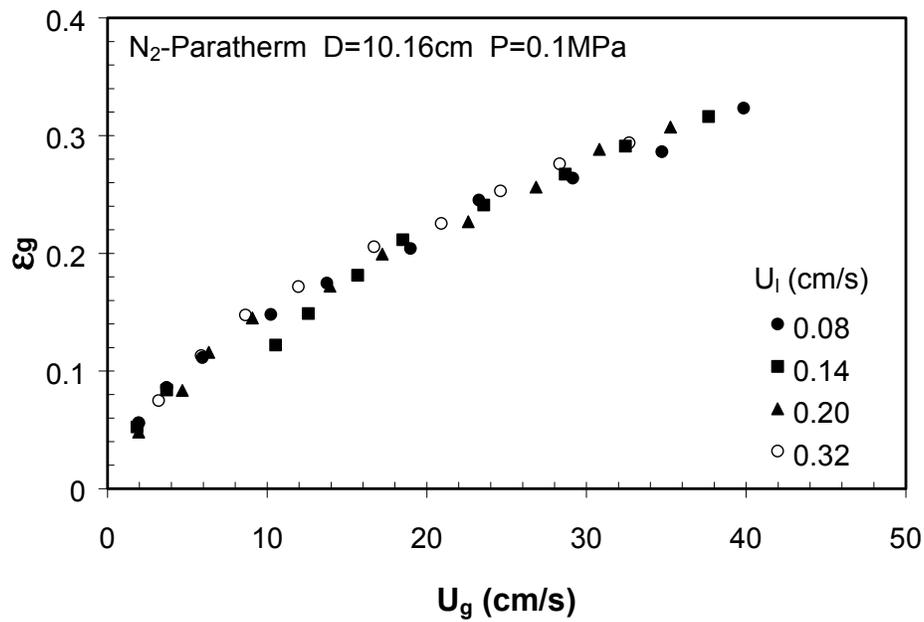
(b) 10.16-cm column

Figure 4-12. Effect of liquid-phase motion on the gas holdup in both the 5.08-cm and 10.16-cm columns.
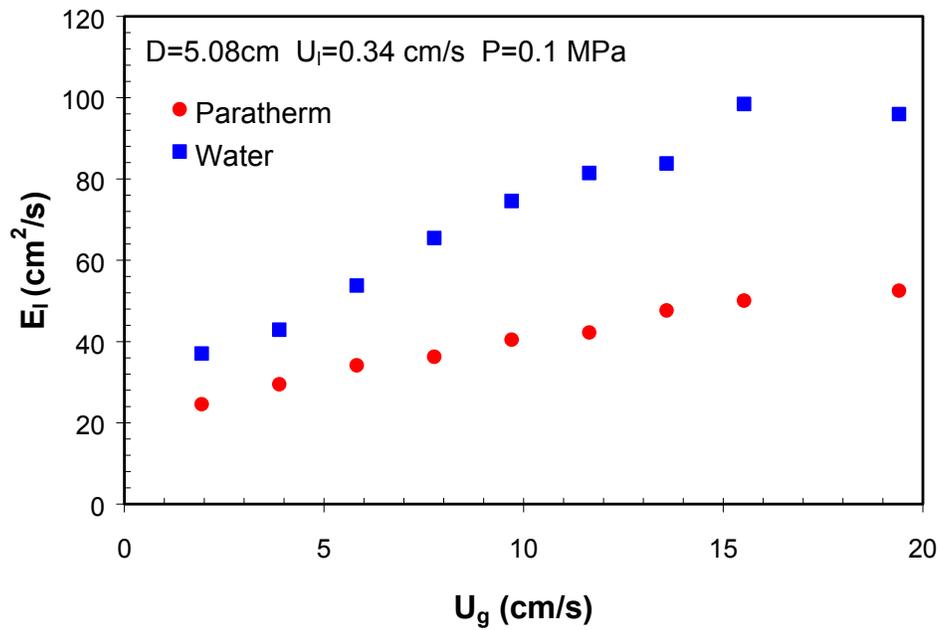
(a) dispersion coefficient
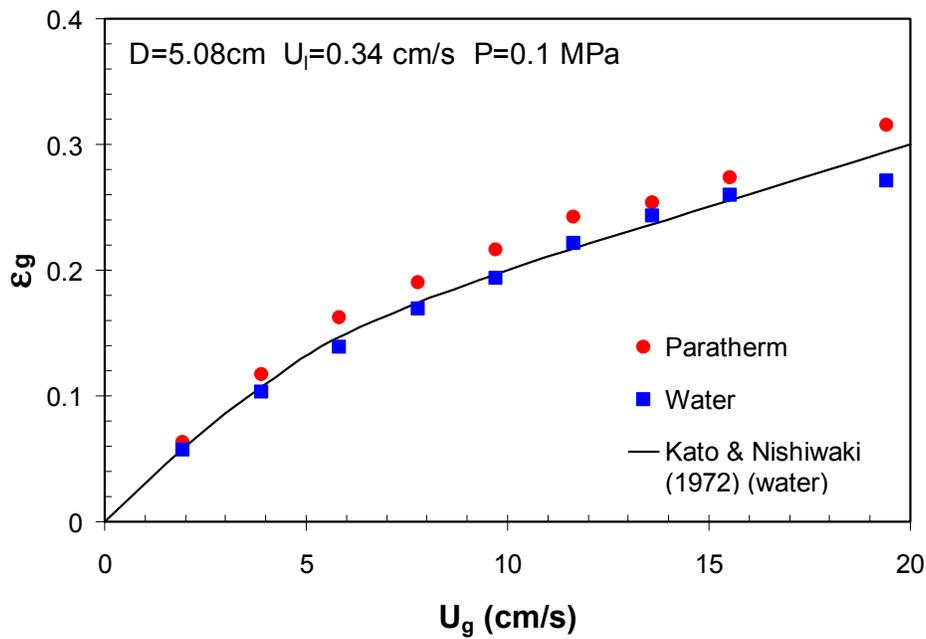
(b) gas holdup

Figure 4-13. Comparison of liquid mixing and gas holdup between water and Paratherm NF heat transfer fluid at ambient pressure.
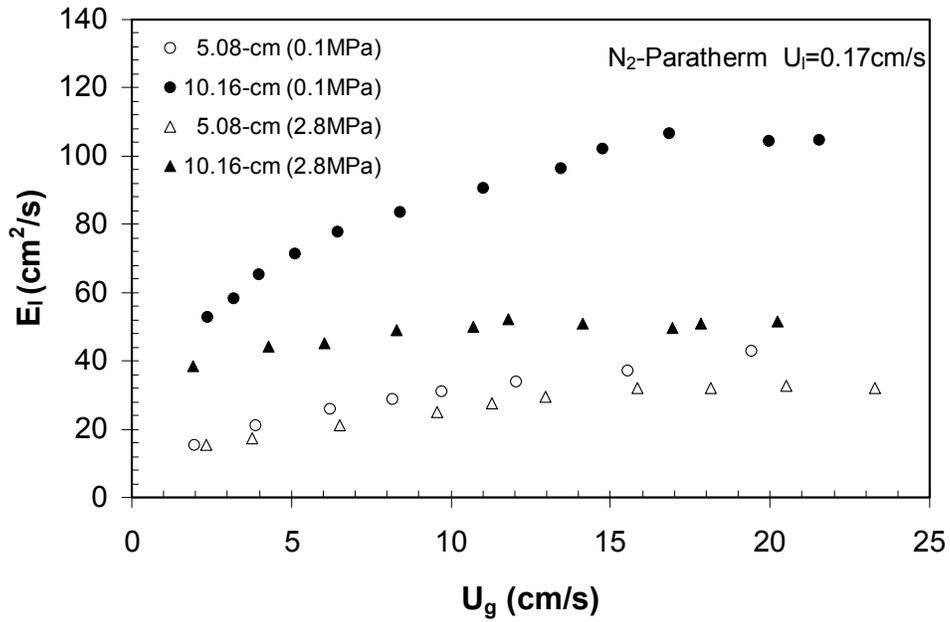
(a) dispersion coefficient
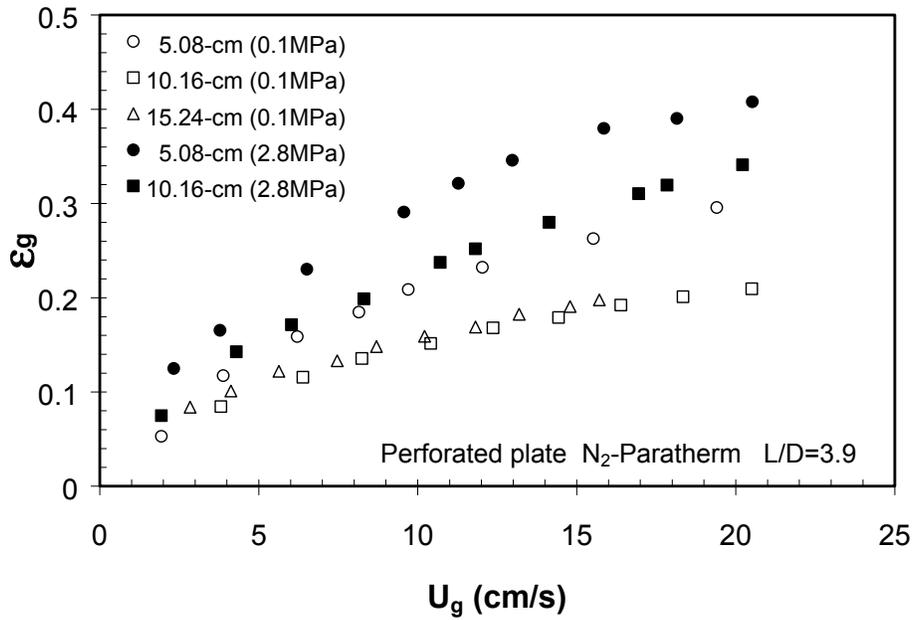
(b) gas holdup

Figure 4-14. Comparison of axial liquid dispersion coefficient and gas holdup between the 5.08-cm and 10.16-cm columns at different pressures.
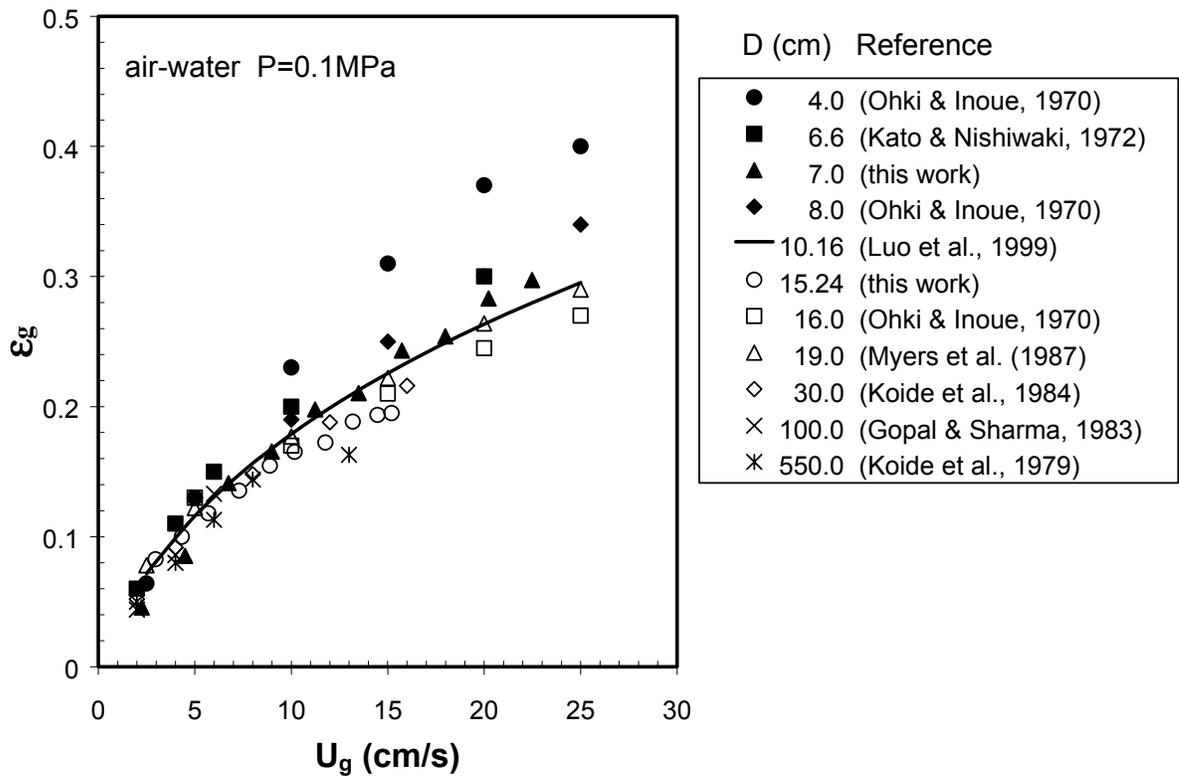
Figure 4-15. Comparison of gas holdup data obtained in different sizes of columns under ambient conditions for the air-water system.
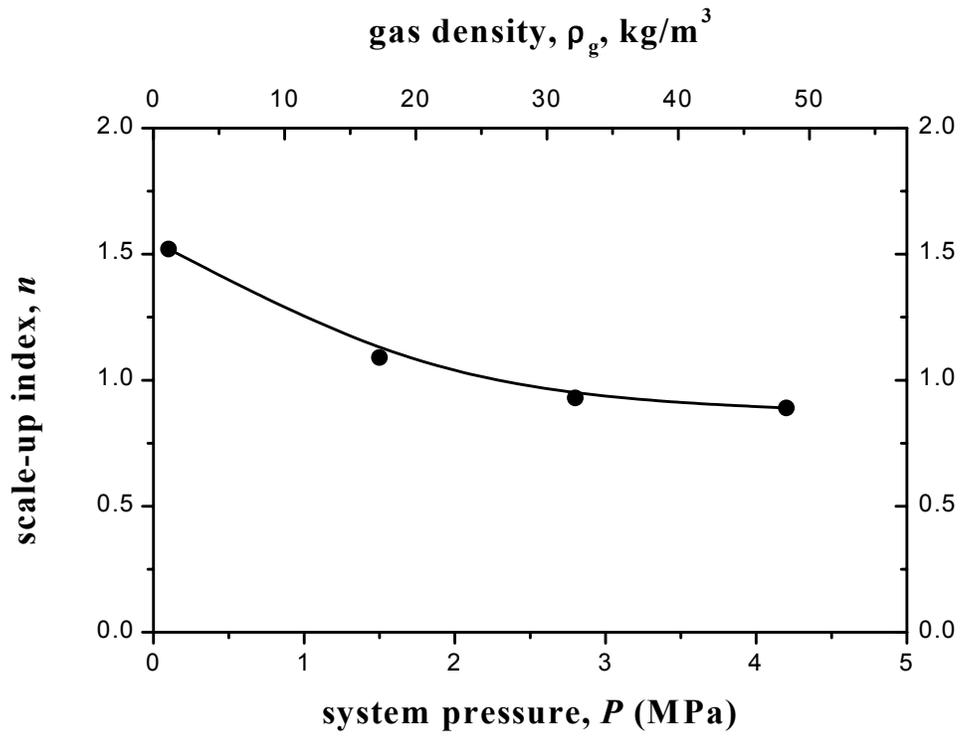
Figure 4-16. Pressure effect on the scale-up index of liquid-phase mixing.

Chapter 5: Heat-Transfer Characteristics in a Slurry Bubble Column

Introduction

  Many fundamental heat transfer studies have been conducted in bubble columns and three-phase fluidized beds at ambient conditions. A comprehensive review is available in the literature (Kim and Kang, 1997). It is known that the heat transfer coefficient in gas-liquid or gas-liquid-solid systems is higher than that in single-phase systems. The high heat transfer rate in multiphase flows is mainly due to turbulence induced by gas bubbles. Kumar et al. (1992) studied the effect of bubbles on the instantaneous heat transfer rate in liquid and liquid-solid systems. They reported that the injection of a single bubble into liquid or liquid-solid systems enhances the heat transfer rate through the bubble wake. The strong vortices and turbulence in the bubble wake region increase the heat transfer surface renewal rate. For gas-liquid or gas-liquid-solid systems, it is commonly accepted that the heat transfer coefficient increases with an increase in the gas velocity, the size of particles, and the thermal conductivity and heat capacity of the liquid, but decreases with an increase in the liquid viscosity (Kim and Laurent, 1991). In multi-bubble systems, the gas holdup may also affect the heat transfer behavior. Magiliotou et al. (1988) studied the effect of gas holdup on the heat transfer coefficient in three-phase fluidized beds. Surfactants were used to attain high gas holdups. It is found that the heat transfer coefficient is much higher in the surfactant system than that in the pure water system at a given gas velocity. Most previous studies were conducted at the ambient pressure and little work was reported for high-pressure conditions. Deckwer et al. (1980b) measured the heat transfer coefficient from an immersed heat source to the surrounding gas-liquid or gas-liquid-solid media under conditions which prevail in the Fischer-Tropsch slurry process (P=0.1 to 1.0 MPa; T=250 to 300 ^{o}C). Based on the surface renewal model and the Kolmogoroff theory of isotropic turbulence, a correlation was proposed to predict the heat transfer coefficient in slurry bubble columns. However, their study did not elucidate the effect of pressure on heat transfer behavior, since it was conducted in systems where the gas holdup is not affected by pressure. Luo et al. (1997b) studied heat transfer behavior in a three-phase fluidized bed over a pressure range of 0.1 to 15.6 MPa. Two types of glass beads, 2.1 and 3 mm in diameter, were used as the solid phase. They found that the heat transfer coefficient increases with an increase in pressure, reaches a maximum at pressures of 6 to 8 MPa, and then decreases. An empirical correlation was proposed to predict the heat transfer coefficient in three-phase fluidized beds at high pressures.

  The effect of particles on heat transfer behavior of slurry bubble columns is not fully conclusive in the literature. Deckwer et al. (1980b) studied the heat transfer behavior in a slurry bubble column. Hydrocarbon liquids and Al_2O_3 powders ($d_p \leq 5\mu m$) were used as liquid and solid phases, respectively. The solids concentration varied up to 16 wt.%. It is found that increasing solids content leads to a higher heat transfer coefficient. They postulated that this increase is possibly due to the independent motion of particles that leads to the increased exchange frequency of fluid elements on the heating surface. Saxena et al. (1990) studied the heat transfer characteristics from a cylindrical probe immersed in a slurry system containing air, water and magnetite particles. They found that the heat transfer coefficient in the three-phase system is slightly greater than that in the corresponding two-phase (gas-liquid) system, and there is only a weak dependence of the heat transfer coefficient on the particle diameter and slurry concentration. In their study,

the particle size and concentration varied in the range of 36-138 μm and 0-30 wt.%, respectively. Li and Prakash (1997) studied the instantaneous heat transfer characteristics in a slurry bubble column involving air-water-35μm glass beads. They found that the time-averaged heat transfer coefficient decreases with increasing slurry concentration up to 40 vol.%. They postulated that the addition of particles may dampen the bubble-wake turbulence and hence reduce the heat transfer rate. All studies in the literature concerning the particle effect on heat transfer behavior were conducted under ambient or low pressures.

The objective of this study is to investigate heat transfer behavior in a high-pressure slurry bubble column. Specifically, the effects of gas velocity, pressure, temperature, and solids concentration on the behavior of heat transfer between an immersed heating surface and surrounding medium are studied experimentally and analytically. The inherent mechanisms of pressure and particle effects on heat transfer behavior are discussed.

Experimental
High Pressure Slurry Bubble Column
Experiments are conducted in a high pressure multiphase flow and visualization system shown in Fig. 5-1. The high pressure column is 10.16 cm in I.D. and 1.37 m in height. The column consists of three sections: plenum, test and disengagement sections. Three pairs of quartz windows are installed on the front and rear sides of the column. A detailed description of the system is given in Luo et al. (1997b). In this study, the gas distributor used is a perforated plate with 120 square-pitched holes of 1.5 mm in diameter. At the top of the column, a copper screen is installed to prevent particle entrainment.

Compressed nitrogen and Paratherm NF heat transfer fluid are used as the gas and liquid phases, respectively. The physical properties of the gas and liquid phases vary with pressure and temperature. To fully understand the effects of pressure and temperature on heat transfer behavior, variations of these properties need to be considered in the correlation or model calculation. The physical properties of the gas and liquid phases at different pressures and temperatures are given in Table 1. At ambient conditions, the heat capacity and thermal conductivity of the liquid phase are 1.926 kJ/kg·K and 0.132 W/m·K, respectively. Glass bead particles with a density of 2,500 kg/m^3 and a mean diameter of 53 μm are used as the solid phase. The heat capacity and thermal conductivity of particles at ambient conditions are 0.837 kJ/kg·K and 0.224 W/m·K, respectively (Perry et al., 1963). The effects of pressure and temperature on the heat capacity and thermal conductivity of the liquid and solid phases are negligible under the experimental conditions of this study (Perry et al., 1963). The liquid phase is in batch operation. The superficial gas velocity, pressure, temperature and solids concentration vary in the ranges of 0 ~ 20 cm/s, 0.1 ~ 4.2 MPa, 35 ~ 81°C and 0 ~ 35 vol.%, respectively.

Heat Transfer Measurement
The heat transfer coefficient is determined by a heat transfer probe (RdF Corporation, microfoil heat flux sensor No. 27075), which is specifically designed for high-pressure and high-temperature conditions. The probe uses a microfoil heat-flow sensor that can directly measure the local heat flux through the heating surface of the probe by detecting the temperature difference across a thermal barrier of known resistance. The thermocouples in the sensor can also give the temperature of the heating surface. The

probe is placed at the center of the column and the overall dimensions of the probe are 25.4×19.1×4 mm. The details of the heat transfer probe are given elsewhere (Luo et al., 1997b). The temperature of the bulk fluid is measured with a T-type thermocouple. For each measurement, the heat flux and temperature difference between the probe surface and the bulk fluid are sampled simultaneously by using a computer data acquisition system at a rate of 100Hz for 30 seconds. The time-averaged heat transfer coefficient can be calculated from the heat flux and temperature difference by

$$h_w = \frac{1}{\tau} \int_0^\tau \frac{q(t)}{T_s(t) - T_b(t)} dt .$$

(5-1)

For each experimental condition, the measurement is conducted 4 or 5 times and the average value is used. The deviation of the results for each experimental condition is about 2~4%.

Results and Discussion
Effect of Pressure

Figure 5-2 shows the variation of heat transfer coefficient with gas velocity and pressure in slurry bubble columns. The heat transfer coefficient increases as the gas velocity increases and then levels off. Many studies conducted under ambient conditions have also shown a similar trend of gas velocity effect (Deckwer, 1980a; Saxena et al., 1990). According to the theory of isotropic turbulence, the heat transfer rate is controlled by the energy dissipation induced by micro-scale eddies. At high gas velocities, the gas flow in the slurry bubble column is in the form of large bubbles. The large bubbles do not significantly affect the energy transfer at the micro-scale level; instead they induce an enhanced liquid internal circulation (Deckwer, 1980a). The internal circulation does not improve the heat transfer coefficient appreciably, and hence a leveling off of the heat transfer coefficients occurs at high gas velocities.

Figure 5-2 also shown that the heat transfer coefficient decreases significantly with the increase of pressure. This behavior can be attributed to the variations of physical properties of the liquid phase, bubble size and gas holdup with the pressure. Since the heat transfer behavior is closely associated with macroscopic flow structures and microscopic flow characteristics, a variation in pressure, which alters the hydrodynamics, would yield a significant effect on the heat transfer behavior in the slurry system. Previous studies on heat transfer in gas-liquid and gas-liquid-solid systems indicated that an increase in the liquid viscosity decreases the heat transfer coefficient (Kato et al., 1981; Kang et al., 1985; Deckwer, 1980a; Kumar and Fan, 1994). The decrease in heat transfer coefficient with increasing liquid viscosity is possibly due to the fact that the thickness of the laminar sublayer in turbulent flow increases with liquid viscosity. Since the liquid viscosity increases with pressure, increased pressure would decrease the heat transfer coefficient due to the variation of the liquid viscosity. Other physical properties of the liquid, such as density, thermal conductivity and heat capacity, are less affected by pressure (Reid et al., 1977).

The heat transfer coefficient is also affected by the bubble characteristics and hydrodynamics such as bubble size and gas holdup. Kumar et al. (1992) found that the injection of a single bubble into liquids or liquid-solid suspensions enhances the heat transfer rate via bubble wake. Since the wake size is proportional to bubble size, a larger bubble would have a larger wake and stronger vortices associated with the wake, thereby

enhancing the rate of heat transfer. Since the bubble size decreases with increasing pressure, the pressure would have a negative effect on the heat transfer coefficient. As mentioned earlier, the gas holdup can also affect heat transfer behavior. Under high gas holdup conditions, the turbulence induced by the intense bubble-wake, bubble-bubble, and bubble-surface interactions would augment the rate of heat transfer surface renewal. Since the gas holdup and the bubble number density increase significantly with pressure, the frequency of bubble passage over the heating surface increases with pressure, and thus increases the heat transfer rate. The combination of above effects gives rise to the overall effect of pressure on the heat transfer rate.

In slurry bubble columns, it is observed that the bubble size reduces significantly with an increase in pressure especially when the pressure is below 6~8 MPa, which would result in a decrease in the heat transfer coefficient. Therefore, the bubble size is a dominant factor affecting the heat transfer rate in slurry bubble columns. For large particle systems, i.e., three-phase fluidized beds, the pressure effect on the heat transfer coefficient may be different as observed by Luo et al. (1997b). The difference in hydrodynamics and bubble characteristics between large particle systems and small particle systems was also observed by other researchers. Luewisutthichat et al. (1997) photographically studied bubble characteristics in multi-phase flow systems. They found that large particle systems (i.e., three-phase fluidized beds) exhibit appreciably different bubble behavior compared to small particle systems (i.e., slurry bubble columns). In small particle systems, the bubble flow behavior is similar to that in two-phase systems, while large particle systems exhibit a broad bubble size distribution with a large Sauter mean diameter. Therefore, the effect of pressure on heat transfer behavior, which is closely dependent on the hydrodynamics and bubble characteristics, would be different in three-phase fluidized beds and slurry bubble columns. In a three-phase fluidized bed, the variation of bubble size with pressure may become less important in affecting the heat transfer coefficient, while the increase in the gas holdup or the frequency of bubble passage over the heating surface could be a dominant factor in determining heat transfer behavior, and thus the heat transfer coefficient would increase with increasing pressure as observed by Luo et al. (1997b).

Effect of Solids Concentration
The effect of particles on the heat transfer coefficient under ambient pressure and elevated pressure (P=4.2 MPa) is shown in Fig. 5-3. For the present system, the addition of particles to the liquid greatly increases the heat transfer coefficient. This behavior can be explained by the larger bubble size in the slurry system compared to the pure liquid. Luo et al. (1999) measured the bubble size distribution in a slurry bubble column by using an optic fiber probe and found that the mean bubble size increases significantly with an increase in solids concentration, especially under ambient pressure. Thus, the heat transfer coefficient increases significantly with an increase in solids concentration. The extent to which solids concentration affects the heat transfer coefficient differs at different pressures. The effect of the solids concentration on the heat transfer coefficient at ambient pressure is more profound than that at high pressure, since the bubble size is relatively large and the effect of solids concentration on the bubble size is more remarkable at ambient pressure (Luo et al., 1999). At high pressures, the heat transfer coefficient in the three-phase system is higher than that in the two-phase system, while the difference in the heat transfer coefficients for the solids concentrations of 20% and 35% appears to be insignificant. The

reason is that the bubble size does not vary significantly with a further increase in the solids concentration at high pressures (Luo et al., 1999).

Effect of Temperature

The effect of temperature on the heat transfer coefficient is shown in Fig. 5-4. For all the pressures considered, when the temperature increases, the heat transfer coefficient increases significantly. This phenomenon can be explained by the significant decrease of the liquid viscosity with increasing temperature. Among the three factors that affect the heat transfer rate, i.e., liquid viscosity, bubble size and gas holdup, the liquid viscosity is the one most affected by the temperature. The liquid viscosity decreases significantly with increasing temperature, which results in an increase in the heat transfer coefficient. For example, at the pressure of 4.2 MPa, the liquid viscosity decreases from 0.024 Pa·s to 0.0053 Pa·s, i.e., a 78% decrease as the temperature increases from 35^oC to 81^oC. Based on the correlation proposed by Deckwer (1980a), the heat transfer coefficient is proportional to the -0.25 power of the liquid viscosity in gas-liquid systems. Therefore, the 78% decrease in liquid viscosity would result in the 46% increase in heat transfer coefficient. From the experimental data shown in Fig. 5-4(a), at the gas velocity of 10 cm/s, the heat transfer coefficient increases from 514 to 676 $w/m^2 \cdot k$, i.e., a 32% increase as the temperature increases from 35^oC to 81^oC. Thus, the change in the liquid viscosity is the determining factor for the effect of temperature on the heat transfer coefficient in the system of this study.

Correlation

Among various factors that affect the heat transfer coefficient from an immersed surface to the surrounding medium in bubble columns, the most important are liquid properties (ρ_l, μ_l, k_l and C_{pl}), operating conditions (u_g), and hydrodynamics (d_b and ε_g). Based on the Higbie surface renewal model and the Kolmogoroff theory of isotropic turbulence, Deckwer (1980a) proposed the following form of semitheoretical correlation to predict the heat transfer coefficient in bubble columns:

$$St = c\left(\text{ReFrPr}^a\right)^b \tag{5-2}$$

where *St, Re, Fr* and *Pr* are Stanton, Reynolds, Froude and Prandtl numbers based on the liquid properties, respectively, and *a*, *b* and *c* are constants obtained by fitting the experimental data. Based on the semitheoretical analysis, Deckwer et al. (1980a) found that *a*, *b* and *c* are equal to 2, -0.25 and 0.1, respectively. Other researchers (Kast, 1962; Shaykhutdinov et al., 1971; Hart, 1976; Steiff and Weinspach, 1978) also used this form of correlation to represent their heat transfer results and found that the values of parameters *a*, *b* and *c* are in the ranges of 1.9 ~ 2.5, -0.27 ~ -0.22, and 0.1 ~ 0.14, respectively, as summarized by Deckwer et al. (1980a). By assuming the liquid-solid suspension as a homogeneous phase, Deckwer et al. (1980b) found that Eq. (5-2) can also be used in a slurry system if the physicochemical properties of the slurry can be estimated from the individual phases. Equation (5-2) is only perceived to be applicable for ambient pressure since this correlation was obtained in systems where the gas holdup is not affected by pressure. However, for systems in which pressure has a significant influence on the hydrodynamics, the pressure effect on the heat transfer coefficient should be considered in the correlation. For the system in the present study, the experimental results indicate that

pressure has a significant effect on heat transfer behavior in both bubble columns and slurry bubble columns. Therefore, in order to extend Eq. (5-2) to the high-pressure conditions, it is necessary to include the terms that account for the effect of pressure in the correlation. Studies in the literature have indicated that the heat transfer coefficient in bubble columns is influenced by the gas holdup (Zehner, 1986; Magiliotou et al., 1988), and since the gas holdup strongly depends on the system pressure (Luo et al., 1999), including the gas holdup term in the correlation would account for the pressure effect on the heat transfer coefficient. Examining the relationship between the heat transfer coefficient and the gas holdup based on the analytical model as will be discussed later, reveals that h_w may be related to $(1-\varepsilon_g)/\varepsilon_g$, i.e.,

$$h_w \propto \left(\frac{1-\varepsilon_g}{\varepsilon_g} \right)^\alpha .$$ (5-3)

Thus, based on Eq. (5-2) and considering the effect of gas holdup on the heat transfer coefficient, the following correlation is proposed to quantify the heat transfer coefficient in a slurry bubble column at elevated pressures:

$$St_m = c \left[\left(\text{Re}_m \, Fr \, \text{Pr}_m{}^a \right) \left(\frac{\varepsilon_g}{1-\varepsilon_g} \right) \right]^b .$$ (5-4)

The constants a, b and c are obtained by fitting the experimental data. For the present system, a, b and c are found to be 1.87, -0.22 and 0.037, respectively.

To use Eq. (5-4) the density and the heat capacity of the suspension can be evaluated by

$$\rho_m = \rho_l(1-\varepsilon_s) + \rho_s\varepsilon_s$$ (5-5)

$$C_{pm} = C_{pl}(1-\omega_s) + C_{ps}\omega_s$$ (5-6)

where ω_s represents the weight fraction of the solid phase. Based on the electrical analogy for liquid-solid suspensions, Tareef (1940) proposed the following equation to calculate the thermal conductivity of the suspension:

$$k_m = k_l \frac{2k_l + k_s - 2\varepsilon_s(k_l - k_s)}{2k_l + k_s + \varepsilon_s(k_l - k_s)} .$$ (5-7)

The suspension viscosity of the present system is calculated based on the correlation proposed by Luo et al. (1997a) as follows:

$$\frac{\mu_m}{\mu_l} = \exp\left[\frac{K\varepsilon_s}{1-(\varepsilon_s/\varepsilon_{sc})} \right]$$ (5-8)

with two parameters correlated by

$$K = \{3.1 - 1.4\tanh[0.3(10 - 10^2 U_t)]\}/\phi$$ (5-9a)

$$\varepsilon_{sc} = \{1.3 - 0.1\tanh[0.5(10 - 10^2 U_t)]\}\varepsilon_{s0}$$ (5-9b)

where U_t is in m/s. The gas holdup in a slurry bubble column at elevated pressures can be calculated by using the empirical correlation developed in our group by Luo et al. (1999):

$$\frac{\varepsilon_g}{1-\varepsilon_g} = \frac{2.9\left(\dfrac{u_g^4 \rho_g}{\sigma g}\right)^\alpha \left(\dfrac{\rho_g}{\rho_m}\right)^\beta}{[\cosh(Mo_m^{0.054})]^{4.1}}$$ (5-10)

where Mo_m is the modified Morton number for the slurry phase, $(\xi\mu_l)^4 g/\rho_m\sigma^3$, and

$$\alpha = 0.21 Mo_m^{0.0079} \text{ and } \beta = 0.096 Mo_m^{-0.011}.$$ (5-11)

ξ is a correction factor which accounts for the effect of particles on slurry viscosity:

$$\ln\xi = 4.6\varepsilon_s\{5.7\varepsilon_s^{0.58}\sinh[-0.71\exp(-5.8\varepsilon_s)\ln Mo^{0.22}]+1\}$$ (5-12)

where Mo is the Morton number of the liquid, $g\mu_l^4/\rho_l\sigma^3$. This correlation is obtained based on numerous experimental data of the gas holdup in high-pressure systems. The experimental data of the gas holdup have been given in Luo et al. (1999), and the correlation can accurately predict the gas holdup at high pressures including the conditions of this study.

The comparison between the experimental data and the correlation calculation is given in Fig. 5-5. It is shown that the deviation of the predictions is within ±20% and the average deviation is 6.9%. The comparison of the predictions based on the correlation proposed by Deckwer et al. (1980b) (i.e., Eq. 5-2) and that obtained in this study (Eq. 5-4) is shown in Fig. 5-6. As shown in the figure, the correlation proposed by Deckwer et al. (1980b) cannot predict the trend of the pressure effect on the heat transfer coefficient for systems in which pressure has a significant effect on hydrodynamics. The correlation obtained in this study can reasonably predict the pressure effect in such systems.

Heat Transfer Model

A consecutive film and surface renewal model originally developed by Wasan and Ahluwalia (1969) could be used to analyze the heat transfer behavior in bubble columns. The schematic diagram of this model is shown in Fig. 5-7. The model assumes that a thin liquid film with a thickness of δ exists surrounding the heating surface, and liquid elements are in contact with the outer surface of the film via the bubble motion or liquid turbulence. The liquid elements contact the film for a short time, t_c, and then are replaced by fresh liquid elements from the bulk fluid. During the contact, the heat is transferred to the bulk liquid through conduction in the liquid film and unsteady state conduction in the liquid elements. Based on the energy balance, the heat transfer coefficient can be expressed in terms of the physical properties of the liquid, the film thickness, and the contact time between the liquid elements and the film as (Wasan and Ahluwalia, 1969):

$$h_w = \frac{2k_l}{\sqrt{\pi\alpha t_c}} + \frac{k_l\delta}{\alpha t_c}\left[e^{\alpha t_c/\delta^2}\left(1-erf\frac{\sqrt{\alpha t_c}}{\delta}\right)-1\right].$$ (5-13)

Based on Eq. (5-13), the heat transfer coefficient depends on the film thickness and contact time between the liquid elements and the film. Thinner film and shorter contact time lead to a higher heat transfer rate. When the physical properties of the liquid-solid suspension are used in Eq. (5-13), this model can also predict the heat transfer coefficient in slurry bubble columns.

Based on the border diffusion layer model (Azbel, 1981), the order of magnitude of the film thickness may be estimated by (Kumar and Fan, 1994)

124

$$\delta = \frac{6.14L}{Re_m^{3/4} Pr_m^{1/3}} \tag{5-14}$$

where Re_m is based on the length of heat transfer probe, i.e., $\rho_m L u_b / \mu_m$. L is the length of the heat transfer probe. The physical properties of the suspension, such as ρ_m, C_{pm}, k_m and μ_m, are calculated based on the corresponding properties of the liquid and solid phases and the solids concentration, as shown in Eqs. (5-5) ~ (5-8).

The contact time between the liquid elements and the film is assumed to be equal to the contact time between the bubbles and the film, when considering the bubble motion as the driving force of the liquid element replacement with negligible effects of liquid turbulence. Based on this consideration, the contact time can be estimated by the following equation (Kumar and Fan, 1994)

$$t_c = \frac{L}{u_b} \tag{5-15}$$

where u_b is the actual bubble rise velocity in a stream of bubbles. If the effects of pressure on the liquid properties and bubble characteristics such as bubble size and bubble rise velocity are known, this model may be used to illustrate the heat transfer behavior in a high-pressure system.

In slurry bubble columns, the bubble size is typically related to the physical properties of gas and liquid phases, gas velocity and solids concentration. Fukuma et al. (1987) measured the bubble size and bubble rise velocity in a slurry bubble column at ambient pressure with a dual-electroresistivity probe. Based on the analysis of the drift flux of gas, they found that the mean bubble rise velocity can be related to the gas holdup in the column

$$u_b \propto \frac{u_g(1-\varepsilon_g)}{\varepsilon_g}. \tag{5-16}$$

Considering the effect of pressure, an empirical equation accounting for the mean bubble rise velocity in slurry bubble columns is proposed to be of the following form:

$$u_b = \alpha \left[\frac{u_g(1-\varepsilon_g)}{\varepsilon_g} \right]^\beta. \tag{5-17}$$

α and β in the equation are obtained by fitting experimental data as $\alpha = 0.8$ and $\beta = 0.5$. The gas holdup can be calculated from Eq. (5-10). Based on Eqs. (5-13)~(5-15) and (5-17), the heat transfer coefficient under high-pressure conditions can be estimated.

The heat transfer coefficients in slurry bubble columns predicted by the model are also shown in Fig. 5-2 by solid lines. The prediction is in good agreement with the experimental data. The comparison between the experimental data and model predictions is shown in Fig. 5-8. The average deviation is less than 10%. In the heat transfer model, some assumptions or simplifications need to be made in order to estimate the film thickness and the contact time, such as neglecting the liquid circulation, and assuming uniform bubble size and bubble rise velocity. The model predictions can be further improved if the internal circulation of liquid flow and the bubble size distribution could be incorporated into the model.

Based on the model, the heat transfer resistance consists of the film resistance and the resistance due to the unsteady state conduction through the liquid elements. The

comparison of heat transfer resistance due to the film (δ/k_m) with the total heat transfer resistance ($1/h_w$) is shown in Fig. 5-9. It is found that the film resistance accounts for 68%~85% of the total heat transfer resistance under various operating conditions in this study. Thus, it can be concluded that the heat transfer in high-pressure slurry bubble columns is predominantly determined by the conduction through the fluid film surrounding the heating surface. The film thickness and contact time between the fluid elements and the film estimated by the model under various operating conditions are shown in Fig. 10. It is shown that the film thickness and contact time are typically in the ranges of 0.1 ~ 0.3 mm and 0.02 ~ 0.1 s, respectively. It is also found that the bubble rise velocity estimated by the proposed equation, i.e. Eq. (5-17), is within 0.3 ~ 1.2 m/s, which agrees well with the literature data given in Fan et al. (1999). Figure 11 shows the comparison of the actual bubble rise velocity predicted by Eq. (5-17) and the bubble swarm velocity (i.e., u_g/ε_g) reported in the literature in high-pressure bubble columns. It can be seen that Eq. (5-17) can reasonably predict the magnitude of bubble rise velocity and the trend of the pressure effect on the bubble rise velocity.

As shown in Table 5-1 and Fig. 5-11, when the pressure increases, the liquid viscosity increases and the bubble rise velocity decreases. The variations of liquid viscosity and bubble rise velocity result in a thicker film and longer contact time at higher pressures, based on Eqs. (5-14) and (5-15). Therefore, from the film and surface renewal model (Eq. 5-13), the heat transfer rate decreases with increasing pressure due to an increase in the film thickness and contact time between the fluid elements and the film. It is also noted that both the liquid viscosity and the bubble rise velocity affect the film thickness according to the relation derived from Eq. (5-14),

$$\delta \propto u_b^{-3/4} \mu_m^{5/12}. \tag{5-18}$$

For instance, when the pressure increases from the ambient pressure to 4.2 MPa, the liquid viscosity increases from 0.019 to 0.024 Pa·s, an increase of 26% at 35°C in gas-liquid systems, which would result in a 57% increase in the film thickness, based on Eq. (5-18). Meanwhile, the bubble rise velocity decreases from 0.7 m/s to 0.3 m/s, a decrease of 57%, as shown in Fig. 11, which would result in a 66% increase in the film thickness. Therefore, the variations of both the liquid viscosity and the bubble rise velocity are important in accounting for the change of the film thickness with the pressure.

Concluding Remarks

Experiments are conducted to study the heat transfer behavior in a high-pressure slurry bubble column. The effects of pressure, temperature and solids concentration on the heat transfer coefficient are examined. It is found that the liquid properties, bubble size, and gas holdup play a key role in determining the heat transfer coefficient under high pressures. The heat transfer coefficient decreases with increasing pressure, due to the reduced bubble size and increased liquid viscosity. The addition of particles to the liquid phase yields larger bubbles and thus a higher heat transfer rate. The effect of temperature on the heat transfer coefficient is mainly determined by the variation of the liquid viscosity. The heat transfer behavior in a slurry bubble column under the pressure range considered in this study can be described using the consecutive film and surface renewal model.

126

Notations

C_{pl} heat capacity of liquid, J/(kg·K)
C_{pm} heat capacity of liquid-solid suspension, J/(kg·K)
C_{ps} heat capacity of solids, J/(kg·K)
d_b bubble diameter, m
d_p particle diameter, m

Fr Froude number, $\dfrac{u_g^2}{gd_b}$

g gravitational acceleration, m/s^2
h_w time-averaged heat transfer coefficient, W/(m^2·K)
K proportionality constant defined in Eq. (9a), dimensionless
k_l thermal conductivity of liquid, W/(m·K)
k_m thermal conductivity of liquid-solid suspension, W/(m·K)
k_s thermal conductivity of solids, W/(m·K)
L vertical length of heating surface, m

Mo Morton number based on liquid properties, $\dfrac{g\mu_l^4}{\rho_l\sigma^3}$

Mo_m modified Morton number based on slurry properties, $\dfrac{(\xi\mu_l)^4 g}{\rho_m\sigma^3}$

P system pressure, Pa

Pr Prandtl number based on liquid properties, $\dfrac{C_{pl}\mu_l}{k_l}$

Pr_m Prandtl number based on slurry properties, $\dfrac{C_{pm}\mu_m}{k_m}$

q heat flux through the heating surface, W/m^2

Re Reynolds number based on liquid properties, $\dfrac{u_g d_b \rho_l}{\mu_l}$

Re_m Reynolds number based on slurry properties, $\dfrac{u_g d_b \rho_m}{\mu_m}$

St Stanton number based on liquid properties, $\dfrac{h_w}{\rho_l C_{pl} u_g}$

St_m Stanton number based on slurry properties, $\dfrac{h_w}{\rho_m C_{pm} u_g}$

T system temperature, K
t time, s
T_b temperature of the bulk fluid, K
t_c contact time between the liquid elements and the film, s
T_s temperature of the heating surface, K
u_b actual bubble rise velocity in a stream of bubbles, m/s

u_g superficial gas velocity, m/s

U_t particle terminal velocity in liquid, m/s

Greek letters

α thermal diffusivity of liquid, $\dfrac{k_l}{\rho_l C_{pl}}$, m^2/s

α_m thermal diffusivity of liquid-solid suspension, $\dfrac{k_m}{\rho_m C_{pm}}$, m^2/s

δ film thickness, m

ε_g gas holdup, dimensionless

ε_s solids concentration, dimensionless

ε_{sc} critical solids holdup, dimensionless

ε_{s0} solids holdup at incipient fluidization/packed state, dimensionless

ϕ particle sphericity, dimensionless

μ_l liquid viscosity, Pa·s

μ_m viscosity of liquid-solid suspension, Pa·s

ρ_g gas density, kg/m^3

ρ_l liquid density, kg/m^3

ρ_m density of liquid-solid suspension, kg/m^3

ρ_s solids density, kg/m^3

σ surface tension, N/m

τ total sampling time, s

ξ parameter accounting for the effect of particles on the viscosity, dimensionless

ω_s weight fraction of the solid phase, dimensionless

References

Azbel, D. *Two-Phase Flows in Chemical Engineering*; Cambridge University Press: Cambridge, UK, 1981.

Deckwer, W. D. On the Mechanism of Heat Transfer in Bubble Column Reactors. *Chem. Eng. Sci.* **1980a**, 35, 1341.

Deckwer, W. D.; Louisi, Y.; Zaidi, A.; Ralek, M. Hydrodynamic Properties of the Fischer-Tropsch Slurry Process. *Ind. Eng. Chem. Proc. Des. Dev.* **1980b**, 19, 699.

Fan, L. S.; Yang, G. Q.; Lee, D. J.; Tsuchiya, K.; Luo, K. Some Aspects of High-Pressure Phenomena of Bubbles in Liquids and Liquid-Solid Suspensions. *Chem. Eng. Sci.* **1999**, 54, 4681.

Fukuma, M.; Muroyama, K.; Yasunishi, A. Properties of Bubble Swarm in a Slurry Bubble Column. *J. Chem. Eng. Japan* **1987**, 20, 28.

Hart, W. F. Heat Transfer in Bubble-Agitated Systems: A General Correlation. *Ind. Eng. Chem. Process Des. Dev.* **1976**, 15, 109.

Kang, Y.; Suh, I. S.; Kim, S. D. Heat Transfer Characteristics of Three-Phase Fluidized Beds. *Chem. Eng. Comm.* **1985**, 34, 1.

Kast, W. Analyse Des Warmeubergangs in Blasensaulen. *Int. J. Heat Mass Transfer* **1962**, 5, 329.

Kato, Y.; Uchida, K.; Morooka, S. Liquid Holdup and Heat Transfer Coefficient between Bed and Wall in Liquid-Solid and Gas-Liquid-Solid Fluidized Beds. *Powder Technology* **1981**, 28, 173.

Kim, S. D.; Laurent, A. The State of Knowledge on Heat Transfer in Three-Phase Fluidized Beds. *Int. Chem. Eng.* **1991**, 31, 284.

Kim, S. D.; Kang, Y. Heat and Mass Transfer in Three-Phase Fluidized-Bed Reactors-an Overview. *Chem. Eng. Sci.* **1997**, 52, 3639.

Kumar, S.; Fan, L. S. Heat Transfer Characteristics in Viscous Gas-Liquid and Gas-Liquid-Solid Systems. *AIChE J.* **1994**, 40, 745.

Kumar, S.; Kusakabe, K.; Raghunathan, K.; Fan, L. S. Mechanism of Heat Transfer in Bubbly Liquid and Liquid-Solid Systems: Single Bubble Injection. *AIChE J.* **1992**, 38, 733.

Li, H.; Prakash, A. Heat Transfer and Hydrodynamics in a Three-Phase Slurry Bubble Column. *Ind. Eng. Chem. Res.* **1997**, 36, 4688.

Letzel, H. M.; Schouten, J. C.; van den Bleek, C. M.; Krishna, R. Influence of Elevated Pressure on the Stability of Bubbly Flows. *Chem. Eng. Sci.* **1997**, 52, 3733.

Luewisutthichat, W.; Tsutsumi, A.; Yoshida, K. Bubble Characteristics in Multi-Phase Flow Systems: Bubble Sizes and Size Distributions. *J. Chem. Eng. Japan* **1997**, 30, 461.

Luo, X.; Lee, D. J.; Lau, R.; Yang, G. Q.; Fan, L. S. Maximum Stable Bubble Size and Gas Holdup in High-Pressure Slurry Bubble Columns. *AIChE J.* **1999**, 45, 665.

Luo, X.; Zhang, J.; Tsuchiya, K.; Fan, L. S. On the Rise Velocity of Bubbles in Liquid-Solid Suspensions at Elevated Pressure and Temperature. *Chem. Eng. Sci*. **1997a**, 52, 3693.

Luo, X.; Jiang, P.; Fan, L. S. High Pressure Three-Phase Fluidization: Hydrodynamics and Heat Transfer. *AIChE J.* **1997b**, 43, 2432.

Magiliotou, M.; Chen, Y. M.; Fan, L. S. Bed-Immersed Object Heat Transfer in a Three-Phase Fluidized Bed. *AIChE J.* **1988**, 34, 1043.

Perry, R. H.; Chilton, C. H.; Kirkpatrick, S. D. *Chemical Engineers' Handbook;* McGraw-Hill: New York, 1963.

Reid, R. C.; Prausnitz, J. M.; Sherwood, T. K. *The Properties of Gases and Liquids;* McGraw-Hill: New York, 1977.

Saxena, S. C.; Rao, N. S.; Saxena, A. C. Heat Transfer from a Cylindrical Probe Immersed in a Three-Phase Slurry Bubble Column. *Chem. Eng. J.* **1990**, 44, 141.

Shaykhutdinov, A. G.; Bakirov, N. U.; Usmanov, A. G. Determination and Mathematical Correction of Heat Transfer Coefficients under Conditions of Bubble Flow, Cellular, and Turbulent Foam. *Int. Chem. Eng.* **1971**, 11, 641.

Steiff, A.; Weinspach, P. M. Heat Transfer in Stirred and Non-Stirred Gas-Liquid Reactors. *Ger. Chem. Eng.* **1978**, 1, 150.

Tareef, B. M. Thermal Conductivity of Colloidal Systems. *Colloidal J. of USSR* **1940**, 6, 545.

Wasan, D. T.; Ahluwalia, M. S. Consecutive Film and Surface Renewal Mechanism for Heat and Mass Transfer from a Wall. *Chem. Eng. Sci.* **1969**, 24, 1535.

Wilkinson, P. M.; Dierendonck, L. L. v. Pressure and Gas Density Effects on Bubble Break-up and Gas Hold-up in Bubble Columns. *Chem. Eng. Sci.* **1990**, 45, 2309.

Zehner, P. Momentum, Mass and Heat Transfer in Bubble Columns. Part 2. Axial Blending and Heat Transfer. *Int. Chem. Eng.* **1986**, 26, 29.

Table 5-1. Physical properties of nitrogen and Paratherm NF heat transfer fluid at different pressures and temperatures

(a) T=35°C

P(MPa)	ρ_g(kg/m^3)	ρ_l(kg/m^3)	μ_l(Pa·s)	σ_l(N/m)
0.1	1.09	864	0.019	0.029
0.8	8.74	865	0.020	0.028
1.5	16.4	866	0.021	0.027
4.2	45.9	870	0.024	0.026

(b) T=81°C

P(MPa)	ρ_g(kg/m^3)	ρ_l(kg/m^3)	μ_l(Pa·s)	σ_l(N/m)
0.1	0.95	845	0.0047	0.025
0.8	7.61	847	0.0049	0.025
1.5	14.3	848	0.0050	0.024
4.2	39.9	854	0.0053	0.022
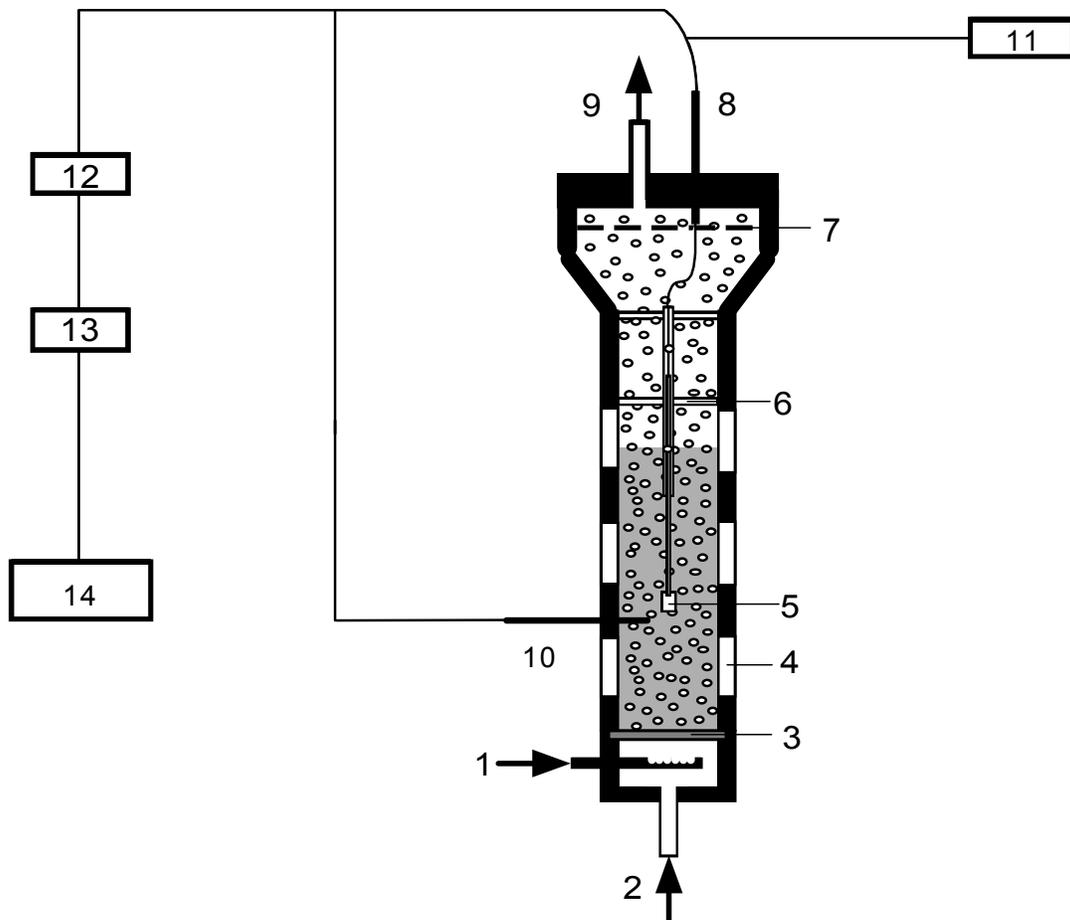
Figure 5-1. Experimental setup for the measurement of heat transfer coefficient in high-pressure slurry bubble columns.

1. Gas inlet; 2. Liquid inlet; 3. Perforated plate distributor; 4. Quartz windows; 5. Heat transfer probe; 6. Support of the probe; 7. Copper screen; 8. Sealing and signal cables; 9. Gas and liquid outlet; 10. Thermocouple; 11. DC power; 12. Signal amplifier; 13. Data acquisition system; 14. Computer.
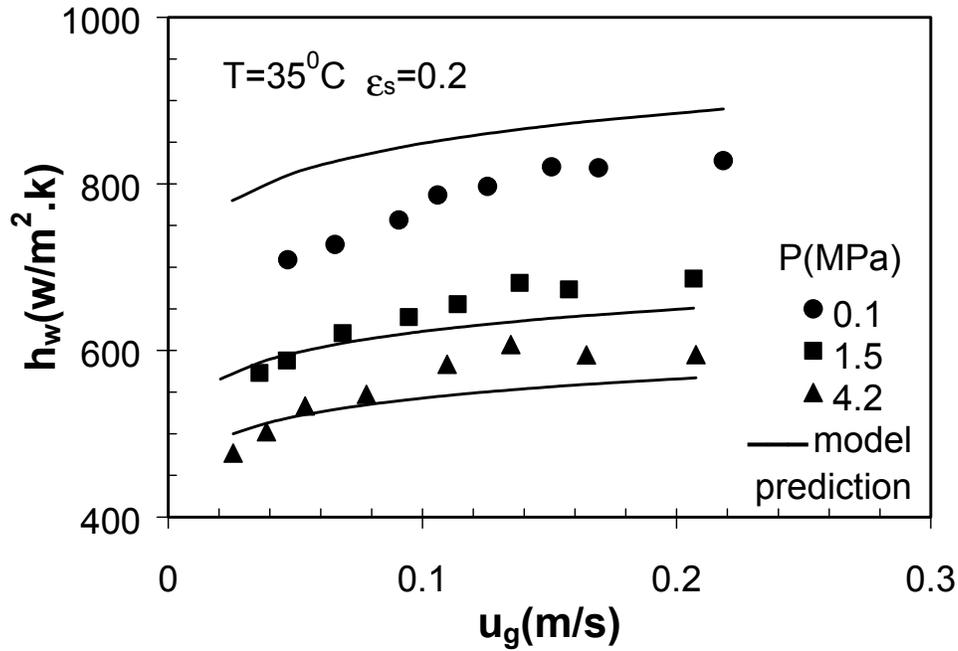
(a)
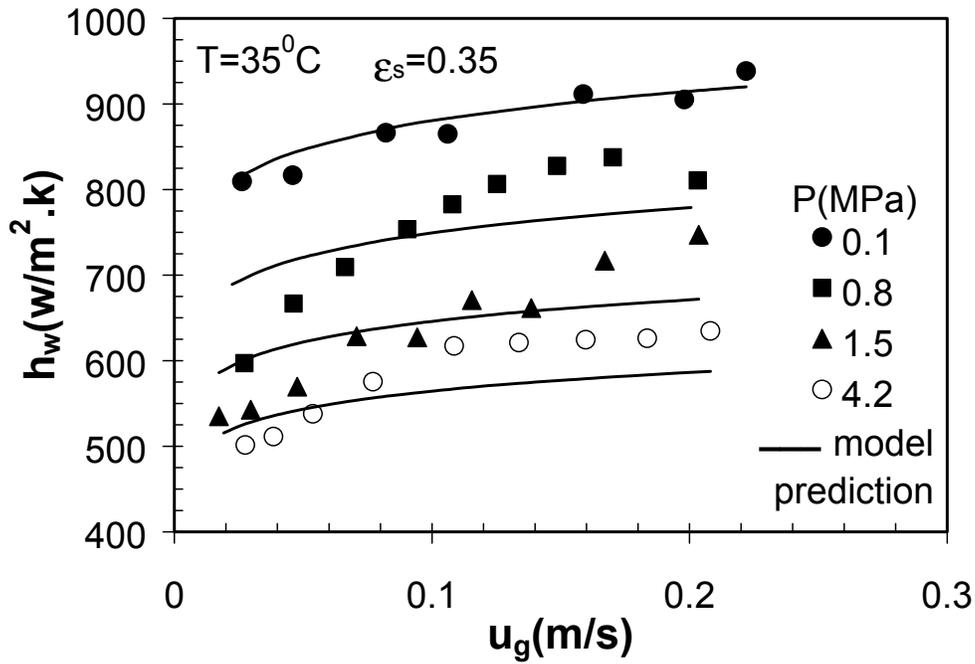
(b)

Figure 5-2. Pressure effect on heat transfer coefficients in slurry bubble columns
(T=35°C): (a) ε_s=0.2; and (b) ε_s=0.35.

133
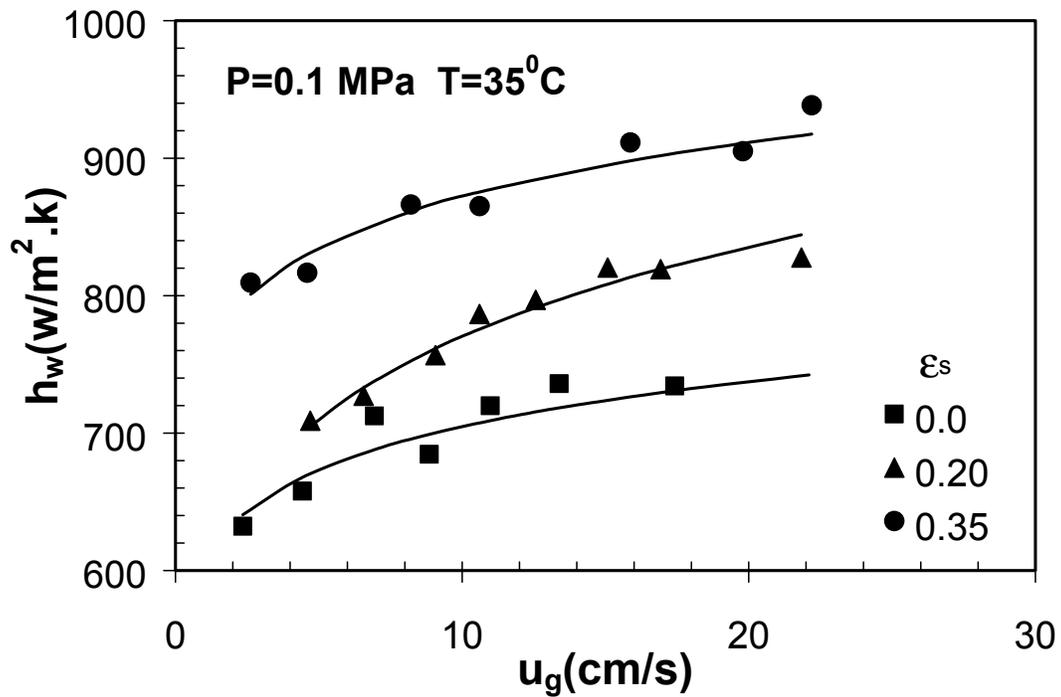
(b) ambient pressure
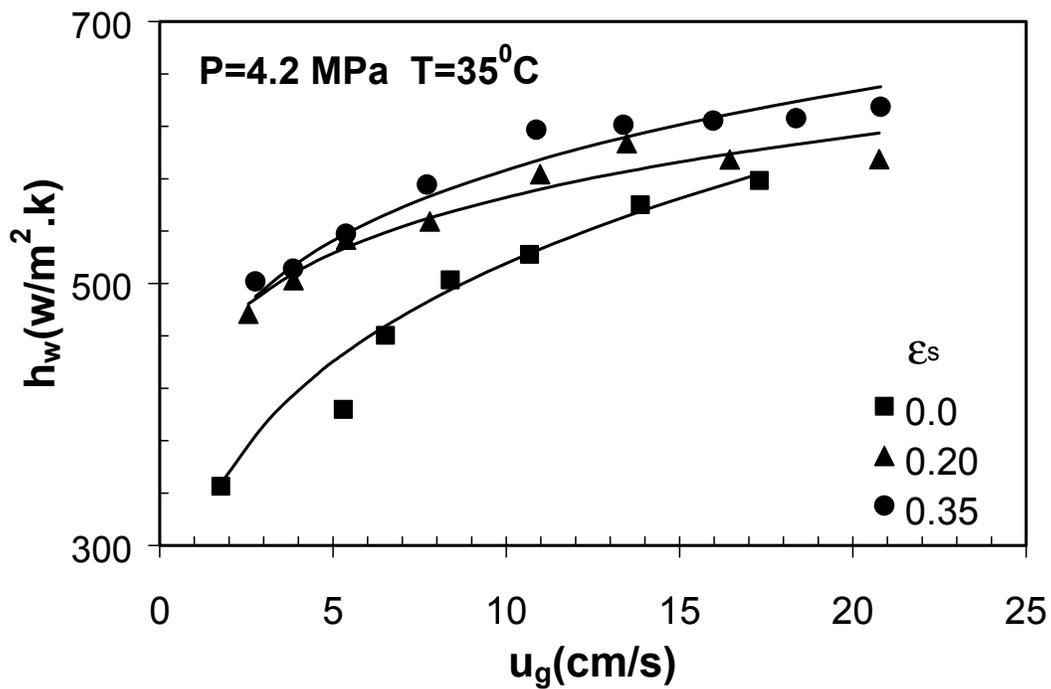
(c) high pressure

Figure 5-3.   Heat transfer coefficient as a function of gas velocity at different solids concentrations (T=35°C) under: (a) ambient pressure; and (b) high pressure (P=4.2 MPa).
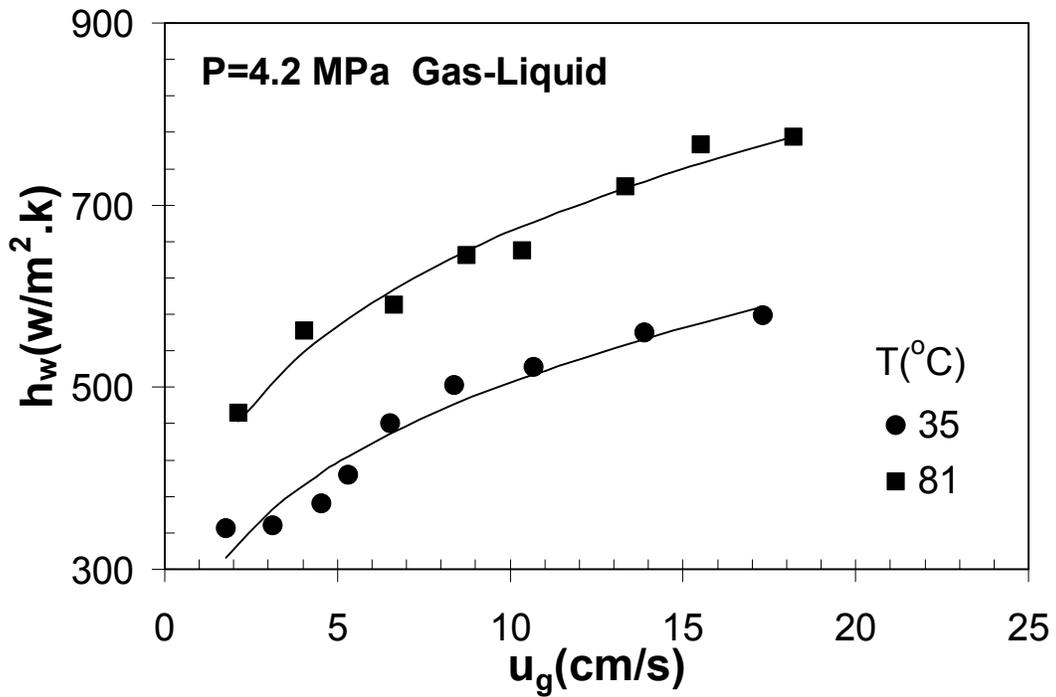
(b) bubble columns
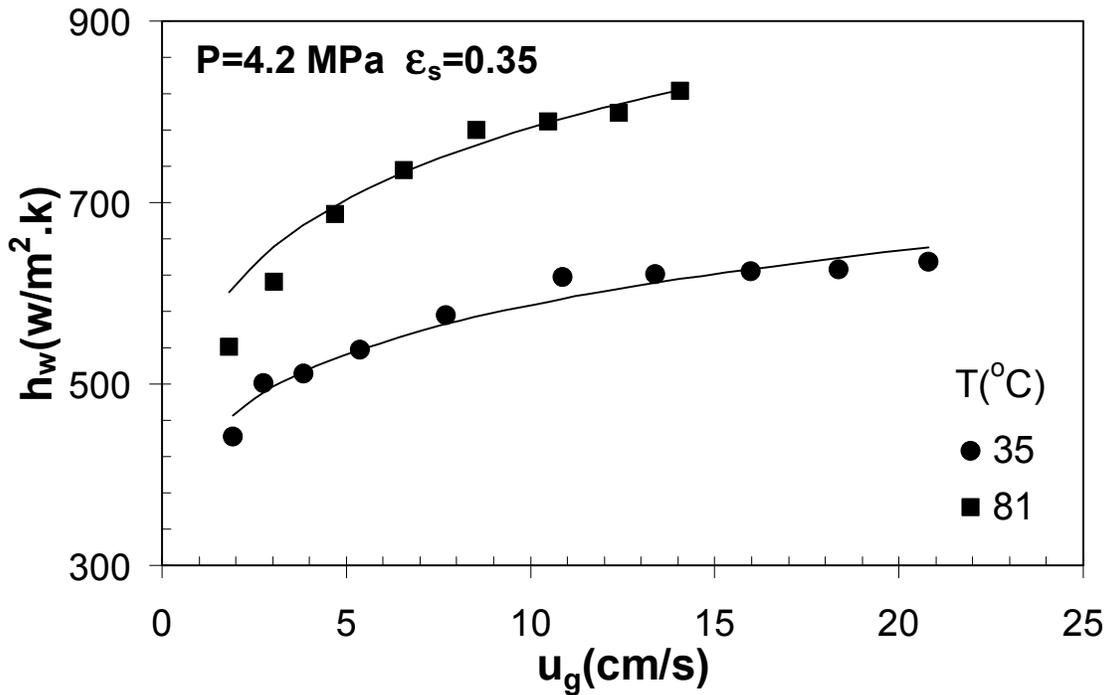
(c) slurry bubble columns

Figure 5-4.   Heat transfer coefficient as function of gas velocity at different temperatures (P=4.2 MPa) in: (a) bubble columns; and (b) slurry bubble columns (ε_s=0.35).
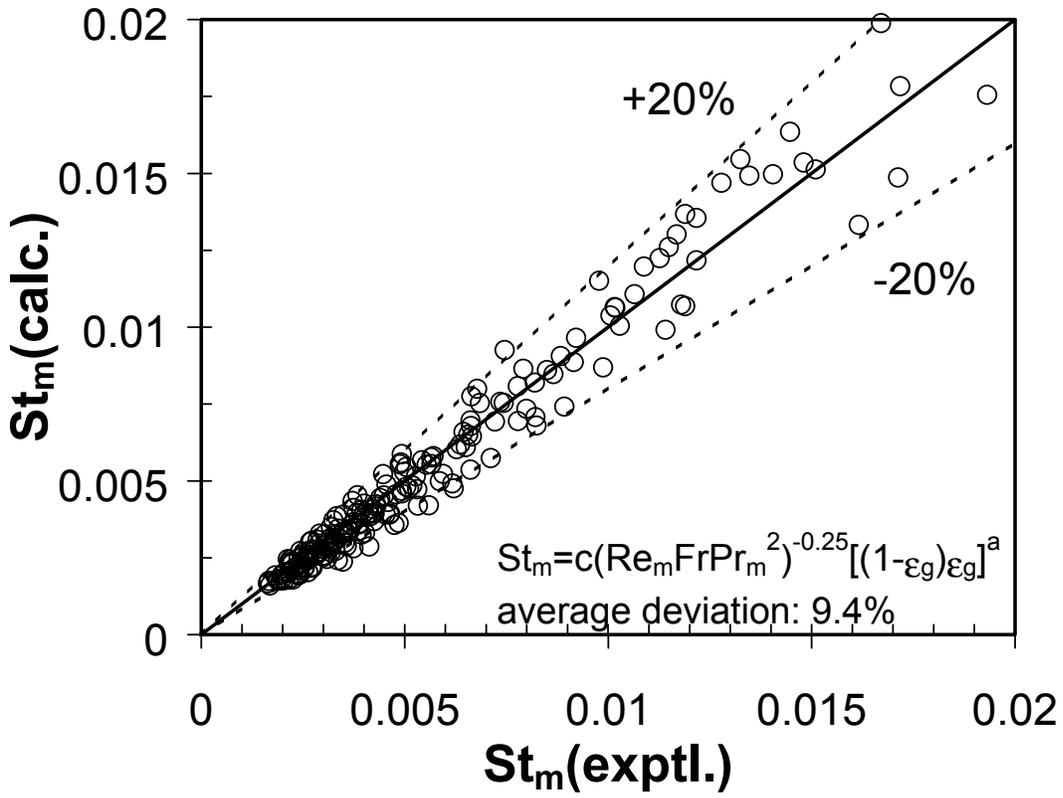
Figure 5-5. Comparison between the correlation predictions and the experimental data of the heat transfer coefficient in terms of Stanton number
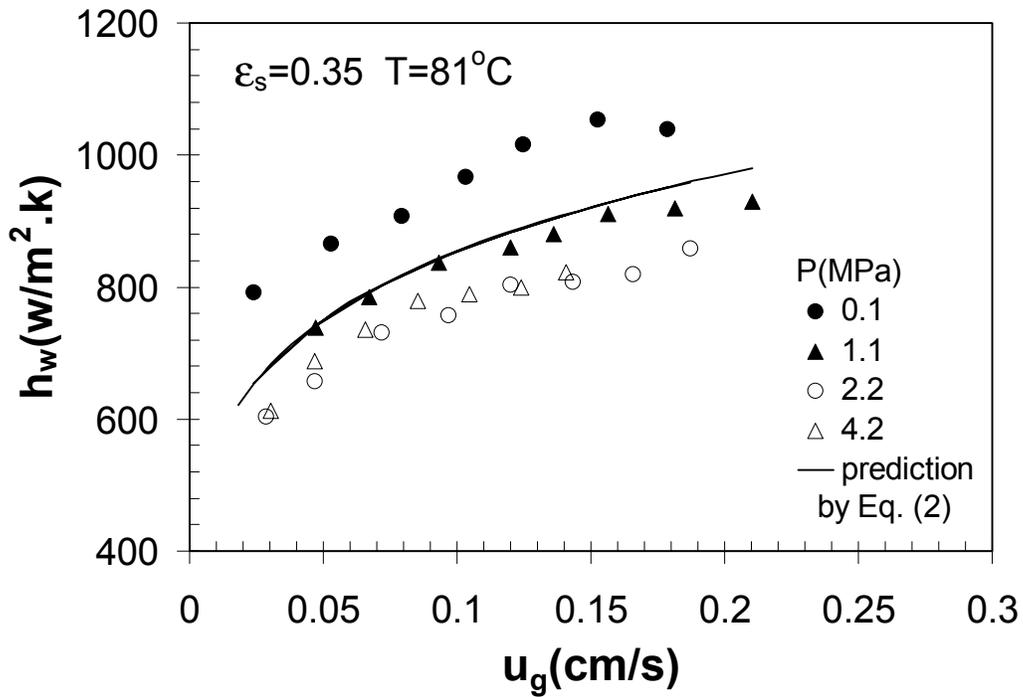
(a) Deckwer's correlation
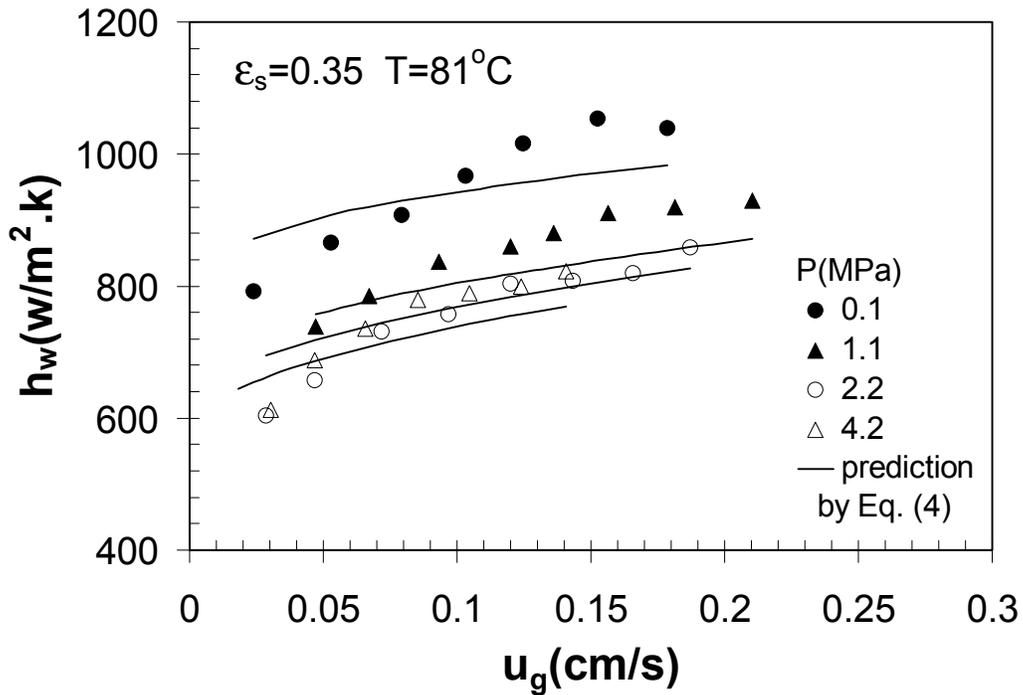
(b) Correlation proposed in this study

Figure 5-6. Comparison of the predicted results of heat transfer coefficients in slurry bubble columns under high pressure and high temperature conditions by using (a) Deckwer's correlation; and (b) correlation proposed in this study.
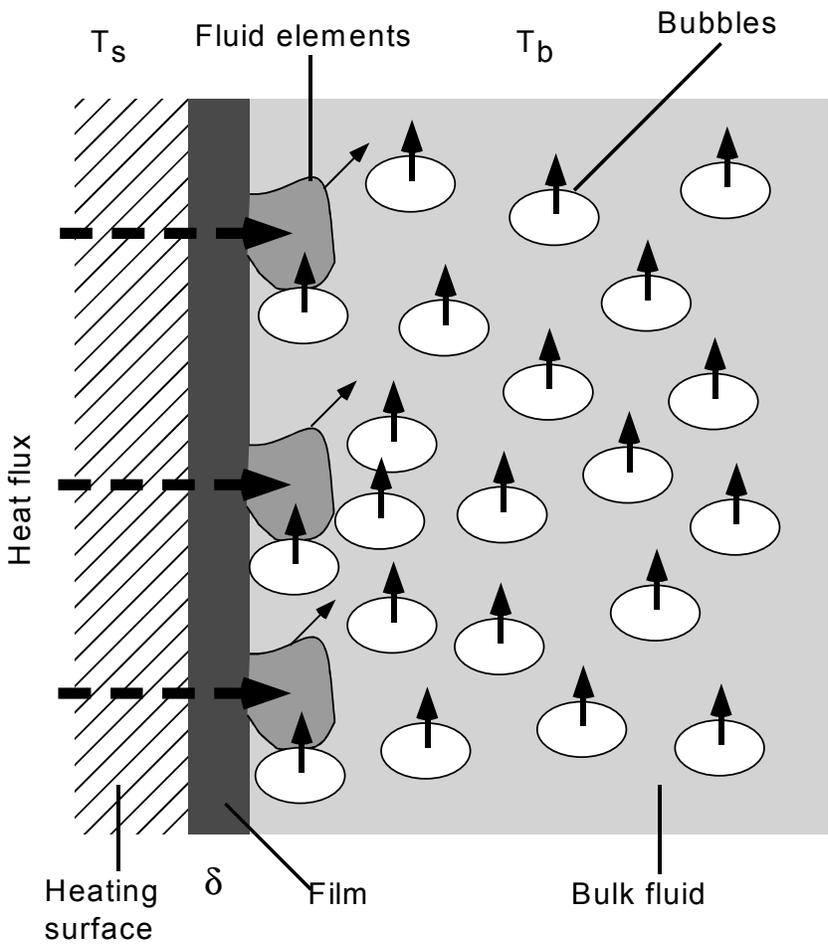
Figure 5-7. Schematic of the consecutive film and surface renewal model (Wasan and Ahluwalia, 1969).
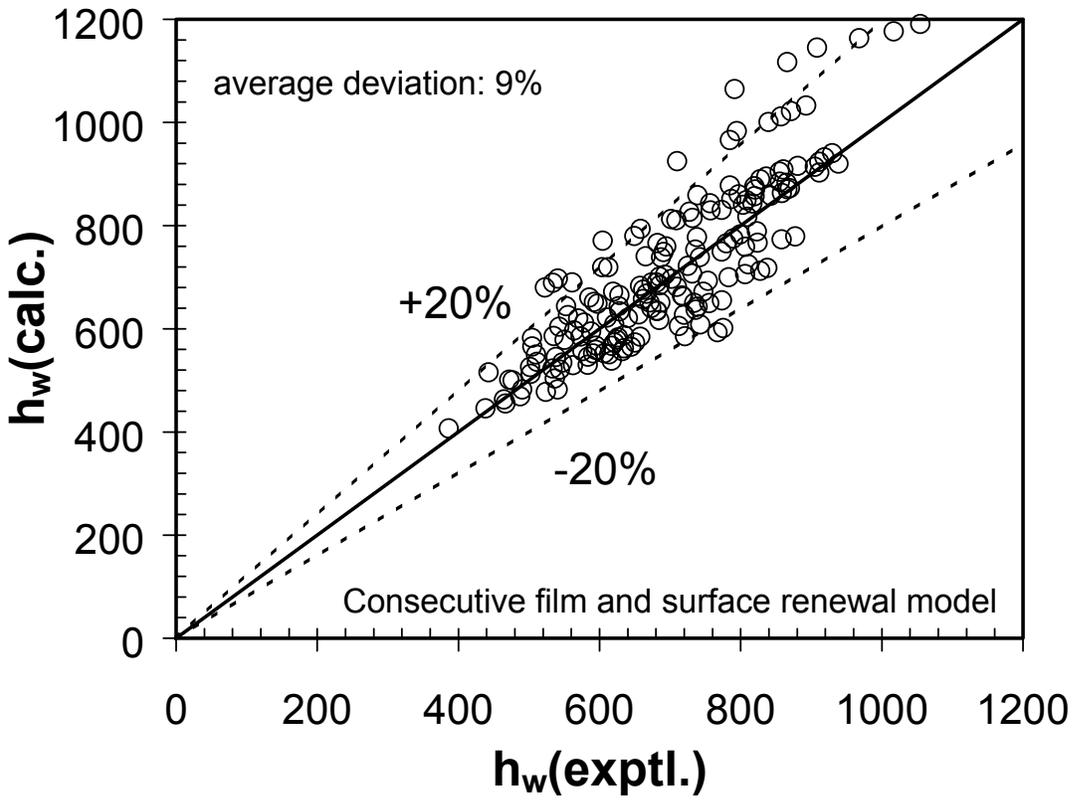
Figure 5-8. Comparison between the predictions and the experimental data of the heat transfer coefficient based on the consecutive film and surface renewal model.
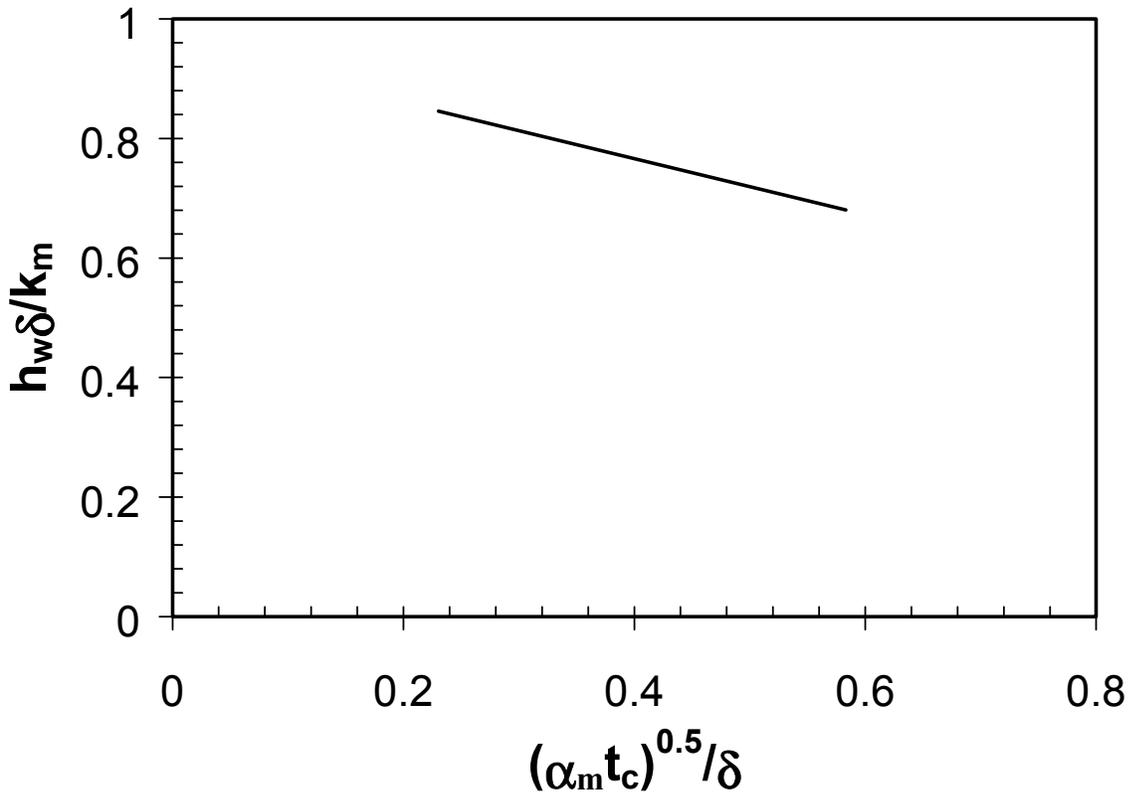
Figure 5-9. Comparison of heat transfer resistance due to the film with the total heat transfer resistance.
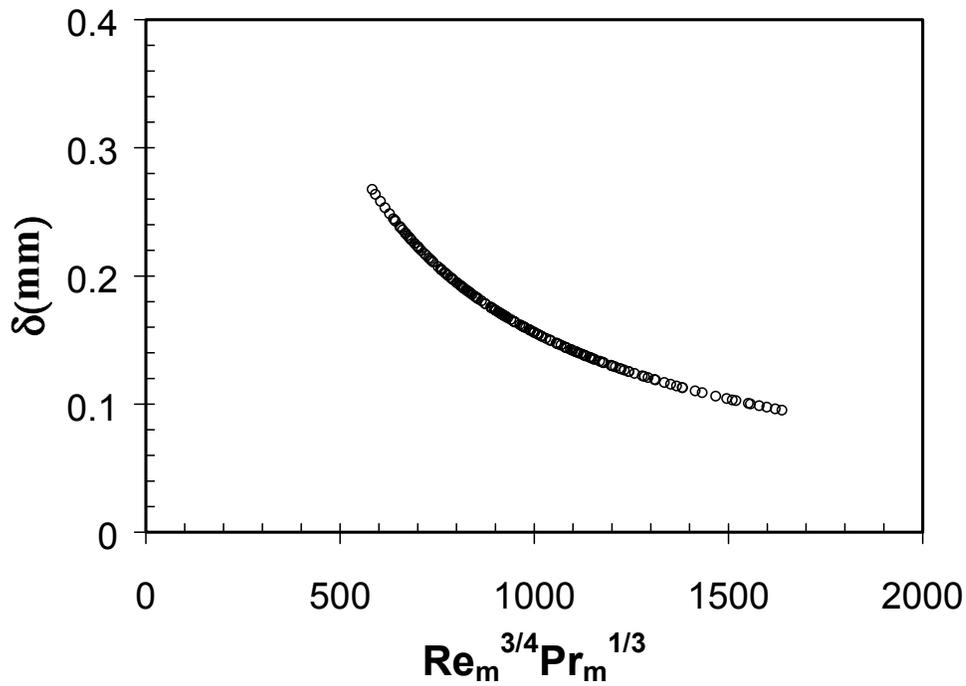
(a) film thickness
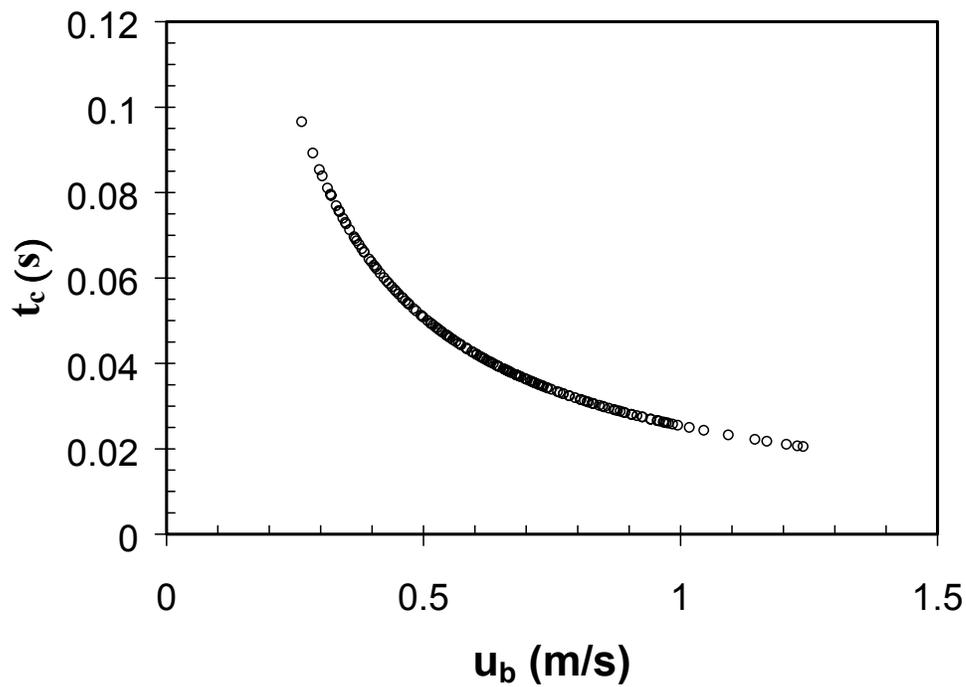
(b) contact time

Figure 5-10. The typical values of (a) film thickness; and (b) contact time between the liquid elements and the film estimated by the model under various operating conditions.
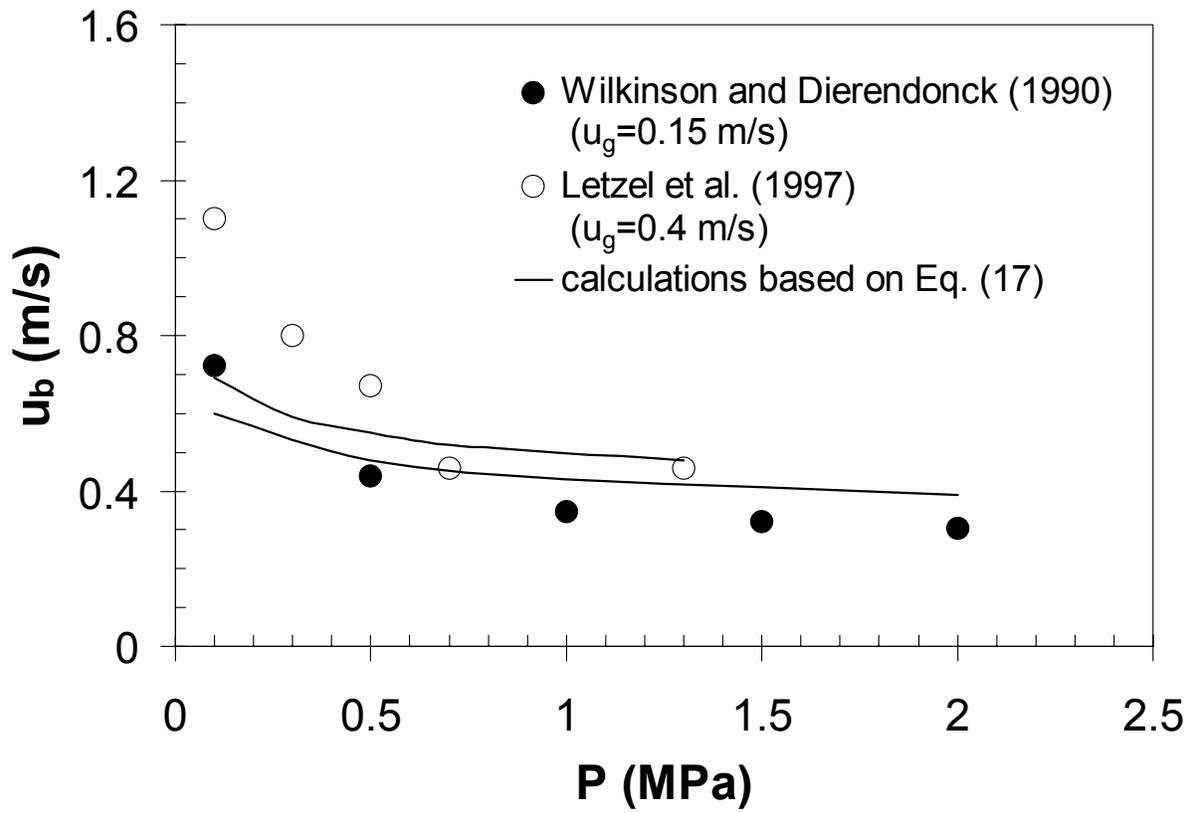
Figure 5-11. Comparison of bubble rise velocity predicted by Eq. (17) and that in the literature for high-pressure bubble columns.

Chapter 6: Future Studies

In this work, pressure was found to have a strong effect on the heat transfer characteristics. The heat transfer coefficient in a slurry bubble column decreases appreciably with an increase in pressure, which in turn increases liquid viscosity, decreases the bubble size, and increases the gas holdup resulting in a larger resistance to heat transfer. In addition to the effects of the pressure, temperature and particle concentration investigated in this work, future studies on the mechanics of enhanced heat transfer due to the fluid-bubble interaction can be emphasized for high velocity bubbling systems. Furthermore, much remains to be examined regarding the heat transfer mechanism between the immersed objects and the slurry medium such that the information obtained can be applied to industrial systems with internals or heat exchangers. The strategic placement of heat exchangers in the fluidized bed reactors in light of the complex hydrodynamic behavior of the reactor system needs to be explored.

Another crucial element of transport properties is mass transfer. The interfacial area and the liquid-side mass transfer coefficient are considered the most relevant design parameters associated with mass transfer. The interfacial area depends on the bubble size and the bubble density in the system. An elevation in pressure increases the gas holdup and reduces the bubble size. Therefore, a significant increase in the interfacial area at high pressures would occur. The liquid-side mass transfer coefficient depends on the bubble characteristics. An increase in pressure results in a decrease in surface tension and reduces the bubble size. These variations contribute to a decrease of the liquid-side mass transfer coefficient with increasing pressure. The combined effects of interfacial area and liquid-side mass transfer coefficient give rise to the overall change of volumetric mass transfer coefficient with pressure. In the literature, the mass transfer behavior in bubble columns at elevated pressures has been reported (Wilkinson et al., 1994; Letzel, 1997). However, these studies are limited in applicability in that the pressure range covered is not sufficiently high (normally less than 1.0 MPa). The development of appropriate measurement techniques and systematic studies to encompass higher pressure and gas velocity conditions are needed. Furthermore, little is known regarding the mass transfer behavior in gas-liquid-solid three-phase systems, especially with the presence of fine particles. The oxygen absorption method with the utilization of optical fiber oxygen probes can be developed to determine the liquid-side mass transfer coefficient in a high-pressure slurry bubble column. Optimization schemes to enhance the overall mass transfer behavior in slurry bubble column reactors can also be explored.

FLUID AND BUBBLE DYNAMICS OF SLURRY BUBBLE COLUMNS AT HIGH PRESSURES AND HIGH TEMPERATURES

Contract No. DE-FC-22-95 PC 95051

Final Report (Reporting Period: January 2002 – June 2002)

From

Dr. Liang-Shih Fan
Distinguished University Professor and Chair
Department of Chemical Engineering
The Ohio State University
140 West 19th Ave.
Columbus, OH 43210

Submitted to

Dr. Bernard Toseland
DOE Contract Program Manager
Air Products and Chemicals, Inc.
P. O. Box 25780
Lehigh Valley, PA 18007

cc:
R. Klippstein, Air Products and Chemicals, Inc.
M. Phillips, Air Products and Chemicals, Inc.
M. P. Dudukovic, Washington University
R. O. Fox, Iowa State University
K. Shollenberger, Sandia National Laboratory

Executive Summary

Gas-liquid bubble columns and three-phase fluidization systems are widely used in industry, particularly chemical and petrochemical industries. Three-phase fluidization describes a gas-liquid-solid flow system in which particles are in motion induced by gas and/or liquid phases. High pressure operations are common in industrial applications of slurry bubble columns for reactions, such as resid hydrotreating, Fischer-Tropsch synthesis and methanol synthesis. The design and scale-up of slurry bubble column reactors require knowledge of the hydrodynamics and mass transfer characteristics. Studies reported in the literature for such characteristics have been limited to ambient conditions. Little has been reported for high-pressure conditions.

The studies conducted under this program examine the effects of pressure and temperature on some areas pertaining to fundamental hydrodynamics in slurry bubble columns. These areas include the effects of distributors on gas holdup in high pressure and high temperature system, and gas-liquid mass transfer behavior in high pressure bubble columns.

The specific findings in this study for each of these areas are summarized below:

The effects of pressure and temperature on the overall gas holdup in bubble column reactors with a porous gas distributor, sparger gas distributor and perforated plate gas distributor are investigated. The overall gas holdup results are compared and the effects of different gas distributors on the gas holdup in high pressure and high temperature bubble columns are obtained. The pressure, temperature conditions investigated are up to 7.0 MPa and 78°C.

The study of gas-liquid mass transfer at high pressure is initiated. Previous studies on the gas-liquid mass transfer at elevated pressures and measurement techniques are reviewed. The gas-liquid mass transfer experiments are conducted in high pressure bubble columns, and the effect of the gas velocity and column diameter on the gas liquid mass transfer coefficient are investigated using the oxygen stripping method.

Chapter 1: GAS Distributor Effect on Gas Holdup in High Pressure and High Temperature Bubble Columns

Introduction

In chemical engineering operations and practice, bubble column reactors operating at high pressures and high temperatures are widely used for carrying out reactions and mass transfer operations such as stripping and absorption. Gas holdup is one of the most important properties in bubble column systems. Many kinds of gas distributors are used in bubble columns systems. Therefore, study of the effect of gas distributor on gas holdup in high pressure and high temperature bubble columns is necessary for design of industrial reactors.

Experimental

A schematic diagram of the bubble column used for high pressure and high temperature studies is shown in Figure 1. The column is 5.08 cm in diameter and 1.37 m in height. It has three pairs of planar quartz windows, with dimensions of 12.7 mm in width and 92 mm in height.

Three types of gas distributors are used in the experiments: (1) a porous plate; (2) a perforated plate with 120 square-pitched holes of 1.5 mm diameter, 4.8 mm thickness; (3) a multi-orifice sparger with 3 rows of triangular pitched holes of 3 mm.

Nitrogen is used as the gas phase and as the pressurizing source. Paratherm NF heat transfer fluid, a stable organic liquid (with a boiling point of 327°C at 0.1 MPa), is used as the liquid phase. Experiments are conducted at pressures of 0.1, 1.5, 4.2, and 7.0 MPa and at temperatures of 28°C and 78°C under batch condition for liquid. The superficial gas velocity, U_g, varies up to 25 cm/s.

The mean gas holdup is determined based on the dynamic pressure gradient obtained from a differential pressure transducer located at 0.16 m and 0.50 m above the gas distributor. The liquid level is maintained near the top of the column so that foaming does not affect the flow measurements.

Results and Discussion

Porous Plate Distributor

Figure 2 shows the effect of pressures on the gas holdup for a porous plate distributor at the temperature of 28ºC. The gas holdup linearly increases steadily as U_g increases. A higher gas holdup is observed at higher pressures due to the fact that a higher pressure yields smaller bubbles resulting in a smaller bubble coalescence rate, leading to an increase in the gas holdup (Jiang et al. 1992, Luo et al. 1999). There is no significant evidence of regime transition from the gas holdup results at 28ºC.

At 78ºC, the gas holdup is considerably higher than that at 28ºC. As seen from Figure 3, bubble regime transitions are evidenced from the gas holdup variation with U_g at elevated pressures. At low U_g conditions, very small and uniformly dispersed bubbles are generated. The gas holdup increases sharply as U_g increases. As the slope of the variation curve decreases, it signifies the onset of bubble clustering and hence, the onset of the churn-turbulent bubble regime. As U_g further increases, bubble collisions enhance, leading to more bubble clustering. Larger bubble clusters rise faster and tend to aggregate in the center of the bubble column. As they rise, the momentum of these clusters is

transferred to the smaller bubbles and hence increases their rising velocity. The clustering effect contributes to a decrease in the rate of increase of the gas holdup with increasing U_g. This maximum point corresponds to the onset of bubble coalescence. These larger bubbles have a much higher rise velocity, causing a decrease in the gas holdup. As the gas velocity further increases, the gas holdup increases solely due to higher through flow of the gas. For ambient pressure, the sharp increase in gas holdup at low U_g is not observed. The regime transition is believed to occur at U_g lower than the minimum measurement condition.

The temperature effect on the gas holdup can be observed by comparing Fig. 2 with Fig. 3. An increase in temperature introduces a more drastic increase in gas holdup at low U_g but a more moderate increase at high U_g. The significant change in gas holdup at different pressures and temperatures is due to the change of physical properties of the liquid and gas phases. The variation of the physical properties of the fluids with pressure and temperature, which affects the rates of bubble coalescence and break-up, contributes to this gas holdup behavior.

Sparger Gas Distributor

Figure 4 shows the effect of pressures on the gas holdup for a sparger gas distributor at 28ºC. There is little difference in overall gas holdup for ambient pressure and 1.5 MPa. The overall gas holdup increases almost linearly with increasing U_g up to around 15 cm/s. At higher pressures, the linearity of overall gas holdup and U_g holds for higher U_g.

At 78ºC, the gas holdup is higher than that at 28ºC especially at low U_g. The effect of pressures on gas holdup for a sparger gas distributor at 78ºC is shown in Figure 5. The gas holdup increases sharply as U_g increases at low U_g for elevated pressures. This phenomenon is not observed at 28ºC nor ambient pressure. This is because the lower viscosity and higher surface tension of the liquid phase at low pressures and low temperatures (Lin et al. 1998) hinder the formation of small bubbles at low U_g. The sharp increase in overall gas holdup quickly dissipate off before a U_g of 15 cm/s and provide lesser increase in overall gas holdup with further increase in U_g. Comparison between Figure 4 and Figure 5 shows that temperature has stronger effect in the increase gas holdup at low U_g in contrast to the relatively minor increase at high U_g. The effect of temperature indicates that the change in fluid properties with increasing temperature allows more small bubbles and reduces the rate of bubble coalescence.

Perforated Plate Gas Distributor

Figure 6 shows the effects of pressure on the gas holdup for a perforated plate gas distributor at 28ºC. It shows a steady increase in overall gas holdup with U_g. Elevated pressures lead to higher gas holdups under all the experimental conditions.

The effect of pressures on gas holdup for a perforated plate gas distributor at 78ºC is shown in Figure 7. At elevated temperatures, the gas holdup is higher than at 28ºC especially at low U_g. Both the effects of pressure and temperature on overall gas holdup are more profound at low U_g than at high U_g. For example, the overall gas holdup at 7.0 MPa, 20 cm/s increases from 0.45 at 28ºC to 0.52 at 78ºC (15.5% increase) whereas the overall gas holdup at 7.0 MPa, 10 cm/s increases from 0.33 at 28ºC to 0.5 at 78ºC (51.5% increase). This is because at high U_g, the vigorous bubble breakup and coalescence

4

reaches a rate that dominates the effect of the small bubbles formed due to the lower viscosity and higher surface tension of the liquid phase at low pressures and low temperatures (Lin et al. 1998).

Comparisons of Porous Plate, Sparger, and Perforated Plate Gas Distributors
Figure 8 shows the comparison of overall gas holdup for porous plate, sparger and perforated plate gas distributors at various pressures and temperatures. As shown in the figure, the sparger and perforated plate gas distributors give very similar gas holdup at all conditions. Porous plate distributor generally gives lower gas holdup than sparger and perforated plate gas distributor especially at high U_g. The regime transition of porous plate distributor is more apparent as compared to sparger and perforated plate distributors. The effect of distributors is generally smaller at high pressure and high temperature conditions because the bubble formation is dominated by the physical properties of the liquid phase instead of the distributor type.

Concluding Remarks
In the bubble column reactors, the overall gas holdup increases with the increase of pressure and temperature. The significant change in gas holdup at different pressures and temperatures is due to the change of physical properties of the liquid and gas phases. It is also found that the sparger and perforated plate gas distributors give very similar gas holdup at all conditions, while porous plate distributor generally gives lower gas holdup than sparger and perforated plate gas distributor especially at low U_g. The regime transition of porous plate distributor is more apparent as compared to sparger and perforated plate distributors. The effect of distributors is generally smaller at high pressure and high temperature conditions because the bubble formation is dominated by the physical properties of the liquid phase instead of the distributor type.

References

Jiang, P., Arters, D. and Fan, L.-S., "Pressure Effects on the Hydrodynamic Behavior of Gas-Liquid-Solid Fluidized Beds," *Ind. Eng. Chem. Res.*, **31**, 2322 (1992).

Lin., T., Tsuchiya, K., and Fan, L.-S., "Bubble Rise and Flow Characteristics in Bubble Columns at Elevated Pressure and Temperature," *AIChE J.*, 44(3), 545 (1998).

Luo, X., Lee, D.J., Lau, R., Yang, G.Q., and Fan, L.-S., "Maximum stable bubble size and gas holdup in high-pressure slurry bubble columns", *AIChE J.*, 45(4), 665 (1999).

List of Acronyms and Abbreviations

P   Pressure, MPa
T   Temperature, ºC
U_g Superficial gas velocity, cm/s
ε_g Gas holdup
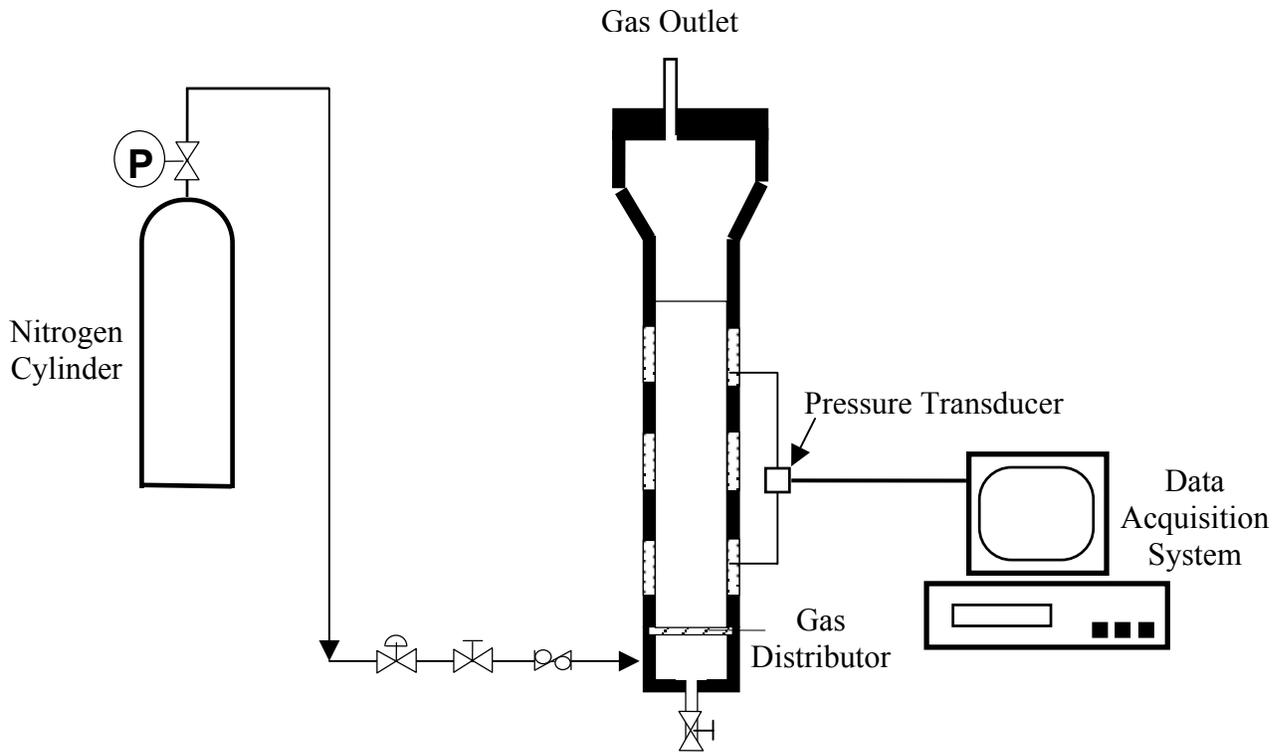
Figure 1. Schematic of experimental setup for the measurement of gas distributor
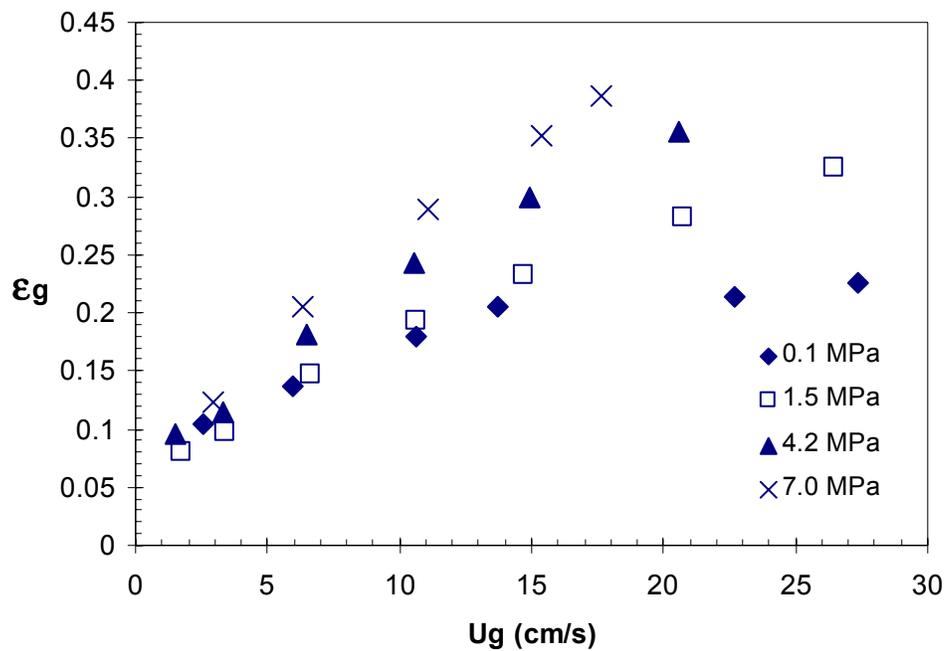

Figure 2. Relationship between the gas velocity and the gas holdup for the porous plate at various pressure and T = 28ºC
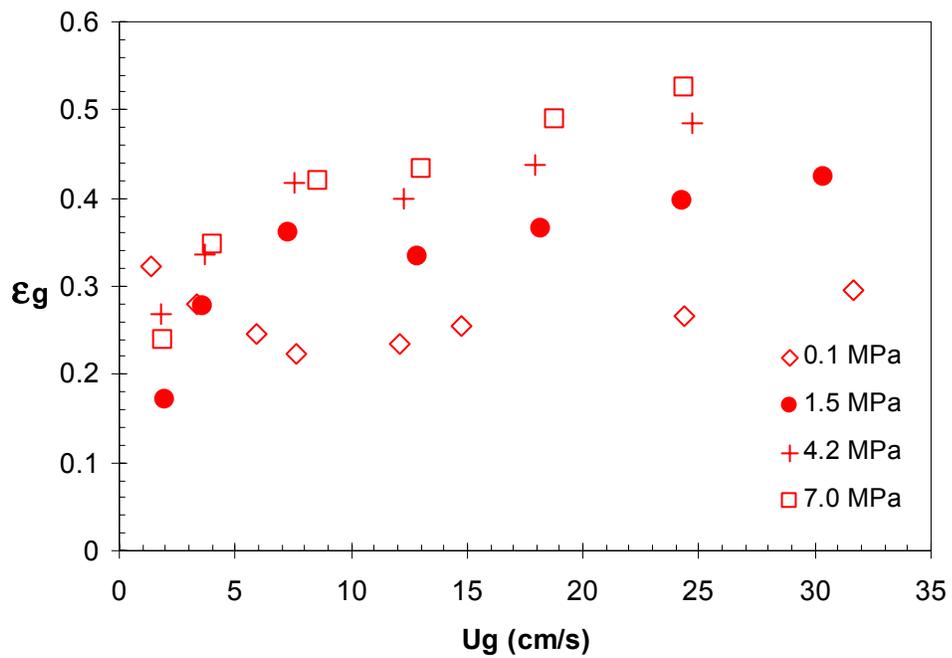
Figure 3. Relationship between the gas velocity and the gas holdup for the porous plate at various pressure and T = 78ºC
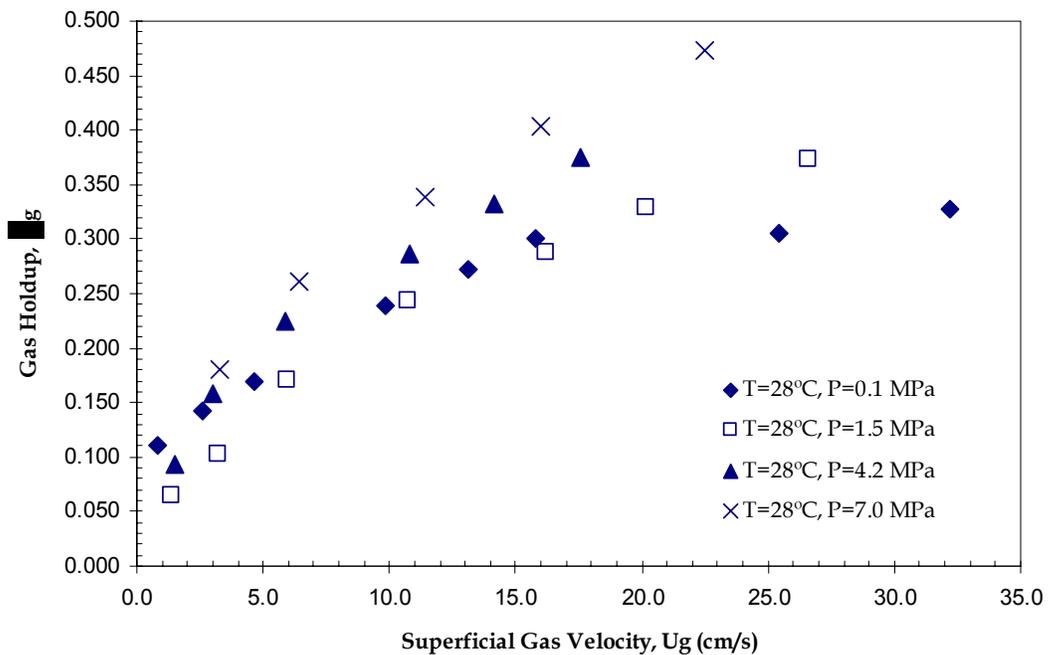
Figure 4. Relationship between the gas velocity and the gas holdup for the sparger gas distributor at various pressure and T = 28ºC
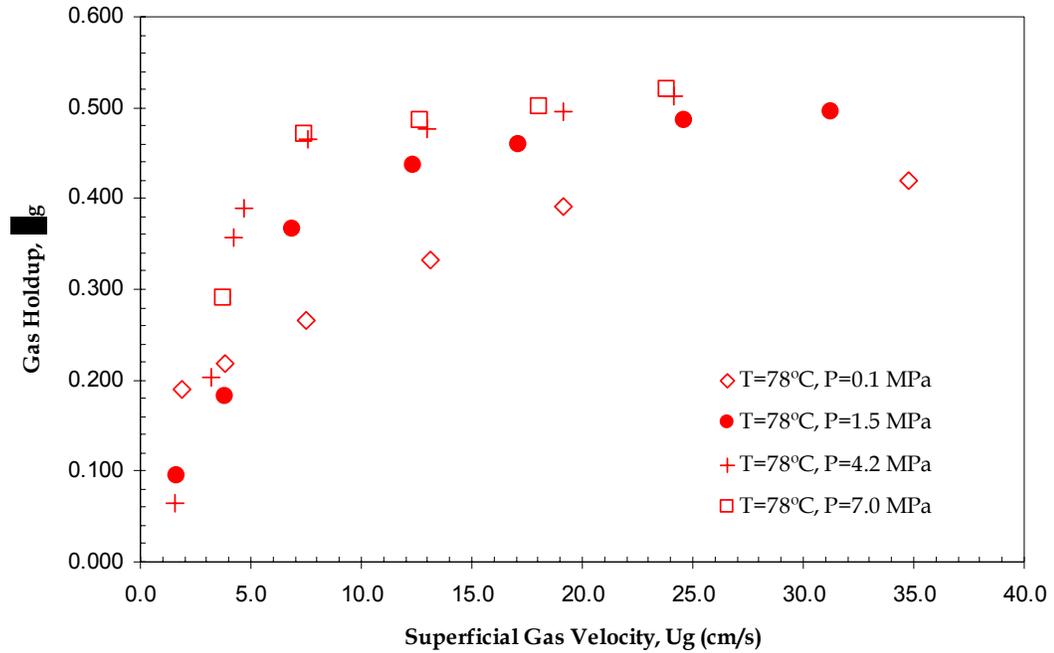
Figure 5. Relationship between the gas velocity and the gas holdup for the sparger gas distributor at various pressure and T = 78ºC
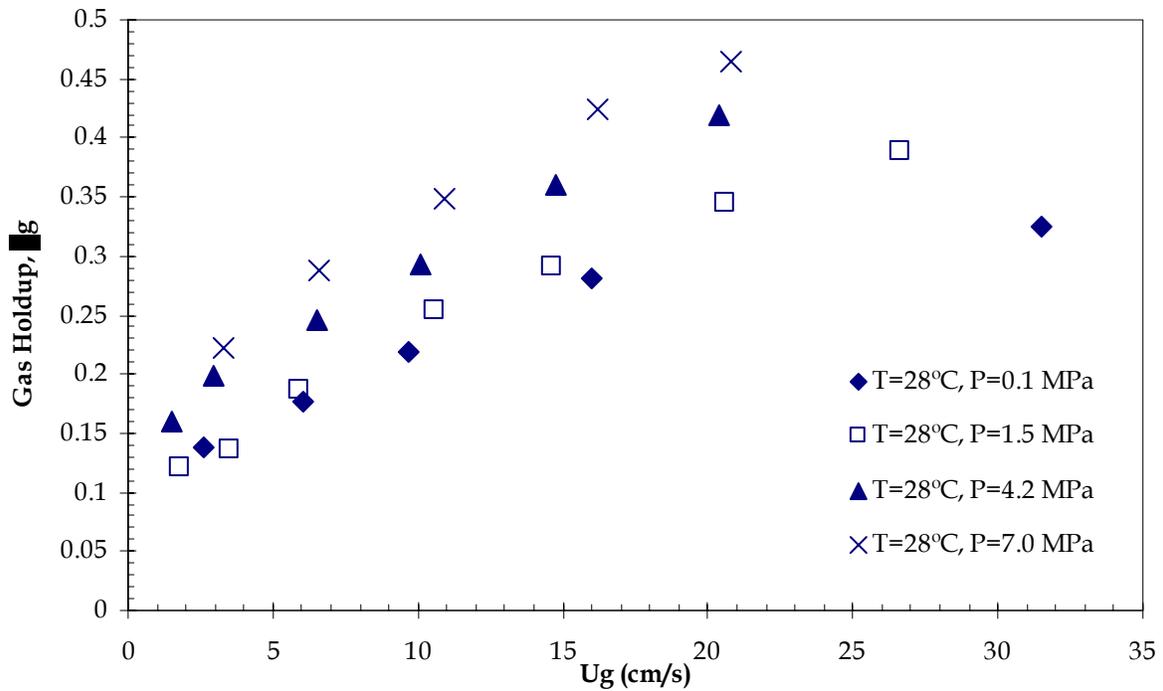
Figure 6. Relationship between the gas velocity and the gas holdup for the perforated plate gas distributor at various pressure and T = 28ºC

8
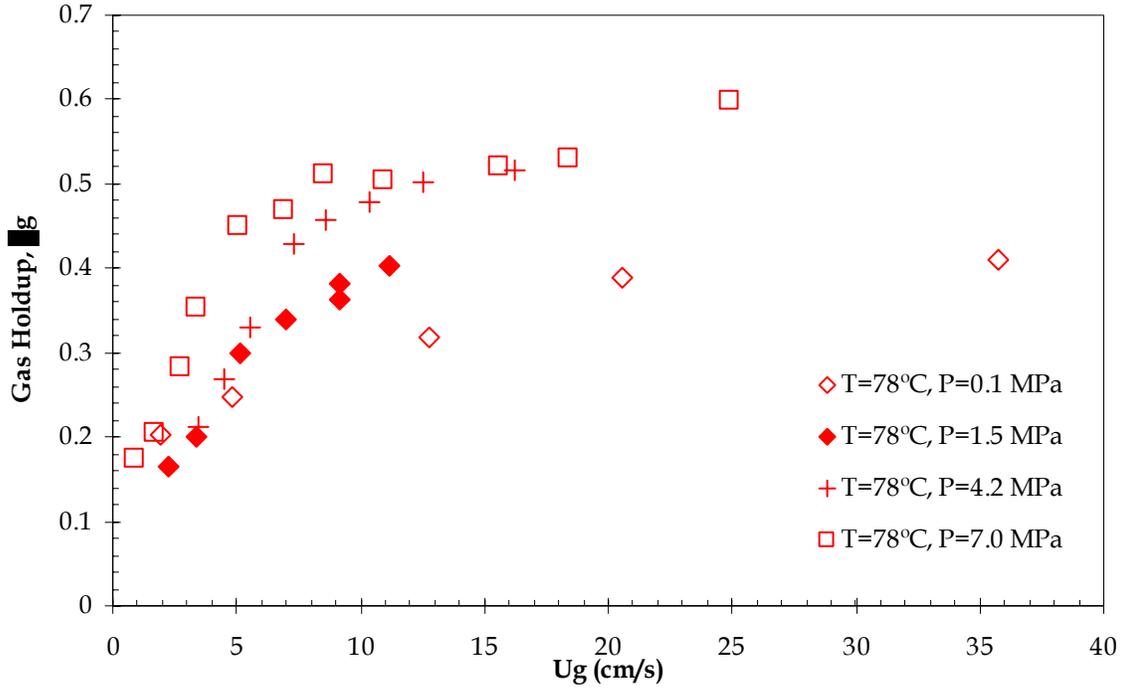
Figure 7. Relationship between the gas velocity and the gas holdup for the perforated plate gas distributor at various pressure and T = 78ºC
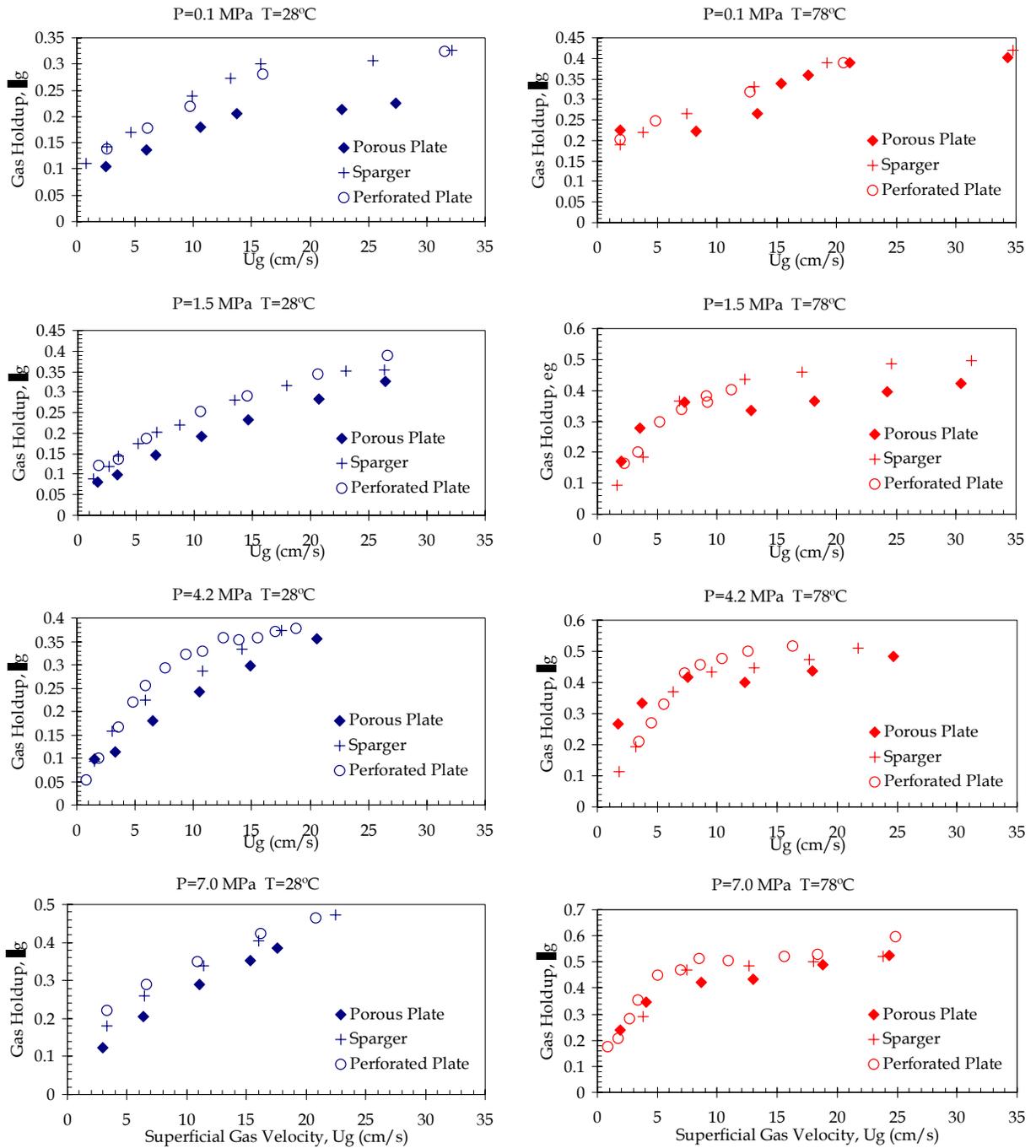
Figure 8. Comparison of overall gas holdup between porous plate, sparger and perforated plate gas distributors at various temperatures and pressures.

Chapter 2: Gas-Liquid Mass Transfer in High Pressure Bubble Column

Introduction

Bubble columns and slurry bubble columns reactors are widely used for industrial processes like Fischer-Tropsch synthesis, coal liquefraction, methanol synthesis, and other reactions (Fan, 1989). The design and scale-up of these reactors require knowledge of the hydrodynamics and the mass transfer behavior of three-phase fluidized beds at high pressures. Although the hydrodynamics of bubble columns and slurry bubble columns has been extensively studied, mass transfer studies are limited to ambient conditions and little has been reported on high pressure phenomena with relevance to industrial processes. It is known (Luo et al., 1999) that pressure has a significant effect on the hydrodynamics of slurry bubble columns. The bubble size decreases and gas holdup increases with increasing pressure. As the mass transfer coefficient depends strongly on the hydrodynamics, the pressure thus affects the mass transfer behavior.

Liquid side mass transfer is considered one of the most important phenomenon in mass transfer studies and results reported in the literature are concentrated on the gas-liquid mass transfer coefficient. Calderbank and Moo-Young (1961) found that k_l is lower for smaller bubble size and since an increase in pressure decreases the bubble size, the liquid-phase mass transfer coefficient would decrease with increasing pressure. Lewis and Davidson (1985) measured the volumetric mass transfer coefficient in a 0.45m diameter column and found that the mass transfer rates were enhanced by the breaking of gas bubbles but the effect was small due to the rapid coalescence of the small bubbles produced.

Sada et al. (1986) found that the influence of the type of suspended particles and the electrolyte concentration on $k_l a$ is insignificant and the increase of $k_l a$ in low concentration of fine particles was due to an increase of a. Ozturk et al. (1987) determined the volumetric mass transfer coefficient in a 0.095 m diameter glass column with different gas phase and organic liquids. The gas holdup and $k_l a$ are found to increase with gas density but $k_l a$ in mixed liquids do not correlate with high gas holdup. They suggested that the tiny bubbles do not contribute to the mass transfer but only circulate in the dispersion. The study of the mass transfer and bubble size in a bubble column under pressure (up to 0.4 MPa) by Wilkinson et al. (1994) also found an increase in $k_l a$ for higher pressures and they argue that the increases in $k_l a$ is partly limited due to the higher gas phase mass transfer resistance and a decrease in liquid reaction phase volume.

Kojima et al. (1997) found that gas holdup and volumetric mass transfer coefficient increased with pressure and the effect of pressure on gas holdup and $k_l a$ became significant at higher superficial gas velocities for single nozzle gas distributor. The liquid properties also affect the pressure effects. Lezel et al (1999) also found an increase in $k_l a$ with increasing pressure is due to the increase in total gas holdup and the ratio of $k_l a/$ is determined to be approximately 0.5. Yang et al. (2000) separated the $k_l a$ into k_l term and a term. There is little variation in k_l values with superficial gas velocity in the range of study (up to 2 cm/s). The interfacial area, a increases with increasing pressure and superficial gas velocity but decrease with increasing temperature and solid concentration.

In conclusion, although there is literature available on the study of gas-liquid mass transfer behavior in bubble columns and slurry bubble columns, those studies were confined to low gas velocities or low pressures, small column sizes and limited systems (air-water). Further systematic studies are needed to cover a wide range of operating conditions and be conducted in systems close to industrial applications. The objective of this study is to develop the suitable measurement technique to investigate the gas-liquid mass transfer coefficient in a hydrocarbon liquid at high pressures.

Experimental

The gas-liquid mass transfer experiments are currently being conducted in the 2-inch high-pressure column. The measurement in the 4-inch vessel will also be carried out later to study the scale-up effect on the gas-liquid mass transfer coefficient.

The gas-liquid mass transfer coefficient is measured using oxygen stripping method with a discontinuous switch from air to nitrogen. A high pressure optical fiber oxygen probe is developed to measure the liquid oxygen concentration up to a pressure of 3000 psi. A 470 nm light source is sent to the probe. The tip of the oxygen optical fiber probe is coated with a fluorescence dye which is excited by the light source. When the fluorescence gel is excited, it gives out light of wavelength 590 nm. The dye fluoresces most brightly when no oxygen is present and decreases with increasing oxygen concentration. A two point calibration of the oxygen optical fiber probe is performed by applying atmospheric air and an aqueous solution of sodium dithionite. The addition of sodium dithionite to water will chemically remove the dissolved oxygen to generate a zero oxygen environment. At the beginning of experiment, the liquid oxygen concentration is saturated with air. Then the air flow is shut down so that all bubbles escape from the liquid. Then nitrogen is fed into the column. Simultaneously, the oxygen concentration is monitored. Assuming that the liquid is perfectly mixed, the dissolved oxygen concentration can then be described by the equation

$$\frac{dC}{dt} = k_l a (C_{eq} - C) \tag{1}$$

where $k_l a$ is the gas-liquid mass transfer coefficient, C is the liquid phase oxygen concentration and C_{eq} is the equilibrium oxygen concentration. Equation (1) can be integrated with the boundary condition that at $t=t_0$, the oxygen concentration is C_0 and at $t=\infty$, $C=0$. In order to compensate for the fact that there is a finite response time for the oxygen probe, a correction term is proposed by Letzel et al. (1999)

$$\frac{dC_{probe}(t)}{dt} = k_{probe} \left[C(t) - C_{probe}(t) \right] \tag{2}$$

where k_{probe} is a probe constant that takes into account the probe response time and C_{probe} is the direct oxygen concentration reading from optical fiber oxygen probe. Equations (1) and (2) can be solved simultaneously to obtain the actual mass transfer coefficient from the probe measured oxygen concentration.

$$C_{probe}(t) = C_{eq} - \frac{C_{eq} - C_0}{k_{probe} - k_l a}(k_{probe}e^{-k_l at} - k_l ae^{-k_{probe}t}) \qquad (3)$$

In this study, nitrogen and air are used as the gas phase, and water is used as the liquid phase. Paratherm NF heat transfer fluid will be used in the future to study the effect of liquid properties on mass transfer behavior. A perforated plate with 45 square pitched holes of 1.6 mm diameter is used as the distributor. The schematic of the experimental setup is shown in Figure 1. The gas velocity varies up to 30 cm/s, which covers both the homogenous bubbling and churn turbulent regimes.

Typical oxygen concentration signals sampled by the high pressure oxygen optical fiber probe are shown in Figure 2. As can be seen, the oxygen concentration in the liquid phase is constant when saturated with air before introduction of nitrogen. As nitrogen is introduced into the liquid, the oxygen concentration reduces exponentially to essentially zero.

Based on Equation (3), a least square fit is performed to find the sensor constant and the mass transfer coefficient. A sample graph of the least square fit is shown in Figure 3. It can be seen that the relations fit the data fairly well, which indicates that the correction model is capable of describing the mass transfer behavior in bubble columns.

Results and Discussion
Comparison with Literature Data
To verify the validity of the measuring technique, the mass transfer coefficient measurement is first conducted in the air-water system under ambient conditions, and the measured mass transfer coefficients are compared with the literature data. The effects of gas velocities on the mass transfer coefficient in the air-water system are shown in Figure 4. It can be seen that the mass transfer coefficient increases significantly with increasing gas velocity and the results agree with the literature. The detailed information of various literature studies used in the figure is shown in Table 1.

Effect of Gas Velocity
Figure 5 shows the effect of gas velocity on gas-liquid mass transfer coefficient. It can be seen that the gas-liquid mass transfer coefficient increases with increasing gas velocity. At high gas velocities, the gas-liquid mass transfer coefficient tends to level off. As the gas velocity increases, the contact time between the liquid and bubbles is reduced, resulting in a lower mass transfer coefficient. An increase in gas velocity increases the gas holdup and decreases the mean bubble diameter. Mass transfer coefficient is known to be lower for small bubbles (Calderbank and Moo-Young, 1961). However, it is believed that $k_l a$ is dominated by the variation of interfacial area. A decrease in the mean bubble diameter at increasing gas velocities provides a larger interfacial area for gas-liquid contact. The significant increase in interfacial area predominates over the decrease of mass transfer coefficient due to shorter gas-liquid contacting time and result in an increase in $k_l a$. As indicated by Letzel et al. 1999, $k_l a$ is proportional to the gas holdup and the ratio $k_l a/$ is approximately equal to one half. Moreover, the turbulence generated by the gas bubbles as well as the liquid internal circulation at higher gas velocities also contribute to the increase in the gas-liquid mass transfer.

Effect of Column Diameter

Figure 5 also shows the comparison of experimental results obtained from 2" ID and 4" ID bubble columns. The gas-liquid mass transfer coefficient is higher in 2"ID column than in 4" ID column. The effect of column diameter on gas-liquid mass transfer coefficient is mainly due to the difference in gas holdup, which directly affect the interfacial area for gas-liquid contact. The effect of column diameter at ambient conditions in air-water system is shown in Figure 6. In small columns, the column wall effect is significant and the bubble size is limited by the column size. As column diameter increases, the bubble size is no longer limited to the column dimension but to the gas and liquid properties. The rate of bubble coalescence and breakup will then dictate the bubble size.

Concluding Remarks

A high pressure bubble column system is set up for the study of gas-liquid mass transfer. To verify the validity of the measuring technique, the mass transfer coefficient measurement is first conducted in the air-water system under ambient conditions. The mass transfer coefficient increases significantly with increasing gas velocity and the results agree with the literature very well. The effect of column diameter on gas liquid mass transfer coefficient is investigated using the oxygen stripping method. It is found that in small columns, the gas-liquid mass transfer coefficient is higher than that in large columns.

References

D.A. Lewis, and J.F. Davidson, "Mass transfer in a recirculating bubble column", *Chem. Eng. Sci.*, 40 (11), p.2013-2017 (1985).

Eizo Sada, Hidehiro Kumazawa, and C.H. Lee, "Influences of suspended fine particles on gas holdup and mass transfer characteristics in a slurry bubble column", *AIChE J.*, 32 (5), p.853-856 (1986).

Gopal, J. S., and M. M. Sharma, "Mass Transfer Characteristics of Low H/D Bubble Columns," *Can. J. Chem. Eng.*, 61, 517 (1983).

Hiromitsu Kojima Jun Sawai, and Hideyuki Suzuki, "Effect of pressure on volumetric mass transfer coefficient and gas holdup in bubble column", *Chem. Eng. Sci.*, 52 (21/22), p.4111-4116 (1997).

H.M. Letzel, J.C. Schouten, R. Krishna, and C.M. van den Bleek, "Gas holdup and mass transfer in bubble column reactors operated at elevated pressure", *Chem. Eng. Sci.*, 54, p.2237-2246 (1999).

Kato, Y., and A. Nishiwaki, "Longitudinal Dispersion Coefficient of a Liquid in a Bubble Column," *Int. Chem. Eng.*, 12, 182 (1972).

Koide, K., S. Morooka, K. Ueyama, A. Matsuura, F. Yamashita, S. Iwamoto, Y. Kato, H. Inoue, M. Shigeta, S. Suzuki, and T. Akehata, "Behavior of Bubbles in Large Scale Bubble Column," *J. Chem. Eng. Japan*, 12, 98 (1979).

Koide, K., A. Takazawa, M. Komura, and H. Matsunaga, "Gas Holdup and Volumetric Liquid-Phase Mass Transfer Coefficient in Solid-Suspended Bubble Columns," *J. Chem. Eng. Japan*, 17, 459 (1984).

K. Terasaka, D. Hullmann, and A. Schumpe, "Mass transfer in bubble columns studied with an oxygen optode", *Chem. Eng. Sci.*, 53 (17), p.3181-3184 (1998).

L.-S. Fan, *Gas-Liquid-Solid Fluidization Engineering,* Butterworths, Stoneham, MA (1989).

Letzel, H.M., J.C. Schouten, R. Krishna, and C.M. van den Bleek, "Gas holdup and mass transfer in bubble column reactors operated at elevated pressure", *Chem. Eng. Sci.*, 54, p.2237-2246 (1999).

Luo, X., D. J. Lee, R. Lau, G. Q. Yang, and L. S. Fan, "Maximum Stable Bubble Size and Gas Holdup in High-Pressure Slurry Bubble Columns," *AIChE J.,* 45, 665 (1999).

Myers, K. J., M. P. Dudukovic, and P. A. Ramachandran, "Modelling Churn-Turbulent Bubble Columns – I. Liquid-Phase Mixing," *Chem. Eng. Sci.*, 42, 2301 (1987).

Ohki, Y., and H. Inoue, "Longitudinal Mixing of the Liquid Phase in Bubble Columns," *Chem. Eng. Sci.*, 25, 1 (1970).

Peter M. Wilkinson, Herman Haringa, and Laurent L. Van Dierendonck, "Mass transfer and bubble size in a bubble column under pressure", *Chem. Eng. Sci.*, 49 (9), p.1417-1427 (1994).

P.H. Calderbank, and M.B. Moo-Young, "The continuous phase heat and mass-transfer properties of dispersions", *Chem. Eng. Sci.*, 16, p.39-54 (1961).

S.S. Ozturk, A. Schumpe, and W.-D. Deckwer, "Organic Liquids in a bubble column: Holdups and mass transfer coefficients", AIChE J., 33 (9), p.1473-480 (1987).

Xukun Luo, D.J. Lee, Raymond Lau, Guoqiang Yang, & Liang-Shih Fan, "Maximum stable bubble size and gas holdup in high-pressure slurry bubble columns", AIChE J., 45(4), 665-680, (1999)

Weiguo Yang, Jinfu Wang, and Yong Jin, "Gas-liquid mass transfer of H_2 and CO in a bubble column with suspended particles at elevated temperature and pressure", Fluidization X, p.525-532 (2000).

Yang, G.Q., and L. S. Fan, "Axial Liquid Mixing in High-Pressure Bubble Columns," *AIChE J.*, In Press (2002).

List of Acronyms and Abbreviations

a   interfacial area
C Oxygen concentration in liquid phase
C_0 Oxygen concentration in liquid phase at the start of experiment
C_{eq} Equilibrium oxygen concentration at the gas-liquid interface
C_{probe} Direct oxygen concentration reading from optical fiber oxygen probe
$k_l a$ Gas-liquid mass transfer coefficient
k_l gas-liquid mass transfer coefficient
k_{probe} Probe constant
P System Pressure
ε gas holdup
T System Temperature
t Time
U_g Superficial gas velocity
ε_g Gas holdup

Table 1. Relevant information of various references used in Figure 4 regarding mass transfer coefficient measurement in air-water system under ambient conditions.

| Paper Reference	System	Operating Temperature, pressure and superficial gas velocity	Sensor response time	k_La range	Correlations
Kojima et al. (1997)	45 mm stainless steel column, N₂/O₂-tap water, aqueous buffered solution, aqueous enzyme solution	293 K, 0.1-1.1 MPa, up to 0.15 m/s	Clark type sensor, 4-6 sec	0.1-1 s⁻¹	$k_L a = C\varepsilon_G^{D}\left(\rho Q^2 d_0^{-3}\gamma^{-1}\right)^{E}\left(P/P_0\right)^{F}$
Letzel et al. (1999)	0.15 m steel column, N₂/O₂-demineralized water	293 K, 0.1-1.3 MPa, up to 0.3 m/s	Clark type sensor, 5 sec	0.02-0.3 s⁻¹	N/A
Terasaka et al. (1998)	0.06 and 0.114 m column, N₂/O₂-tap water, solutions of microbial polysaccharides xanthan or gellan	292 K, 0.1 MPa, up to 0.15 m/s	Optical sensor, 6 sec	0.001-0.11 s⁻¹	Schumpe and Deckwer (1987)
Lewis and Davidson (1985)	0.45 m column, Air-water	293 K, 0.1 MPa, U_g up to 0.23 m/s, U_L up to 0.68 m/s	Clark type sensor, 5 sec	0.01-0.16 s⁻¹	N/A
Wilkinson et al. (1994)	0.158 m metal column, 0.8 mol/l sodium sulphite deionized water solution-Air	293 K, 0.1-0.4 MPa, up to 0.15 m/s	Clark type with uncatalysed oxidation of sodium sulphite reaction model, 5 sec	0.02-0.25 s⁻¹	$k_L a = \left(\frac{k_M D_l}{D^2}\right)\left(\frac{\eta_l}{\rho_l D_l}\right)^{0.5}\left(\frac{gD^2 \rho_l}{\sigma}\right)^{4/7}\left(\frac{gD^3 \rho_l^2}{\eta_l^2}\right)^{2/7}\varepsilon_g^{1.18}$ Akita (1989)
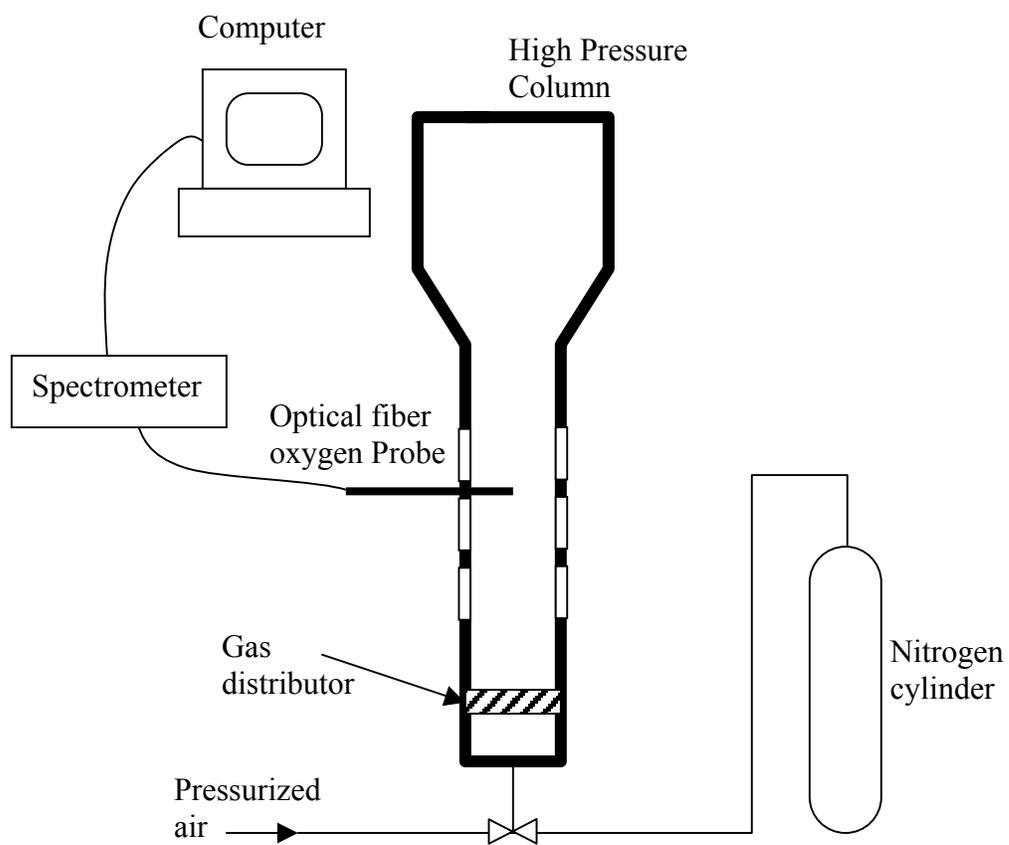
Figure 1.   Schematic of experimental setup for the measurement of mass transfer coefficient
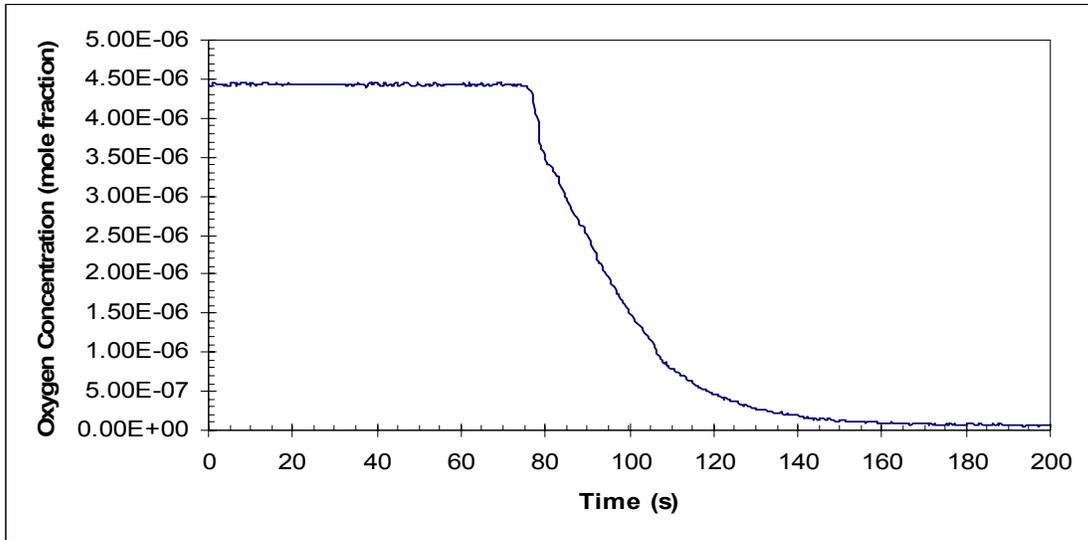
Figure 2.   Typical liquid phase oxygen concentration during the stripping process.
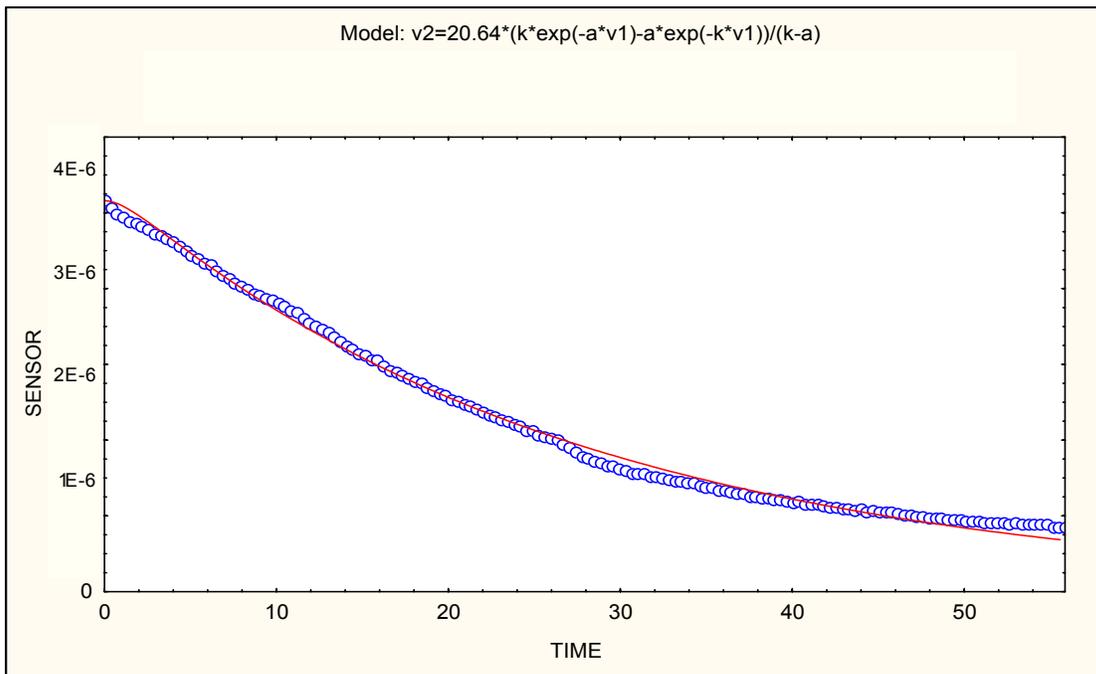

Figure 3.   Least square fit of experimental data to model
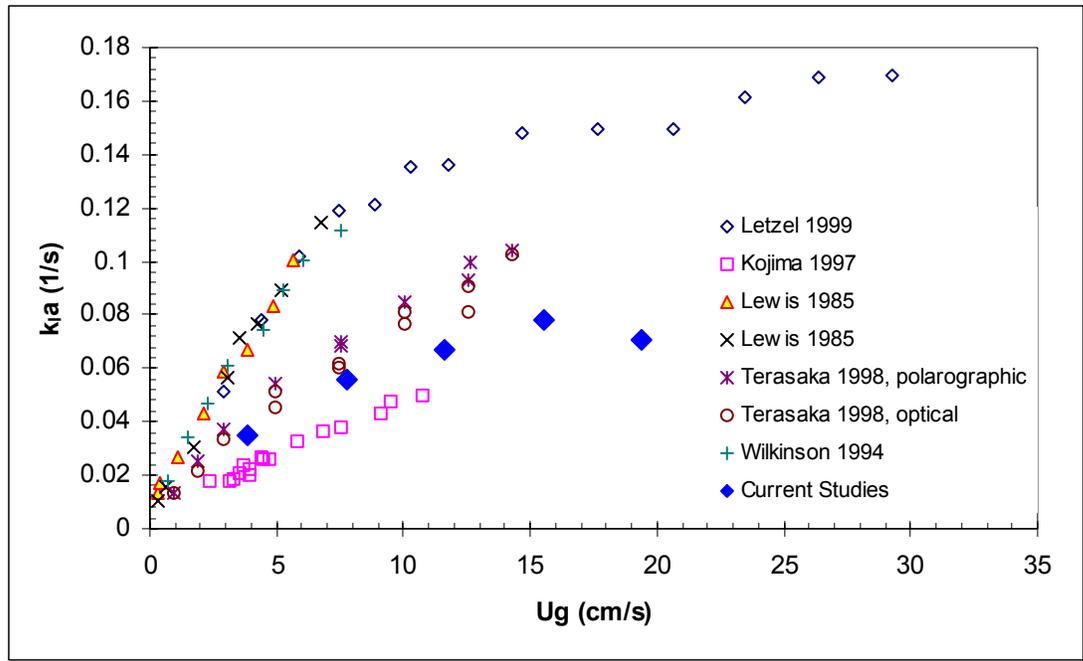
Figure 4.   Comparison of experimental data with available literature data for air-water system under ambient conditions
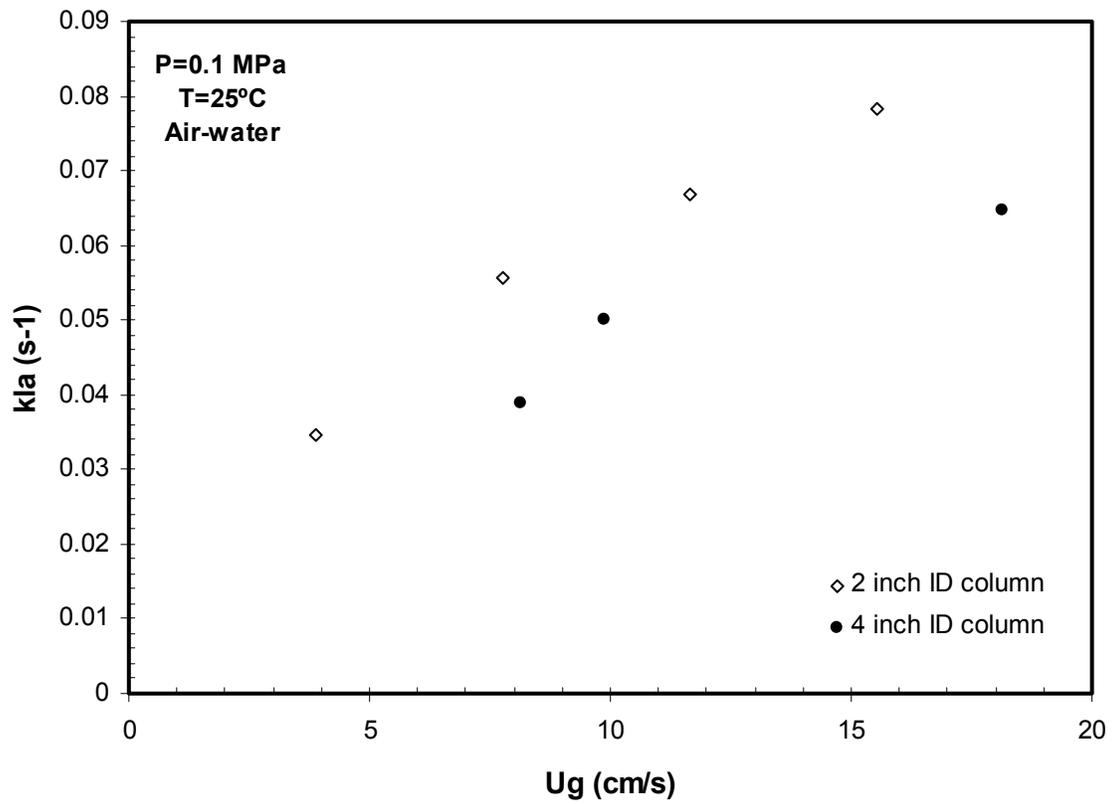
Figure 5.　　　Effect of gas velocity on gas-liquid mass transfer coefficient in air-water system under ambient conditions in different column dimensions.
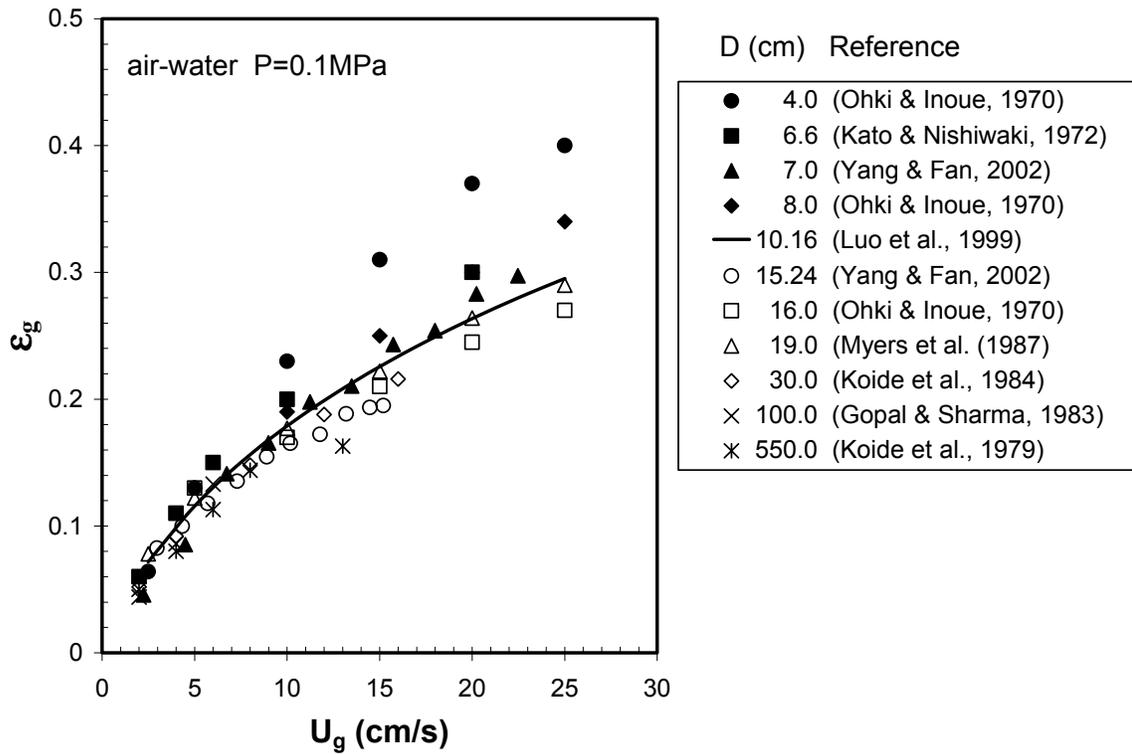
Figure 6.   Comparison of gas holdup data obtained in different sizes of columns under ambient conditions for air-water systems.

FUTURE STUDIES

In the next period, an optical fiber oxygen probe will be tested and used to determine the liquid-side mass transfer coefficient by oxygen absorption method in the high-pressure slurry bubble column. An optical fiber probe will be also be used to determine the interfacial area. The axial dispersion model will be used to determine the mass transfer coefficient. Optimization schemes to enhance the overall mass transfer behavior in slurry bubble column reactors will be developed.

Supplementary: Measurement of Liquid Physical Properties in Bubble/Slurry Bubble Column

Most industrial bubble/slurry bubble columns are operated at extreme conditions of high pressures and temperatures. However, most research reports have been focused on ambient conditions and very little data has been published regarding high pressure and temperature systems. It is known that the physical properties of the gas and liquid greatly affect the hydrodynamic behaviors of bubble/slurry bubble columns. Therefore, it is necessary to know the exact physical properties of the liquid phase at high pressure and temperatures in order to characterize the actual system.

Liquid properties can be characterized at elevated pressures and temperatures in the high pressure and high temperature multiphase visualization system developed at The Ohio State University. The schematic diagram of the experimental system is shown in Figure 1. The column is made of stainless steel with maximum operating pressure and temperature of 21 MPa and 250ºC, respectively. The column is 80 cm in height and 5.08 cm in diameter. The column is comprised at three sections: plenum, test, and disengagement. Three pairs of quartz windows are installed on the front and rear sides the column. Each window is 12.7 mm wide by 93 mm long and allows the entire test section of the column to be viewed. Different gas distributor design can be installed to achieve uniform gas distribution. Nitrogen from the high pressure cylinders is introduced into the column after the pressure and temperature are adjusted to the desired value. The system pressure is controlled by a back pressure regulator installed at the outlet of the bed, while a high pressure turbine flowmeter is used to measure the gas flow rate. The system temperature is maintained by preheated nitrogen gas and a set of wall heaters.

The density, viscosity and surface tension of the liquid at elevated pressure and temperature can be characterized by the hydrostatic weighing method, the dropping weight method and the emerging bubble technique, respectively. For the hydrostatic weighing method, a cylindrical aluminum tube of 30.5 cm in length and 0.717 cm OD, shown in Figure 2(a), has an adjustable metal weight that is submerged in the liquid. The volume of the tube above the liquid surface varies with the liquid density specifically, the relation is based on the Archimedes principle; thus, the liquid density can be determined from the submerged float volume change as

$$S\left[\rho_f l_1 + \rho_g (l - l_1)\right] = (m_1 + m_2) + S_1 \rho_g l_2 \tag{1}$$

where m_1 and m_2 are the masses of the aluminum tube and the metal weight; ρ_f and ρ_g are the densities of liquid and gas; and S_1 and S_2 are the cross-sectional areas of the tube based on the outer and inner diameters.

The viscosity of the liquid under elevated pressures and temperatures is determined using the falling-ball technique. As shown in Figure 2(b), the system consists of a ball-releasing device and a guiding tube. The magnetically operated ball-releasing device is placed inside the column to release the ball into the guiding tube. The falling process is recorded by a CCD camera with an infinity lens. The falling distance (L) of the ball within a time interval (Δt) at its terminal velocity is obtained by a particle tracking system. The viscosity can then be calculated based on the Stokes law as

$$\mu_l = f_w \frac{2 d_p^2 (\rho_p - \rho_l) g \Delta t}{9L} \tag{2}$$

where f_w is the correction factor for the wall effect.

The emerging bubble technique is applied to measure the surface tension between the gas and liquid phases at various pressures and temperatures. A 3.2-mm OD steel tube is inserted vertically into the column and submerged in the liquid. A stable bubble generated on the tip of the tube is recorded by a high-resolution (800×490 pixels) CCD camera with an infinity lens. The boundary of gas-liquid interface in Cartesian coordinates fixed on the bubble (see Figure 3) is determined through the image processing. Then, the boundary coordinates are used as a basis to calculate the surface tension. The image processing incorporates six steps: inverting the gray levels of the bubble and the background images, subtracting one inverted image from the other, inverting the subtracted image, pasting the reflecting area, and defining the boundary based on the difference of the gray level as shown in Figure 4. The preliminary coordinates of the bubble boundary, which are measured in the pixel coordinates, are converted to the actual physical coordinates with the aid of a micro-ruler attached on the tip of the tube.

When an axisymmetric bubble emerges in the liquid and the bubble is in an equilibrium state, the pressure difference across the curved interface can be described by the Laplace equation:

$$\sigma\left(\frac{1}{R_1} + \frac{1}{R_2}\right) = \Delta P \tag{3}$$

where R_1 and R_2 are the two principal radii of curvature and ΔP is the pressure difference across the interface. At the apex of the bubble, the radius of curvature is R_o ($= R_1 = R_2$) and

$$\Delta P_o = P_2 - P_1 = \frac{2\sigma}{R_o} \tag{4}$$

Discounting all external forces besides gravity, the pressure at any point can be related to that at point P_1 or P_2 by

$$\left.\begin{array}{l} P_3 = P_1 + \rho_l g z \\ P_4 = P_2 + \rho_g g z \end{array}\right\} \tag{5}$$

Combining Eq. (4) with Eq. (5) yields the pressure difference across any point on the interface

$$\Delta P = P_4 - P_3 = P_2 - P_1 + (\rho_g - \rho_l)gz = \Delta P_o - \Delta \rho g z \tag{6a}$$

or
$$\sigma\left(\frac{1}{R_1} + \frac{1}{R_2}\right) = \frac{2\sigma}{R_o} - \Delta \rho g z \tag{6b}$$

From trigonometric relationships, it can be shown that $1/R_1 = \mathrm{d}\phi/\mathrm{d}s$ and $1/R_2 = (\sin\phi)/x$ where ϕ is the turning angle. Substituting these two relationships into Eq. (6b) yields

$$\frac{\mathrm{d}\phi}{\mathrm{d}s} = \frac{2}{R_o} - \frac{\Delta \rho g}{\sigma}z - \frac{\sin\phi}{x} \tag{7}$$

Taking the derivative of the trigonometric function with respect to s yields

$$\frac{\mathrm{d}x}{\mathrm{d}s} = -\cos\phi \tag{8}$$

$$\frac{\mathrm{d}z}{\mathrm{d}s} = \sin\phi \tag{9}$$

25

with the conditions $x(0) = z(0) = \phi(0) = 0$. In order to calculate the surface tension, Eqs. (7), (8) and (9) must be solved for several hundred coordinate points on the bubble boundary. The rotational discrimination method is used to obtain an optimized solution for the surface tension. The optimized solution for the surface tension of nitrogen bubble in Paratherm heat transfer fluid is shown in Figure 5. To verify the method, experimental results for N_2-water and N_2-methanol systems are obtained; the estimated values of surface tension for these systems are found to be consistent with the literature values within a deviation of 1%. This finding indicates that for practical purposes instead of determining the dynamic surface tension, the equilibrium/static surface tension is adequate for characterizing the gas-liquid interfacial properties in the system.

Physical properties of Paratherm

Physical properties of Paratherm are measured and shown in Figure 6, 7, and 8.
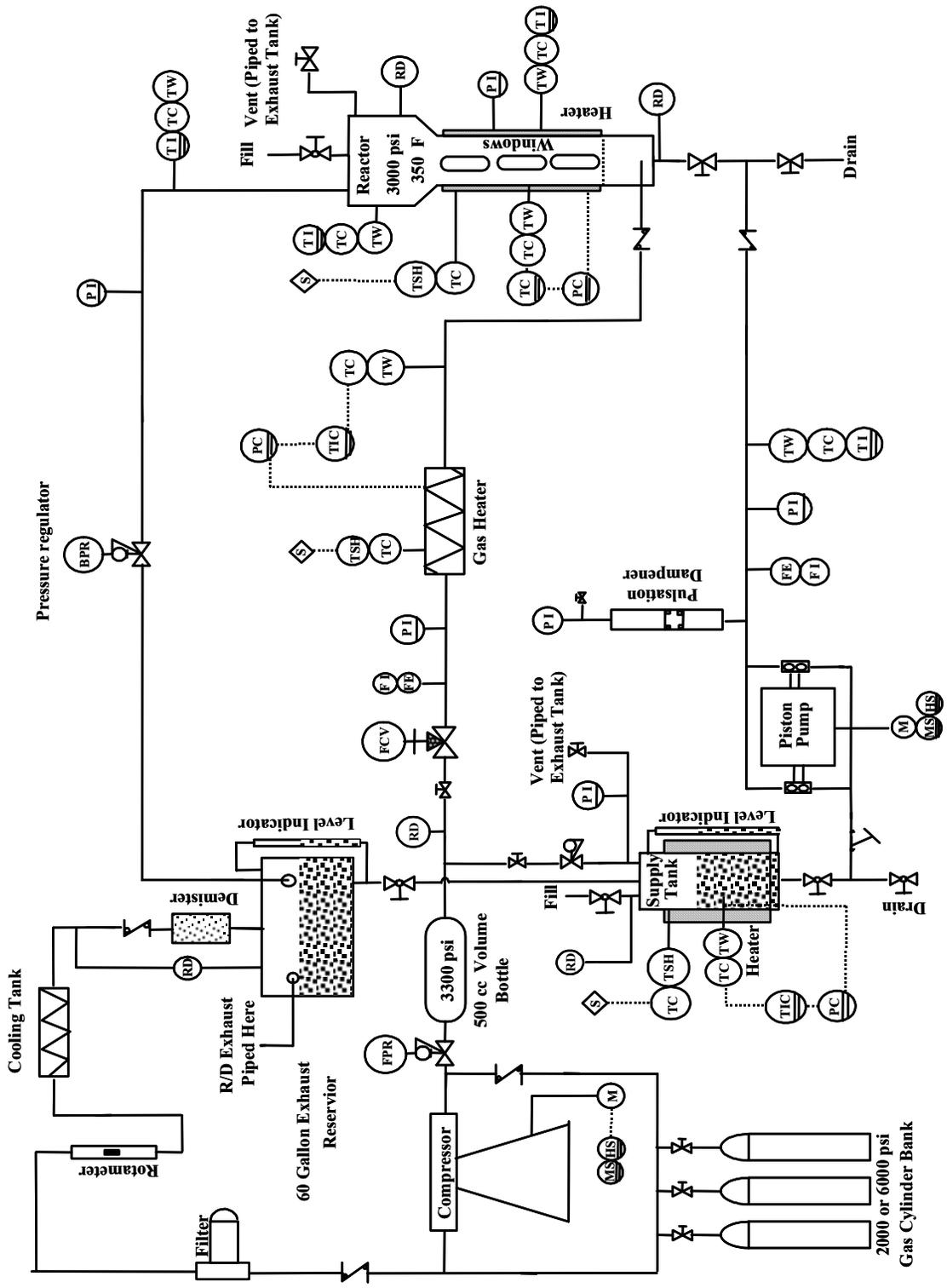
Figure 1. Schematic of high pressure and high temperature multiphase flow and visualization system

27

Figure 2.   Experimental setup for the measurement of (a) liquid density and (b) viscosity

1. Column
2. Window
3. Aluminum tube
4. Adjustable weight
5. Particles
6. Solenoid
7. Tubing
8. Wire
9. Guiding tube

Figure 3.   Coordinate definition for an emerging bubble
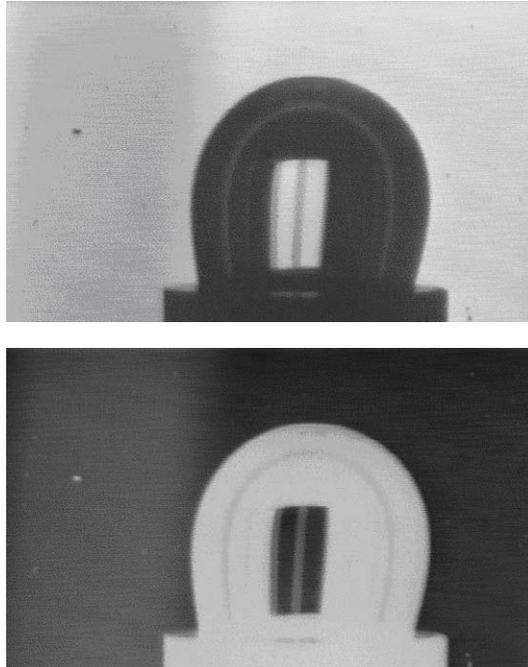
Figure 4.   Procedures of image processing of bubble boundary
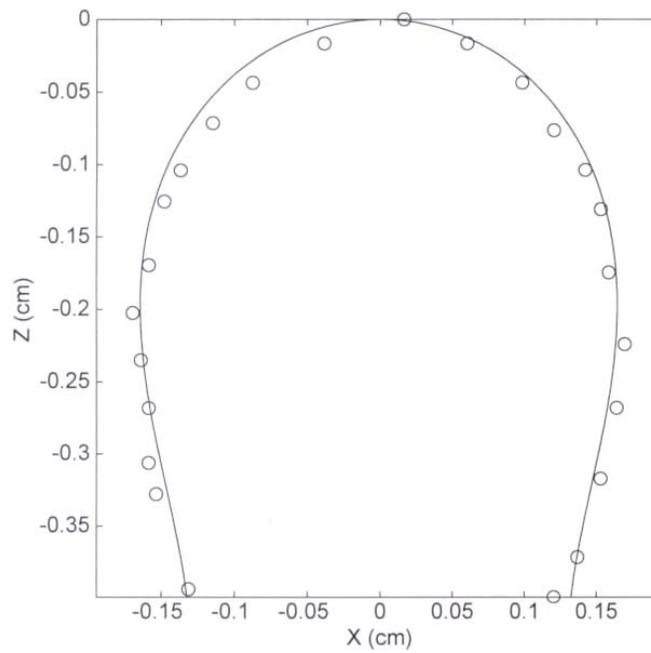
Figure 5.   Optimized results for surface tension determination
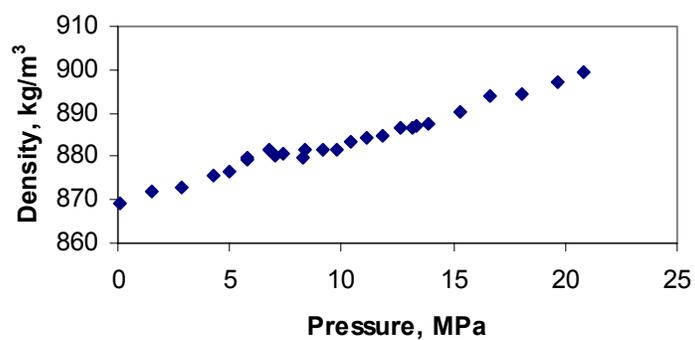
Figure 6. Density of Paratherm, T = 26°C
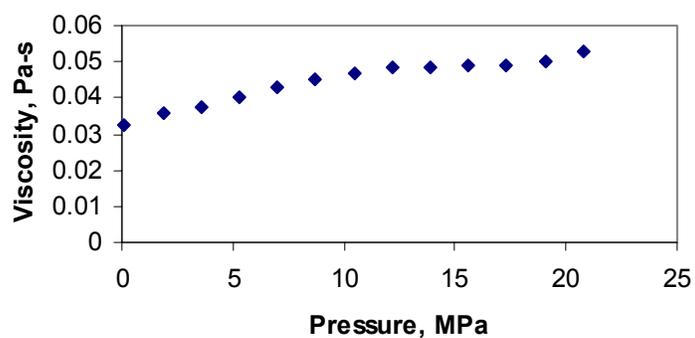
Figure 7. Viscosity of Paratherm, T = 26°C
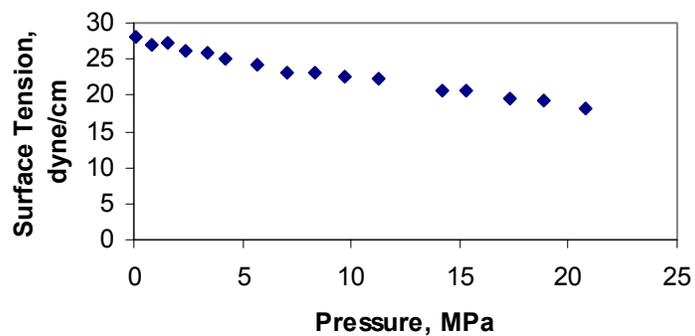
Figure 8. Surface Tension of Paratherm, T = 26°C